# Development of Boundary Conditions for Building Drainage System Components through Novel Numerical, Laboratory and Photogrammetric Methods.

Thesis submitted for the degree of

**Doctor of Philosophy**

**by**

**Nicole J. Jean**

School of Energy, Geoscience, Infrastructure and Society

Heriot Watt University

November 2015

# Abstract

Improvements in public health through better sanitary plumbing systems has been mainly due to the prevention afforded by barrier technologies to the ingress of foul air, which can contain toxic gases and pathogens, notwithstanding the nuisance of malodour. The main defence against this ingress is the 'trap seal' which comes in two forms; the 'water trap seal' and the 'waterless trap seal'. Whilst these devices form effective barriers, they are vulnerable to, or can produce, transient air pressure fluctuations in the system which can lead to seal loss. Greater understanding of the characteristics of these devices is essential for the development of better protection strategies. The development of novel analytical techniques is central to this research as it increases computer model resolution at these important system extremities.

Current methods employ a laboratory only approach, whereby a single loss co-efficient is developed. These laboratory derived boundary conditions are inherently static and in the case of the waterless trap seal, ignore structure flexibility. This research has produced new methodologies to evaluate performance and generate dynamic boundary conditions suitable for inclusion in an existing 1-D Method of Characteristics based model, AIRNET, which solves for pressure and velocity via the St. Venant equations of continuity and momentum in a finite difference scheme. The first novel technique developed uses photographic image and pressure data, transformed via photogrammetric and Fourier analysis to produce mathematical representations of the opening and closing of a waterless trap under transient pressures. The second novel technique developed focusses on the dynamic response of a water trap seal. Current boundary conditions use a steady state friction factor, ignoring separation losses. Analysis via ANSYS CFX allowed a frequency dependent dynamic representation of velocity change in the water trap seal to be developed, integrating unsteady friction and separation losses for the first time. Incorporation of these new boundary conditions in AIRNET confirms that frequency dependent whole system responses are possible and more realistic, reflecting both laboratory and on-site observations.

*To my Mom*

# Acknowledgements

I would like to first express wholehearted gratitude to my supervisor Dr Michael Gormley for his support and guidance before and during my PhD, as this opportunity and thesis is due to his belief in me as a researcher. It is difficult to summarise all the challenges which were faced during this endeavour, but the many months where I struggled to gather any significant data remain imprinted in my memory as the hardest. I will never forget your relief when I returned from St. Lucia one Christmas, and said "I was afraid you weren't coming back". Though giving up was never an option, I felt complete comfort in knowing that you understood just how hard the previous months had been, for one of the biggest challenges of a PhD is the solitude of the journey. Many, many, many thanks for enduring the difficult and frustrating times that came along and for your constant words of encouragement. I am in debt to you for life.

To Dr John McDougall, and Dr Doug Pender, please accept my gratitude for providing your computational expertise to the analysis of my research data.

To my officemates, Francesca, Menan, Jenny, Prince, Ehsan, Hari, Alaa and Jurbe, thank you for allowing me to pick your brains as often as needed and for making our space a home away from home. I pray we remain good friends though separated by land and sea.

The financial support provided by Heriot Watt University, McAlpine Plumbing, and the Reid Trust is thankfully acknowledged.

My friends (particularly Mariel, Shivani, Wilfreda, Kirmone, Lucy, Emma, Mariam, and Brittany) who have lent strength and been cheerleaders, dinner makers and proof readers and so much more throughout this journey, (and even more so at the end, when life poured out ample sadness,) I thank you until. Special thanks to Mariel for making me believe. Though I know you may never believe me, your words carried me through the obscurest of times over the last 9 years, and your kindness continues to overflow.

Thanks to my family, most especially, Aunty Rufina, Aunty Angie, Aunty Gigie, Uncle Popie and Uncle Angus for being the community who loved and supported always.

Finally, I would like to express gratitude to my late Aunty Christine who quietly and fundamentally supported this journey, and my Mom who encouraged me to follow my heart regardless the sacrifices- for God would always provide. For showing me the patience I truly required, and being my one and true confidant, I thank you and love you dearly. This is as much your accomplishment as it is mine.

To the ONE who knows and sees ALL, THANK YOU!

ACADEMIC REGISTRY

# Research Thesis Submission

| | | | |
|---|---|---|---|
| Name*:* | Nicole J. Jean | | |
| School/PGI: | School of Energy Geoscience Infrastructure and Society | | |
| Version: *(i.e. First, Resubmission, Final)* | Final | Degree Sought (Award **and** Subject area) | PhD Construction |

## Declaration

In accordance with the appropriate regulations I hereby submit my thesis and I declare that:

1) the thesis embodies the results of my own work and has been composed by myself
2) where appropriate, I have made acknowledgement of the work of others and have made reference to work carried out in collaboration with other persons
3) the thesis is the correct version of the thesis for submission and is the same version as any electronic versions submitted*.
4) my thesis for the award referred to, deposited in the Heriot-Watt University Library, should be made available for loan or photocopying and be available via the Institutional Repository, subject to such conditions as the Librarian may require
5) I understand that as a student of the University I am required to abide by the Regulations of the University and to conform to its discipline.

* *Please note that it is the responsibility of the candidate to ensure that the correct version of the thesis is submitted.*

| | | | |
|---|---|---|---|
| Signature of Candidate*:* | | Date: | |

## Submission

| | |
|---|---|
| Submitted By *(name in capitals):* | |
| Signature of Individual Submitting: | |
| Date Submitted: | |

## For Completion in the Student Service Centre (SSC)

| | | | |
|---|---|---|---|
| Received in the SSC by *(name in capitals):* | | | |
| *Method of Submission* *(Handed in to SSC; posted through internal/external mail):* | | | |
| *E-thesis Submitted* ***(mandatory for final theses)*** | | | |
| Signature: | | Date: | |

# Table of Contents

# List of figures

# List of tables

## Nomenclature

| | |
|---|---|
| A | Opening area |
| $A$ | Acceleration |
| $a$ | Cross sectional area of the valve |
| $a_f$ | % opening of the frame |
| $a_s$ | Cross sectional pipe area. |
| **B** | Viscous damper |
| $B$ | Binary logic |
| $b_1$ | Binary logic 1 |
| $b_0$ | Binary logic 0 |
| C | Acoustic velocity |
| **c** | Y intercept |
| $C_R$ | Boundary reflection coefficient |
| $C_0$ | Local acoustic velocity |
| $C^+$ | Characteristic slope |
| $C^-$ | Characteristic slope |

| | |
|---|---|
| D | Internal pipe diameter |
| $D_h$ | Hydraulic diameter |
| $d$ | Distnace from inner surface of bend |
| d | Thickness |
| $d_i$ | Solid displacement |
| $\boldsymbol{\varepsilon}$ | dissipation rate |
| $\varepsilon$ | Roughness |
| F | Force |
| $F_i$ | Body forces acting on the solid |
| $f$ | Friction factor |
| $f'_{av}$ | Average frequency of opening area data |
| $f'_D$ | Dominant frequency of opening area data |
| f | Pixel intensity |
| $f_t$ | Binary image function |
| $g$ | Gravity |
| $H$ | Trap fluid height |
| $h$ | Distance |
| $i$ | Distance factor |
| $K$ | Pipe roughness height |
| $\boldsymbol{k}$ | Turbulence kinetic energy |
| $k$ | Separation loss coefficient |
| *K1-K4* | Constant in characteristic equations |
| $L$ | Pipe length |
| $L_I$ | Inner length of bend |

| | |
|---|---|
| $L_O$ | Outer length of bend |
| l | Cord length |
| $M$ | Mass |
| $m$ | hydraulic mean depth |
| $n$ | number of pipes, nodes or selected points along a plane |
| $O(h^n)$ | sum of n- and higher order terms and is a function of the mesh spacing, |
| P | Wetted perimeter |
| $p$ | Pressure |
| $p_a$ | Appliance side pressure |
| $P\varepsilon$ | Predicted variable |
| $p_r$ | Reflected pressure |
| $p_s$ | System side pressure |
| $\Delta p$ | Pressure increment |
| $\rho$ | Density of the fluid |
| $\rho_\omega$ | Wall density |
| $Q$ | Volumetric flow rate |
| Re | Reynold's number |
| $r^n$ | Residual error |
| $S_v$ | Slope of velocity plot |
| $S_o$ | Slope of pipe |
| **T** | Trap reference number |
| $T$ | Threshold |
| $t$ | Time |
| $t^*$ | Non-dimensional time |
| $\Delta t$ | Time increment |

| | |
|---|---|
| $\boldsymbol{V}$ | Voltage |
| $V$ | Mean velocity |
| $V_{mf}$ | Mean velocity across applied frequency |
| $V_w$ | Liquid column velocity |
| $v$ | Fluid velocity |
| $\Delta v$ | Frequency dependant change in velocity |
| $x$ | Position |

**Subscript**

| | |
|---|---|
| A, B, C, R, S | Nodes with known values of *p*,*c*,*u* at time *t* |
| $atm$ | Atmospheric conditions |
| $av$ | Average |
| Max | Maximum values |
| $Max^x$ | Max value against Max value |
| $MR^x$ | Max value against RMS value |
| $_{rms^x}$ | RMS value |
| Trap | Trap conditions |
| $w$ | Water flow |
| $x, xi$ | Relationship descriptors |

**Other**

| | |
|---|---|
| $C_\mu$ | Dimensionless constant |
| $\mu$ | Fluid viscosity |

| | |
|---|---|
| $\mu_k$ | Kinematic viscosity |
| $\mu_t$ | Turbulent viscosity |
| $\mathcal{T}$ | Viscous stresses |
| $\gamma$ | Ratio of specific heat at constant pressure to constant volume |
| Ø | Diameter |

## Abbreviations

---

AAV – Air Admittance Valve

APDL - ANSYS Parametric Design language

BBA – British Board of Agrément

BBC - British Broadcasting Corporation

BC- Boundary condition

BDS – Building Drainage System

CDC- Centre of Disease Control and Prevention

CEL - CFX expression language

CFD – Computational Fluid Dynamics

D – Dimension

Eq - Equation

FD – Finite Difference

FDM- Finite Difference Method

FE – Finite Element

FEM – Finite Element Method

FSI – Fluid Structure Interaction

FV – Finite Volume

FVM – Finite Volume Method

HDD – Hard disk drive

HHD- Hybrid hard drive

HPC – High performance computing

fps – frames per second

MoC – Method of Characteristics

PDE – Partial differential equations

SARS – Severe acute respiratory syndrome

SSD – Solid state drive

UDFs - User Defined Functions

UN – United Nations

UPFs - User Programmable Features

VF – Volume fraction

VOF – Volume of Fluid

wg – water guage

WHO – World Health Organisation

# Chapter 1

# Introduction

## 1.1 Introduction

The existence of modern day societies owes much to developments in the fields of Public Health, Sanitation, Microbiology, and Immunology. Of all these fields of advancement, sanitation provision exceeds advances in the field of Medicine (for instance, antibiotics and anaesthesia) as the most significant of medical advances by readers of the British Medical Journal in 2007.

> *"The greatest medical milestone of the last century and a half."(Boseley, 2007)*

C.E.A. Winslow in 1920 notes Public Health to be, the science and art of preventing disease, prolonging life, and promoting physical health and efficiency. This focus on preventing disease and prolonging life can be seen in the developments of control and prevention measures of the spread of infectious diseases addressed through immunoprophylaxis, prophylaxis, antiviral chemotherapy, interferons, cytokines, vector control and the use of adequate sanitation practices. These measures are paramount in ensuring health and wellbeing in the developed world, and their absence determines many of the poor health indicators in developing countries.

The safe removal of disease carrying human waste is the primary goal of any sanitation system. Preoccupations with malodours have now given way to more realistic concerns

about the spread of disease via ‘invisible particles’ containing micro-organisms. The isolation of people from this waste is of primary concern to the designer of any sanitation system; history shows the ‘stop/start’ nature of developments in this regard.

Though the Romans, Greeks and early ancient civilisations provided transportation systems for human waste, the odour still provided great discomfort and anxiety to building inhabitants. The development of the water trap seal remains the greatest public health development in the building drainage sector as this device offers protection from harmful biological matter deposited into the network. The threat of Building Drainage System (BDS) protection device vulnerability due to poor system design, installation or maintenance, along with effects of climate change, should be of great concern to all building inhabitants.

Built environment professionals collectively hold the responsibility for safeguarding the health of building occupants, as far as the building envelope, and associated devices and components can provide. The link between sanitation and disease spread, first made by Sir Edwin Chadwick, promoted the use of piped water and flushed drainage systems to contain foul smells. His efforts saw to a decrease in the mortality rate of London, thus providing society with an appreciation years after of the BDS, to not just limit sewer gas propagation but to prevent disease and prolong life.

Evidence of sanitation as a marker for social development is no better shown than during the Roman Imperial period, when the provision of over 1000 litres of water per person per day provided great pride to the Romans. The empire flourished during this time as greater levels of sanitation reflected the affluence of the time and engineering superiority of the Romans. Contrary to this, at the end of the “era of cleanliness” and the fall of the Roman Empire, sanitation was in large neglected, leading to epidemics which claimed many lives.

Improvements in Public Health continue to arise as a result of intensive research into new methods and techniques, often inspired by a desire for improved social conditions, and are often the measure of progress.

## 1.2 The spread of infectious disease

The free movement of pathogens in the built environment, especially via airborne transmission routes, have great potential for the rapid spread of disease. This concern about air as a transmission route of infection has existed for as long as there has been recognition of the transmissibility of disease (Bennett and Brachman, 1998), as in the past, deficiency in the control and therefore transmission of pathogens, led to more deaths than wars. For instance, between 1918 and 1919, an estimated 20 to 40 million people were killed from influenza, while 16.5 million civilians and military died in the World War I conflicts. In the era of the American Civil war, it is estimated that 440,000 of the 660,000 deceased soldiers, died of disease, and not battle wounds (Connolly and Heymann, 2002) as one would expect.

It is widely acknowledged today that the free movement and propagation of a pathogen from a host to another occurs via skin and hair shedding, defecation, vomiting, coughing, sneezing, and or via insect/arthropod vectors (Hathway *et al*, 2011) and so not solely through airborne routes. Regardless of the method however, the mass grouping of vulnerable individuals provides an adequate opportunity for large scale transmission of disease.

The high death toll from infectious disease due to compromised water and sanitation systems persists to present day. In June 1994, the cholera outbreak in Goma claimed 12,000 Rwandan lives, and in Zimbabwe from August 2008 to June 2009, cholera affected a suspected 98,424 lives, killing 4276 persons (WHO, 2009). More recently, the World Health Organisation (WHO) situation report published on the 18$^{th}$ February 2015, stated that the Ebola outbreak in West Africa (primarily in Guinea, Liberia, and Sierra Leone), had killed approximately 9442 of the possible 23,371 infected person cases between March 2014 and February 2015.

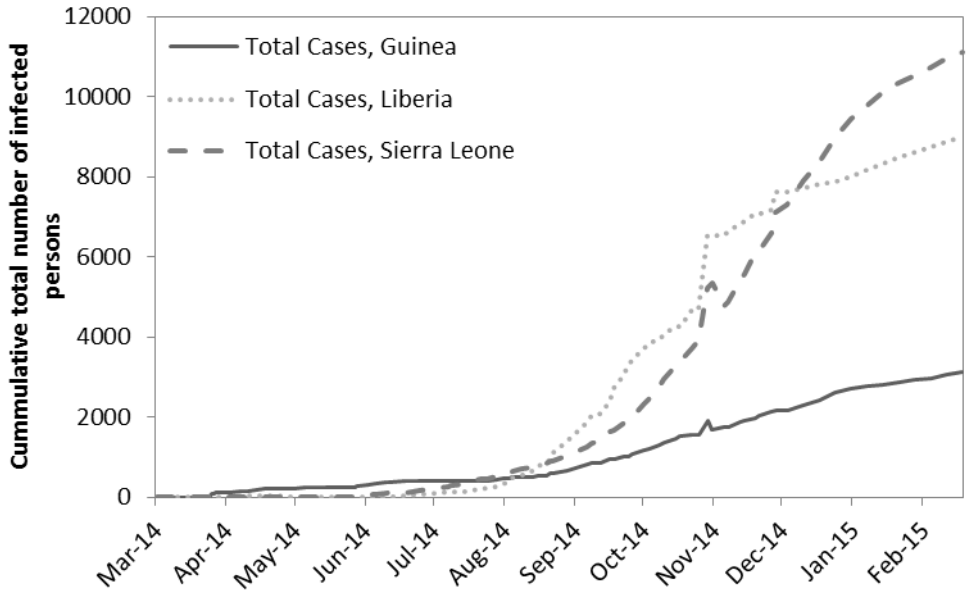


**Figure 1. 1, A cumulative count of the total number of Ebola cases in Guinea, Liberia, and Sierra Leone from March 2014 to February 2015.**

The years 2012-2013 and also 2014 saw outbreaks of measles in Swansea (U.K.) and several states in America respectively. Showing that though vaccination and other public health measures have significantly increased life expectancy and lowered the incidence of certain infectious disease outbreaks, (even to the point where America claimed to have eradicated measles in 2000) continued efforts are required to tackle ongoing and potentially recurrent public health issues. These issues include the reluctance and failure of many parents in America and Britain to vaccinate their children due to concerns of induced Autism.

This refusal as a result of the fear of individual health consequence, led the increased rate of transmission of this disease, leading to a total of 1200 cases in Swansea and 668 cases across America. These cases highlight that the key to ongoing Public Health success, lies in ensuring that measures does not rely solely rest on a single pre-emptive method of disease prevention.

> *"…even more important than dealing with the immediate threat is ensuring that this Ebola outbreak encourages greater levels of preparedness against the future spread of infectious diseases, of which the treat is growing rapidly with rising population density and international travel." (Goldin, 2014)*

Protection from infectious diseases can also be afforded through the proper design of our habitable spaces; ensuring that complete isolation can be afforded in densely populated areas. This is to begin with the BDS which connects all households in a building through a single pipe network.

## 1.3 Historical development of sanitation and hygiene methods for infectious disease control

The portfolio of activities involved under the field of public health is ever changing as the hazards to society evolve. A constant focus however, is placed on the provision of safe drinking water, controlling transmissible diseases, and improving the environment. This focus is shown currently in the Millennium Development Goals, and the present push to ending open defecation practices (United Nations, 2015).

The following subsections describe the developments and improvements in sanitation often brought about by environments in dire need for infectious disease control measures.

### *1.3.1 Early thinking and sanitation developments for infectious disease control*

Religious texts, such as the Bible, the Vedas and the Qur'an, all make note of humankind's need for cleanliness and careful disposal of human physiological waste. In the Book of Deuteronomy it is stated:

*"If there is among you a man who is not clean by reason of nocturnal emission, he shall go and stay outside the camp….you shall have a place outside the camp for your natural necessities. You shall bring a stick with your equipment with which you may dig a hole, and then cover up the excrement with the unearthed soil." (The Bible – Book of Deuteronomy 23:11-14)*

Such religious guidance shows the thinking of the time, and helped safeguard future public health within the built environment by instructing the separation of waste and host, through distance and covering, as it is perceived that the presence of the faecal matter (or its resulting odour) was unclean. The practice of separation is noted also in archaeological findings. These show the first known people to link proper sanitation and disease transmission, to be the early Minoan and Harrappan civilisations.

Of note here, is another religious text, the Bhagavad-gita, which instructs its followers to practice proper sanitation to remain free of demons, stating:

*"One should always be careful to keep his body clean by bathing, brushing teeth, shaving, changing clothes etc. …the demons neither like now follow all these rules for external and internal cleanliness."(Bhagavad-gita 16:7)*

The "age of cleanliness" during the Harappan period of the third millennium BC is said to be the period where the first toilets, latrines and sewers (soak pits, pipe networks for rainwater, and wastewater removal and drains with sedimentation cesspits) were invented. Some of the most advanced of these is found in the ancient civilisation of Mohenjo-Daro located in the Indus valley of Pakistan, in 2800BC (see Figures 1.2a, 1.2b, 1.3a and 1.3b) (Angelakis and Rose, 2014). Here, dwellings with its their own drinking water supply, private bathroom, and lavatory built into the outer walls of the house, are also found to house a connection to a communal main drain (constructed of earthenware) which ran through the streets of the village. Excavations of the civilisation show that waste water and solid matter from toilets were transported as far away from the dwellings and into unpopulated areas by subsurface drains covered by flat stones (Angelakis and Rose, 2014).


(a) (b)

**Figure 1. 2, Early below ground drainage and sanitation system in Indus Valley, Pakistan. (Source: Kenover, 2009)**

It is interesting to note here that these first toilets existed only for the affluent in society, and were constructed from brick, overlain with a wooden seat for comfort (see Figure 1.3a). They operated much like modern day toilets in that the design allowed the user to sit during use and the waste was disposed of through the vertical chute (Pathak, 1995 cited in Angelakis and Rose, 2014). Manual flushing was then required to carry the waste through the clay pipes and into the street drains and to the cesspit. Cleaners were required to dig out the pit and manually remove the solid waste, along with any other household waste (Angelakis and Rose, 2014). The lay man in society could not afford such luxury and so for physiological relief he would squat over a hole in the ground (an open pit) (see Figure 1.3b). Today this waste disposal tool is referred to as a pit latrine.

(a) (b)

**Figure 1. 3, Indus Valley Open toilets (Source: Angelakis and Rose, 2014)**

The Minoans between 2100 – 1100BC installed water supply to the palace of Knossos using earthenware pipes which carried water from nearby mountains to the palace (Antaki, 2003). The design of each pipe section was tapered or conical in shape; larger on one end than the other to allow the narrow pipe section to fit into another large section and so on. These terracotta pipes connected to stones sewers and toilet, at the Knossos Palace, Crete (Angelakis and Rose, 2014).

Between 1600BC and 300 BC the Greeks used not just earthenware, and stone pipes, but also, the then modern materials of bronze and lead in plumbing design (Antaki, 2003). This progression in plumbing design suggests that clearly these civilisations considered sanitation a noble endeavour. Not only were they meeting the requests of religious teachings, but they endeavoured to have the best and most modern systems available.

The link between health and water usage however, had not yet been made. Not until the period, 460-377BC when Hippocrates noted his theories on the occurrence of disease. His Treatise *Airs, Waters and places* dismissed supernatural explanations of disease and instead attributed illness to characteristics of the climate, soil, water, mode of life, and

nutrition surrounding the patient (Nelson and Williams, 2007). This recognition of the importance of water for public health led to adequate provision of baths, toilets and sewerage drainage systems.

The Roman imperial period between 400 BC and 150AD saw the building of over 200 stone aqueducts to supply portable water to public baths, city fountains and a selection of private homes (Antaki, 2003). The fountains were built to act as surge tanks in instances of pressure transient generation due to sudden changes in flow regimes and the water supply of around 1364 litres (300 gallons) per person per day, compared to 140-160 litres in the U.K. today. Sanitation was highly regarded as a show of affluence of health, finance and wellbeing.

An indulgent recognition of the public health accomplishments of the Romans is noted by the Roman water commissioner, Frontinus.

> *"in as much as the seven then existing seemed insufficient to meet both the public needs and the luxurious private demands of the day…With such an array of indispensable structures carrying so many waters, compare, if you will, the idle pyramids or the useless, though famous, works of Greeks!". (*Frontinus, trans. By Bennett, 1961, p. 353;357*)*

Frontinus highlights the link between living standards, and sanitation development. This as sanitation is seen as a noble endeavour and can be said to be synonymous with development in the context of a progressive society.

Rightfully, the Romans were proud to have surpassed previous civilisations in their innovation and technological advances, but by the end of 476AD the era of cleanliness ended and, sanitation standards began to fall. This degrade in living standards, was linked to the fall of the Roman Empire. Although exceptions exist, in large, waterworks were ignored in middle age Europe.

### *1.3.2 Developments in the 16th to 18th century*

Knowledge and innovation in drainage science remained at a standstill from the middle ages until the 1500's when the first flush water closet was invented. The invention of the water trap seal by Sir John Harington in 1596 brought about the opportunity for increased comfort within the built environment.

Sir John Harrington, an Elizabethan poet, designed the water closet which operated: using water for the removal of human waste, the cleaning of the appliance bowl and limiting the propagation of foul odours (see Figure 1.4). After each use, a barrier was created by placing a plate at the base of the bowl, and ensuring adequate water existed to provide a six inch seal. This invention referred to in his book *The Metamorphosis of Ajax* (1596) as "the odourless toilet", provided users freedom from the unpleasant smell created by decomposing faecal deposits, and also peace of mind during use; as the act of defecation was no longer associated with poor health.

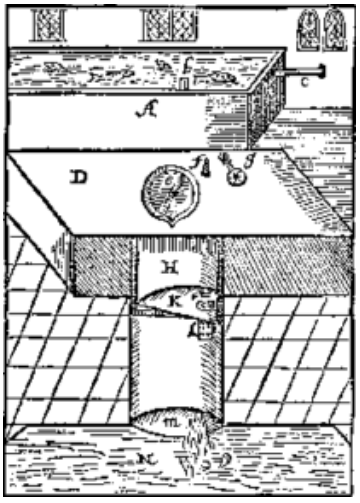


**Figure 1. 4, Sir John Harrington's sixteenth Century water closet the 'Ajax' (Billington and Roberts, 1982)**

In the 1600 and 1700s advancements in plumbing technology arrived with the expanded use of cast iron pipes and by the mid-1700s, the London bridge waterworks Company reported over 54000 yards of wooden pipe and 1800 yards of cast iron. (Antaki, 2003).

In 1775, came a semi self-sealing modification to Harrington's water closet invented by Alexander Cummings. Cummings, a Bond Street watchmaker from Edinburgh,

designed what is the traditional water trap seal. The first patent registered for the trap seal was made by Joseph Bramah, a cabinet maker in 1778, three years later. This design altered the original by including a hinged outlet value, and a connection directly to a cesspool to the design (Wright, 1980 cited in Kelly, 2009). These two innovations would later become the most widely used and most vital components to public health for the BDS.

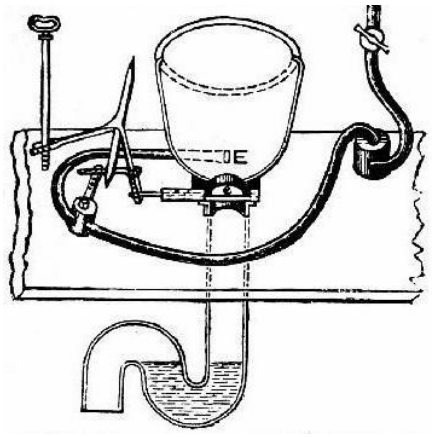

**Figure 1. 5, Alexander Cumming's patented water seal closet of 1775 (Billington and Roberts, 1982)**

The invention of the water seal closet bought an end to BDS developments between the 15th and 18th century.

These developments by Cummings and Sir Harrington are significant as though the Romans and Greeks invented transportation systems to remove the waste from the building; these were the first inventions to address and control the propagation of air or sewer gases in the home.

### *1.3.3 Developments in the 19th to 20th century- The link between sanitation and health*

The belief that the foul odour from human excreta was equivalent to pestilence was prevalent well into the 19th century, becoming the major influence behind all sanitation development in the 19th to 20th century. It is ironic however, that the foul odour was

regarded to be equivalent to pestilence causing extreme annoyance at a time when the German Pathologist Friedich Henle (1809-1885) discovered the germ theory of infectious disease transmission. This theory opposed the miasma theory proposing instead that disease was spread via microorganisms too small to be seen with the human eye.

> "*the material of contagions is not only an organic but a living one and is indeed endowed with a life of its own, which is, in relation to the diseased body, a parasitic organism."* (Henle, FGJ. Von den Miasmen und Contagien und von den miasmatisch-contagiösen Krankheiten, 1840)

However, due to the high death toll of epidemics, and increased fears, little could be done initially to convince society and disprove the Miasma theory. In the U.K., this theory of the disease transmission, continued through the mid-19th century. Sir Edwin Chadwick's report *'The Sanitary Conditions of the Labouring Population'* in 1842 led the sanitation movement in London by eventual major expansion to sewer provision (Swaffield and Galowin, 1992; Kelly, 2009). In 1846 Chadwick (who remained despite his works, an avid believer in the Miasma theory) is noted to have said:

> *"All smell is, if it be intense, immediate acute disease." (Parliamentary Papers, 1846, vol 10, p.651)*

A year later, in 1847, William Farr, the chief statistician for the Office of the Registrar-General, affirmed Chadwick's view on the spread of disease stating in his Tenth Annual Report:

> *"the disease mist, arising from…cesspools…is continually kept up and undergoing changes; in one season it was pervaded by cholera, in another by influenza ; at one time it bears Small pox, Measles, Scarlantina and Whooping Cough among your children; at another it carried fever on its wings. Like an angel of death it has hovered for centuries over London". (Tenth Annual report of the Registrar-General, 1847, p.xvii).*

Widespread use of sanitation devices during this time included a full scale sewer system in Hamburg, Germany, and the growing acceptance and use of water closets in England.

However, this report by William Farr mentions the grave state of public health at the time, approximating a minimum of 38 deaths per day in London due to living conditions associated with poverty. In 1848, in response to Chadwick's 1842 report, sanitary legislation was passed, including the Public Health Act, Metropolitan and City Sewers Act and the Nuisances Removal and Disease Prevention Act; introducing the first law in London requiring the draining of all domestic waste into sewers. Unfortunately, the removal of stagnant physiological waste with the new renovated sewer system did little to calm fears of infectious disease transmission as the sewer gases seeped through every possible opening, entering on many occasions into dwellings.

> *"It therefore becomes a point of the utmost importance that the seeds of disease should at once be arrested: that they should not be carried from house to house from street to street, from unhealthy parts to salubrious districts, by the construction of monster sewers, impregnated with the feculent matter of each locality, and sowing it again broadcast,...." (Booth, 1853)*

Repeated epidemic cholera disease outbreaks between 1831 to 1832, 1848 to 1849 and 1853 to 1854, only confirmed the belief that the sewer gas was the source of the infection, and that the noxious emanations were carried from a disease infected household, to hosts in a healthy household. Dr John Snow's (1855) paper *On the Mode of Communication of Cholera* in which he presented his investigation of the spread of Cholera on Brood Street, presented the finding that cholera was spread via the faecal contamination of portable water. Snow's work proved Henle's germ theory by identifying the waterborne nature of infectious disease transmission. The Miasma theory was proven false as the reason for the spread of cholera and replaced later with the understanding of the germ theory.

In 1858, parliament was suspended due to the intensity of the foul odour entering the chambers. The incident produced an immediate response of the parliamentarians who set in action provision for a £3m sewer project involving, sewer drains, pumping stations, and treatment plants. This system for the city of London was designed by Sir Joseph Bazalgette. It took these catastrophic events in major cities (such as Paris, and London) to stir the population and their elected officials to demand the installation of portable water and sewer systems (Parmley, 2001).

By the end of the 19th Century, great strides had been made in improving sanitation within dwellings, isolating human faecal matter and controlling the transmission of sewer gases; through the innovations of Sir John Harrington, and Alexander Cummings. These inventions and actions by Chadwick had significantly aided in the reducing the casualties of infectious disease, thus leading to the link between poor sanitation and the spread of disease. An ensuing new design for the BDS far above standards previously met was now had. Sanitation was embraced as a necessity to the protection of public health and the field of study began – embracing a twofold focus; the design and regulation and maintaining the criteria of system operation.

## 1.4 Built environment health security risks in the 21st century

Public health in an evolving modern society is influenced by serval factors. These factors include: urbanisation, globalisation, environmental conditions, the introduction of new technologies, new disease prevention measures and advances in medical science, to name a few. It is expected that continued advances in the field of medicine will introduce new vaccines and treatments to prevent and cure infectious diseases which still burden society today. However, developments in the field of medicine should not be seen as a singular fix to ensuring the health of a community.

The Centre of Disease Control and Prevention (CDC) (2014) states that the health security risks which the global public faces now and in the future include the following:

- The emergence and spread of new microbes
- The globalisation of travel and food supply
- The rise of drug-resistant pathogens
- The acceleration of biological science capabilities and the risk that these capabilities may cause the inadvertent or intentional release of pathogens
- Continued concerns about terrorist acquisition, development, and use of biological agents.

In addition to this list, the effect of changing climatic conditions on existing BDS protection devices (in use across the globe), and the acceleration of disease spread due

to urbanisation is considered. The following subsections provide a brief discussion of the risks due to inadequate performance of BDS protection devices, the emergence and spread of new microbes, globalisation of travel and urbanisation. Health security risks such as increased drug resistance to infectious disease, biological scientific advances, and terrorism are subjects outside the scope of the built environment and this study though they do present significant risk to public health; as pathogens will likely propagate between hosts through the BDS, these factors are not discussed.

### *1.4.1 The emergence and spread of new microbes*

It is commonly accepted that climate plays a role in the transmission of many infectious diseases, some of which are among the most important causes of mortality and morbidity in developing countries (WHO, 2005). Pathogens and insect vectors are capable of surviving over a certain temperature threshold. Their reproductive rates may increase with an increase in ambient temperature, but additionally, temperatures in excess of the tolerance range of the pathogen may increase mortality rates and in insect vectors, increase egg production and frequency of feeding (WHO, 2005). For instance, peak instance of gastroenteritis is known to become prevalent during temperate months (Altekruse *et al* 1998, cited in WHO, 2005). The World Health Organisation (Halstead, 1996, cited in WHO, 2005) continues by stating that the strong seasonal pattern of influenza infections in Europe, is thought to reflect the increased tendency among humans to spend more time indoors during the winter months.

### *1.4.2 Risk to BDS protection devices*

BDS protection devices such as the water trap seal (first designed by Alexander Cummings), are reliant on numerous factors for sustained defence of the spread of infectious disease. These factors include: the amplitude and frequency of system generated pressure transients, the ambient air temperature, and water availability.

The IPCC (2007, 2014) makes clear that an overall negative effect as a result of climate change is expected, predicting an average global warming of 1.5 to 5.8 ºC in the 21st century. In its upper range, this level of temperature increase poses a risk of the water trap seal becoming an unsuitable device in certain regions, or in buildings with irregular occupancy levels. In addition to, and as a consequence of increased temperatures,(a negative effect on the water resources and fresh water systems of the world is to be expected). In other words climatic changes will cause an adverse effect on the water availability. The risk therefore to the water trap seal is twofold. Water supply may be insufficient to provide a seal, in may become quickly susceptible to evaporative trap seal loss due to the ambient temperature in buildings.

In the UK, anxiety over local water availability is confirmed by the Environment Agency and Natural Resources Wales (2013) report which shows that the problem of water availability in England and Wales is a current issue and not just a concern in the future. The current water stress indicators suggest 9 of the 24 companies in England and Wales, to be currently experiencing severe water stress which persists in all future predictions. This number increases to 10 companies across the 4 mentioned future water stress models.

Frequent and sustained trap seal loss creates insecurity in the operation and ability of the BDS to protect the health of building inhabitants. Special consideration therefore is required in the design of the BDS to ensure that the protection device selected is capable of operating satisfactorily under current environmental and predicted future conditions. Under current predictions, the greatest risk is posed to existing buildings where isolation of the indoor and sewerage network is allowed through the sole use of a single protection device – the water trap seal.

A recent addition to the range of available plumbing products is the development of the waterless appliance trap seal which is advantageous due to its climate resistant characteristics. The continued evaluation of the criteria of BDS performance is pivotal to isolating a need for innovation and maintaining public health; while being out of sight and mind to the average user.

Protection of public health through the safe operation of the BDS is an important factor as the BDS throughout history, has provided a measure of social development and therefore should not be considered a minor risk. Climatic changes are expected which will affect environmental conditions, and therefore, impact the choice of BDS protection system and components. The protection systems are important for health and hygiene and therefore the thought of system vulnerability should be a concern to all.

### *1.4.3 Globalisation of travel and trade*

The growing cross border threat of infectious disease spread is facilitated by the unprecedented mobility of people (international tourists, business persons, and war refugees), food and commodities across the globe. Never before have people moved faster, and more frequently across multiple time zones, thus bringing with them, new pathogens to previously unexposed regions. In response to the recent measles outbreak it is said by Tom Frieden (CDC Director) that today,

> *"A measles outbreak anywhere is a risk everywhere" (CDC Newsroom, 2013)*

This means that, deadly diseases anywhere in the world test each and every country's public health security. Transmission can be expected through any of the known routes: direct contact, waterborne, blood borne or insect and arthropod vector. Diseases which have successfully travelled across countries to new regions via global travel and trade are: HIV/AIDS, SARS, chikungunya, tuberculosis, cholera and malaria.

> *"Today, diseases as common as the common cold and as rare as Ebola are circulating the globe with near telephonic speed, making long distance connections and intercontinental infections almost as if by satellite. You needn't even bother to reach out and touch someone." (Angier, 2001)*

As global population continues to grow, a major concern, is the growing disparity between economic classes; as this widens the numbers of vulnerable persons in society, many more will migrate in search of a better standard of living, continually ensuring the

struggle countries face in protecting their citizens. Evidence of this is already being found in the Migrant crisis of April 2015. Leaning, 2002 (cited in Knobler, Mahmoud and Lemon, 2006) refers to the 21st century as the "Century of Migration".

**Figure 1. 6, Mediterranean migrant crisis of 2015 (The Independent, 2015)**

### *1.4.4 Urbanisation*

The continued movement of people into cityscapes and large communities provides the perfect condition for multiple points of contamination from a single event. Take for instance persons travelling during peak hours being enclosed in a carriage. Kumar *et al* (2007) explains that pathogens expelled by coughing or sneezing may cause contagion if inhaled, and so, in such an instance, the case for disease spread through airborne transmission relies on the number of persons in the carriage forced to inhale the pathogen. The concern however, lies in the opportunity for a single individual, in a single event, to infect as many as 280-356 persons (Transport for London, 2015).

As transportation systems evolve to adapt to and serve growing populations, control of infectious disease spread becomes an even more difficult task, therefore leaving the continued existence of the civilisation vulnerable. Within the built environment, disease transmission can occur through all forms, but specifically airborne, insect vector, and waterborne through the building drainage network.

Fidler (1996) explains that, previous successes in controlling infectious diseases caused interest in infectious diseases to wane in the international medical and scientific communities, and the consequence of which is seen in the hampering control effects of emerging infectious diseases. His statement though not directly (pointed at this field), speaks also of the Building Drainage Systems, which since its present day design development in the $19^{th}$ century has seen little advancement. The continued events of disease outbreak however, continue to emphasise the need for a clear understanding of potential areas for failure within the built environment and continued growth and innovation.

It should be noted here that the extent of risk to public health can be seen in the closeness of living quarters. The population densities of the following cities are as follows: in London 5285 persons per $km^2$, 10 694 persons per $km^2$ in New York, 18 150 persons per $km^2$ in Lagos and 29 650 persons per $km^2$ in Mumbai. .

## 1.5 The limitations of present numerical modelling of Public Health systems

While the risks are not always known, the technology and methodology exists to predict sanitation system responses to an increasing number of threats. These tools aid the classification of a safe system, or one at risk of frequent cross contamination into the building occupied spaces. AIRNET a 1D Method of Characteristics model allows whole systems to be evaluated from a protective seal standpoint, thus ensuring that people are protected from the toxic gases and bio-aerosols which can emanate from the BDS/ sewer system.

It is imperative therefore, that this protective seal (the appliance trap seal) is accurately represented in the 1D model. At present, three hindrances exist to realistic whole system modelling. They are:

- That the current boundary condition over estimates the water trap seal height under certain transient conditions
- The more recent models aimed at addressing the aforementioned limitation can only be applied to a single trap seal.

- No boundary condition presently exists for more recent innovations such as the waterless trap seal

There is a fundamental need therefore, to bring AIRNET into the present by enabling the representation of appliance trap seals typical of today's system. This thesis focuses on improving understanding of barrier technology operation and seeks to improve prediction methods to ensure that modelling techniques are accurate and appropriate.

## 1.6 Aims and Objectives

The aim of this research is to establish novel methodologies for the development of boundary conditions of responsive BDS protection devices suitable for incorporation in a Method of Characteristics (MoC) numerical model. The study investigates the analysis of appliance trap seals (both water and waterless forms) using Computational Fluid Dynamics (CFD), laboratory methods and photogrammetric (the process of gaining image data from the use of pixels and light) analysis. The focus here is to provide a more in depth qualitative and quantitative analysis of BDS protection systems.

These reference products (the water and waterless appliance traps) have been chosen due to their importance to public health and the significant lack of knowledge about its performance.

The research objectives were:

Objective 1: Determine the unsteady flow characteristics in a U-bend- water trap seal through numerical methods using a commercially available CFD tool, (ANSYS CFX) to digitally produce deterministic data.

Objective 2:Develop a methodology for the evaluation of transient flow friction representation using a commercially available CFD program – ANSYS CFX, to establish a boundary condition for a water trap seal, which incorporates a frequency dependent representative of friction. This

boundary condition must be compatible with the MoC numerical model, and more accurately describe the unsteady multiphase flow regime within the seal.

Objective 3: Develop a novel methodology for determining the operational characteristics of flexible components (waterless trap seals) using photographic methods.

Objective 4: Validate the potential of computational fluid dynamic investigations as an alternative or comparable method to laboratory evaluation.

Objective 5: Validate new boundary conditions (for the waterless and water trap seals) by modifying the existing numerical model - AIRNET (developed at Heriot Watt University), for simulation of the unsteady air flow conditions in building drainage networks – providing characteristic data of the reference products.

## 1.7 Focus of subsequent chapters

*Chapter 2, Public Health – Plumbing and drainage context*

The following chapter in this thesis, continues the introductory notes on Public Health by providing an in-depth look at the Building Drainage System, and the methods employed to protect building inhabitants from pathogens. The criteria, design history, disease transmission routes and fluid mechanics of the system are provided, and followed by the latest solutions to control both negative and positive air pressure transients.

*Chapter 3, Numerical Modelling Literature Review*

Chapter 3 provides the theoretical background in the popular discretisation methods for solving both fluid and solid problems. The chapter begins by providing a general background into the Finite Volume, Finite Element, and Finite Difference method of

numerical modelling. The problems for which each method is best suited are discussed along with the rationale for the noted advantages. Whole system modelling of the Building Drainage System is traditionally performed using the MoC technique for which boundary conditions are developed empirically. Details of this process are provided along with the limitations to existing boundary condition development methods. Fluid Structural Interaction (FSI) is introduced and suggested as a suitable method of assessing non-rigid system components.

*Chapter 4, Laboratory and Numerical Investigation*

This chapter details the experimental (laboratory and numerical) methods employed in the investigation of the reference water trap and waterless trap seals. General CFD and FSI software and hardware requirements are provided along with the limitations and findings during the use of several computing solutions. The chapter then continues by providing details of the methodology implemented to fulfil the requirements of the objectives of this study.

*Chapter 5, Numerical Analysis of Multiphase flows in Appliance Traps*

This chapter presents the results and analysis of unsteady flow in two appliance water traps using CFD. The results lead to the identification of zones of movement, and the variation in motion according to the applied frequency. Using this data, a frequency dependant friction factor which provides the existing governing equation with a more realistic impression of the trap seal movement is developed.

*Chapter 6, Fluid Structure Interaction – Laboratory and Numerical Investigations*

This sixth chapter presents the investigation of aero-elasticity of the waterless trap seal using high speed digital photography, pressure measurements, and numerical FSI to analyse the self-oscillating waterless trap seal. Programmatic analysis required a custom

cell/pixel colour recognition software to determine the pipe opening size, length, breadth, shapes and opening and closing patterns. Fourier analysis determined the dominant pressure and opening frequencies, and post-processing of the FSI data enabled investigation of the flow within the sheath.

*Chapter 7 Discussion and Validation of the Novel Boundary Condition Techniques*

Chapter 7 presents the methodology for boundary condition development for a waterless and water trap seal, and exhibits the results of the system modelling conducted in AIRNET incorporating the new boundary conditions derived in chapters 5 and 6. This data provides validation of the computational (CFD and FSI) and laboratory experimental data.

*Chapter 8 Conclusions and Recommendations for Future Work*

This chapter provides the main conclusions of the research through a summary of findings and concludes by providing suggestions for future work which would extend this body of work.

## 1.8 Conclusion

The devastating effect of the spread of infectious diseases in the past is seen in the number of deaths recorded through history. Though great strides in the Medical and Sanitation fields allow society to reside in close proximity today, challenges are still fought by public health engineers in the 21$^{st}$ Century. Outbreaks of rare diseases like, cholera, ebola, SARS, have tested our global systems and led to a greater appreciation to the risks urbanisation and globalisation pose to all.

This chapter has detailed the history of humankind's efforts to control the spread of disease through the eras and society's changing acceptance, ignorance and

understanding of the role that air and water play in disease transmissibility. Concerns of Public Health Engineers, surrounding future climate change predictions have been discussed as climate change poses significant challenges to the operation of the BDS. The rationale for developing boundary conditions through novel techniques for whole system modelling and the importance of accurate models is explained along with the objectives to be met in order to achieve this research project's goal.

# Chapter 2

## Public Health: Drainage and Plumbing system contexts

### 2.1 Introduction

Physical barriers provided by walls, floors, doors and ceilings, present the illusion of complete isolation when in fact, the internal space of every household in an urban setting, is connected by a physiological waste removal (drainage) network. This network (the communal transport system for household urine, faecal matter, synthetic wipes, cleaning agents and other waste) is terminated by protection devices (appliance trap seals) at each sanitary appliance.

This seal acts as the sole defence mechanism to protect residents from pathogens originating from the drainage network, and so it could be argued that the trap seal between the sewerage system and the living space is the single most important innovation in building plumbing and drainage science since its acceptance in the 19$^{th}$ century. This invention acts to prevent the spread of disease by limiting human exposure to pathogens, and thus making the solid waste transportation system a safeguard to public health.

This chapter begins by exploring the role of the BDS in Public Health Engineering, how the design has changed through the years and what factors have influenced these changes. An understanding of the importance of ventilating the system is brought to the fore, along with the influence that transient system fluid mechanics play in compromising protection devices – the water trap seal and the waterless trap seals.

These trap seals are formally introduced, providing the scope, design and limitations of the devices.

In the event of device failure, transmission of disease becomes likely (if biological conditions are favourable), and so the methods and the types of pathogens along with their lifespan within the network are introduced. This is particularly important in the fomite transmission route, where inanimate objects within the building can become contaminated thus leading to disease spread when touched. Understanding the transient pressure regime within a BDS is an essential first step in predicted protection device responses. Air pressure control, via ventilation pipes or active ventilation devices such as air admittance valves are additional protection systems and offer a stable pressure regime for system terminations such as water trap seals and waterless trap seals.

Protecting the seal between the sewer and the building is a complex task and this chapter raises issues surrounding the modern day rationale for the inclusion of these protection devices and the consequences to public health of a seal breach.

## 2.2 The criteria of the Building Drainage System performance

An effective BDS is required to transport human and sanitary waste away from the appliance, and to the sewer connection. Safe operation of this system requires that transportation within the network occur without possibility of cross contamination, leakage or interruption to system usage (Swaffield, 2010). Under current climate change predictions, meeting the safe operation criteria is expected to pose pressure on existing devices and require designers to ensure safe operation under low water availability, and extreme temperature conditions.

## 2.3 The Building Drainage System design

The criteria for safe operation of the BDS along with consideration for cost effective, and resource sensitive design, have fuelled many of the advances made in the design of the BDS over the years. Figures 2.1, 2.2, and 2.3 show the gradual shift over a century,

from the traditionally oversized systems towards a more efficient and economical use of materials.

The traditional two pipe system designed during the Victorian era divided the transport of grey and black water into two networks. This design method ensured that faecal oral transmission could occur solely via contact with the toilet and that the instance of system failure reduced due to the low volume of water discharged via multiple appliances. Additionally, in many cases of this era, the toilet held a separate room in the house from other sanitary appliances, abiding with the practice of separation of habitable comfort spaces and physiological matter.

From the late 19$^{th}$ century, the focus of the BDS rested on design and regulation and the criteria of the system. This shift is first noted in the beginning of the 20$^{th}$ century when the stipulation of a London county council Bye-Law required that where more than one w.c. was connected to a soil pipe, each w.c. should be ventilated by a pipe not less than 50mm in diameter (Wise, 1957). The then widely used two pipe system led to use of excessive amounts of pipework in the need to ensure safe and comfortable living conditions.

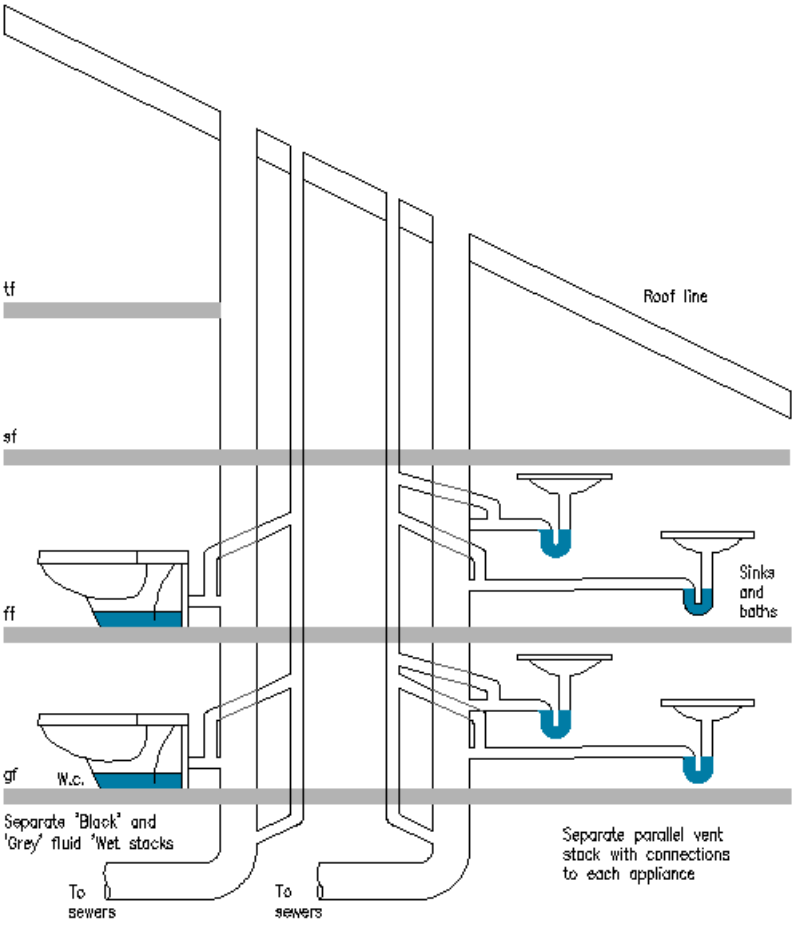


**Figure 2. 1, The two pipe system**

Factors such as the economic implications of excessive pipework, along with ill system operation due to the severe weather conditions, fuelled further research in the USA in the 1930s. This work led to the development of the one pipe system. This system was first tried in the U.K. in 1934, however the potential savings were somewhat lessened by the venting requirements stipulated by the London county council Bye-Law (Gormley, 2002).

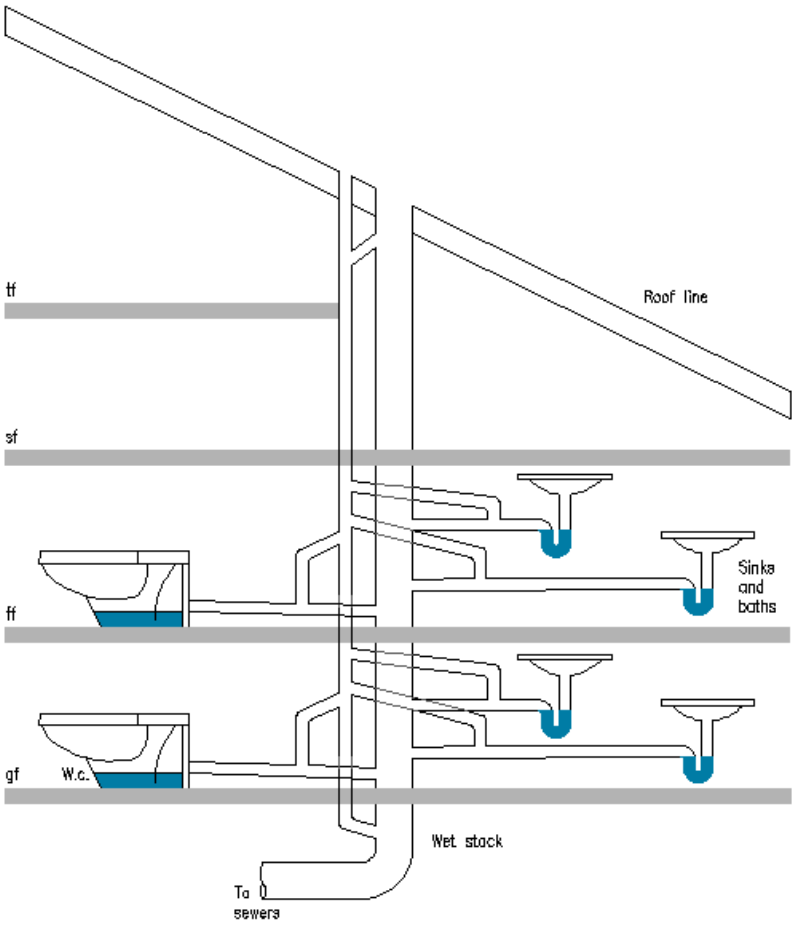


**Figure 2. 2, The one pipe system introduced in the 1930s**

During this time, concern for the retention of appliance trap seals during operation led to research aimed at providing design guidance that linked acceptable water flow capacity to the ensuing air pressure regime within the pipe network. This research focus commenced with the earliest recorded research work due to Hunter (1924), and continues today. At the National Bureau of Standards (NBS), Washington DC, Hunter established the limit for stack water annular flow – namely an annular film whose cross-section is no more than 25 per cent of the stack cross section. In 1940, Hunter developed the concept of discharge units relating the flow requirements of appliance use, and in so doing the considering the effect of simultaneous use. This design tool remains relevant to this day.

In the 1950s Wise, aided by research work from his colleagues at the UK Building Research Establishment (BRE), developed the single stack system that reduced the

venting complexity (Swaffield, 2010) "on behalf of local authorities who were concerned about the excessive use of pipework in their large building programme following World War II"(Gormley, 2002). This system however, was found to still be susceptible to pressure transients and so research continued into the 1970s and led to the modified one-pipe system which is widely used by designers to this day. (Kelly 2009) explains that research leading to this development included site as well as laboratory testing.

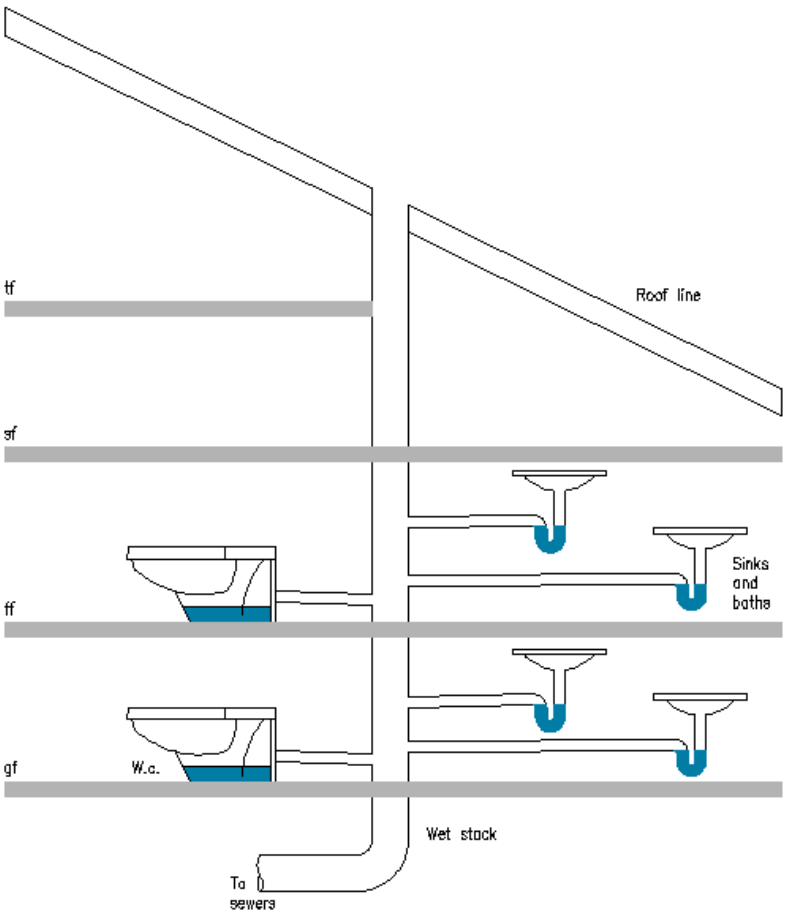


**Figure 2. 3, Single stack drainage system introduced in the 1950s**

Focus on the criteria of the BDS post the 1950s is seen in work by Wise, (1952), Wylie and Eaton, (1961) and Lillywhite and Wise, (1969) who developed semi-empirical relationships between terminal water flow and induced air flow, as well as in work by Wise and Croft (1954), Wise (1957), Campbell (1992), and Jack (1997) on the vertical stack length effects, providing finding that such as discharge water flow rate, pipe

diameter and the roughness of the pipe carried the magnitudes of negative pressure transients generated throughout the stack (Filsell, 2006). These works challenged the thinking that air entrainment was based solely on appliance discharge, and instead considered the effect of system resistances.

Research efforts continued into positive air pressure transient propagation in building soil stacks. This research led to the development of Studor's P. A. P. A$^{TM}$(Discussed further in Section 2.5.2). Further investigation of the system has led to greater use of the single stack system due to the ability to ensure safe operation through venting appliances suitable for alleviating either negative or positive pressure, thus restoring the system to atmospheric conditions. Venting and attenuation devices are discussed further in Section 2.5.2.

### *2.3.1 The water trap seal*

The appliance water trap seal has since the 18$^{th}$ century acted as the 'final defence mechanism' against the propagation of sewer gas into the indoor space. This barrier though sometimes altered in design (see Fig 2.4), remains relatively unchanged in its operation in the last two centuries. It is particularly important for inhabitants at low levels of a building as they present the shortest travel path for sewer gas and liquid ingress through appliances. However, as noted from the SARS virus outbreak in 2003 (as discussed in Section 2.4.1), the spread of disease through appliance trap seals across multiple levels of a building can occur; in this instance due to aerosolised contaminated matter assisted in travel by mechanical fans and the opportunity of through flow in the appliance trap.

The seal between the indoor space and the potentially contaminated BDS is created by the addition of sufficient water to an appliance trap; thus creating what is known as the appliance water trap seal. This seal, typically greater than 50mm above the base of the inner bend, prohibits the passage of air pressure transients into the indoor environment. UK drainage codes (BS EN12056:2000) specify that pressure fluctuations within the

appliance trap should not exceed ±37.5mm wg, and so to ensure retention the required minimum seal height is 38mm.

Research by Gormley and Kelly (2011), Gormley *et al* (2011), Swaffield (2010), and Gormley (2011) provide evidence of the importance of the trap seal as pathogens (such as the Norovirus and SARS) contained in bio-aerosols, contaminated buildings through the drainage network, reaffirming that transmission of infection can occur through contact with aerosolised contaminated sewer fluid.

Improvements in sanitation since the middle ages make such occurrences rare thus attesting to role the traditional water trap seal as the main isolator for a building and its inhabitants from the microbiological matter contained in a BDS. That is, until the invention of the waterless trap seal.

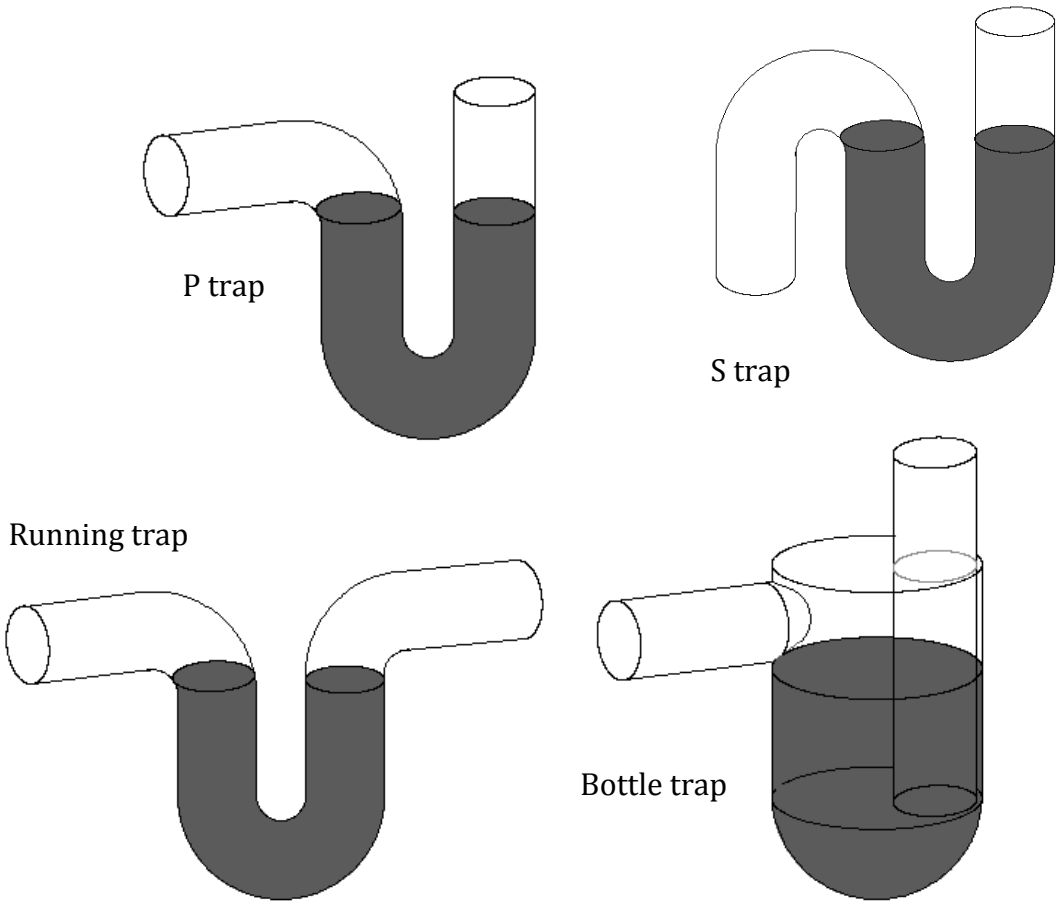


**Figure 2. 4, Types of water trap seals**

### *2.3.2 The waterless trap seal*

Among recent innovations within the building drainage sector is the introduction of the waterless trap seal. Developed in the 1990s by Hepworth HepvO® (now Wavin HepvO®), for the purpose of isolating the BDS from the rest of the building components. This seal holds the advantages of being devoid of the risk of depletion or compromise due to vibration, while also limiting the through flow movement of insects, and maintaining operation under extreme cold and low water usage conditions.

Waterless traps are broadly analogous to each other, in that the mechanical construction, (from the general shape of the trap to the material composition), are similar, and each forms an obstruction to airflow. These deformable valves differ however, in their size, thickness, colour and elasticity. With Sample 1 (of the waterless trap seal reference products) being the smallest, thinnest and most elastic, and Sample 3 being the largest, thickest, and stiffest of the set. All three reference products (waterless trap seals) are enlarged (in circular form) at one end to enable uniform fixed connection to, and uniform flow from the pipe, and slimmed to two parallel lips (in rectangular form when closed) at the other to provide an adequate seal to the pipe (see Figure 2.5).

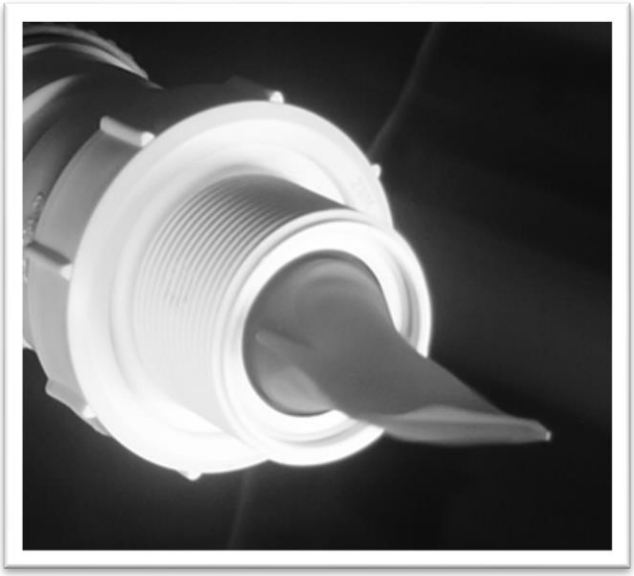

**Figure 2. 5, The waterless trap seal connected to a 50mm pipe**

The waterless trap seal is made up of a flexible sheath enclosed within a waste water pipe (which is set open at one end and closed in a rectangular form at the other end) and is likened to the behaviour of an air admittance valve in that, it enables air flows to enter the network under negative air pressure gradients, and seals instantaneously on the arrival of a positive transient. Therefore under normal appliance operation, liquids and air entering from the appliance are allowed to propagate into the BDS, but reverse flow is prohibited.

**Figure 2. 6, The reference waterless trap seal - Sample 3.**

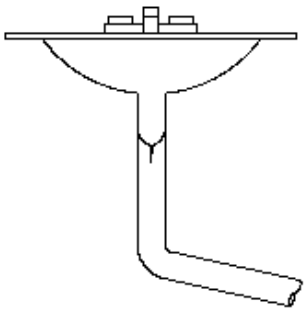

(a) Vertical : closed

When:

$p_a \leq p_s$

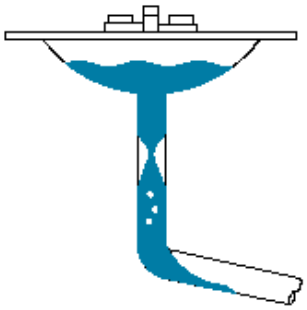

(b) Vertical : in use

Water introduced by appliance usage holds the valve open

When:

$p_a > p_s$

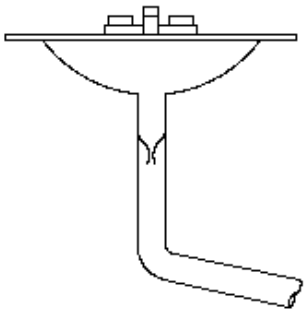

(c) Vertical : in use

Waterless trap seal here acts as an AAV remaining open until the negative pressure applied downstream increases

When:

$p_a > p_s$

**Figure 2. 7, Schematics of an installed waterless trap seal: (a) closed in vertical position, (b) opened in vertical position by appliance usage, (c) opened by self siphonage**

The water and waterless trap seals though likened in the purpose of their operation differ in many ways. Following the event of an intermittent negative pressure flow regime in a branch connected to a waterless trap seal, the device would quickly reseal and return the network to a healthy state. This occurrence in a water trap seal, could likely lead to significant loss in trap seal height, less than required to ensure retention of the seal. On the other hand, an unobserved fault in the waterless trap seal is possible

under high positive pressure. Dependant entirely on the trap design, the material is capable of inverting. Unknown to the inhabitants in both scenarios where the seal is lost, return to a healthy state would require the use of the appliance to top up the seal height in the case of the water trap seal and manual movement of the sheath's lips in the case of the waterless trap seal. These disadvantages of the waterless trap are however an unlikely event as the required pressure for inversion is rare to the BDS. If a satisfactory seal exists, this product prevails over the water trap seal as the circumstance for potential evaporation of contaminated sealing fluid ceases to exist. The mode of compromise differs in these two traps making one's advantage the other's weakness and vice versa.

A compromise is reached when both seals are installed to work in unison. Alternatively, the use of sensory tools could also assist in ensuring the inhabitants are aware of possible inversions.

## 2.4 Transmission routes of infectious disease

Human waste of a healthy or infected person may contain several types of pathogens. These microbes or organisms can be classified as either a: virus (20 -300 $nm$), chlamydiae (200-1000 $nm$), cickettsiae (300-1200 $nm$), mycoplasmas (125-350 $nm$), bacteria (0.8-15$nm$), fungi (2-200 $\mu m$), protozoa (1-50 $\mu m$) or helminth (3 $nm$ -10 $m$). Within the built environment, the hardiness of a particular microbe is of particular interest as secondary transmission may occur through inanimate objects such as: toilets, sinks, showers, or other drainage appliances. The lifespan of certain organisms is suggested in Table 2.1. It should be noted that microbe survival times increase if housed in dust, food, water, bacterial spores, protozoan cysts, or thick shelled helminth eggs (Kumar *et al*, 2007). For an individual to become at risk of disease transmission, an infectious dose of the disease must be present and make contact with the person (Fewtrell and Bartram, 2001). Typically transmission of disease through a BDS occurs under 3 categories: waterborne transmission (faecal oral routes), airborne transmission (respiratory droplets), and insect/arthropod vectors.

### *2.4.1 Waterborne transmission*

Waterborne transmission refers to the infection of a host via the ingestion of or contact with contaminated water by faecal matter. In the BDS, this transmission route is likely in instances where pathogens expelled by faecal matter into water are ejected through an appliance and proceeds to reach the gastrointestinal system. Eggs shed by some helminths (e.g. hookworms, schistosomes) into stools gain access to new hosts via larval penetration of the skin (Kumar *et al*, 2007).

| **Organism** | **Freshwater** | **Saltwater** | **Soil** |
|---|---|---|---|
| Viruses | 11-304 days | 11-871 days | 6-180 days |
| Salmonellae | <10 days | <10 days | 15-100 days |
| Cholera | 30 days | >285 days | <20 days |
| Faecal coliforms | 10 days | <6 days | <100 days |
| Protozoan cysts | 176 days | 1year | >75 days |
| Ascaris eggs | 1.5 years | 2 days | 1-2 years |
| Tapeworm eggs | 63 days | 168 days | 7 months |
| Trematodes | 30-180 days | 2 days | <1 days |

**Table 2. 1, Pathogen and indicator survival in freshwater, saltwater and soil. Sources: Feachem *et al*, 1983; Mara and Cairncross, 1989; National Research Council, 1998; Robertson *et al*, 1992; Rose and Slifko, 1999; Schwartzbrod, 2000; Tamburrini and Pozio, 1999 cited in Fewtrell and Bartram, 2001.**

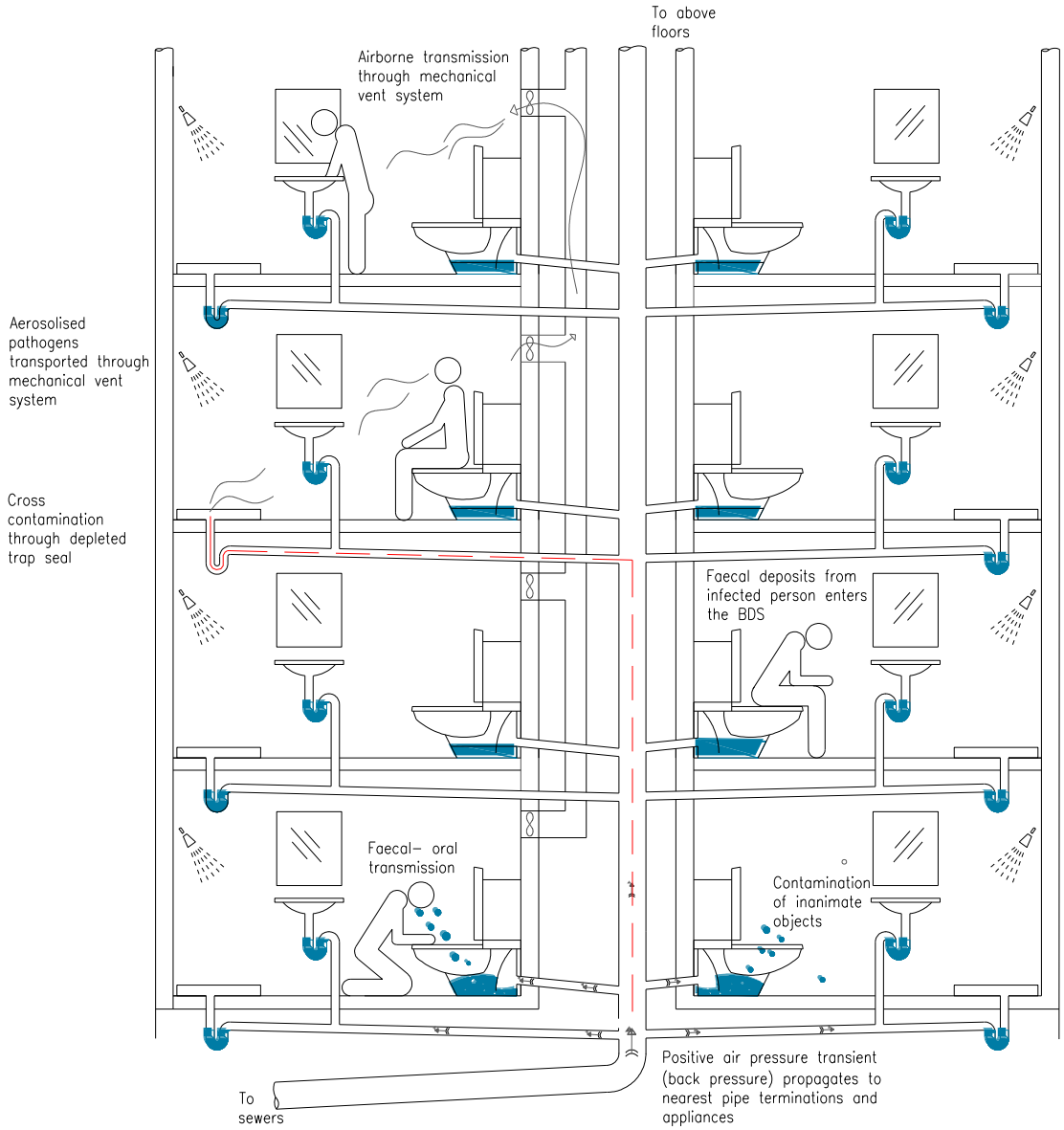


**Figure 2. 8, Infectious disease transmission routes within a high rise building designed with both passive (right) and mechanical ventilation (left) solutions.**

Expelled pathogens which are likely to persist after defecation include: poliomyelitis, norovirus acute gastroenteritis, giardiasis, hepititis A, hepititis E, poliovirus, rotavirus (gastroenteritis), shigellosis, typhiod fever, vibrio parahaemolyticus infections,

enteroviruses, vibrio cholera (cholera), clostridium difficile, cryptosporidiosis, ascariasis, and helicobacter pylori.

### *2.4.2 Airborne transmission*

The airborne route of transmission is said to possibility account for between 10 to 20% of all endemic nosocomial infections (Brachman, 1970). Airborne transmission of disease occurs by the propagation of pathogens through the air from one host to another. This method of infectious disease transmission is particularly suited to 'less hardy microorganisms which must be quickly passed from person to person, often by direct contact' (Kumar *et al*, 2007). Examples of such infectious diseases include: the common cold, influenza, mycobacterium tuberculosis, rhinovirus, measles, chickenpox, anthrax and cryptococcosis.

### *2.4.3 Insect or arthropod vector transmission*

This method of infectious disease transmission involves a vector, a carrier which transmits an infectious agent through an arthropod. Common carriers include: mosquitos, flies, sand flies, rats, cockroaches, triatomine bugs, mites, ticks, lice and fleas, and are known to spread diseases such as malaria, chikungunya, trypanosomiasis, yellow fever, west nile virus and lassa fever.

### *2.4.4 Transmission through the Building Drainage System – a single case*

It is often difficult to link the source of the infectious disease outbreak with the BDS, however in 2003, the severe acute respiratory syndrome (SARS) epidemic presented at a local site - the Amoy Gardens housing complex in Kowloon Bay, Hong Kong. Here, 12 years ago, early concerns about the airborne transmission of a contagious disease were reaffirmed, and further, the transmission through pipework which housed no physical barrier to divide the indoor space and the building drainage and vent system.

The complex houses 19,000 residents, within 19 blocks. Each block consists of between 30 to 40 floors with typically 8 flats per floor. See Figure 2.9.

**Figure 2. 9, Amoy Gardens housing complex, Hong Kong. Source, SKK (HK), (2015).**

The SARS outbreak at the Amoy Gardens occurred primarily as a result to insufficient water in an appliance trap seal. This failure in system criteria enabled cross contamination to occur and the subsequent propagation of aerosolised biological matter to propagate through the complex.

WHO (2003b) reported a total of 321 cases of which 41% resided in Block E, 15% resided in Block C, 13% resided in Block D and 18% of the total number of cases resided in the remaining 11 other Blocks in the complex (Hong Kong Dept. of Health Report, 2009, cited in Kelly, 2009). This occurrence highlights the importance of control of such microorganisms in the built environment. Prevention of cross contamination however, is especially vital in hospitals and care homes, where inhabitants are in a likely immuno-compromised state.

This occurrence highlighted that the BDS may present upon given conditions, the platform for pathogen propagation through multiple housing compartments.

## 2.5 Fluid dynamic characteristics

Omnipresent air in the BDS presents as full bore flow until it is displaced by water through an appliance discharge. The operation and thus, discharge of water, urine, faecal matter, and hygiene wipes by a sanitary appliance into a drain pipe, is considered a random and unsteady occurrence, due to the unpredictability of use, and the short duration of water flow. The safe travel of solid items along this surge wave is dependent on the characteristics of the solid, the size of the pipe, the flow rate and volume and the attenuation time of the discharge wave. An optimised design would seek to prevent the deposition of a single, or multiple items which could form an obstruction or interruption to the operation of the network.

Focus on the understanding of fluid mechanic profiles is important to identifying the areas of greatest concern; the areas where pressure transients are generated and the where within the system they cause greatest effect.

### *2.5.1 Air pressure transients*

The unsteady nature of fluid flow in a BDS offers a prolific environment for air pressure transient generation as they develop as a consequence of changes in flow conditions. These transients are identical in nature to those occurring in classical water hammer cases, meaning that they propagate at the relevant wave speed, experience transmissions and reflections at discontinuities and are gradually diminished by frictional effects. In this case the relevant wave speed is the acoustic velocity in air which is approximately 325 m/s. The generation and propagation of air pressure transients within BDSs can be seen to represent a potential threat to the integrity of appliance trap seals, although normally of a low amplitude.

#### *2.5.1.1 Propagation and reflection of air pressure transients*

The propagation and reflection of an air pressure transient was first theorised by Joukowsky, a Russian scientist, at the beginning of the 20th Century. He provided an explanation of the pressure rises that were being experienced in the water supply in Moscow. His research identified the relationship that existed between wave speed, pressure rise, fluid density and flow velocity for a fluid brought to rest within a certain time:

$$\Delta P = \rho c \mathrm{V} \qquad \textbf{Eq. 2. 1}$$

Where, $\Delta P$ is the pressure rise, $\rho$ is the fluid density, $V$ is the mean velocity of the fluid brought to rest and, $c$ is the local acoustic velocity. Subsequently, Joukowsky understood the importance of wave reflectance from system boundaries and the timing implications of this occurrence. He thus introduced the idea of pipe periods.

$$Pipe\ period = \frac{2L}{c} \qquad \textbf{Eq. 2. 2}$$

Where, $L$ is the pipe length, and $c$ is the acoustic wave speed. This expression considers the distance to be travelled and the wave speed of the transient flow. Kelly (2009) makes use of this Eq. 2.2 to determine the location of depleted trap seals within a network. In Eq.2.3, $\gamma$ is the ratio of specific heat and, $p$ here is the absolute pressure.

$$c = \sqrt{\frac{\gamma p}{\rho}} \qquad \textbf{Eq. 2. 3}$$

The reflected transient flow can be quantified using a dimensionless coefficient which is a ratio of the applied pressure transient to a branch against the reflected transient in the branch. In the event that the water column presented a dead end to the imposed air velocity at the fluid interface the expression $v = 0$ holds, and the resulting reflection coefficient would be $+1$. If however the seal became compromised due to the applied

pressure, the resulting reflection coefficient would be less than 1. The exact figure is entirely dependent on the quantity and position of the water in the trap. Figure 2.10 presents pictorially the reflection coefficient according to the conditions present in the trap seal.

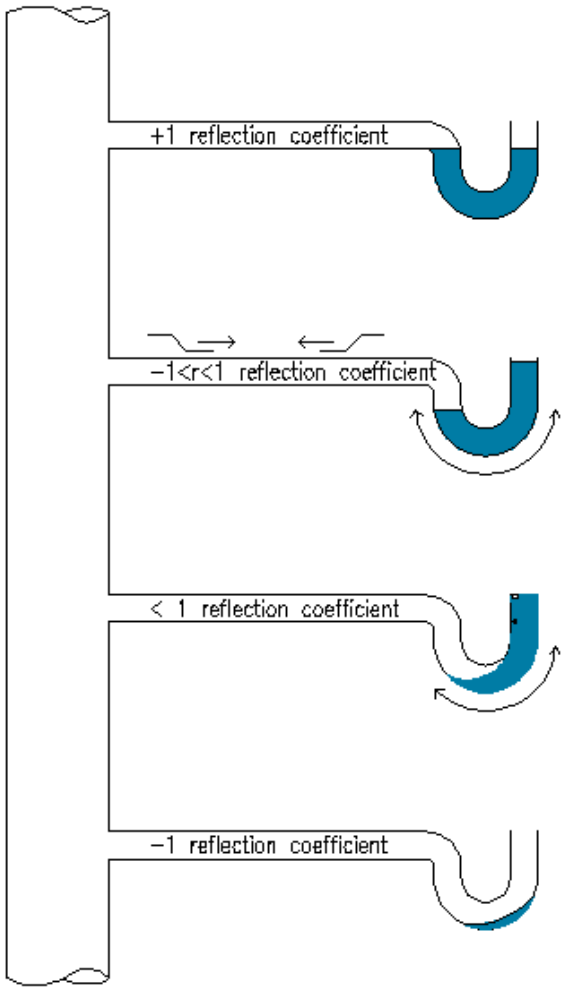


**Figure 2. 10, Reflection and transmission process in a BDS based on the response of the water trap seal to an applied air pressure transient**

#### *2.5.1.2 Branch pressure profile*

The pressure profile of water flow in a pipe branch is reliant on the nature of the induced flow. Generally it is expected that the flow is full bore for a certain period of

time, with an air pocket towards the end of the discharge. This air pocket is created due to gravity acting on water flowing through the appliance trap into the branch. Separation occurs as water attempts to remains in the appliance trap, thus separating from the momentum of the flow. Static pressure of the air here, is sub-atmospheric, as air from the habitable space and the stack, bubbles through the water to equalise the pressures within the branch. This movement of air through the water produces noises audible to the habitants of the immediate room (Chadderton, 2004).

#### *2.5.1.3 Stack pressure profile*

Water flowing from the branch enters the vertical soil stack and develops as annular flow (a concentric film) along the pipe wall, enabling air to establish the central core. This fluid moves downwards through the stack in parallel with an entrained airflow from the open termination in the dry stack. Such flows subject the stack to negative pressure caused by losses associated with appliance discharge. These time dependent fluid flows move at a rate equal to the air velocity under no-slip conditions, which is dependent on the location of the discharge, the length of the vertical path travelled, quantity of fluid and duration of discharge.

A frequent occurrence in the soil stack is the generation of low amplitude pressure transients. This pressure transient may be generated due to sudden change in flow regime of the annular flow once arriving at the base of the stack and transitioning to horizontal flow. Grant (1997) explain that the entrained air flow rate increases with water flow until the water conditions approach full bore at the base of the stack. Here, as a result of the rapid reduction in free cross sectional area, a prohibition of air movement is experienced. This positive transient could potentially cause harm to appliance trap seals as it travels upward through the stack and through branches. It should be noted that though of low amplitude, pressure transients generated within the network are capable of destroying the system protection provided by the appliance trap seals, thus allowing the ingress of contaminated sewer gas.

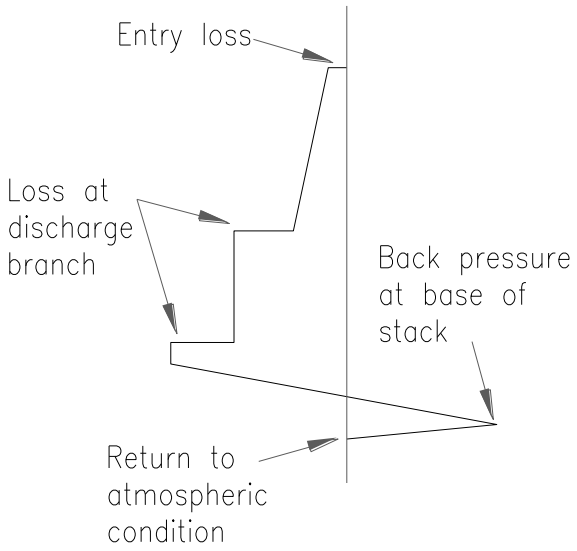


**Figure 2. 11, Pressure profile for a single stack system with 2 active branches**

#### *2.5.1.4 Methods of water trap seal depletion*

The appliance trap seal is designed to act as a protection device, and therefore, can be considered a termination boundary. The water column providing this seal, by nature of its simple design, is ever responsive through water height fluctuations, to the pressure differential between the appliance and system side of the trap. In an ideal system all transients propagating towards this boundary would be reflected upon contact and transmitted elsewhere in the network until the air pressure attenuated. Therefore, the water column is left virtually unaffected by the applied force. This ideal is crucial to meeting the criteria of the BDS, and is compromised by the fundamental requirements of its operation. For instance, the vacuum created via flow past a branch connected to an appliance trap seal, the back pressure created by the sudden stoppage of flow at the base of the stack, and the sudden flux of a large amount of fluid through the trap .These features of the system are likely to compromise its safe operation and are discussed further below.

(i). ***Induced siphonage*** **-** Induced siphonage occurs, upon appliance discharge and as water moves into the vertical stack or flows horizontally past another branch.

The motion, across this junction pulls air from the nearest branch causing with it the suction of water from the appliance trap seal.

(ii). ***Back pressure*** **-** The flow of fluid within the BDS and specially the soil stack, leads to several simultaneous reactions. One of which, is the generation of positive air pressure transients upon the blockage to air propagation by the water curtain at the base of the stack.

(iii). ***Momentum*** **-** The momentum generated within a branch by the discharge of a sanitary appliance, if of sufficient inertia, may allow the water column in the appliance trap to travel with the discharge fluid, leaving little or no fluid behind to create a safe seal.

Other methods of trap seal depletion independent of appliance discharge are:

(iv). ***Evaporation*** **-** Unused appliance traps are at risk of slowly losing their seal due to latent heat transfer. The rate of evaporation in the U.K. is noted to be in the region of 3mm per week under normal ambient conditions. (Wise, 1957; Swaffield, 1995). If this is the case, a 50mm seal would deplete in 17 weeks, and a 75mm seal in 25 weeks (Kelly, 2009). High temperatures experienced in the summer months or trap located near heat sources are likely to deplete at a much faster rate.

(v). ***Leakage*** **-** Improper installation of the water trap seal may leave the device vulnerable to constant leakage. If left unobserved for a significant length of time, the constant loss of water from the water column leaves the immediate inhabitant susceptible to the transmission of disease through the BDS.

(vi). ***Self Siphonage*** **-** Appliance discharge into horizontal drains (branches) can generate air flows which lead to trap seal depletion. The likely magnitude of the entrained air flow induced through discharge make such an event a rarity.

(vii). ***Wind shear -*** Due either to gusts of wind or annular water flow in the stack, as the entrainment of air into the dry stack presents a positive transient to the system. The pressure fluctuations brought on via external air pressure force the movement of the water column towards the appliance side of the trap. The frequency of the gust may cause the backward and forward movement of the seal, and eventually under certain condition lead to trap depletion.

It should be noted that apart from the factors so far mentioned, retention of the appliance trap seal is reliant also on external influences such as improper system design and construction, excessive pressure excursions due to sewer surcharge, pressure fluctuation through the dry stack due to wind shear, and evaporation of the seal due to lack of use and/ or high temperatures (Kelly, 2009).

The uncompromised retention of the trap seal and thus maintenance of the dead end boundary is however, reliant on the nature of the transient. This description of the appliance trap seal is of a passive boundary, though the resulting oscillations induced by an applied transient can lead to the weakening of the seal. This reactive characteristic requires the water seal boundary to be considered an active boundary as it be characterised in four states (See Table 2.2), and may enter into this form as a consequence of the scenarios described above and presented in Figure 2.12.

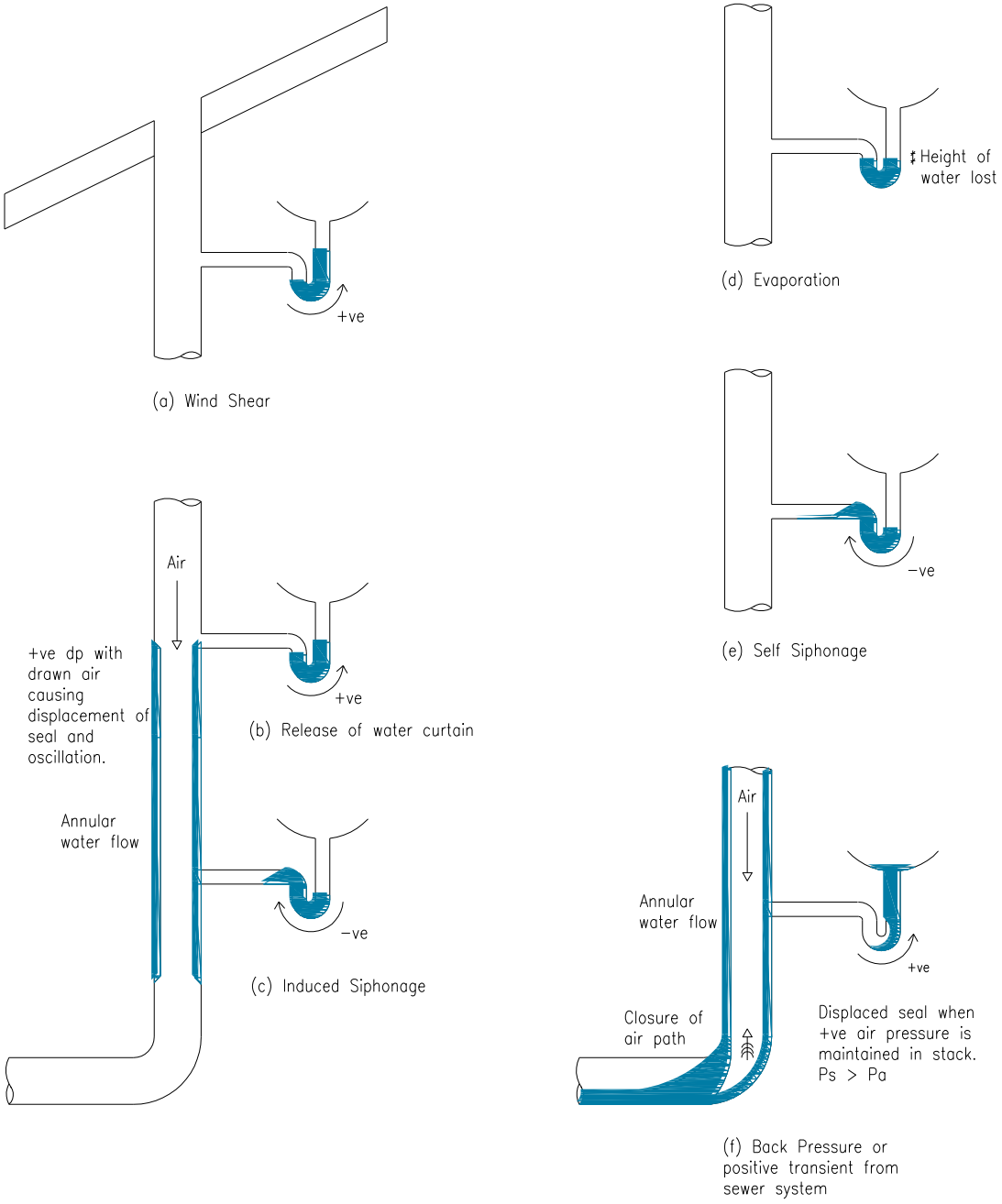


**Figure 2. 12, Recurrent conditions affecting an appliance water trap seal.**

| | Description | Flow type |
|---|---|---|
| **1** | The seal at rest (dead end)- no significant change to water column as a result of system or atmospheric changes | Full bore (water flow) |
| **2** | The seal is oscillating due to applied pressure transient, but remains uncompromised | Full bore (water flow) |
| **3** | The seal is compromised for a short period | Transitional free surface |
| **4** | The seal is fully depleted. | Full bore (air flow) |

**Table 2. 2, Possible flow regimes in an appliance water trap**

### *2.5.2 Control and suppression of air pressure transients*

Concerns for the retention of the sanitary appliance trap seal have dominated developments in the BDS since the end of the 19$^{th}$ century- at which time it was first acknowledged that air pressure transient propagation, generated as a natural consequence of appliance discharge, could in fact compromise the integrity of the water trap seal and ultimately lead to trap depletion (Kelly, 2009).

Focus on creating a system which responds immediately (thus safeguarding the seal) to changes in the pressure regime can be seen in the traditional two pipe system and one pipe system. As described in Section 2.3, the need for a more cost effective and resource conservative solution became a more topical requirement leading the design from a two pipe, to the one pipe, the single stack system, then the modified one pipe system. The consequence however, being poor system performance. Though venting was in fact considered here, poor design often lead to situations such as that shown in Figure 2.13 (below).

Such instances steered Engineers to a greater appreciation of the need for venting of the BDS, and adequate design procedures. It should be noted here, that this need applies more typically, in high rise multi-occupancy buildings.

**Figure 2. 13, Effect (in ground floor flat shower room) of positive pressure transient generated upon the discharge from the top floor bath in a two pipe system.**

Note in Figure 2.13 (right) the ripple movement of the water caused by the incoming air pressure wave. In the case of a single stack system, the debris shown could likely be faecal matter alien to the household. However, the system for which these pictures are shown, is a two pipe system and so, more likely to be hair and dirt,

Developments in Building drainage system components which address the venting requirements and the want for a more conservative design, can be seen in the invention of the Air Admittance Valve (AAV) in the 1980s, then later in 2000 invented by Swaffield and Campbell and developed by Gormley (2002) the Positive Pressure Air Transient Attenuator (P.A.P.A.). The AAV operates by equalising system pressure if a negative pressure transient in induced locally in the system. This device therefore, allows air at atmospheric conditions into the network and seals under a positive pressure regime.

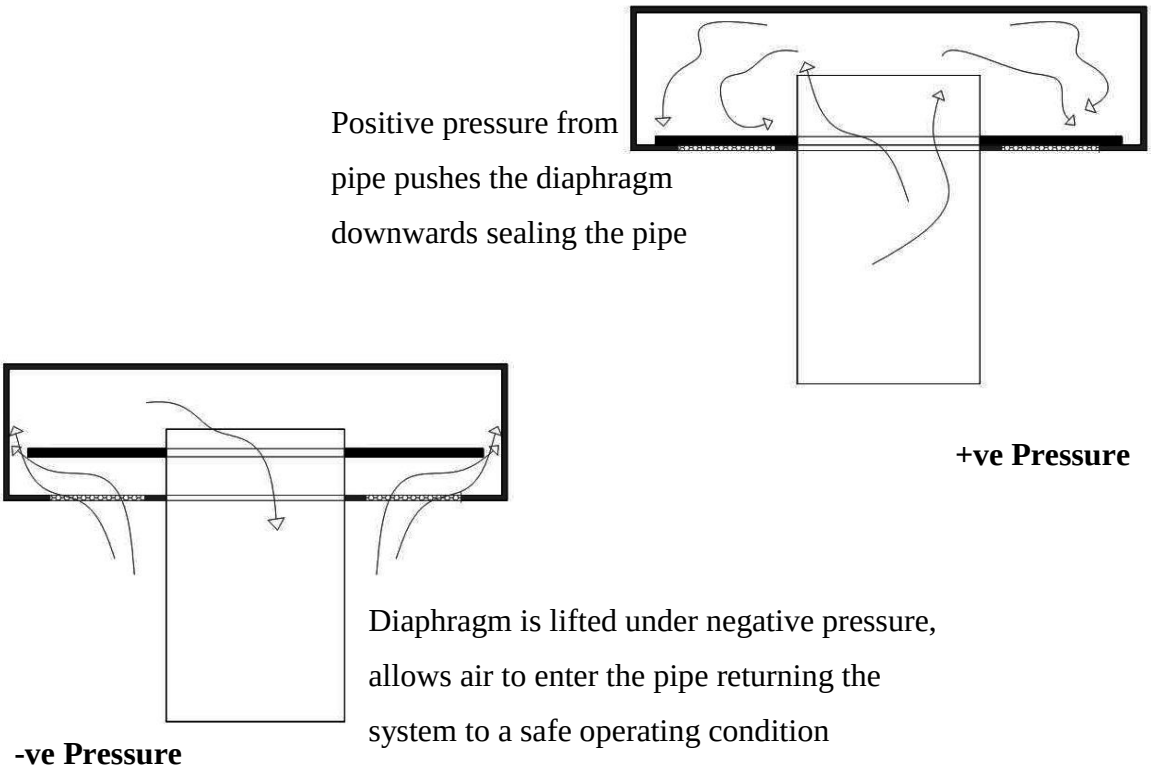


**Figure 2. 14, The operation of the Air Admittance Valve**

The PAPA performs the opposite function of the AAV. This device contains a flexible membrane encased by a rigid plastic shell, and is positioned near the base of the stack. The positioning here is vital to its operation as it must present the path of least resistance to the propagating air flow. Upon entering the device, the internal walls swells to absorb the energy, then slowly in time releases the air back into the soil stack at a lower velocity.

Current research trends lean towards the use of mathematical modelling, and computational studies which afford designers a greater understanding of fluid mechanics and assessment of the network on a minute scale.

Figure 2.15 to 2.17, presents the results of numerical and laboratory testing of the pressure profile within the soil stack of a single stack system.

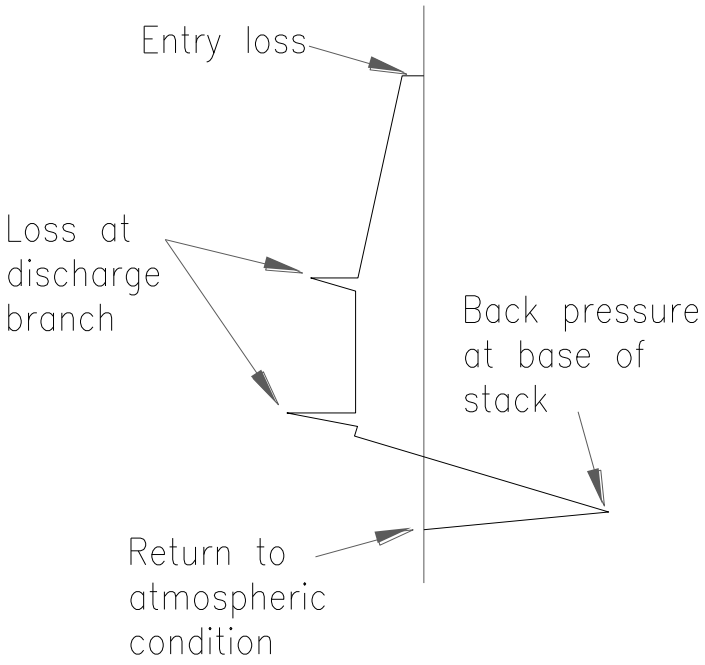


**Figure 2. 15, Pressure profile for a modified one pipe system with 2 active branches**

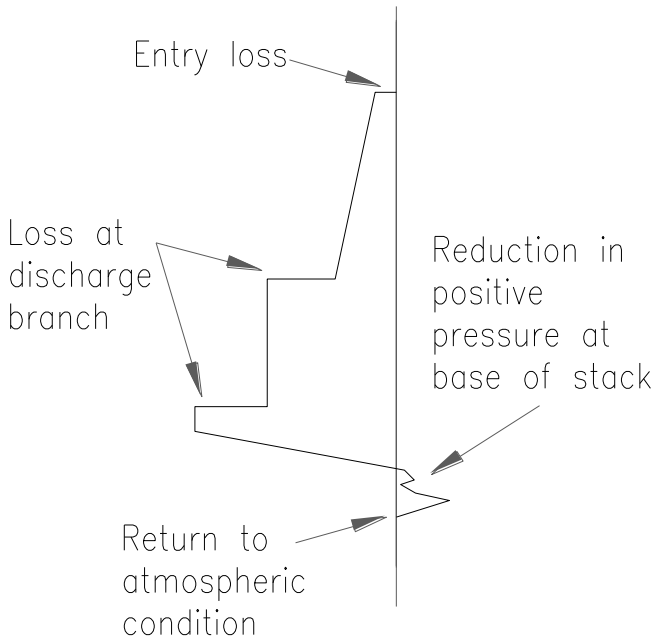


**Figure 2. 16, Pressure profile for a single stack system with 2 active branches using a PAPA at the base of the stack.**

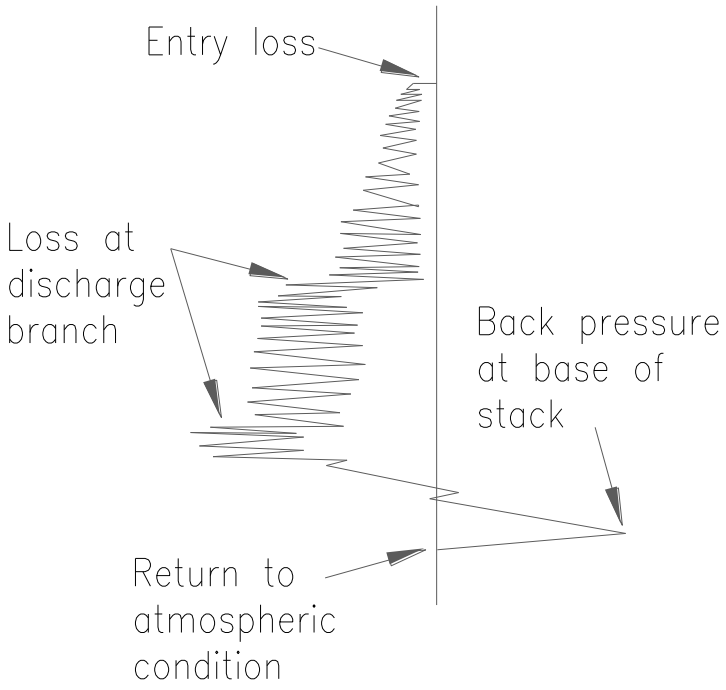


**Figure 2. 17, Pressure profile for a single stack system with 2 active branches using an AAV fitted at intervals along the stack.**

### *2.5.3 Flow Internal Energy in the BDS*

Flow specific energy in a BDS is considered to be a relationship between potential energy and flow kinetic energy. The steady flow energy equation describing this relationship between potential energy and kinetic energy at each section of the network, includes a fluid internal energy term to represent frictional resistance and separation losses (Swaffield *et al*, 2015). Here, change in *e* (internal energy) is the result of friction and separation losses.

The understanding of friction and separation losses in a BDS is vital to attaining a full grasp of the fluid dynamics of system air propagation. Flows enclosed by a pipe wall all possess a loss due to the shear stresses acting at the pipe wall. This loss is noted as a fall in fluid pressure in the direction of fluid flow. Darcy's equation may be used to express this relationship. The general form is as stated below.

$$\Delta P = \rho f L \frac{V^2}{2m} \qquad \textbf{Eq. 2. 4}$$

Where, $\rho$ is the fluid density, $L$ is the pipe length , $V$ is the flow mean velocity, $m$ is the hydraulic mean depth and $f$ is the friction factor defined by the Colebrook White friction factor relationship.

This equation for full bore cross sectional flows becomes,

$$\Delta P = 4\rho f L \frac{Q^2}{2DA^2} \qquad \textbf{Eq. 2. 5}$$

Where, $D$ is the pipe diameter, and $V = {}^{Q}/_{A}$

The Colebrook white relationship is discussed in detail in Section 2.5.3.1.

Separation losses occur when a steady uniform fluid flow is interrupted by an obstruction or change in direction, causing the flow to separate from the duct walls. Eddy currents are generated as a result of this disruption to the flow and present localised pressure losses (Swaffield and Galowin, 1992). Conventionally, in the BDS, separation loss is defined in terms of the kinetic pressure and an empirical loss coefficient, *K* (Swaffield and Galowin, 1992)

The Steady Flow Energy Equation, may be expressed as,

$$\left(P + \rho g Z + \frac{1}{2}\rho v^2\right)_{IN} = \left(P + \rho g Z + \frac{1}{2}\rho v^2\right)_{OUT} + \Delta P_{friction} + \Delta P_{separation} \qquad \textbf{Eq. 2. 6}$$

Separation losses encountered at pipe bends, fittings (such as the appliance trap seal, grilles, AAVs) and at entry and exit can be expressed in terms of an experimentally derived coefficient and the flow kinetic energy.

$$\Delta P_{separation} = \frac{1}{2}\rho v^2 = \frac{1}{2}\rho\left(\frac{Q}{A}\right)^2 \qquad \textbf{Eq. 2. 7}$$

#### *2.5.3.1 Frictional representation of flow in the water trap seal*

Friction is defined by the shear forces which oppose motion, and in this instance the resistance to motion of the water seal is a result of the pipe wall surface, water quantity, density, and gravity; all of which contribute to prohibiting the propagation of the air flow through the curved conduit (the appliance water trap seal).

The assumption of a steady uniform frictional resistance model is made involving for example the Colebrook white friction factor relationship, which provides a satisfactory approximation of the event but not wholly justified (Swaffield, 2010). Swaffield continues by stating that the quasi-steady model is universally used within surge analysis using MoC for the pragmatic reason that the rate of change of the flow conditions are sufficiently slow, in terms of time and pipe period, for the predictions to remain valid within normal engineering limits (when accuracy of system parameters are not known to be highly accurate). This flaw in the assumption of uniformity, introduces further errors to the model.

$$f_{unsteady} = f_{steady} + 0.449\frac{D}{V^2}\frac{\partial V}{\partial t} \qquad \textbf{Eq. 2. 8}$$

With frictional loss defined as:

$$\Delta P = \frac{4f\rho LV^2}{2D} \qquad \textbf{Eq. 2. 9}$$

Where, $\Delta p$ is the pressure differential or pressure head lost, *f* is the Darcy friction factor, *L* is the length of pipe, D is the inner diameter of the pipe, $\rho$ is density, and *V* is the flow velocity.

Early research in the representation of friction in unsteady flow in conduits was conducted by Carstens and Roller (1959), Zilke (1968) and Vitkovsky *et al* (2004). Carstens and Roller (1959), term based on local time acceleration developed an additional empirical term to be added to the friction factor

$$\Delta P = \frac{4f\rho LV^2}{2D} + \frac{16\rho L}{D^2}\sum \begin{bmatrix} V(time - j\Delta t + \Delta t) \\ -V(time - j\Delta t - \Delta t) \end{bmatrix} W\left(t^*(j\Delta t)\right) \qquad \textbf{Eq. 2. 10}$$

Zilke (1968) study of unsteady friction in laminar flows produced the basis for the prediction of the rate of change. The unsteady frictional pressure loss in pipe flow is calculated using

$$\Delta P = \frac{4f\rho LV^2}{2D} + \frac{16\rho L}{D^2}\int_0^1 \frac{\partial V}{\partial t^*} W_o(t - t^*)dt^* \qquad \textbf{Eq. 2. 11}$$

Where $t^*$ is non-dimensional time

$$t^* = \frac{4vt}{D^2} \qquad \textbf{Eq. 2. 12}$$

Vitkovsky *et al* (2004) extends Zilke's work, presenting an equation which is applicable to turbulent flows.

$$\Delta P = \frac{4f\rho LV^2}{2D} + \frac{16\rho L}{D^2}\sum_{1,3,5}^{M} \begin{bmatrix} V(time - j\Delta t + \Delta t) \\ -V(time - j\Delta t - \Delta t) \end{bmatrix} W\left(t^*(j\Delta t)\right) \qquad \textbf{Eq. 2. 13}$$

The Colebrook-white relationship was developed in 1939 is based on an earlier body of research by C.F. Colebrook and C.M. White '*Experiments with fluid friction in roughened pipes'*. Colebrook's 1939 publication *'Turbulent flows in pipes with particular reference to the transition region between smooth and rough pipes laws'* set out the following equation which is still used today for the calculation of the friction factor in turbulent air flow in pipes.

$$\frac{1}{\sqrt{f}} = -4log_{10}\left(\frac{\varepsilon/D_h}{3.7} + \frac{1.26}{Re\sqrt{f}}\right) \quad \textbf{Eq. 2. 14}$$

Where, $f$ is the friction factor, $\varepsilon$ is the roughness (m), $D_h$ is the hydraulic diameter or internal diameter of a pipe, $Re$ is the Reynolds number.

For free surface flows, the Colebrook equation is written as (Bridge and Swaffield (1983):

$$\frac{1}{\sqrt{f}} = -4log_{10}\left(\frac{K}{14.84m} + \frac{0.315}{Re\sqrt{f}}\right) \quad \textbf{Eq. 2. 15}$$

Where, $m$ is hydraulic mean depth.

$$Re = \frac{\rho VL}{\mu} = \frac{VL}{\mu_k} \quad \textbf{Eq. 2. 16}$$

Where, $V$ is the mean velocity of the flow in the pipe (m/s), $L$ is the pipe length, $\mu$ is the dynamic viscosity of the fluid, $\mu_k$ is the kinematic viscosity and $\rho$ is the density of the fluid.

Frictional resistance for trap seal oscillation is represented by:

$$T3=\tau LP = 0.5\rho fLPV_{trap}^2 \quad \textbf{Eq. 2. 17}$$

Where, the first term represents the differential pressure within the branch to trap boundary. The second term in the equation represents the differential between water surface levels at a stated time with term 4 representing the mass time acceleration. (Swaffield, 2007)

## 2.6 Conclusions

The role of the Building Drainage System, to transport fluids and solids away from the habitable space quickly without causing harm to inhabitants, relies on the simple design made up of appliances, protection devices and pipe work. The evolution of the system design and an overview of the protection devices is presented in Sections 2.3. Section 2.4 highlights that through the BDS, the greatest risk of host to host transmission is through inhalation of aerosolised contaminated liquid, direct contact with contaminated liquid or solid matter, and contact with pathogens through inanimate objects. These routes of transmission express the importance of BDS pressure transient control and suppression devices (such as the PAPA and AAV), to the protection of responsive BDS barriers as they ensure the health and wellbeing of building occupants. Section 2.5 of this chapter, detailed the flow regimes which are expected and the methods in which pressure transients can cause trap seal depletion.

Recent research in this field acknowledges the role mathematical modelling presently plays in preventing poor system designs; systems unfit for purpose. The consequence of poor system design is frequent trap seal depletion and thus, the possible transmission of disease. Chapter 3 continues by providing a discussion of the relevant issues surrounding available mathematical modelling techniques.

# Chapter 3

# Numerical Modelling

## 3.1 Introduction

Fluid flows in BDS are intrinsically unsteady. In the main this is due to random discharges of wastewater and the resulting entrained airflows which are required to equalize naturally occurring pressure fluctuations. Air flows are just as important as water flows in a gravity drainage system since it is air pressure disruptions which can compromise the seal between the system and habitable space. The prediction of air flow and pressure within the system is best dealt with as full bore flow while horizontal water flows are more appropriately predicted using free surface modelling techniques; both transient in nature. Methods employed to predict BDS fluid flows must therefore be capable of simulating multiphase or single phase flows, shock waves, transient flow and time dependant flow regimes. The MoC numerical method enables satisfactory prediction of these system characteristic flows in building drainage networks to be analysed, but requires adequate knowledge of the system boundary conditions.

The existing methods of boundary conditions development (by theoretical analysis and laboratory investigations), currently present many limitations, and so, identification and investigation of novel methods for development of these conditions is pivotal to the development of whole system modelling techniques. Among these limitations are the economic requirements of necessary apparatus, the inability to investigate the effect of minute changes to product geometry, the requirement of personnel during testing, and

the limited product detail provided through empirical methods. This limited data imposes restrictions on the quantitative analysis of the product, as boundary conditions for the FD model typically requires a relationship between pressure and flowrate (Beattie, 2013).

This chapter is provides the theoretical background to existing computer based flow prediction techniques; Computational Fluid Dynamics (CFD), and the coupling of known techniques for the calculation of complex problems. The research presented focuses on the fundamentals to the common CFD techniques (the Finite Difference, Finite Volume and Finite Element methods), and also discusses the historical application and existing MoC methods used in the prediction of air transient propagation in pipes and sanitary appliances. Section 3.7.1 to 3.7.3 highlights the importance of the associated network boundaries and the methods for developing this physical characteristic data. Section 3.8 provides an overview of the commercial CFD software used for the fluid flow assessment and Section 3.9 concludes the chapter.

## 3.2 Computational Fluid Dynamics

Multi-dimensional modelling techniques which assess fluid dynamics digitally, is commonly referred to as Computational Fluid Dynamics (CFD). This field of study is based on the calculation of flow movement using the Navier Stokes equations. The existing techniques under this broad umbrella each possess unique advantages applicable to different flow problems. Some of which are suitable for predicting unsteady, transient and random discharge flows in BDS. This technique holds the advantage of being able to:

- Assess complex systems not capable of solving experimentally, digitally
- Allow comprehensive visualisation
- Provide large data sets than afforded experimentally due to economic, or technical resource limitations

The most popular methods under this heading are the Finite Difference (FD), Finite Element (FE) and Finite volume (FV) methods. The modelling process includes: the

definition of system geometry, creation of discrete calculation regions, or cells, setting up boundary conditions, the calculation process and finally post processing. Enhancements over the years in both the fields of physics and computer science have led the way in the development and progress of CFD. Relatively inexpensive and powerful computing hardware and software, along with application of the fundamental basis of any CFD code, the Navier-Stokes momentum equations, (which define single phase fluid flow) (Nicholls-Lee, 2011 and Griebel *et al*, 1997); enable the development and continued augmentation of CFD. These equations are simplification by elimination of terms describing viscosity. This simplification yields the Euler equations.

The solution of the partial differential equations which describes fluid flow is critical in CFD. The earliest tools used in the solution of partial differential equations: Finite Difference Method (FDM) and Finite Element Method (FEM), were developed years apart and for different purposes.

The finite difference method, the oldest and simplest modelling tool was first noted in 1910, at the Royal Society of London, when Richardson (1910) presented a paper on the approximate arithmetical solution by finite differences of physical problems involving differential equations with an application to stresses in a masonry dam (Chung, 2010). In 1928, Courant, Friedriches, and Lewy, presented the method of solution of hyperbolic partial differential equations through a solution of the differencing scheme using a rectangular or rhombus like mesh. Courant *et al* (1928) also makes note within this paper of the criteria for convergence under the parabolic, elliptical and hyperbolic differencing schemes. Other researchers of note who contributed to the development of the FDMs are: Lax (1954) for work on the earliest shock capturing schemes which laid the foundation of shock wave theory of importance to BDS due to the transient nature of fluid flows, Godunov (1959) for developing a differencing numerical method for the solution of wave equations in partial differential form, Lax and Wendroff (1960), provided the systems of conservation laws, and MacCormack (1969), (1971) developed the two stepped FD scheme which is suitable to the approximation of free surface wave problems to second order accuracy.

The MoC is used to transform the St. Venant equations of continuity and momentum into a pair of total derivative expressions solvable by the FD technique. It was first

mentioned by Monge in 1789, whose work focused on solving the St. Venant equations through graphical methods and further developed by B. Riemann in the 1850s. Massau in 1900, Lamoen in 1947, and Gray in 1953, applied the MoC method to the study of free surface wave motion, open channel flows, analysis of water hammer and fluid transient problems, and were followed by Mary Lister (1960), a mathematician who first proposed the technique to transform partial differential equations into ordinary partial differential equations. This approach has since been widely accepted as a suitable method for the calculation of unsteady fluid flows in the MoC technique and by extension, low amplitude air pressure transient propagation in building drainage systems (Swaffield, 2010). Lister's research is proceeded by work by Streeter and Lai (1962), Fox (1968), Evangelisti (1969), Swaffield (1970), Boldy (1976) and Wylie and Streeter (1978); and then after the introduction of mainstream computer technology: Fox, (1989), Campbell, (1992), McDougall (1995), Jack (1997), and Wright (1997). These developments all led to the development of the MoC based numerical model utilised within the industry. CFD however, is a much broader subject area involving the FE, FV and other immerging numerical techniques.

The development of the FEM in 1950s arose from the need to examine and predict structural behaviour. Early attempts in this field were made by Hrennikoff (1941) and McHenry (1943), who developed analogies between a one dimensional lattice line elements, and the corresponding stress regions of a continuous solid (Logan, 2010). These semi analytic techniques were subsequently applied to the structural design of aircrafts. This development was followed by Argyris (1955) who discovered matrix methods for the solution of structural questions. This minimisation process forms the basis of the FEM mathematical technique. Argyris's approach however was found to be inadequate to the solution of high speed jet aircrafts and so what is considered as the first FEM work was published in the Aeronautical Science Journal by Turner *et al*, (1956) paper titled *Stiffness and deflection analysis of complex structures* for applications to aircraft stress analysis in 1956.

From the 1960s onwards the aerospace industry has integrated CFD techniques into the design, R&D and manufacture of aircraft and jet engines (Versteeg and Malalasekera, 1995), however although initially limited to the high technology engineering disciplines

of Aeronautics and Astronautics (Tu *et al*, 2008, Bakker *et al.*, 2001), it is now popular among industrial applications and academic research fields; areas requiring solutions to complex problems. Credit to the further enhancement of this technique is given to researchers such as: R.W. Clough, H.C. Martin, J.H. Argyris, and O.C. Zienkiewicz. The FEM used extensively for the analysis of structural problems, now offers the BDS the platform to assess the structural response of BDS components (active boundary conditions). Such likely components are: the waterless trap seal, the PAPA and the AAV. Modelling of the PAPA and waterless trap seal in particular, offer a complex problem due to elastic membrane offering linear and non-linear movement of the material and thus unpredictable responses to pressure transients.

The third and final technique discussed in this thesis, is the Finite volume method (FVM). This method relates to both the Finite Difference Method (FDM) and Finite Element Method (FEM), have become increasingly popular in recent years, becoming the preferred solution method because of its straightforward data structure, in commercially available packages. This popularity of the FVM is due also to its ability to conserve physical quantities both locally and globally. Giannopapa (2004) however, notes that the FEM is preferable over the FVM in cases where the material is linearly elastic. She continues by stating that in cases where the material concerned is non-linear or viscoelastic, resulting in constant changes in the material properties, the FV will have an advantage over the FE method. This advantage to the FVM is due to the intense computational time and memory requirement on the CPU by the FEM (Demirdzić and Martinović, 1993 cited in Giannopapa, 2004). The FVM is also found to more easily (than the FEM) approximate fluid flow problems due to the non-linear characteristics of the governing equations. However, when for simple linear fluid flow equations where a simple solution matrix is adopted, the FEM is significantly faster.

Tu *et al*, (2008) asserts that the different disciplines of fluid mechanics and heat transfer from which CFD is derived are becoming commonplace in every aspect of engineering now, including chemical, civil and environmental engineering. While these techniques are more common now, they are not without challenges and are not the panacea that was hoped.

CFD techniques have been applied on a broad scale in the process industry to gain insight into various flow phenomena, to examine different equipment designs or compare performance under different operating conditions resulting in enhanced efficiency and lower operating costs (Eesa, 2009, Tu *et al*, 2008). Fluid flow simulation in the Building Drainage sector has relied mainly on Finite difference - MoC schemes, though three main techniques exist. By understanding the advantages of each technique (the FD, FE, and FV methods), the possibility exists to improve the modelling of the BDS.

## 3.3 Governing equations

This section provides the fundamental equations of fluid movement (required for CFD) and solid deformation assessment. The Navier Stokes equations for Newtonian incompressible fluid flow in pipes, is presented in Section 3.3.1 along with the hookean equations for elastic structure deformation in Section 3.3.2.

### *3.3.1 Fluid flow equations*

The continuity equation is derived by applying the principle of mass conservation to a small expanse of fluid (Abbott and Basco, 1989; Fletcher, 1997) first order hyperbolic equation

$$\frac{\partial \rho}{\partial t} + \frac{\partial}{\partial x_i}(\rho \boldsymbol{v}_{\mathrm{i}}) = 0 \qquad \textbf{Eq. 3. 1}$$

Here $\rho$ represents the density of the fluid, u the fluid velocity, the subscripts $i$ indicates the Cartesian coordinates and the respective velocity components, $x$ is the position and $t$, time. In incompressible flows however, $\rho$ is constant and autonomous of both space and time and so $\frac{\partial \rho}{\partial t}$ equals to 0. The equations of continuity for incompressible flows becomes expressed in its Cartesian coordinates as

$$\frac{\partial v_i}{\partial x_i} + \frac{v_i}{x_i} + \frac{\partial v_j}{\partial x_j} = 0 \qquad \textbf{Eq. 3. 2}$$

Newton's second law of motion states that the rate of change of momentum is equivalent to the sum of the forces acting on a patch of fluid. The momentum equation can be expressed in Cartesian coordinates (Abbott and Basco, 1989).

$$\frac{\partial \rho}{\partial t}(\rho v_{\mathrm{i}}) + \frac{\partial}{\partial x_j}(\rho v_j v_i) = -\frac{\partial P}{\partial x_i} + \frac{\partial}{\partial x_j}\left[\mu\left(\frac{\partial v_i}{\partial x_j} + \frac{\partial v_j}{\partial x_i}\right)\right] \qquad \textbf{Eq. 3. 3}$$

and becomes,

$$\frac{\partial v_{\mathrm{i}}}{\partial t} + \frac{\partial v_j v_i}{\partial x_j} = -\frac{1}{\rho}\frac{\partial P}{\partial x_i} + \frac{\partial}{\partial x_j}\left[\mu\left(\frac{\partial v_i}{\partial x_j} + \frac{\partial v_j}{\partial x_i}\right)\right] \qquad \textbf{Eq. 3. 4}$$

Where, $\mu$ is fluid viscosity, and $P$ is pressure. It should be noted that water and air (in this context) are considered Newtonian fluids and so their viscosity is constant. For non-Newtonian fluids, the shear rate-dependence of viscosity is taken into account using a constitutive equation for viscosity (Eesa, 2009).

$$\mathcal{T}_{ij} = \mu\left(\frac{\partial v_i}{\partial x_j} + \frac{\partial v_j}{\partial x_i}\right) \qquad \textbf{Eq. 3. 5}$$

Here, $v$ denotes the velocity, the subsript $i$ the radical direction or $j$ the axial direction, $x$ is the distance along the given direction, $p$ is the pressure, $\rho$ is the density of the fluid, r is the radius, is and $\tau_{ij}$ represents the strain tensor of the fluid which is only relevant in the characteristics of a viscous fluid.

Equation 3.5 (seen above as part of equation 3.4) describes the relationship between an incompressible, constant viscosity fluid's shear stress. This term is called a tensor (or symmetric tensor in this case) which describes the viscous stress components. Versteeg

and Malalasekera (2007) suggests that the most useful forms of the conservation equations for fluid flows are obtained by introducing a suitable model for the viscous stresses, $T_{ij}$.

### *3.3.2 Structural equations*

In cases where the movement of the fluid proportionally influences the behaviour of a surrounding solid, the effects of this vibration or material displacement should be considered as the resulting effect on the fluid behaviour may be significant. The waterless trap seal investigated in this thesis presents such a phenomenon, and so FSI is considered a suitable approach. Fluid structure interaction (FSI)) is the study of this relationship (and is further discussed in Section 3.5 and 3.6. For FSI simulations, the stress and displacement relationship is defined by

$$\rho_w \frac{\partial^2 d_i}{\partial t^2} = \frac{\partial \sigma_{ij}}{\partial x_j} + \rho_w F_i for\ i,j = x,y,z \qquad \textbf{Eq. 3. 6}$$

Here, $d_i$ is the displacement $\rho_w$ is the wall density, $F_i$ are the components of body forces acting on the solid and imported from the fluid field solver.

From Eq. 3.6, the stress tensor of a Hookean elastic solid is expressed as:

$$\sigma_{ij} = e_{ij} \quad _{ij} + 2 \quad _L e_{ij} \qquad \textbf{Eq. 3. 7}$$

## 3.4 Discretisation techniques

Digital computers inherently can only read and manipulate numerical forms of data. For this reason the above governing equations of momentum, continuity, and, stress and displacement, written in the form of partial differential equations (PDE) cannot be solved without first undergoing a process called discretisation; the process of

transforming partial differential equations into numerical equations, through the use of approximations. It should be noted that these approximations introduce error to the numerical simulation.

The accuracy of solution relies on the form of the partial differential equation assumed, whether linear, quasi-linear, or a second order equation they are classified as elliptic, hyperbolic or parabolic respectively. Each category of equations relates to a certain physical phenomena.

- Elliptic equations describe steady state phenomena
- Parabolic equations typically presents problems where the magnitude of a variable varies and is of greater interest that the propagation of random motion. For instance, equations of heat and diffusion.
- Hyperbolic equations describe propagation problems so requires the definition of boundary conditions such as the inlet, outlet and wall functions. This form is adopted for the description of fluid flow in BDS.

The transformation of an Elliptic, Parabolic or Hyperbolic partial differentiation into an ordinary differential equation is generally performed though either of three popular methods of discretisation are namely: the FD, FE, and the FV methods.

### *3.4.1 Finite Difference Method*

The FDM is the oldest flow prediction method and is based upon the application of the local Taylor expansion to approximate the differential equations (Peiro and Sherwin, 2005). This method uses a square network of lines to construct the discretisation of the partial differential equations. The Taylor series expansion method of network transformations of the partial differential equations provide a library of numerical equations that describe the derivatives of a variable as the differences between values of the variable at various points in space and time (Shaw, 1992).

According to the FDM, if the velocity value is known at one point *p*, then the Taylor series expansion can be used to determine the values of *u* at two points a small distance *h* away from *p* (Eesa, 2009). Here the numerical equations at a given point are based on the values and approximations at neighbouring points.

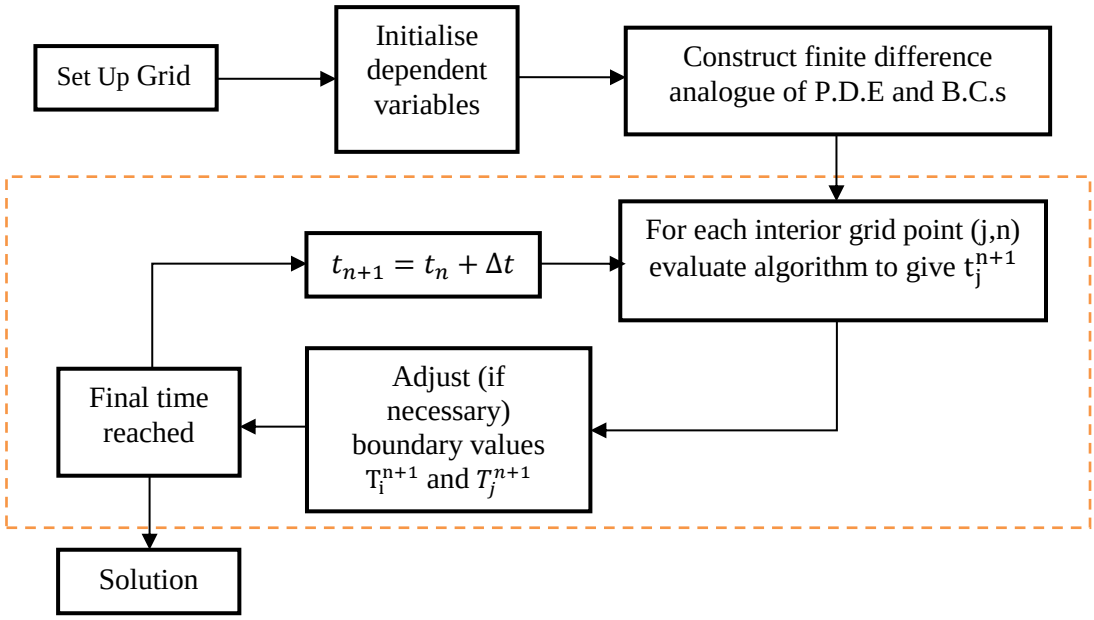


**Figure 3. 1, The process schematic for the FD discretisation method. Source: Fletcher (1997).**

The Taylor series expansion enables the solution of variables using a 1D or 2D grid. The 2D solution method allows for the determination of two unknowns $x + h$ and $x - h$ since $x$ is known. Once a single variable is known, the value of the dependent variable at a value of the independent variable a small distance from the reference value can be determined (Shaw 1992).

$$u_{x+h} = u_x + h\frac{du}{dx} + \frac{1}{2}h^2\frac{d^2u}{dx^2} + \frac{1}{6}h^3\frac{d^3u}{dx^3} + \cdots \qquad \textbf{Eq. 3. 8}$$

and

$$u_{x+h} = u_x - h\frac{du}{dx} + \frac{1}{2}h^2\frac{d^2u}{dx^2} - \frac{1}{6}h^3\frac{d^3u}{dx^3} + \cdots \quad \textbf{Eq. 3. 9}$$

By adding or subtracting these two equations, the first and second derivatives respective to position x can be found (Shaw 1992).

$$\frac{d^2u}{dx^2} = \frac{1}{h^2}\left(u(x+h) - 2u(x) + u(x-h)\right) + O(h^2) \quad \textbf{Eq. 3. 10}$$

and

$$\frac{du}{dx} = \frac{1}{2h}\left(u(x+h) - u(x-h)\right) + O(h^2) \quad \textbf{Eq. 3. 11}$$

Here $O(h^n)$ known as the truncated term, represents the sum of n- and higher order terms and is a function of the mesh spacing, represented by the distance h (Eesa, 2009). The degree of error in the discrete approximation is determined by the exponent term of h. The increase in this term reflects the truncated errors are reduced more rapidly with decreasing mesh, increasing the order accuracy of an approximation implies that errors are reduced more rapidly with decreasing mesh size. According to Fletcher (1997), the truncation error is likely to be a progressively more accurate indicator of the solution error as the grid is refined. Limitations however, do exist; a larger exponent or higher order approximations are less robust (Abbott and Basco, 1989).

#### *3.4.1.1 Method of Characteristics*

Since its development in the 1960s, the Method of Characteristics (MoC) has been extensively used for solving the Saint Venant equations (a 1D simplification form of the fully developed Navier Stokes equations) to describe the laws of continuity and momentum in shallow water flow problems. This 1D technique based on characteristic lines along which the governing equations are transformed (from partial differential

equations to become ordinary differential equations), provides the advantage of rapid computation of supersonic flows within simple geometries.

The MoC has numerous advantages: the simplicity of programming and efficiency of computations, even for complex systems with numerous boundary conditions; and its particular suitability to applications where the event to be simulated is of relatively short duration (Kelly, 2009). Kelly continues by stating that additionally, the method deals with networks in terms of internal nodes and boundaries which, when linked to a first order difference scheme, only involves the simultaneous solution of two equations at each internal pipe node and, at boundaries, the solution of one characteristic per pipe and an equation defining the boundary condition (see Swaffield and Boldy, 1993; Fox,1968; Streeter 1969). This feature enables the development and analysis of complex boundary conditions as calculations can be conducted in isolation. The MoC calculation method is wholly appropriate for BDS, although issues do exist with conservation of mass – since it is 1D, it can lose mass with distance and time, an occurrence called a 'leak'.

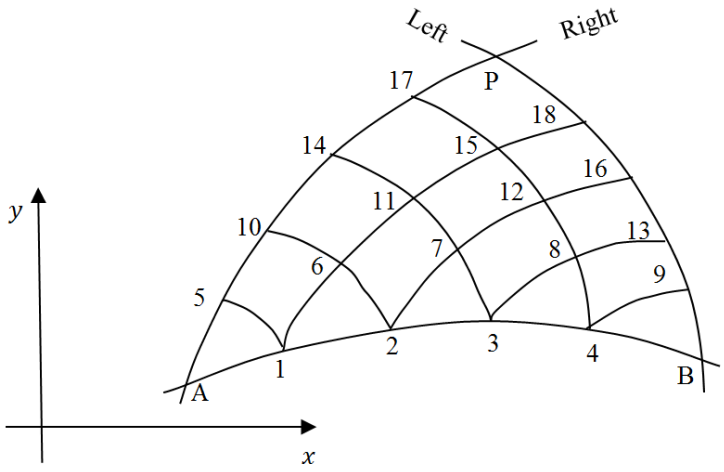


**Figure 3. 2, Computation of characteristic network PA, PB which corresponds to the characteristic lines names $C^+$ and $C^-$ in Figure 2.3. Source: Niyogi (2006)**

The St. Venant equations of continuity and momentum are shown as a pair of quasi–linear hyperbolic partial differential equations that are transformed into a pair of total derivative equations which can be solved by a FD scheme via the MoC (Swaffield and Boldy, 1993, Swaffield, 2010). These total derivative equations, once linked to the FD technique is expressed in terms of air velocity and wave propagation speed and defined against time and distance variables. It should be noted here, that the simulation of the whole building drainage system in this thesis makes reference only to full bore air flows.

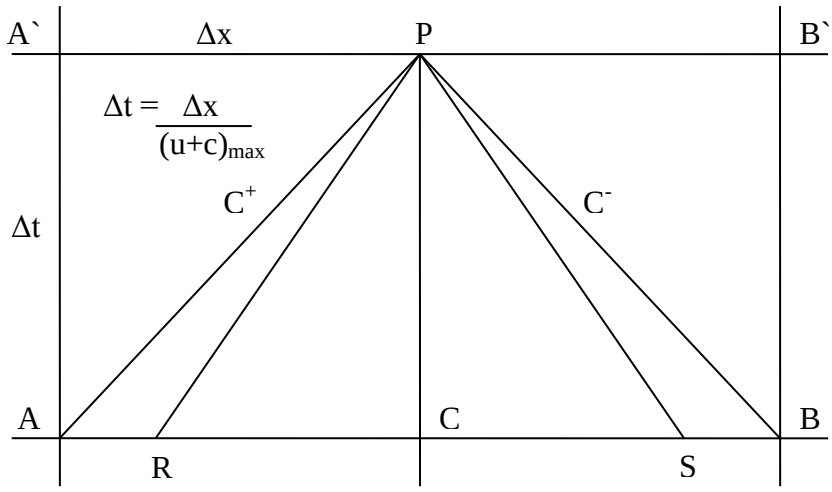


**Figure 3. 3, Typical grid representative of the scheme used for the calculation of the propagation of pressure transients through a pipe. Source: Swaffield *et al*, (2015)**

This method is based on the fact that the supersonic flow is hyperbolic, meaning that a given point has effect on some region downstream of it, but not upstream (Murzionak, 2013). The characteristic lines which emanate from or intersect at a given point, describe the two boundaries of the region in reference. The calculation at a certain time on the grid is based on the conditions upstream and downstream, as one step in the past, and requires a definition of the characteristic slope as a foundation for all future predictions. Abbott (1979) explains that in fact the characteristic lines between *A* and *P* and *B* and *P* in Fig 3.3, should be curved, but as the time step are normally very small, it is allowable to represent this data in straight lines. The margin of error is very small.

Point P is calculated using the characteristics lines between R and P and S and P. Information regarding air velocity and wave speed and hence pressure, is calculated and transferred through these lines of communication formed by the characteristic slopes allows to be propagated throughout the system (Swaffield and Boldy, 1993).

The set of equations presented below form the basis of air flow predictions for Building Drainage Systems. The pair of quasi-linear hyperbolic partial differential equations are presented in Eq. 3.12 and Eq.3.13.

$$L_1 = \left(\frac{2}{\gamma - 1}\right)\rho C\frac{\partial C}{\partial x} + \rho v\frac{\partial v}{\partial x} + \rho\frac{\partial v}{\partial t} + \frac{4fv|v|}{2D} = 0 \qquad \textbf{Eq. 3. 12}$$

and

$$L_2 = \rho\frac{\partial v}{\partial x} + \left(\frac{2}{\gamma - 1}\right)\frac{\rho}{C}\left[v\frac{\partial c}{\partial x} + \frac{\partial C}{\partial t}\right] = 0 \qquad \textbf{Eq. 3. 13}$$

therefore,

$$L = L_1 + \lambda L_2 = \frac{\partial v}{\partial x}(\lambda + v) + \frac{\partial v}{\partial t} + \left(\frac{2}{\gamma - 1}\right)\left[\frac{\partial c}{\partial x}\left(\lambda\frac{v}{C} + C\right) + \frac{\lambda}{C}\frac{\partial C}{\partial t}\right] + \frac{4fv|v|}{2D} = 0 \qquad \textbf{Eq. 3. 14}$$

Where terms: $u$ is flow velocity, $\lambda$ is ratio of specific heat at constant pressure to constant volume and $C$ is acoustic velocity. Friction is represented by the term $\frac{4fu|u|}{2D}$ where the factor $f$ in air pressure transient modelling and not multiphase flows, is determined by the Colebrook-White equation.

$$\frac{1}{\sqrt{f}} = -4log_{10}\left[\frac{k}{14..8m} + \frac{0.315}{\rho\frac{v}{\mu}\sqrt{f}}\right] \qquad \textbf{Eq. 3. 15}$$

Applying the MoC yields the following total differential equations.

$$\frac{\partial v}{\partial t} \pm \left(\frac{2}{\gamma - 1}\right)\frac{\partial c}{\partial t} + \frac{4fv|v|}{2D} = 0 \qquad \textbf{Eq. 3. 16}$$

Provided that:

$$\frac{\partial x}{\partial t} = v_R + c_R \qquad \textbf{Eq. 3. 17}$$

$C^+$ Characteristic may be expressed by

$$v_P - v_R + \frac{2}{\gamma - 1}(c_P - c_R) + 4f_R v_R|v_R|\frac{\Delta t}{2D} = 0 \qquad \textbf{Eq. 3. 18}$$

However when,

$$\frac{\partial x}{\partial t} = v_s - c_s \qquad \textbf{Eq. 3. 19}$$

The $C^-$ Characteristic may be expressed by

$$v_P - v_S - \frac{2}{\gamma - 1}(c_P - c_S) + 4f_S v_S|v_S|\frac{\Delta t}{2D} = 0 \qquad \textbf{Eq. 3. 20}$$

This expression described above is applicable to cases where the $\frac{\partial x}{\partial t}$ condition, is given by Eq. 3.19 and the Courant criterion Eq. 3.26, is satisfied. The simplification of Eq's 3.18 and 3.20, are found in Eq 3.21 and 2.22.

$C^+$ Characteristic: $v_P = K1 - K2h_P$ **Eq. 3. 21**

and

$C^-$ Characteristic: $v_P = K3 - K4h_P$ **Eq. 3. 22**

Where:

$$K1 = v_R + \frac{2}{\gamma - 1}c_R - 4f_R v_R|v_R|\frac{\Delta t}{2D} \quad \textbf{Eq. 3. 23}$$

$$K2 = K4 = \frac{2}{\gamma - 1} \quad \textbf{Eq. 3. 24}$$

and

$$K3 = v_S + \frac{2}{\gamma - 1}c_S - 4f_S v_S|v_S|\frac{\Delta t}{2D} \quad \textbf{Eq. 3. 25}$$

The $C^+$ and $C^-$ characteristics which link the inter-nodal distances, $\Delta x$ to $\Delta t$ in Figure 3.3 due to the rectangular form of the grid, are required for a stable solution to conform to the relationship,

$$\Delta t = \frac{\Delta x}{(v + c)_{max}} \quad \textbf{Eq. 3. 26}$$

To ensure that R and S are always adjacent to each other, the size of the time step must remain equal and not exceed that given by the Courant stability criterion (Courant and Fredrichs, 1948). Values $v$ and $c$ present the maximum throughout the whole network at

time $t$ for each time step. Courant Criterion limits the calculation time step (in terms of the local flow and acoustic velocities).

### *3.4.2 Finite Element Method*

Originally developed by aircraft structural engineers in the 1950's to analyse large systems of structural elements in the aircraft, and named the direct stiffness method, independently became , an established technique in engineering sciences for computations in structural mechanics (Braess, 2002). Today, the method has reached such a state of maturity that is now thought of as a method for solving general field problems (Gosz, 2006). The application of the FEM to non-structural problems such as fluid flow and electromagnetism was initiated by Zienkiewiez (1965), and applications to a wide class of problems of interest in nonlinear mechanics was contributed by Oden (1973).

The FDM produces the numerical equations at a given point based on the values at neighbouring points, the FEM differs by producing equations for each element independently of all the other elements (Shaw, 1992). This technique requires that the continuum be divided into many 'elements', and the variable considered is calculated at the node within each element. Using the simple polynomial interpolation functions known as shape functions the variable of interest throughout the domain can be discretised. An assumption of a variable is first made to determine a description of variables across the entire domain. The discovered variation the variables within each element are determined based on the values of the variable at the end points of the element. These points are known as the nodes of the element. The equations obtained for each element are then assembled in global matrices, and boundary conditions are imposed on the matrices so that the equations can be solved (Eesa, 2009). The understanding of the interaction of elements is considered only when element descriptors and placed into matrix form.

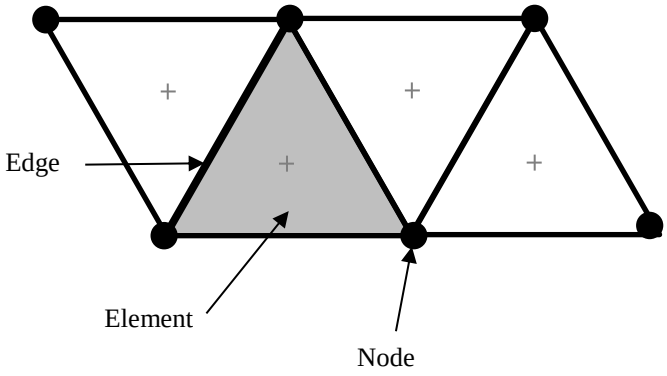


**Figure 3. 4, Typical terminology of a FE mesh**

The solution of a flow problem through the FE mesh requires these major steps:

- Determine the strong form of the governing equations
- Transform the strong form of the governing equations to the weak form
- Select suitable interpolation (shape) functions
- Select the weight functions and setup the algebraic equations for each element
- Obtain the global matrix system of the equations through the assembly of all elements
- Impose boundary condition
- Solve the system of algebraic equations
- Post process the results

### *3.4.3 Finite Volume Method*

The FV based method of numerical solution has become the favoured solution method of discretisation among commercial CFD codes. This method is well suited for the numerical simulation of various types (elliptic, parabolic or hyperbolic, for instance) of the conservation laws; it has been extensively used in several engineering fields, such as fluid mechanics, heat and mass transfer or petroleum engineering (Eymard *et al*, 2006). Likened in many ways to the finite difference method, some of its implementations draw on features taken from the FE method (Eesa, 2009). For instance: the common use

of arbitrary geometries, the flexibility of use of structured or unstructured meshes. Both the FV and FE methods are viewed to be robust schemes (Eymard *et al*, 2006). The method initially introduced by researchers like McDonal (1971), Maccormack and Paullay (1972), and Rizzi and Inouye (1973), discretises the integral form of the conservation equations directly in the physical space (Tu *et al*, 2009).

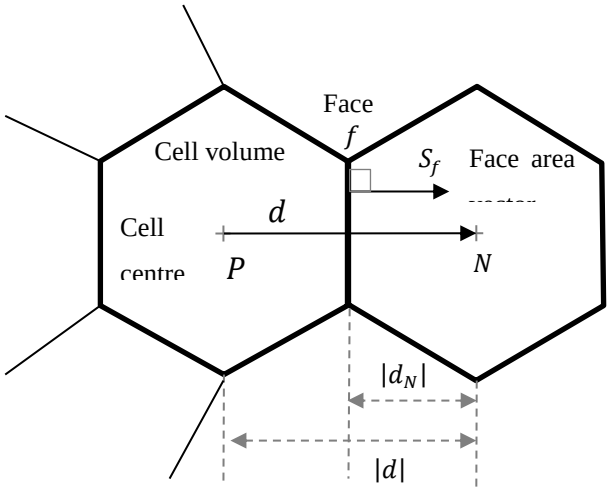


**Figure 3. 5, Typical cell characteristics in a FV mesh**

The application of solving the partial differential equations in relation of the physical problem is conducted though the generation of a grid or mesh from which the enclosed area is of relevant and not the grid intersection points. This grid often similar to that shown in Figure 4 encloses what is referred to as a control volume. As discussed previously discretisation is required to provide numerical data for the solution process. The FVM integrates the differential form of the governing equations across all control volumes. Each integral is then converted into a discrete form, thus yielding discretised equations at the centroids, or nodal points, of the control volumes (Eesa, 2009).

Through this approach, when solving the Navier Stokes equations, the region is often discretised using a staggered grid, in which the different unknown variables are not located at the same points (Griebel *et al*, 1997). Here, the values of u, v, and p of importance to hyperbolic problems are not determined at the same location along the gird, and so an extra boundary layer along the grid exists.

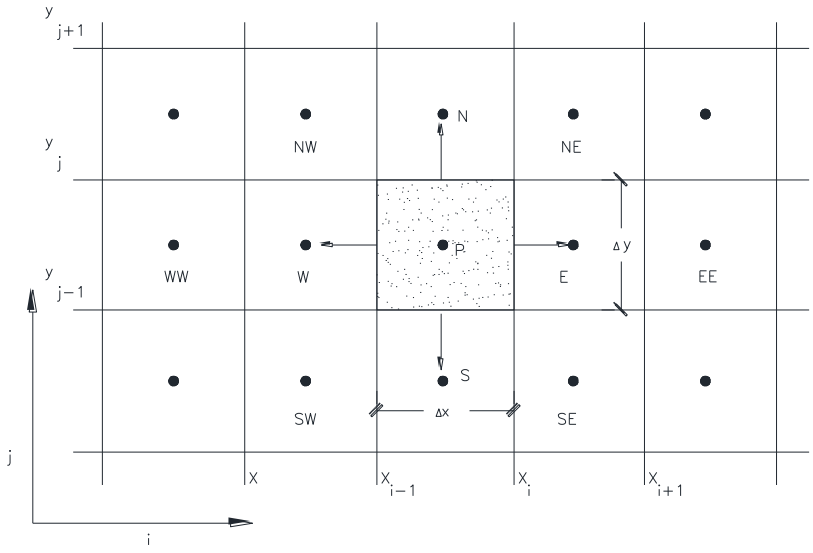


**Figure 3. 6, FVM – co-located grid. Source: Cheng H. (2003)**

Figure 3.6 illustrates a co-located grid within which, all relevant values are located in the cell centres. The finite volume discretisation method interpolates to determine the flux across the four edges of the cell.

## 3.5 Fluid Structure Interaction

This section introduces the computational field of FSI and proposes its use in the study of the behaviour of flexible building drainage system components. The advantage of FSI to the field of BDS fluid flow study, lies in the ability to examine newly developed system component whose behaviour is not easily determined in a laboratory setting. FSI is a general term used to describe the numerical calculation of the mutual interaction of a fluid and a solid at their interface; when the fluid influences the physical behaviour of the solid structure and in return, the mechanical response of the solid on the flow regime of the fluid, and so on and so forth in distance and time. A flexible tube, in this context, is a general term used to describe any membrane which contains a viscous or non-viscous fluid and deforms proportionally with variations in internal pressure. The greatest amount of research in this area has been done in the biomedical engineering field; in the study of blood flow in viscoelastic vessels.

FSI was originally used to simulate cases of aero-elasticity for aerodynamic research interests, such as: fluttering of the wings of an aircraft (Amsallem *et al*, 2007), (Farhat *et al*, 2006), and (Lieu and Lesoinne, 2004), blades of a turbo machine (Marshal and Imregun, 1996), (Willcox *et al*, 1999). Within biomechanical research interests this method has recently been used to investigate, for instance, blood flows through stenosed arteries (Chan, 2006), blood flow through the elastic walls of large arteries (Bazilevs *et al*, 2006), (Perktold and Rappitsch, 1995), (Riemslagh *et al*, 1998), (Tezduyar *et al*, 2008), (Vierendeels *et al*, 2007), blood flow through the heart and specifically through the heart valves (Dumont, 2005), (Dumont *et al*, 2007), (Peskin, 1972), (Van Loon *et al*, 2006), and prototype development and improvement of artificial heart valves and Ventricular assist devices (Moosavi *et al*, 2008), stents and other medical devices (Degroote, 2010).

Studies such as Lee and Xu (2002), where a Newtonian fluid (with a sinusoidal varying input velocity) is modelled within an isotopic elastic membrane representing blood flow in an artery can be likened to single flow problems in flexible building drainage system components. Deformation of the artery due to the internal arterial pressure shows that slower fluid flow and maximum stress occurred at the shoulders of the stenosis (Degroote, 2010). Precedent sent by the modelling of flexible structures such as blood vessels provide this research project with the knowledge to investigate computationally the flow of air in a waterless trap seal.

Early research which led to the development of elastic deformation theory in tube like structures include: Lamb (1898) who studied the wave propagation in cylinders, Skalak (1956) extended Lamb's work with the inclusion of bending stiffness and rotary inertia in an axially symmetric tube model, by investigating the fluid structural interaction in a straight liquid filled pipe. Research by Lin and Morgan (1956a, 1956b) are similar to Skalak's work but this work a counted for the effects of transverse shear deformation in a tube. Paidoussis and Denise (1972) and Paidoussis (2003) regarded the oscillation of an elastomer cantilevered cylindrical shell and provide equations of motion.

### *3.5.1 Historical development of FSI techniques*

Numerical methods (or rather non-computational methods) for the analysis of the interaction between a fluid and a structure have been studied since the early 19th Century. Young (1808), is considered the first investigator in this field to have performed studies of wave propagation of incompressible fluids in elastic tubes, pipes, and blood vessels. His work led to the development of a formula for the velocity of pressure waves in an elastic tube with thin homogenous and isotropic wall, filled with an incompressible fluid (Giannopapa, 2004). Witzig (1914), noted as the first author to publish the results on wave propagation in distensible tubes, and Womersly (1957) continued research in this field by investigating the dynamic response of a tube with a sinusoidal flow, with each defining an analytical solution for the flow field. Witzzig's (1914) analytical solutions was later found to be impractical when realistic geometries and physiological conditions are considered, which creates the need for numerical simulation (Pericevic and Moatamedi, 2007), and (Bessams *et al*, 2007). An overview of these methods for analytical solutions of the equations of axisymmetric motion of visous, incompressible fluid in the frequency domain is presented in Cox (1968) cited in Bessems *et al*, 2007).

Reuderink *et al* (1989) is among the first researchers to compute pulsatile flow in elastic arteries based on one dimensional wave propagation developed from Aniliker *et al* (1971), and Hughs and Lubliner (1973) work on one dimensional wave propagation model describing non-linear flow behaviour in large elastic vessels. Note that this development came post the 1970s, and the introduction of computing technology. Bessems *et al* (2007) explains that until the early seventies these models were mainly based on analytical solutions of the equations of axisymmetric motion of viscous, incompressible fluid in the frequency domain. An overview of these methods is presented by Cox (1968).

In 1998, Zhao *et al* (1999) cited in Pericevic and Moatamedi, (2007) it noted to have coupled ANSYS CFX (a computation fluid dynamics code discussed in Section 3.8) with ABAQUS (a structural dynamics code) via their own iterative algorithm for their study of blood vessels (Pericevic and Moatamedi, 2007). This work was followed by Kunts and Mentor (2004). Kuntz and Menter, (2004) developed a unique method to

approaching the solution of FSI problems. ANSYS 8.0 (an FE solver) and CFX 5.7 (a FV solver), both codes of ANSYS Inc, were coupled in a Partitioned method using a third party code – MpCCI release 2.0. This coupling between ANSYS and ANSYS CFX for evaluating FSI problems persists to the present versions of the software; ANSYS Mechanical and ANSYS CFX 15.0. ANSYS. Inc however does not stand alone in the market of commercial black FSI solvers. Other available packages are provided by: Star CCM+, Abaqus, Openfoam, and COSMOL.

### *3.5.2 Arbitrary Lagrangian Eulerian*

The Arbitrary Lagrangian Eulerian formulation (ALE) used in FSI calculations was first developed by Hirt *et al,* (1974), by the presentation of a solution of the Navier Stokes equations using both Eulerian and Lagrangian approaches. This solution method is based on the principle that the mesh motion can be chosen arbitrarily and allows automatic remapping of the mesh. The ALE formulation consists of a Lagrangian time step followed by an advection step. This advection step describes the mapping of the mesh from a distorted Lagrangian mesh to an undistorted mesh (Pericevic, and Moatamedi, 2007). The mesh modifies itself to match material boundaries in large deformations limiting the need for re-meshing as would be typically required under the langragian method. This disadvantage is found in the semi Lagrangian approach also. The ALE solution method explained in Hirt *et al* (1974) adopts either an Eulerian or a fully Lagrangian approach.

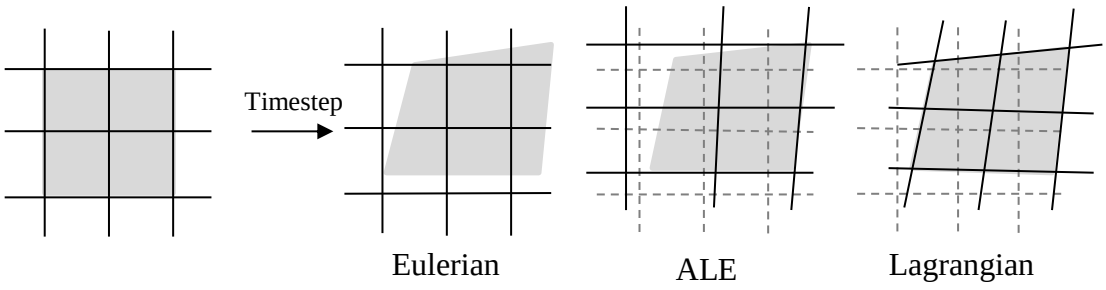


**Figure 3. 7, The comparison between the Eulerian, Arbitrary Lagrangian-Eulerian (ALE) and Langrangian formulation. Source; Degroote (2010)**

In Figure 2.6 it is shown that the ALE method differs significantly from the Eulerian method in the method the new mesh in time is described as the Eulerian formulation grid is fixed, while, in the ALE formation, disparity exists between the grid and the material (which moves at a different velocity). The solution here is mapped onto a new mesh by a distorted mesh. The nodes of this new mesh are placed at an arbitrary position between their locations on the original mesh and their locations on the distorted mesh (Pericevic and Moatamedi, 2007). In the Lagrangian formulation the grid and the material travel at the same velocity. This pictorial representation highlights the fact that the ALE method is a somewhat, semi-Lagrangian and semi Eulerian method.

## 3.6 FSI Coupling:

Typically in FSI, the fluid and solid components are modelled using different techniques to different levels of complexity, ranging from simple analytical solutions to 3-dimensional numerical schemes with advanced physical models. In addition to the range of techniques available for modelling the individual fluid and solid components, there is also the question of exchanging information, typically in the form of boundary conditions, at the interface. The options here are limited and can be classified on the basis of the level of coupling between fluid and solid.

Coupling schemes include:

- Non iterative over time
- Iterative over time
- Non iterative over each time step
- Iterative over each time step

### *3.6.1 Interpolations methods on fluid/structure interface*

This section presents the three methods for the calculation of fluid and structural problems. An objective comparison of the strength and weaknesses of the two main methods – the partition and monolithic approaches are presented.

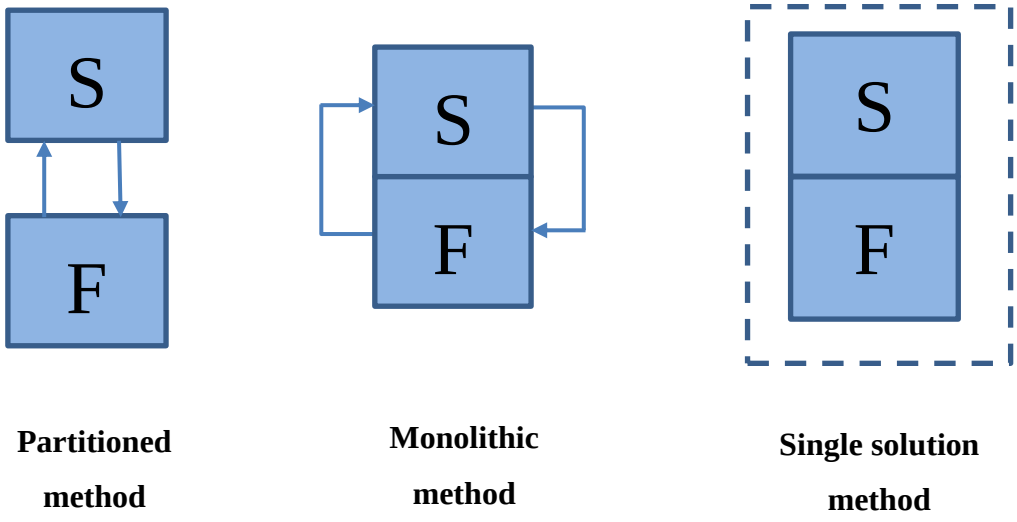


**Figure 3. 8, Schematic of the connections between fluid and solid solvers in the partitioned, monolithic and single solution interpolation methods**

The partitioned method as the name implies partitions the fluid and solid solvers, and calculates for the solution of the fluid and structural equations alternatively. This modular approach holds the advantage of being able to use two separately developed, reliable and optimised codes, which were developed specifically for the physical problem at hand. For instance in the case of the discretisation method employed, as described in Section 3.2, the FVM calculates complex fluid flow problems more

accurately then the FEM and in return the FEM developed for structural problems is likely to approximate structural deformation more accurately than the FVM.

A coupling algorithm exists in the partitioned method as the link between the two solvers. This algorithm allows the interaction between the fluid and solid variables, and stipulates the order in which the flow equations and the structural equations are solved. Generally iterations occur within the set of equations to provide greater accuracy of results.

A distinct advantage of the monolithic approach to FSI coupling which is in direct relation to the solvers having a single method of discretisation, is that no iterations have to be performed between the solution of the flow equations and the solution of the structural equations. The monolithic approach however allows the solution of the flow equations and structural equations simultaneously and therefore the FSI problem calculation time is quicker in this approach. On the other hand many commercial codes operate on black box solvers and therefore little control may exist over the coupling and data transfer method. In the partitioned method it is possible to modify the coupling algorithm

## 3.7 AIRNET

AIRNET, a MoC based FD model, developed at Heriot-Watt University over the past 30 years (initially by the late Professor Swaffield), simulates real system boundaries and appliance trap seals within a building drainage vent system. The AIRNET programme which is the first of its kind within the drainage sector, enables the whole BDS to be evaluated.

The simulation software calculates system variables such as air pressure and air flow velocity and airflow rate at any point in the installation. Results of the simulation therefore, reflect the air pressure transient reflection positions and enable complete understanding of the effect system operation and components poses to the safe workings of the network.

The equations of momentum and continuity (see Eq. 3.12 and Eq. 3.13) are expressed in terms of local air flow velocity and wave speed propagation. The MoC can then be used to convert the results into a FD form, and a simplified, total derivative equation is then developed and used to determine the gradient of lines used in the graphical representation of this data. These lines are known as characteristic lines. This numerical simulation technique has facilitated the effective and efficient design and analysis of transient airflows, enabling a comprehensive assessment of the potential for integration of innovative and sustainable design solutions.

The simulation of low amplitude air pressure transient propagation by Swaffield and Campbell (1992b) proved AIRNET's capability to model real flow scenarios. Swaffield (2007) tested this ability by modelling the effect of a sinusoidal transient wave on the trap seal displacement. Such testing however, requires the application of established MoC solutions introduced the categories of active and passive to differentiate boundaries.

Campbell (1992b) became the first to categorise boundary conditions to be either, active and passive (Swaffield, Jack and Campbell, 2004). Where active boundaries are based on a variable for instance: time, or pressure. On the other hand, passive boundaries are described as a steady state condition.

### *3.7.1 Boundary conditions*

The MoC solution technique divides the BDS up into its constituent parts. Therefore creating what can be considered a listing of domains each with a wall boundary, inlet and outlet. At each boundary, a $C^+$characteristic (at a downstream boundary) and a $C^-$characteristic (at the upstream boundary), represents the conditions at the entry and exit of each conduit length. A single equation is used to describe the effect of the domain's characteristic on the flow regime. This equation is known as the boundary equation.

The choice of appropriate boundary equations is fundamental to the application of the MoC. In the case of air pressure transients it will be necessary to model the boundary

conditions by reference to either ambient pressure at the boundary or some expression linking pressure at the boundary to flow across it (Douglas *et al*, 2011).

Boundary condition can be subdivided in three general categories. They are:

- *Passive boundary conditions*

Passive boundary arises as the result of normal system operation. This covers inactive pipe junctions (whether dry or subjected to annular film flow past the connection), junctions of two of more pipes, constant pressure reservoirs, pipe dead ends, open ended pipes, or changes in the cross sectional area of a pipe.

- *Active boundary conditions*

An active boundary does not possess a steady state of operation, meaning that the boundary condition is entirely reliant on the environmental characteristics. This covers building drainage system components such as the Air admittance valve (AAV), the positive air pressure attenuator (PAPA) which are considered active because of their moving parts. Building drainage system protection devices also fall under this category of boundary conditions.

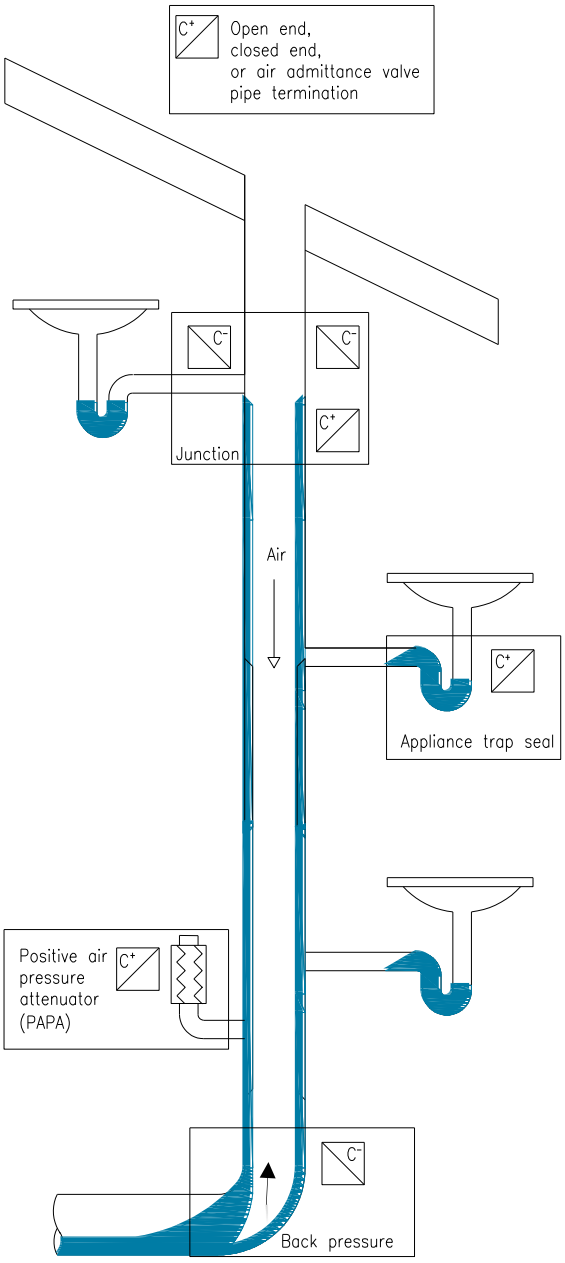


**Figure 3. 9, Boundary conditions and characteristic curves for a typical single stack building drainage system**

### *3.7.2 Boundary condition development approaches*

The method of characteristic techniques described (in Section 2.4.3), requires the initial conditions to be known so that the process of numerical modelling can begin. These

nodes are solved by first developing boundary conditions which are compatible with a single $C^+$ and $C^-$ characteristic. For every entry to and exit from a pipe section one characteristic exists.

Boundary conditions describing the network model are critical in determining the accuracy with which a transient analysis may be modelled. This boundary condition data simply expressed as pressure or fluid flow velocity through the boundary in time, is required at time step zero to enable the commencement of the simulation, and then after for every subsequent time step throughout the network. This data is linked to create an expression which describes the element's treatment of imposed flows.

### *3.7.3 Existing boundary conditions*

Douglas *et al* (2011) notes that the great strength of the MoC technique is that the solution allows internal pipe sections and boundary conditions to be considered independently. The accuracy of the calculation therefore, rests on the identification of the appropriate relationship to describe the flow regime within the boundary and the response under transient conditions.

Over forty years of research has been invested in the developments of AIRNET and by extension, BDS boundary conditions. Campbell (1992) regarded the pressure responses of the vertical stack systems, and found it acceptable to allow the force of the annular water column with a central entrained air column from the upper termination, to be represented by a fan positioned at the base of the stack (Swaffield, Jack and Campbell, 2004). This work using a pseudo-fan as an analogue to a suction force which draws air down the vertical stack enabled AIRNET to model the distributed air pressure recovery (Campbell 1992).

Jack (1997) through a site investigation involving a 20 storey public housing high rise building in Dundee, Scotland, enhanced the work by Campbell (1992). This work linked the resistance coefficient of the water column to the discharge flow rate and to the diameter and roughness of the wet stack, leading to the representation of the force in the wet stack as traction or a negative friction force, and so allowing the effects of multiple

branch discharges to be predicted in numerical models. AIRNET was then able (using this pseudo friction factor) to simulate air pressure transient propagation and traction forces exerted by the entrained air core (Swaffield, and Jack 1998).

Further work by Jack (2000) introduced the theory of traction force exerted on the entrained air core by the downward movement of the annular water flow, and substituted the friction factor terms, $f_r$ and $f_s$, with a 'pseudo friction factor' term. In 2002, Jack and Swaffield (2002), investigated the effect of the water curtain at the base of the wet stack, noting the generation of a positive air pressure transient (back pressure).

***Passive boundary conditions***

Any instance where airflow between the building drainage system and the internal building, sewer network or external environment is presented with unobstructed positive or negative flow, is considered an opening. This opening to the piped network is expressed mathematically with local loss coefficient K.

$$P = P_{atm} + 0.5\rho K v|v| \qquad \textbf{Eq. 3. 27}$$

The $C^+$ equation is combined with the local loss equation

$$v_{N+1} = K1_N - K2_N C_{N+1} \qquad \textbf{Eq. 3. 28}$$

and Eq.3.27 becomes

$$P_{N+1} = P_{atm} - 0.5\rho K v_{N+1}|v|_{N+1} \qquad \textbf{Eq. 3. 29}$$

Where, $P_{atm}$ is the atmospheric pressure (the pipe exit pressure), the suffix $N+1$ denotes the pipe exist node, and K is the loss coefficient

In the instance of a closed ended pipe, or closed valve,

$$v = 0 \qquad \textbf{Eq. 3. 30}$$

and so, substituting Eq.3.30 into Eq. 3.28, the equation describing a closed end of a pipe becomes

$$C_{N+1} = \frac{K1_N}{K2_N} \qquad \textbf{Eq. 3. 31}$$

***Active boundary conditions***

The air admittance valve (AAV) developed in the 1980s as a venting device, introduces positive airflow to the system under negative pressure and seals under positive pressure (preventing cross contamination). This opening and closing valve positioned near an appliance trap seal or at termination of a pipe, has an associated valve loss coefficient ($K$) at time $t$ during either opening or closing valve motion. The $C^+/C^-$ characteristic lines are solved with

$$P = P_{out} + 0.5\rho K_t v|v| \qquad \textbf{Eq. 3. 32}$$

and written as,

$$P = P_{N+1} + 0.5\rho K_t v_{N+1}|v_{N+1}| \qquad \textbf{Eq. 3. 33}$$

Where, $P_{out}$ equal to $P_{N+1}$ is the prevailing pressure upstream or downstream of the valve.

If time t > closing time,

$$v_{N+1} = 0 \qquad \textbf{Eq. 3. 34}$$

If time t > opening time

$$P_{atm} = P_{N+1} + 0.5\rho K_t {v^2}_{N+1} \qquad \textbf{Eq. 3. 35}$$

If fully open,

$$K_t = K_{min} \qquad \textbf{Eq. 3. 36}$$

If valve is partially open,

$$K_t = K \qquad \textbf{Eq. 3. 37}$$

$\Delta P$ across valve $= 0.5\rho K_{fully\ open} V_{upstream} |V_{upstream}|$

It should be note here that the equations describing a fully open valve boundary condition covers the orifice between two pipe boundary.

Another example of an active boundary is the water trap seal which acts as a foremost measure of security to the BDS. This device, connected to a network is immediately vulnerable as it is responsive to positive and negative pressure transients, causing fluctuations in water level (much like in a manometer).

Frictional resistance for trap seal oscillation is represented by Eq. 2.13 restated here,

$$T3{=}\tau LP = 0.5\rho f L P V_{trap}{}^2 \qquad \textbf{Eq. 3. 38}$$

Where, the first term represents the differential pressure within the branch to trap boundary. The second term in the equation represents the differential between water

surface levels at a stated time with term 4 representing the mass time acceleration. (Swaffield, 2007)

$$T1 = A\left[0.5\left(P_{pipe,t+\Delta t} + P_{pipe,t}\right) - \left(P_{atm} + P_{room}\right)\right] \quad \textbf{Eq. 3. 39}$$

$$T2 = \rho g A(H_o - H_1 + 2dH) \quad \textbf{Eq. 3. 40}$$

$$T4 = \rho L A \frac{V_{trap,t+\Delta t} - V_{trap,t}}{\Delta t} \quad \textbf{Eq. 3. 41}$$

Where Eq 3.39 is the pressure differential between the room air and the transient pressure profile in time, Eq 3.40 is the height differential between the water surface on the system and appliance side of the curved conduit, Eq. 3.38 is the frictional resistance to the movement of water in the trap or trap oscillation, and Eq. 3.41 is the mass acceleration.

The existing boundary condition for a water trap seal is expressed as T1+T2-T3-T4 = 0

Eq. 3.42 describes this movement.

$$A\big(p(j,N(j)+1) - p(atm)\big) + \rho_w A g(H_1 - H_0) - \tau_o L P = \rho_w L A \frac{dV_w}{dt} \quad \textbf{Eq. 3. 42}$$

Where, $A$ is the cross sectional area, $L$ is the liquid column length, $H_1$ is the liquid seal height on the system side of the trap, and $H_o$ is the liquid seal height and $P$ is the wetted perimeter.

$$\big(p(j,N(j)+1) - p(atm)\big) + \rho_w \left[(H_1 - H_0) - L\left(\frac{4fV_w|V_w|}{2D} - A\frac{dV_w}{dt}\right)\right] = 0 \quad \textbf{Eq. 3. 43}$$

Where $V_w$ is the liquid column velocity, $f$ is the friction factor of the water which is base d on the Colebrook-white steady state friction expression and, D is the trap diameter.

Gormley and Beattie (2010) improved this boundary condition by making equations T3 a product of a $\beta$ function which reflects the effects of air pressure transient frequency. This factor however, though easily incorporated into the MoC model accounts for fluid in a single trap seal.

Boundary conditions not noted here include the: positive air pressure attenuator, exist for trapped air, time dependant inflow at the channel entry, free outfall of a liquid and moving hydraulic jumps which are formed upstream of a junction.

The waterless trap seal boundary condition has been likened to the AAV boundary condition in so that they both open and close under a given pressure. The behaviour and construction of these devices differ significantly and so in the instance of a non-rigid device like the waterless trap seal the oscillatory motion of the object should be considered in the model.

## 3.8 ANSYS CFX

ANSYS CFX is a general purpose computational fluid dynamics software which uses a hybrid discretisation method for the solution of partial differential equations. This hybrid "element based FVM" requires the generation of an unstructured grid where elements, nodes and control volumes are determined. ANSYS CFX is an Implicit solver meaning that no limitation exist on its time step size. This modular tool combines part of the preprocessing requirements with a complete postprocessor. ANSYS CFX is used to solve a multitude of flow situations, of which include: Steady state and transient flows, laminar and turbulent flows, heat transfer, bouyancy, combustion, newtonian and non-newtonian flows, particle tracking, transport of non-reacting scalar components, mutliphase flows, and flows in multiple frames of refernce.

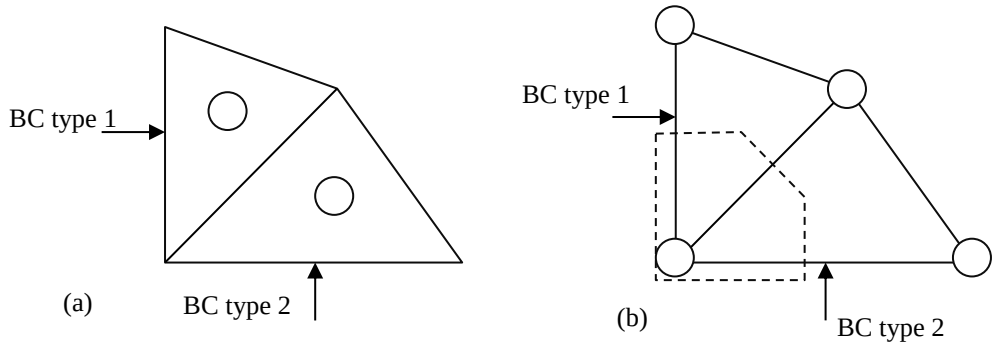


**Figure 3. 10, Boundary condition for (a) cell based and (b) vertex based discretisation**

The algorithms for the analysis of free surface flows can be classified into these three groups: Lagrangian, Eulerian and a combination of the two: a Eulerian Lagrangian method. The lagrangian group mainly consists of strictly Lagrangian and particle methods, while the Eulerian group is composed by fixed grid and adaptive grid methods (Ferzinger and Peric, 2002). Three approaches to the solution of free surface flows exist: Fixed mesh methods, moving mesh methods and free mesh methods. ANSYS CFX solves free surface problems through the fixed mesh approach, using a technique known as VOF (volume of fluid). The algorithm which describes fluid transport is solved for the fraction of each cell (or control volume) occupied by the fluid phase. Although more robust than both the moving mesh method and free mesh method, there are limitations to the approach which the researcher must compensate for. This method is not very effective for resolving a sharp interface and so in transient simulation where the free surface is varying in both time and space, it is required that a fine mesh be specified in the pre-processor and not adaptive grid methods section, and that the free surface interface be clearly defined.

The CFD simulation must progress through three stages: pre-processor, solver, post processor. Their functions are listed below.

| Pre-processing | Solver | Post processing |
|---|---|---|
| Governing equations | Identification of the physical characteristics and boundary conditions | Graphical presentation of results |
| Development of the problem | Specification of the Geometry | Analysis of derived results |
| | Discretisation of governing equations within flow domain | |
| | Solution of flow conditions | |

**Figure 3. 11, Details of the three main components of computational modelling**

CFX Pre, the partial pre-processor is a physics pre-processor, as here, only the physical description of the problem is defined. Features and attributes such as the analysis type, fluid characteristics, initial conditions, boundary conditions (inlets, outlets walls and openings), solver parameters, fluid and solid domains, and sub domains are specified through ANSYS CFX-Pre. The ability to define complex flow scenarios such as (FSI and multiphase flows with temperature controlled inlets are feasible by specifying the physical conditions which are relevant to the flow problem.

The component that solves the CFD problem is called the solver. It produces the required results in a non-interactive/batch process (ANSYS, 2009). A CFD problem is solved as follows:

- The partial differential equations are integrated over all the control volumes in the region of interest. This is equivalent to applying a basic conservation law (for example, for mass or momentum) to each control volume.
- These integral equations are converted to a system of algebraic equations by generating a set of approximations for the terms in the integral equations.
- The algebraic equations are solved iteratively.

Due to the non-linear nature of the governing partial differential equations of fluid flow, iterations must be conducted to continually reduce the calculation error to an acceptable

level. Then the solution is said to have converged. For each iteration, an error, or residual, is reported as a measure of the overall conservation of the flow properties (ANSYS,2009). The accuracy of the solution is dependent on several factors, which are predetermined in the pre-processor stage (and physics processor).

## 3.9 Conclusions

This chapter has outlined the different methods which comprise the field of Computational Fluid Dynamics. The FD, FV and FE methods have been described along with the equations which govern fluid and solid movement. An historical perspective to the development of the FD, FE, FV methods, and the more recent development of computational FSI is detailed in Sections 3.2 and 3.5. Instances of the use of FSI in previous research (in different fields of science) are made, thus providing a link to the possible use of this method in the solution of flexible BDS components.

It is explained that all CFD models require: a grid of points, boundary conditions which define the characteristics at a position of the flow domain and enable approximations, and the fluid characteristics in the system. It is noted that a great advantage of the MoC technique used in the numerical solution of whole BDS, is that the method considers the internal pipe sections and boundary conditions independently, and therefore accuracy of the solution relies on the identification and description of the flow regime within the boundary and the response under transient conditions.

# Chapter 4

## Laboratory and Numerical Investigations

### 4.1 Introduction

This chapter presents the methodologies used in order to establish new techniques for boundary equation development outlined in Chapter 3. The focus of the laboratory and digital experimentation centres on the interaction of responsive Building Drainage System (BDS) protection devices under unsteady flow and transient conditions.

These barriers are designed to prohibit the ingress of foul air (sewer gases), and potentially harmful pathogens from the sewer or other areas within the building drainage network from entering habitable spaces. They can be formed from a small water seal held in a curved conduit - the water trap seal, or, by the installation of a self-sealing flexible membrane - the waterless trap seal. These appliance trap seals will be used extensively in this research as reference products from which boundary condition information will be obtained for later inclusion in a numerical model. The numerical and laboratory experiments carried out in this study reflect the nature of the devices under normal transient conditions and allow the operational phenomenon observed to be presented in subsequent chapters.

The following sections and subsections within this chapter present first, the details of the hardware and software utilised for the digital experiments, followed by the setup of the numerical models of the appliance water traps and the flexible sheath likened to Sample 1 of the waterless trap seals within ANSYS CFX, the laboratory methodology

used for the investigation of the appliance waterless trap seal and the instruments required to conduct the investigation of air transient propagation through waterless trap seals. These details are all provided between Sections 4.2 and 4.6. The methodology presented in Sections 4.4 to 4.6 will contribute to achieving Objectives 2 and 3 by presenting the basis for the boundary condition development methodology. Section 4.7 concludes the chapter.

## 4.2 Numerical Modelling – Software

ANSYS CFX was selected as previous validated research of both multiphase flows and fluid structure interaction problems confirmed readings that ANSYS CFX was considered more advanced in Fluid Structure Interaction problems than ANSYS Fluent at the time and able to calculate transitional laminar to turbulent, and full bore to free surface flow problems adequately.

A conceptual advantage of the use of commercial CFD software was the reduction in the time requirement of a digital experimentation compared to the conventional laboratory experimental methods. This assumption was found to be false, upon practical use. It was discovered that ANSYS CFX (like other 3D commercially available CFD codes), is time intensive; a factor entirely reliant on the available computing power. This fact is magnified by the complexity of the flow characteristics and the degree of accuracy required.

## 4.3 Numerical modelling - Hardware and limitations

The numerical element of this research was conducted on two workstations. They are the: HP Z400 workstation (14GB Intel® Xeon® CPU W3550 3.07Ghz, 4 core machine has a memory of 16GB), and an HP virtual workstation (6GB Intel ® Xeon ® CPU E5-26400 2.5Ghz, 2 core machine has a memory of 4GB). Both workstations run on a 64bit operating system and were operated independently.

High performance computing (HPC) specifications for ANSYS CFX are typically recommended to have installed greater than a 16Gb of ram (ideally 32Gb or more), with 8 or more cores. This however is dependent on the complexity of the flow regime, the resolution of the mesh and time constraints; in essence the amount of data to be handled per second or time step. During the analysis of a multiphase problem, it was noted that the CPU usage comparative to normal use, was low, but that the RAM usage was exceedingly high, approaching full capacity. The issues with slow computing, errors and failure of many simulations was due to the data not being written as quickly as required by the software. This issue became even more prevalent under the FSI models due to the complexity or communication between the two solvers. The addition of a GUI, and/ or ANSYS HPC license is recommended to address this issue. A resolution arrived however, with an upgrade the Z400_workstation hard drive, by the addition of a OCZ 480GB RevoDrive 3 X2 PCIe solid state hard drive.

A vast improvement to the speed of multiphase flow calculations was thus noted. Flow problems which once required 7 days to compute, now required 20 minutes. A 99.8% decrease in computation time (real time). Regrettably this addition came towards the end of the data collection stage of the research project and so the benefits of reduced time investments, was not gained to any great effect.

Table 4.1 below, provides the read/write speeds of the Z400 workstation hard drive before and after the OCZ 480GB RevoDrive 3 X2 PCIe solid state hard drive (referred to as PCIe) installation, and compares the test results with that of other available hard drives available within the department.

| | | SATA 110GB SSD | HDD Hp desktop | External HHD (USB SATA) 3TB | **HDD Z400 (before)** | **PCIe Z400 (after)** |
|---|---|---|---|---|---|---|
| Seq | read | 201.6 | 43.18 | 166 | 22 | 678.1 |
| | write | 140.6 | 92.8 | 139 | 28 | 575.1 |
| Random 4K | Read | 16.33 | 0.345 | 0.59 | 0.048 | 20.56 |
| | write | 27.73 | 0.536 | 0.555 | 0.596 | 87.17 |

**Table 4. 1, Comparison of the read/ write speed (Mbyte/sec) of the PCIe drive against other available hard drives**

Data in Table 4.1 shows quite decisively that the solid state hard drives (SSDs) noted in the tables as the 110GB SSD and the PCIe Z400 (after) recorded faster read/write speeds across the board when compared to the conventional HHDs however the PCIe drive is as much as 3 times faster than even the 110BG SSD. The read/write time on the Z400 PC was 146 times faster with the PCIe drive than its original HDD, a phenomenal improvement.

The following subsections details the numerical methodologies employed for the assessment of the water trap seal and the waterless trap seal.

## 4.4 Model overview of the water trap seal

The model structure within the ANSYS workbench involves three main sections: the pre-processor, the solver, and the post processor. The first, the pre-processor refers to the modules for specification of the geometric parameters of the problem and the module which generates the computational mesh. The solver here is CFX *14.5*, called 'setup and solution' modules within the ANSYS workbench. The setup module provides the medium for the specification of the boundary conditions and physical

details of the model. The postprocessor otherwise named within the program as ‘results’ enables the model simulation data to be assessed.

### *4.4.1 Definition of appliance geometric parameters*

The two appliance water traps modelled can be described as: the glass appliance part swivel water trap by Schott, (typical to the Heriot Watt University Building Services Laboratory), and a typical PVC commercially available appliance water ‘P’ trap. They are henceforth referred to within this text as the laboratory and commercial appliance water traps respectively. The geometric differences between the two reference water traps is noted in the size of the inner bend (12.5mm, 37.5mm), the internal diameter of the conduit (46mm, 40mm), the overall height of the trap (212mm, 172mm), and the overall shape of the trap (P shaped, Swivel) for the commercial and laboratory traps respectively.

The problem was described to be transient in nature, with the end of calculations occurring after 0.5 (simulation) seconds. Transient simulations unlike steady state simulations, solve the governing equations through a number of loop iterations at every time step; in this instance 6 iterations every 0.001 (simulation) seconds, then the calculated result at each node is saved for each time step or stated time interval. Upon the end of an iteration, the convergence value is either met or the maximum number of loop iterations achieved before solution of the subsequent time step can begin.

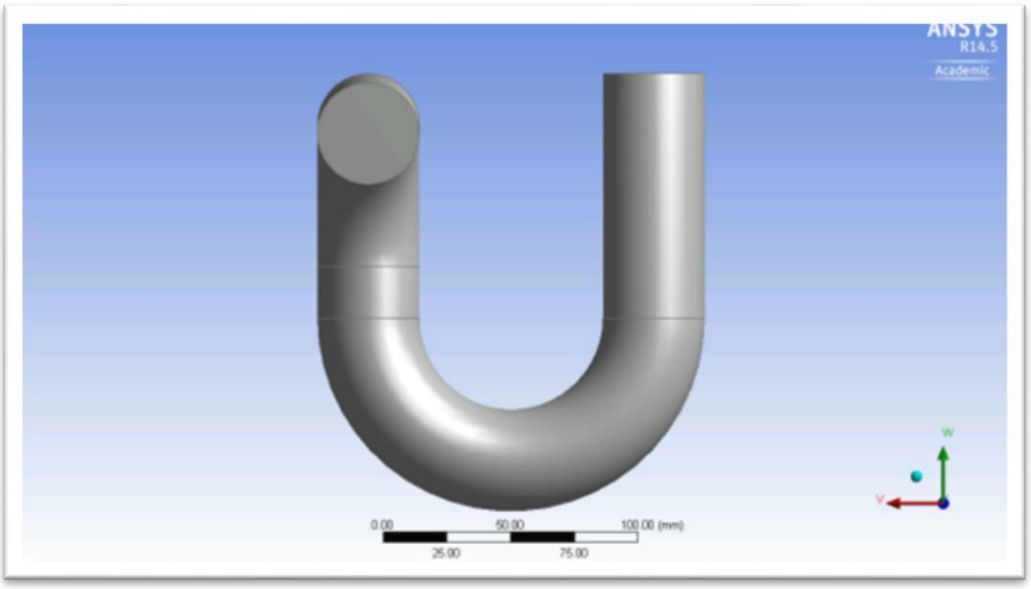


**Figure 4.** 1**, Front view of the laboratory appliance trap designed in ANSYS design modeller. System side of the trap located on the left of the u- bend and the appliance side of the trap on the right.**

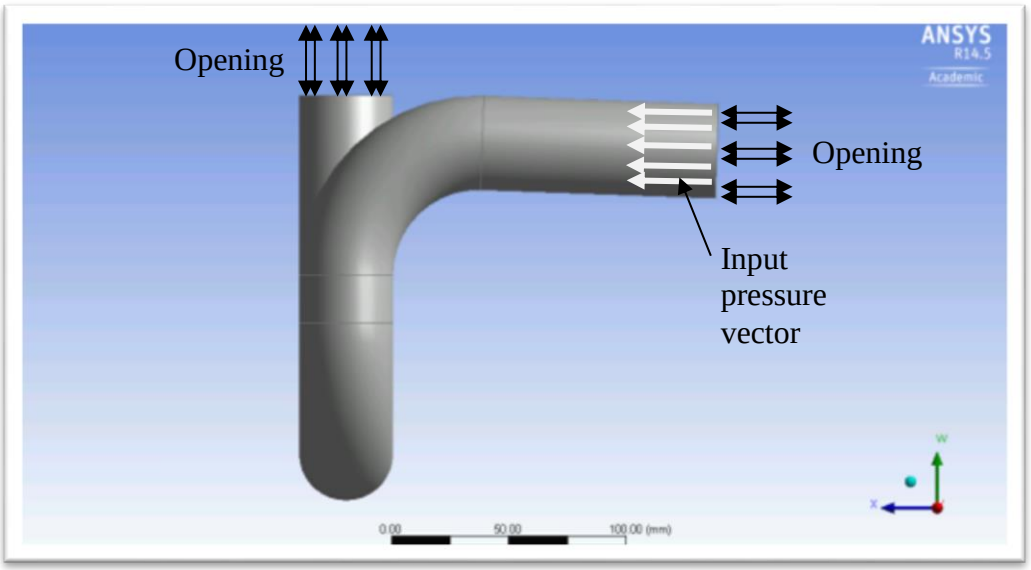


**Figure 4. 2, Side view of the laboratory appliance trap digitally reproduced using ANSYS design modeller showing specified entry and exit boundary conditions.**

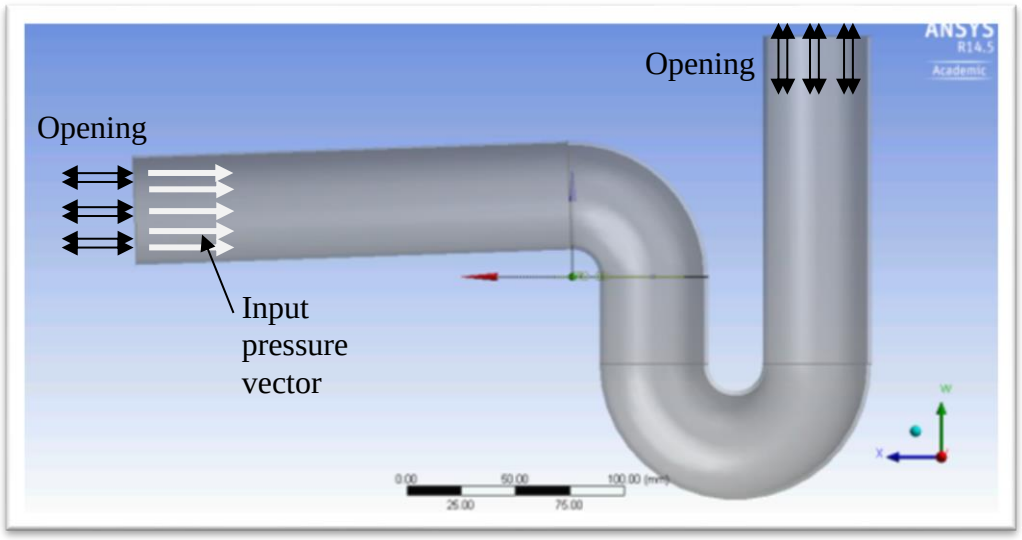


**Figure 4. 3, Front view of the commercial water trap digitally reproduced using ANSYS design modeller, showing specified entry and exit boundary conditions.**

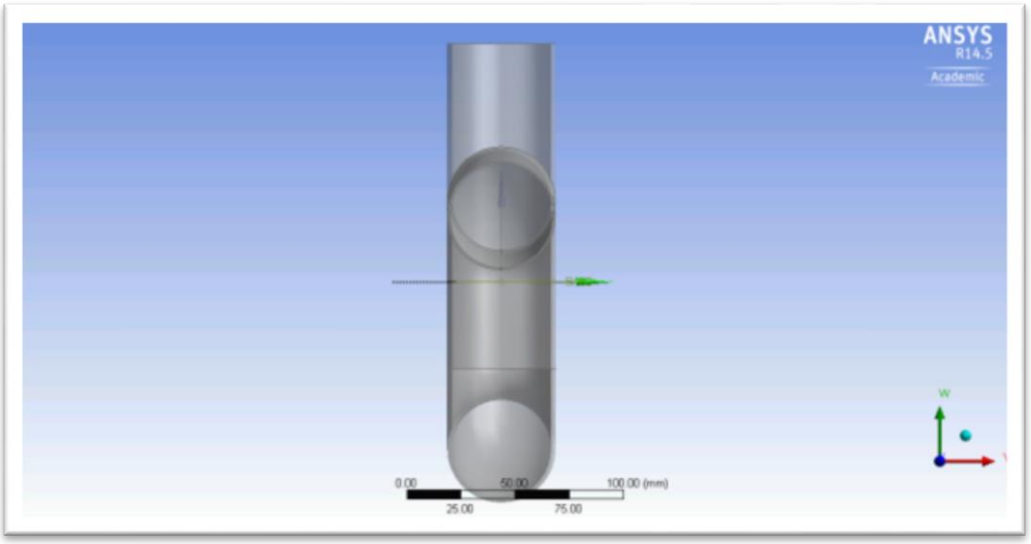


**Figure 4. 4, Side view of the commercial appliance water trap digitally reproduced using the ANSYS design modeller.**

### *4.4.2 Computational mesh*

The finite control volumes specified by the user, are the key to the advantage of this tool, as laboratory investigation poses limitations to such analysis. The finite positions for observation and data collection impose no disruption to the flow regime, therefore the accuracy of the data is largely dependent on the computational specification.

The geometry of the commercial trap was meshed with tetrahedral cells and the laboratory trap was meshed with prisms and hexahedrons. This difference in the shape of each control volume is due entirely to the differences in the shape of the trap (and the allowance for the software to calculate a 'best fit' automatically). This selection of control volume shape was determined by the ANSYS Mesh module. The size of the mesh was determined experimentally by assessing the number of cells generated upon varying the size profile to reach an optimised mesh (fit for purpose). Assessing first the coarse, medium and fine mesh resolutions, (and noting the size descriptors in each,) the mesh was then manually altered to attain consistency in either the number of elements or the mesh resolution in the commercial and laboratory appliance trap. Equality between the number of elements or nodes in the appliance traps was not attainable and so the size descriptors were set to ensure similarity.

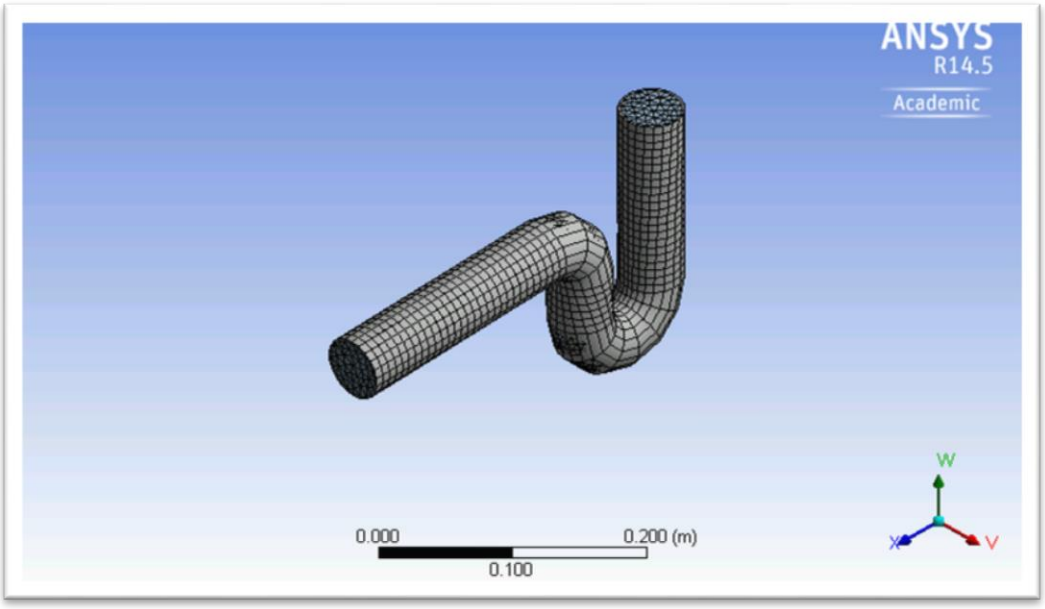


**Figure 4. 5, The computational mesh applied to the commercial appliance water trap**

A no-slip wall boundary was applied at the pipe wall. This no-slip condition is significant as it allows the fluid layer adjacent to the wall to have a velocity equal to that of the wall. Typically, due to this no slip condition at the wall, it is advised that inflation layers are used to refine the mesh along the pipe wall surface. For these simulations this approach was not employed. Simulations run using for instance the ICEM meshing tool, are however expected to be more accurate, without increasing significantly altering calculation time. It will be shown however in Section 4.4 (of the subsequent chapter), the disparity in results between the results from coarse mesh simulation and that on a fine mesh simulation.

The water trap seal was drawn in the ANSYS design module, here, only the fluid element enclosed by the pipe was specified. The mesh generated is derived of 806 215 elements, 832 128 nodes, 52 468 faces, and constructed predominantly from the 80 4683 hexahedrons but also by the addition of 1532 prisms. The commercial trap mesh generated (see Figure 4.5) is derived of 4541 elements, 20 528 nodes, 4116 faces, and

constructed predominantly from the 20 528 tetrahedrons. The comparable fine mesh in the commercial trap model, is derived of 4 424 807 elements, and 889 592 nodes.

A single domain was created within which the inlet, outlet and body of the trap were defined. The inlet pressure profile is set to the system side of the trap, at the end of the branch pipe. Results due to this placement provide a realistic representation of the pressure transients generated under normal working conditions.

### *4.4.3 Appliance water trap boundary conditions*

The definition of a multiphase flow requires as implied, the specification of the multi phases present within the flow region. In typical building drainage systems, water, and air are the main fluids, accompanied intermittently by traces of: detergent, bodily waste and food waste. For the purpose of this research, only water and air are considered.

Early models in this study divided the trap into separate domains where air and water exist, then attempted to model the flow by dispersing air at the face of the water body and not at a specified distance away (preferably at the pipe system entry point). This method prohibited the development of a laminar flow regime before surface interactions and so was considered to not adequately mimic realistic flow conditions. Future models addressed this.

The volume of fluid (VOF) method is an Euler-Euler method suitable for the prediction of free surface flows, movement of large bubbles, and stratified flow. Here, the movement of the phases is tracked by the interfaces. The standard Euler-Euler models are capable of handling very complex flows, but do not however, always give the best results since empirical information is needed in order to close the momentum equations (Andersson B.,*et al*, 2012). For a single domain to contain both air and water whether separated or dispersed, the VOF model in ANSYS CFD is recommended. Dispersed multiphase systems can be solved using either the mixture model or the Euler-Euler model. Andersson *et al*, (2012) explains that the VOF model is the only method available for describing and modelling separated flow conditions, and continues by

explaining that the within this model, single phase modes predict the flow regime where applicable.

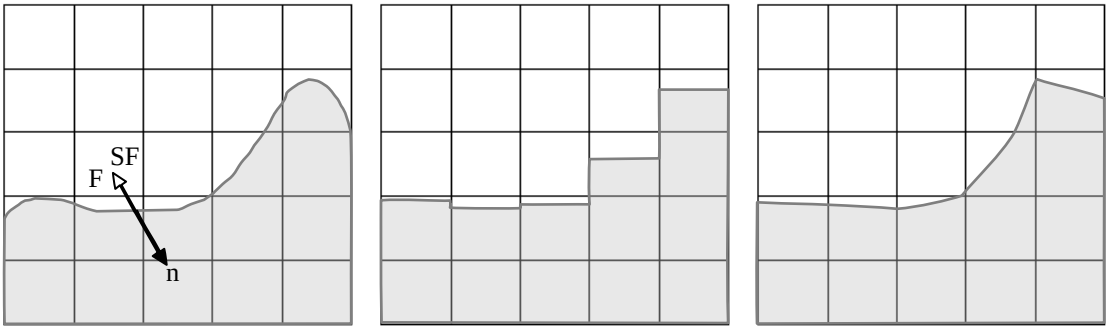


(a) (b) (c)

**Figure 4. 6, Volume of fluid (VOF) modelling of a fluid-fluid surface: (a) is the real surface, (b) the volume fraction calculated by the VOF model and (c) the linear reconstruction of the surface. Source: (Andersson *et al*, 2012)**

In order to clearly define the free surface region an expression is defined and written in ANSYS CFX expression language (CEL). The free surface boundary was after several experimental methods defined by:

$$VF_{air} = if(y\ coordinate > (H - H_s - D - W_T)[m], \\ 1,\ 0) \qquad \textbf{Eq. 4. 1}$$

and the volume fraction of water as,

$$VF_{water} = 1 - VF_{air} \qquad \textbf{Eq. 4. 2}$$

Where, $W_T$ is the pipe wall thickness, D is the uniform diameter of the trap, H is the total height of the trap, $H_s$ is the seal height.

The volume fraction (VF) of air and water is calculated per cell in the domain. For instance, an average scale shows that with a 38mm trap seal in the traditional water trap,

the average initial VF of air is 0.62459 and water, 0.3754. Meaning that at t = 0, 62.5% of the trap is filled with air and 37.5% is filled with water, thus creating the air and water columns. Volume fractions are always written as a ratio of the phases and sum to 1.

Inlet profiles within ANSYS CFX are set to either a velocity, mass flow rate or pressure value, and can seemingly only be defined linearly. To describe a fluctuating, step or ramped fluid flow a user defined subroutine is required or the expressions are to be written using CFX expression language (CEL). ANSYS CFX provides the option of customisation through User Programmable Features (UPFs) and User Defined Functions (UDFs). UPFS provide the user with the ability to customise the ANSYS program, extending the capabilities of the ANSYS Parametric Design language (APDL) of the code (Imaoka, 2009) by allowing user defined boundary conditions, material properties, source terms for flow regime, user customised model parameters, and enhances solution and post processing. (ANSYS, 2009). For this investigation CEL was used to describe the initial positions for the volume fractions of air and water, and the pressure input. Equation below shows the equations used in the simulations.

The boundaries at the pipe inlet (system side) and pipe outlet (appliance side) were pressure specified, and a fully developed sinusoidal altering pressure gradient, and a zero static pressure with atmospheric conditions specified respectively. Five simulations were conducted for each appliance water trap. With each simulation the frequency of the applied pressure varied while the maximum amplitude of the pressure wave remained constant.

$$Sine\ wave\ input = 100[pa] \propto sin(2\pi fT) \qquad \textbf{Eq. 4. 3}$$

Where T (current time), is divided by 1[s] to create a dimensionless figure.

### *4.4.4 Turbulence model*

Many models over the years have been developed to describe turbulent fluid flow conditions. Examples of the *Reynolds-averaged Navier-Stokes* (RANS) based models are: the k-$\varepsilon$ Model, Zero Equation model, Reynolds Stress Model (RSM), Re-normalised Group Model (RNG), New k- ε Model due to shih (NKE), Model due to Girimaji (GIR), Shi, Zhu, Lumley Model (SZL), k-ω Model, Shear Stress Trnasport Model (SST).

The Shear Stress Transport model used in the prediction of the air and water column movement in the water trap is a two equation eddy viscosity turbulence model. Developed by F.R. Mentor (1993, 1994) for the approximation of aeronautic flows with strong adverse pressure gradients and separation (Mentor *et al*, 2003) as the popular k-ε model. Wilcox (1993) notes that other turbulence models failed to capture the realistic behaviour of turbulent boundary layer up to separation.

The k-ω model on the other hand, is used for free surface simulations as it is substantially more accurate than the k-$\varepsilon$ in the near wall layer, and has therefore been successful for flows with moderate adverse pressure gradients, but fails for flows with pressure induced separation (Wilcox, 1993). This standard k-$\omega$ model was developed by Wilcox (1993). It was found however, that the K-ω model was very sensitive to the free stream conditions and so great care was required to reduce calculation errors obtained in regions where the fluid flows away from the wall.

To overcome this issue, the shear stress transport variation of Menter's model, has been developed with the aim of combining the favourable features of the standard k$\varepsilon$ model with the standard k−ω model in order that the inner region of the boundary layer be adequately resolved by the latter, while the former is employed to obtain solutions in the outer part of the boundary layer (Yeoh and Tu, 2009). A blending function is used to provide a smooth transition between the two models.

### *4.4.5 Solution controls*

The ANSYS CFX (FVM) uses a coupled solver where by the equations of pressure and velocity, are solved as a single simultaneous system. Here, the pressure equation is solved using alternate pressure values instead of adjacent ones forming a checker board pattern. Eese (2009) states that this means that an oscillatory pressure field, in which, for example, the pressure at consecutive grid nodes follows the sequence 1, 110, 1, 10, 1 etc, would be treated as a uniform pressure field since alternative grid points have the same value. Shaw (1992) suggests that a staggered grid is used to address this problem but that more recently like in ANSYS CFX, the Rhie Chow algorithm (presented in Rhie and Chow, 1983) is employed to address the vulnerability of decoupling under such conditions.

This solver requires the definition of a set of linear equations to compute the solution. These ordinary differential equations can be written in the form:

$$\begin{cases} a_{11}\emptyset_1 + a_{12}\emptyset_2 + a_{13}\emptyset_3 = b_1 \\ a_{21}\emptyset_1 + a_{22}\emptyset_2 + a_{23}\emptyset_3 = b_2 \\ a_{31}\emptyset_1 + a_{32}\emptyset_2 + a_{33}\emptyset_3 = b_3 \end{cases} \qquad \textbf{Eq. 4. 4}$$

Where, $a$ is a known coefficient of the variable $\emptyset$, and $b$ is a known value in the respective equation. Shaw (1992) cited in (Eesa, 2009) explains that this system can be written in the general matrix form,

$$[A][\emptyset] = [B] \qquad \textbf{Eq. 4. 5}$$

Where $[A]$ is a coefficient matrix, $[\emptyset]$ is the solution vector, and $[B]$ is right hand side of the matrix.

This equation is solved iteratively by starting with a guessed initial solution, $\emptyset^n$, and substituting it in Eq.4.5 to obtain a residual, $r^n$, thus

$$r^n = B - A\emptyset^n \qquad \textbf{Eq. 4. 6}$$

The multiphase solution method also uses the high resolution advection scheme. This scheme is used to discretise the convection terms. In this scheme, the blend factor, $\beta$ in order to satisfy boundedness and accuracy equals to 0 or close to, ensuring the it does not provide non-physical values. Shaw, (1992) suggests solutions under this scheme are easy to obtain as they are robust and therefore converge easily. The criteria for $\beta$ adopted in ANSYS CFX is based on the boundedness principles used by Barth and Jesperson (1989) cited in (Eese, 2009).

The second order backward Euler Scheme also employed is required as a transient scheme as it can accelerate convergence within the time step. The scheme initialises the solution within each time step by extrapolating the solutions from the previous two time steps, to the subsequent time step.

### *4.4.6 Convergence criteria*

For convergence to be reached at each time step, the iterative process must be controlled. The specification of a small time step interval along with sufficient number of iterations allows the solution meeting this aim as greater accuracy is afforded. However, the consequence to this requirement is an increased time requirement for solution.

For the solution of water trap seal movement in both the commercial and laboratory trap seal, the convergence value was set to $10^{-4}$. The simulation at each time step was found to have converged when the RMS value of the residual error $r^n$equalled the convergence value for all equations. In an effort to reach this level of convergence without extending the simulation time to any great level, 6 iteration loops were set. The calculation would terminate upon the achievement of this target of upon the maximum number of iteration being reached.

The imbalances for the multiphase simulation remain typically between 3.6299% to -3.7337% for all equations.

### *4.4.7 Summary of appliance water trap modelling*

The computational experimental setup of the multiphase flow in the commercial and laboratory trap seal was presented in this section. The section began by detailing the geometric requirements of the flow problem, detailing the computational mesh used making special note of the disparity in the resolution of the commercial trap seal mesh and the laboratory trap seal mesh. the method of specifying the boundaries, especially the water and air boundary is discussed in Section 4.4.3 and in 4.4.4, the turbulence model suitable for the modelling of multiphase flow is highlighted and it's computational development discussed. Section 4.5 continues by discussing controls required for a satisfactorily accurate simulation.

## 4.5 Model overview of a flexible sheath

This section presents the development of a simple model of the waterless trap seal for numerical solution, and describes the experimental setup of the geometric, boundary condition, mesh, physical parameters and solution controls.

The multi-physics modelling of a non-rigid structure is an important element in many product development and medical industries. This methodology involves ANSYS workbench within which a partitioned approach in the coupling of the fluid and structural solvers to define the calculation template. ANSYS and CFX are iteratively coupled through MFX using a standalone model in either Mechanical APDL or ANSYS mechanical and CFX. In this instance, ANSYS Mechanical (for solid mechanic solution) and ANSYS CFX (for fluid dynamic solution) are connection by the solvers. The design of the calculation template is completed upon the detailing of the connection algorithm; a one way or a two way connection between modules. One way coupling transfers data uni-directionally and is used in weakly coupled physics, or two way,

where the solid behaviour affects the flow of the fluid and the reaction of the fluid consequently impacts the behaviour of the solid (for example in elastics membrane applications).

The model structure within the ANSYS workbench (as described in Section 3.7.1) involves three main sections: the pre-processor, the solver, and the post processor. Here the pre-processor on the mechanical side of the model enables the detailing of the physical properties of the solid, then the geometric parameters. These geometric parameters are then shared with the fluid side of the model, and so there exist no requirement to draw or import the model repeatedly. The sharing of information occurs again between the solvers. Once the solution is complete, using a single post processor the results are shown comparatively.

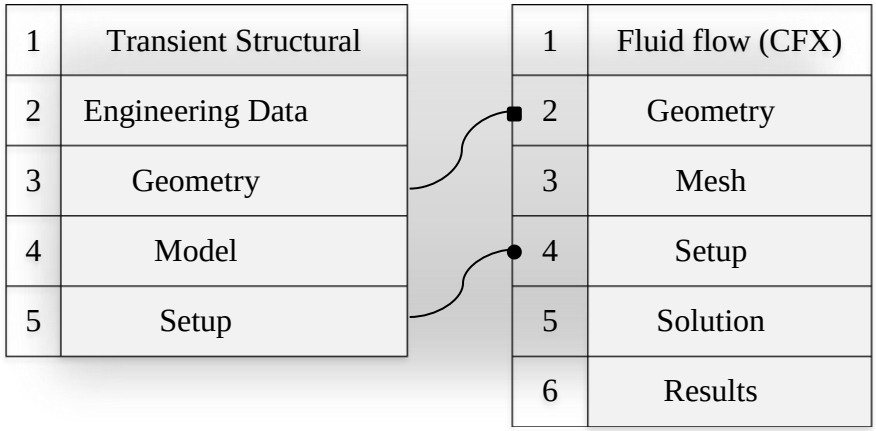


**Figure 4. 7, The setup for two way Fluid Structure interaction in ANSYS workbench**

In order to model the response of a simple non rigid structure comparable to the waterless trap seal, a sheath was assumed to be circular in cross sectional shape and seamless along the entire length. To obtain the dimensions for geometric representation, the lips of a reference product (Sample 1) were measured and the perimeter determined. Equating this perimeter to the circumference of the sheath, the equivalent diameter was determined to be 22.34mm, thickness of 0.16mm and the length, 55.25mm. Within the mechanical segment the properties of the sheath were defined. Table 4.2 provides the details listed in the Engineering Data module.

| | |
|---|---|
| **Density** | 1000 kg/m³ |
| **Young's Modulus** | $1.206 * 10^6$Pa |
| **Poisson's ratio** | 0.48 |
| **Bulk modulus** | $1.005 * 10^7$ Pa |
| **Shear modulus** | $4.074 * 10^5$ |

**Table 4. 2, The mechanical properties of the silicone sheath specified in the Engineering Data module**

Within the solvers the problem was described to be transient in nature, with a homogeneous single phase incompressible flow encompassed by the silicone solid.

.

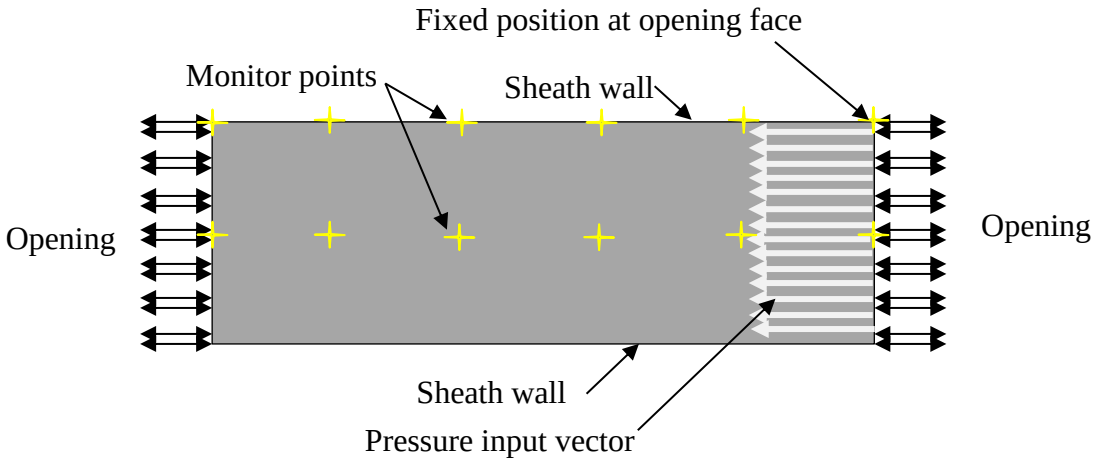


**Figure 4. 8, the setup schematic of the sheath in ANSYS CFX**

The FSI co-simulation model structure within the ANSYS workbench involves the ANSYS Mechanical (structure) setup and the ANSYS CFX (fluid) setup, linked by geometry and solution. Two-way coupling of data, as in a non-rigid structure problem; the flow of neither the structure nor the fluid is independent of the other.

### *4.5.1 Boundary conditions*

This subsection provides the details specified in ANSYS CFX of the physical parameters of the problem. Boundary conditions are required to express digitally what exists in reality. Boundaries can be the interface between two phases, junctions, changes in fluid flow regime, the beginning (inlet) and end of a product (outlet), as well as the interface between fluid and solid elements.

In this FSI simulation, the inner surface of the wall presents as the interface. Displacement of the fluid as it pushes against the structure is recoded as the force in ANSYS CFX and ANSYS Mechanical the total displacement. This force data is relayed to the mechanical solver and the total displacement to the fluid solver in a continuous iterative process.

The inlet and outlet are set to opening as the transient air flow drags air into and out of the boundary. Pressure input was set to 1500Pa for the constant pressure run, and 1000Pa for the stepped pressure run, normal to the Z-axis of the inlet boundary. At the outlet boundary, the static pressure was set to 0 Pa. The flow regime for both remained subsonic.

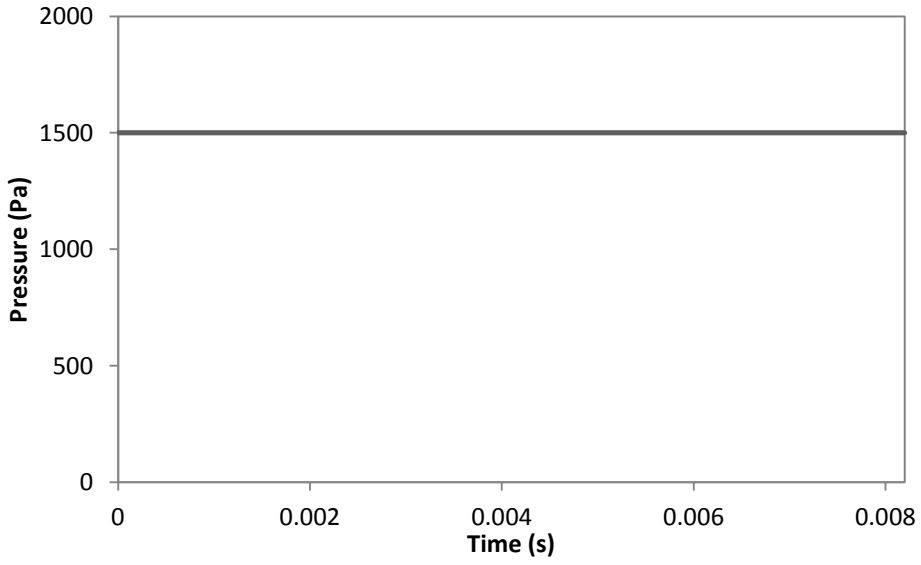


**Figure 4. 9, Steady pressure input profile**

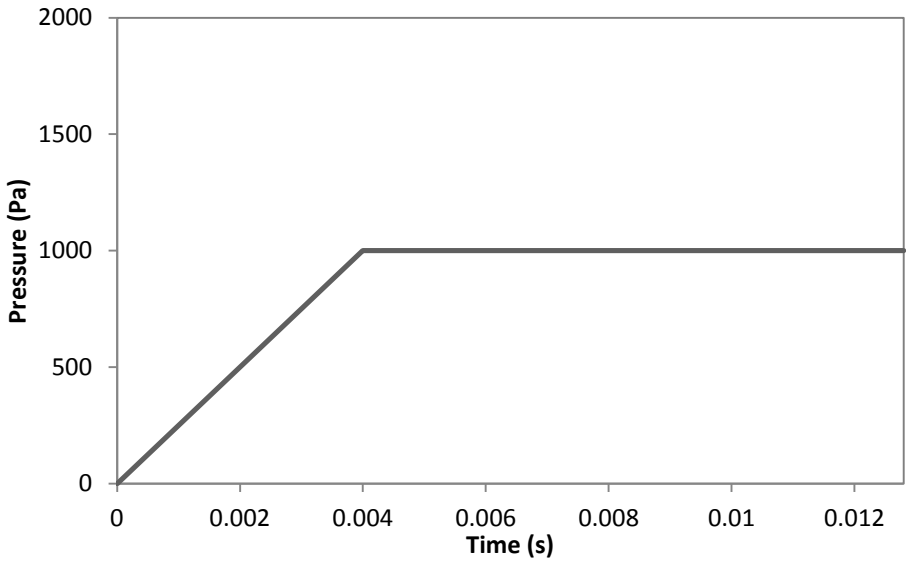


**Figure 4. 10, Stepped pressure input profile**

The brief length (time) of the digital experiment is thought to be due to the limitation of the hardware as after the end time shown in Figure 4.9 and 4.10 the complexity of the problem calls an end to the simulation. A stepped or ramped pressure input approach was hoped to increase the length of the solution. The solution however with a constant pressure input profile terminated at 0.0082s, a time comparable to the time at constant pressure in the simulation with the stepped pressure input profile.

### *4.5.2 Computational mesh*

The computational solution of fluid structure interaction problems is among the most complex in simulation studies. This is as the solution of both the mechanical and fluid elements are occurring simultaneously and so, whether in staggered or simultaneous motion, seamless data transfer between solvers is required. The time required to compute such a problem can be highly intensive and relies upon the selection of hardware, the choice of commercial CFD package (i.e. method of discretisation), the resolution of the mesh and size of each time step interval. The undertaking of the solution of this problem was immensely limited by the available hardware, but as failure in the solution are not always readily understood, experiments were conducted with

varying time steps and mesh resolution in an aim to discern and remedy the cause of the error.

The geometry of the flexible sheath was meshed in the ANSYS mesh module with tetrahedral cells. The selection of control volume shape was determined by the ANSYS mesh module. The size of the mesh was determined experimentally by assessing the number of cells generated upon varying the size profile. First the coarse, medium and fine mesh were assessed, then subsequently manually varying the size of descriptors. In this way, the global mesh size was determined giving a maximum cell size of approximately 0.6334m and a minimum of 0.00317m for the coarse mesh in the core region of the sheath.

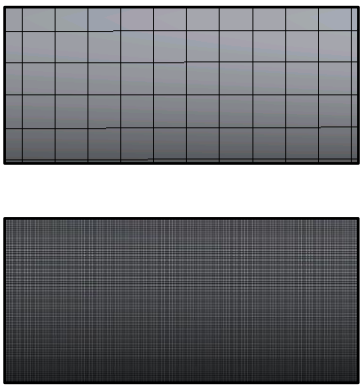

| | Fluid | Solid |
|---|---|---|
| **(a)** | 1872 elements<br>2204 nodes | 396 elements<br>2882 nodes |
| (b) | 119920 elements<br>125469 nodes | 7979 elements<br>55880 nodes |

**Figure 4. 11, Mesh resolution (generated in the ANSYS Mechanical module)**

The solution of the coarse mesh required 21 days to compute and therefore the fine mesh was considered unsuitable due to the time limitations of this study.

### *4.5.3 Turbulence model*

The K-epsilon (***k*-*ε***) turbulence model developed by Launder and Spalding (1974) was selected for this application largely due to its popularity in single phase simulations. The algorithms for transport prediction, calculate for two turbulence quantities, the turbulence kinetic energy ***k*** and its dissipation rate ***ε***. They are solved simultaneously with the equations governing flow behaviour; the momentum and continuity equations.

The width of applicability of the model is demonstrated by reference to numerical computations of nine substantially different kinds of turbulent flow.

The dissipation rate $\varepsilon$ is described by:

$$\text{Velocity scale } u_o = C_\mu^{1/4} k^{1/2} \qquad \textbf{Eq. 4. 7}$$

$$\text{Length scale : } l_m = \ l_e = \frac{u_0^3}{\boldsymbol{\varepsilon}} \qquad \textbf{Eq. 4. 8}$$

Giving a turbulent viscosity by the Kolmogorov-Prandtl expression

$$\mu_t = \ \rho C_\mu \frac{\boldsymbol{k}^2}{\boldsymbol{\varepsilon}} \qquad \textbf{Eq. 4. 9}$$

The constants $k$ and $\varepsilon$ are determined by the following Eq. 4.10 and 4.11.

$$\frac{\partial(\rho \boldsymbol{k})}{\partial t} + div(\rho \boldsymbol{k} \boldsymbol{U}) = div\left[\left(\mu + \frac{\mu_t}{\sigma_k}\right) grad\ \boldsymbol{k}\right] + P_k - \rho \boldsymbol{\varepsilon} \qquad \textbf{Eq. 4. 10}$$

$$\frac{\partial(\rho \boldsymbol{\varepsilon})}{\partial t} + div(\rho \boldsymbol{\varepsilon} \boldsymbol{U}) = div\left[\left(\mu + \frac{\mu_t}{\sigma_\varepsilon}\right) grad\ \boldsymbol{\varepsilon}\right] + \frac{\varepsilon}{\boldsymbol{k}}(C_{\varepsilon 1} P_{\boldsymbol{k}} - C_{\varepsilon 2} \rho \boldsymbol{\varepsilon}) \qquad \textbf{Eq. 4. 11}$$

Where, $P_{\boldsymbol{k}}$ is the turbulence production, $C_\mu$ is a dimensionless constant, $\mu_t$ is the turbulent viscosity.

The dimensionless constants in Eq. 4.7 and 4.8 are

$$\sigma_k = 1;\ \sigma_\varepsilon = 1.3;\ C_{\varepsilon 1} = 1.44;\ C_{\varepsilon 2} = 1.92$$

### *4.5.4 Interpolation and solution methods*

The process of coupling two solvers is performed using one of two methods. These methods provide immediate variable data for each node or element at each time step to the corresponding mesh. They are the globally conservative interpolation method and the profile persevering interpolation method.

The conservative interpolation method ensures that the profile is interpolated in such a way that the total variable data being moved from one mesh is identical to that received by the corresponding coupled mesh regardless of the mesh resolution.

Profile preserving differs as it maps the profile of a variable on one mesh and matches it onto the other mesh ensuring as much accuracy as is possible. Consideration must be taken in setup of the meshes on the fluid and solid or sender and receiver sides as in the profile preserving interpolation method the fine mesh is recommended on the receiving side, but on the sending side if using the globally conservative mesh.

Izhar, Qureshi and Khushnood, (2013) explains that in general, temperature and displacements are sent using the profile preserving scheme while heat flows and forces are sent using the conservative method. The criterion for mesh motion is specified in ANSYS CFX as a physical variable specification; where it is set to regions of motion specified. Upon the selection of Multi-field mode the interface requirement is complete as this automatically sets up the solvers to receive mesh displacement and fluid forces from each other. These two types of interfaces are automatically created when domains are formed.

#### *4.5.4.1 Finite volume-Finite element coupling Solution controls*

The iteration process described in Figure 4.12 shows the looped simulation procedure. The outer loop describes the flow from one time step to another. Within this process however, staggered loops involve the solution through iterations within each solver until the implicit solution is gained. ANSYS Mechanical and ANSYS CFX are able to run

calculation simultaneously or sequentially, with the force or displacement variables exchanged after each staggered iteration. In this study, data was transferred sequentially.

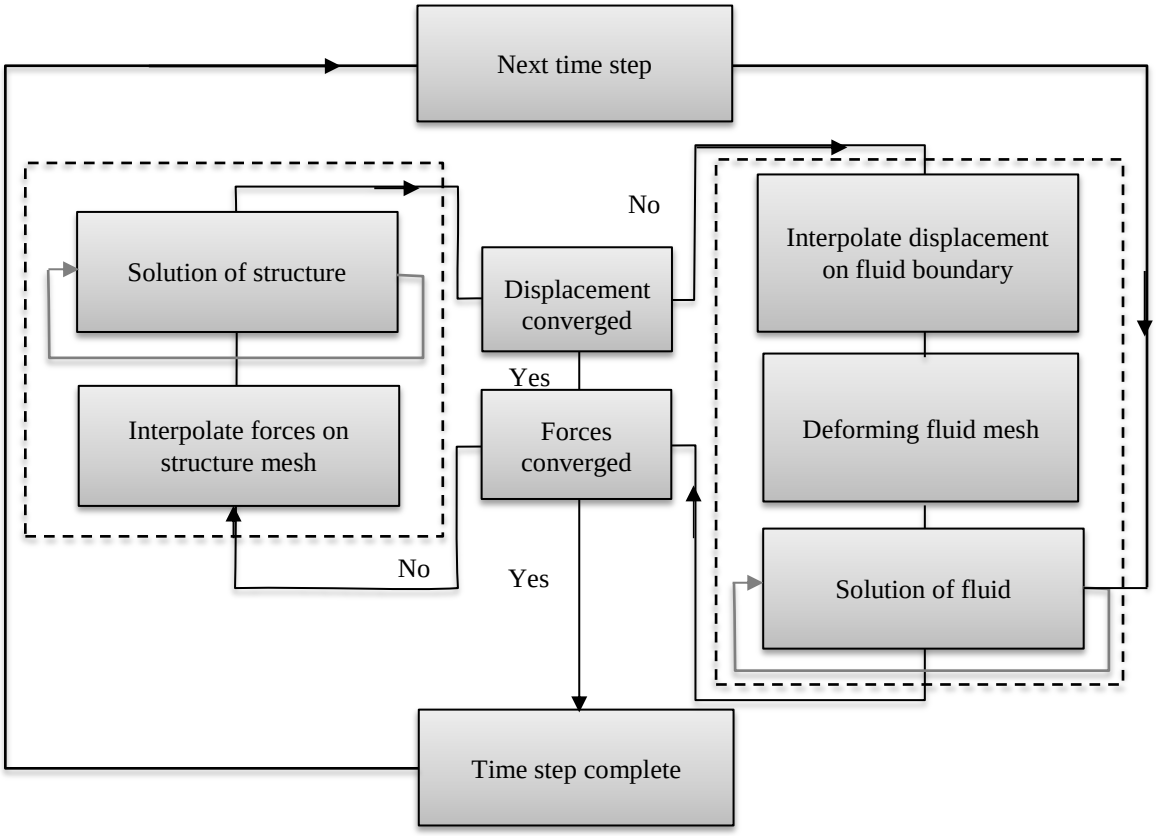


**Figure 4. 12, Flowchart of one and two way FSI solution coupling method**

#### *4.5.4.2 Convergence criteria*

As stated in Section 4.5.1, convergence is linked to the time step interval which plays a vital role on the length of time a solution requires to compute. In the FSI studies two situations where presented, a semi steady state flow and an unsteady flow regime. The time steps were $1 * 10^{-4}$s and $5 * 10^{-5}$s respectively. The solution was assumed to have converged when the root mean square (RMS) of the normalised residual error reached $10^{-4}$ in the fluid solver and $10^{-2}$ in the external solver. To reach this level of convergence, the calculation of the governing equations was conducted through 6 coupling iterations within which 3 coefficient loops. If convergence was not reached

after this number of iterations the solution continued to the next time step calculation and the % error noted in the normalised residual error reached.

### *4.5.5 Summary*

Section 4.5 can be described as the computational FSI methodology of the testing of the flexible BDS devices. The section has detailed the method employed to computationally assess the behaviour of a flexible membrane progressing through the development of the model, detailing the specified boundary conditions (the wall and fluid elements), the turbulence model selected and the rationale for the decision. By Section 4.5.4, the interpolation methods and criteria for the accurate solution of the FSI single phase problem is detailed. This process develops the methodology required to meet Objective 3 of this study.

The following section details the Laboratory method for FSI modelling which also contributes to the meeting of Objective 3.

## 4.6 Laboratory investigation of Fluid Structure Interaction

In addition to the computational FSI work detailed above, a laboratory investigation on the interaction between fluid transient flow and waterless trap sheath structural movement was carried out. The laboratory methods described in this section were designed to assess structural displacement over a range of airflow and pressure regimes. A novel method for assessing air through flow, a measure of sheath opening, was developed using photogrammetric methods from which a novel 1D model boundary condition was developed.

### *4.6.1 Laboratory method*

The Heriot Watt University John Swaffield Laboratory provided the ideal location thanks to the available test rig and apparatus to investigate of the mechanical behaviour and frequency of free through flow of a flexible BDS component (the waterless trap seal). This first attempt at the characterisation of the waterless trap required the development of a new technique, which required the development of a testing and analysis methodology. A twofold approach was developed requiring the simultaneous recording of the pressure response, and the mechanical response. The determination of the pressure response called for the measurement of the pipe static pressure reading, while the mechanical response is characterised through the imaging of the seal movement.

The tests conducted on the three waterless trap seals were performed in a continuous manner. Initial tests aimed to attain a steady state flow reading for the entirety of the test period using a compressor. For a single constant pressure regime a maximum time of 60s of pressure and photographic data could be gained. This method proved to be limited by the maximum available pressure or the size of the available compressor, but there were also limitation due to the time required to perform the tests in this singular manner. It was felt that by using the pressure transient generator, a greater range of pressures could be imposed onto the trap. With this method however, the limitation was imposed by the camera which could record for no longer than 60s, leaving very short time intervals for each pressure regime. The following figures show the chosen data set for each tested sample.

All photographic and corresponding static pressure data recorded during the 60s period was thus divided into data sets with respect to consistent pressure readings.

A test involved the following process:

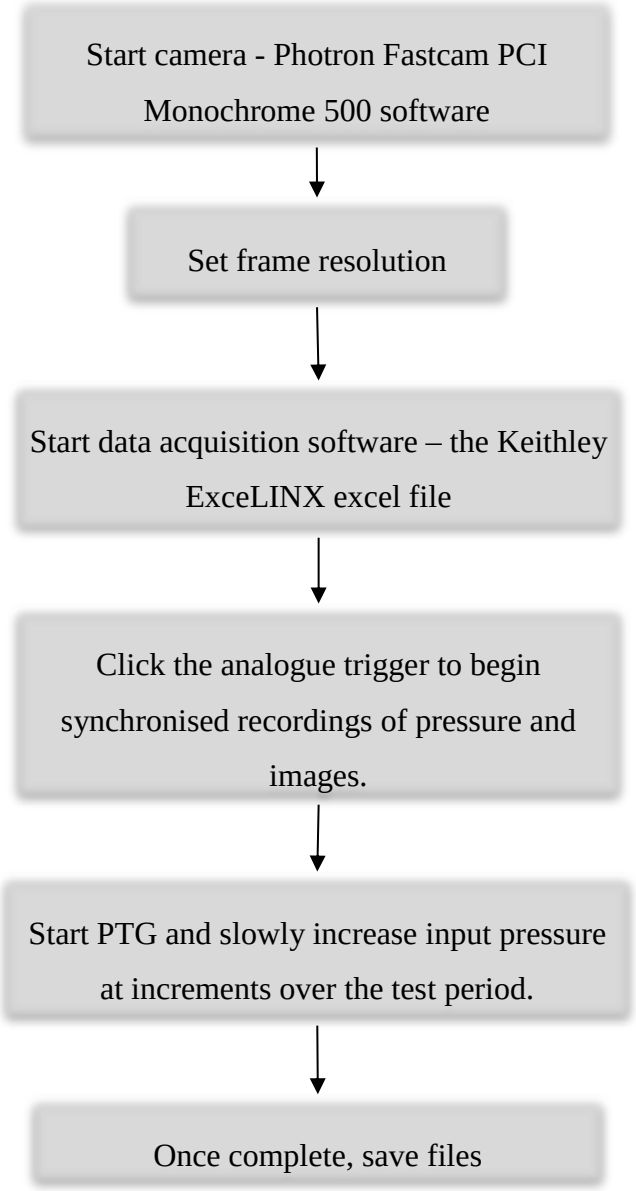


**Figure 4. 13, Flowchart of testing process**

### *4.6.2 Experimental apparatus*

This section of Chapter 4 provides a listing of all apparatus involved in the fluid structural assessment of the waterless trap seals. Details of the equipment used are provided. These include the test rig, the three reference waterless trap seals, the tools for data acquisition, the photographic imagining apparatus, the apparatus for air pressure measurements.

#### *4.6.2.1 Test rig*

At the centre of the laboratory investigation was the Pressure Transient Generator (PTG). The instrument design uses a radial fan housed in an enclosure to generate almost 2m head of water pressure. Since this exceeds the requirements for this research, the extra capacity is exhausted though variable sized vents in the box walls. This box enclosure stands above the ground level and is connected to a 2.5m long PVC pipe with an internal diameter of 51.5mm and an external diameter of 55.8mm, conforming to BS5255.

Static air pressure measurements were recorded using a pressure transducer connected to a high scan rate data logging system. The various waterless trap seals were connected to the end of the 50mm pipe and during a total time of 60 seconds, the pressure introduced to the pipe was gradually increased and the in turn reaction of the waterless trap seal, recorded using a high speed camera.

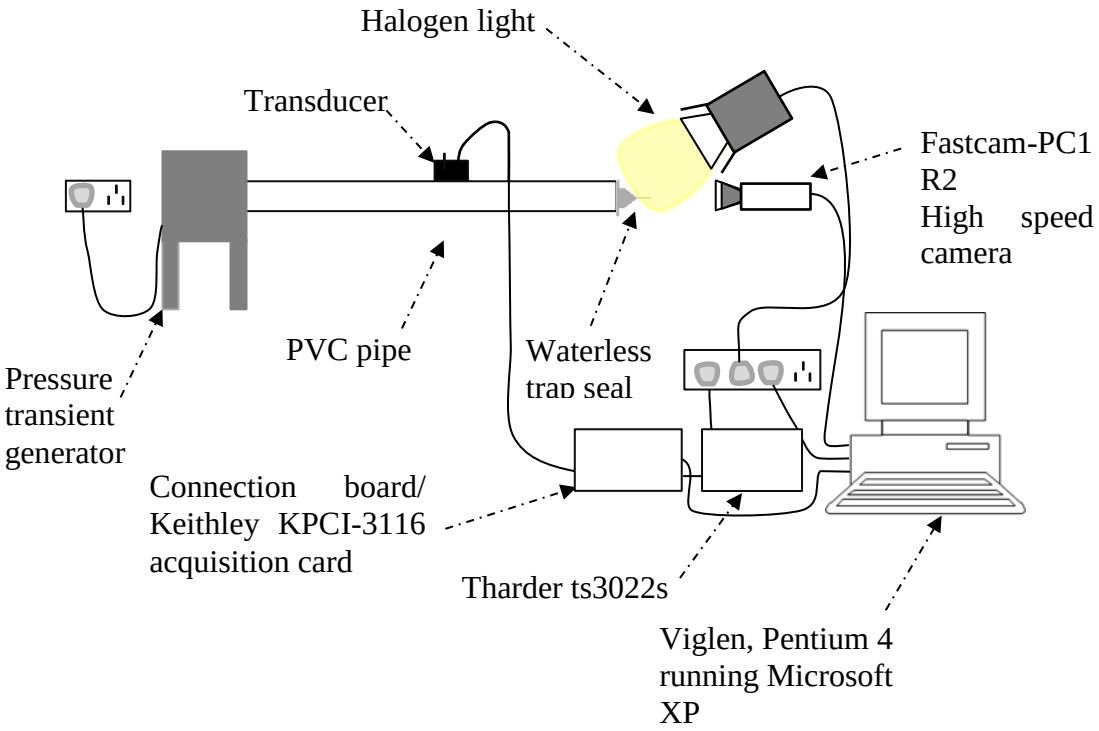


**Figure 4. 14, Laboratory test apparatus**

#### *4.6.2.2 Reference products*

Three sample waterless trap seals were used during the course of this investigation. They are named Sample 1, Sample 2, and Sample 3 due to the number to prototypes available in the laboratory. From Figure 4.15 it can be observed the differences and similarities between the three waterless trap seals. Sample 1 (left) is the smallest and thinnest of the three products while Sample 3 is the longest, thickest and has the largest pipe connector.

**Figure 4. 15, The reference waterless trap seals, Sample 1 (left), Sample 2 (middle), and Sample 3 (right).**

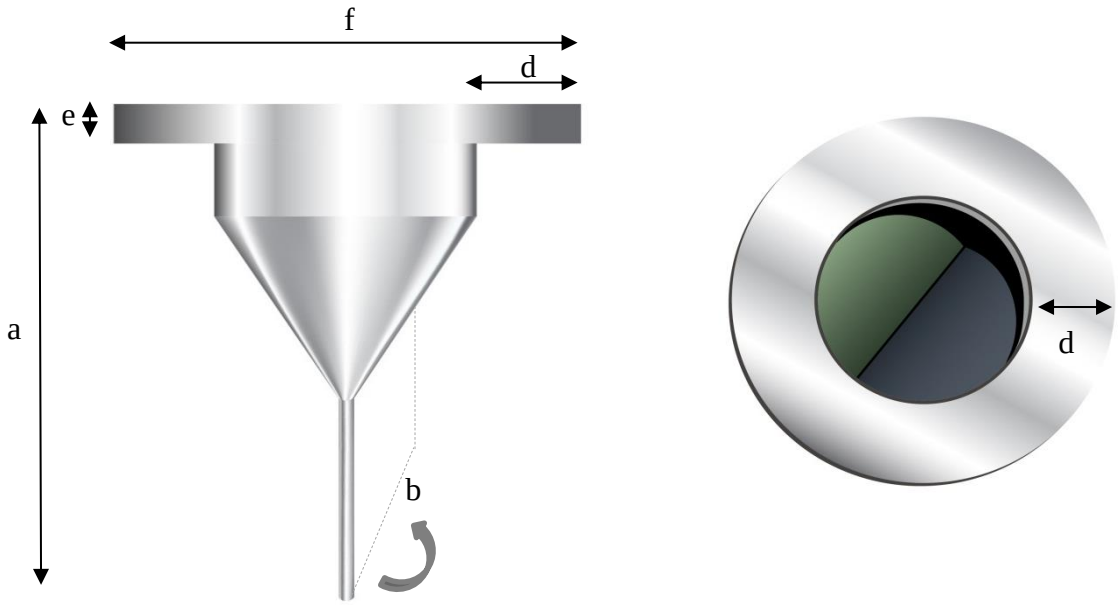


**Figure 4. 16, Side view of the waterless trap seal (left), Isometric top view of the waterless trap seal (right)**

| Key | | Sample 1 | Sample 2 | Sample 3 |
|---|---|---|---|---|
| **a** | **Total height** | 55.25 mm | 54.4 mm | 53.45 mm |
| **b** | **Lip width** | 35.1 mm | 39.44 | 36.18 mm |
| **c** | **Lip thickness** | 0.16 mm | 0.2 mm | 0.35 mm |
| **d** | **Rim width** | 3.04 mm | 2.74 mm | 6.39 mm |
| **e** | **Rim height** | 4 mm | 3.8 mm | 3.9 mm |
| **f** | **External rim Ø** | 33.16 mm | 38.86 mm | 38.72 mm |
| **g** | **Internal rim Ø** | 27.08 mm | 33.38 mm | 25.94 mm |

**Table 4. 3, Dimensions of the reference waterless trap seals**

The orifice, brought about by the end of the pipe fitting has an internal diameter of 31.89mm.This dimension can be compared to the internal and external diameters of the housed waterless trap seals and found that with the rim extending only 0.635mm off the internal edge of the pipe fitting orifice. Therefore, simply positioning the waterless trap

seal (Sample 1) without any additional aid during the prodding of pressure transients will result in significant forward movement. Sample 1 was instead placed within an adaptor 3mm smaller in diameter and positioned over the pipe fitting orifice. The internal diameter of this additional orifice is 28.8mm and external diameter 44.74mm. The pipe fitting external orifice diameter is 47.42mm.

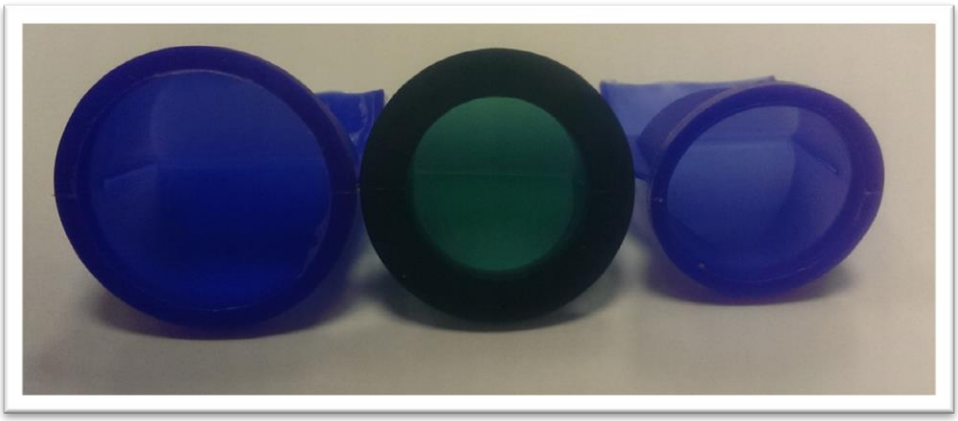

**Figure 4. 17, The three reference waterless trap seal positioned (according to size) to highlight the face connecting with the pipe fitting. Sample 1 (right), Sample 2 (left) and Sample 3 (middle)**

Figure 4.18 to 4.20 show these pictorially connected to the system and under an applied pressure:

**Figure 4. 18, Sample 1 connected to the 50mm pipe using a pipe fitting and adaptor**

**Figure 4. 19, Sample 2 connected to the 50mm pipe using a pipe fitting**

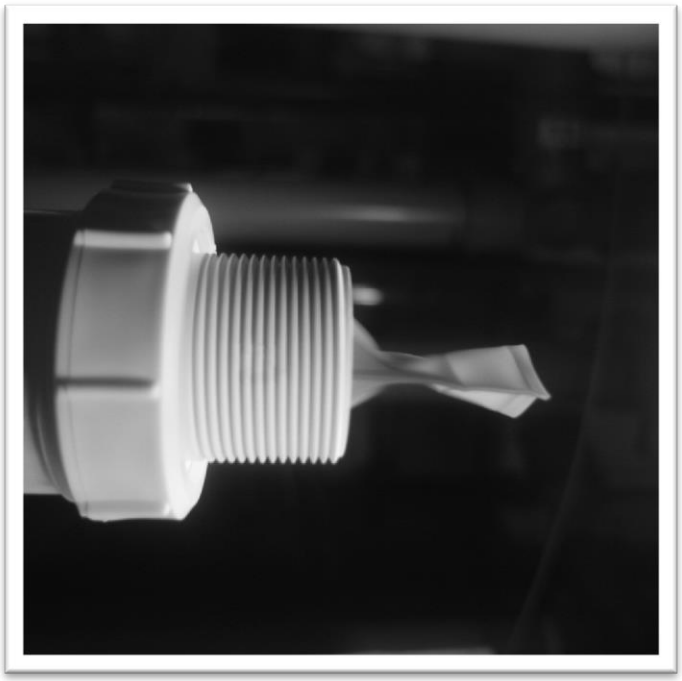

**Figure 4. 20, Sample 3 connected to the 50mm pipe using a pipe fitting**

#### *4.6.2.3 Data acquisition*

Pressure readings from the transducer were recorded through the Keithley KPCI-3116 acquisition card. This acquisition card or electronic board of 12 channels is triggered by a 5V signal. An analogue trigger was wired into the board and linked to the high speed camera, enabling the simultaneous recording of photographic data and pressure readings. The pressure readings and photographic images were set to record at a rate of 250 fps.

#### *4.6.2.4 Photographic imaging (camera and lighting)*

The camera used to conduct this investigation is the Photron Fastcam PCI Monochrome 500. The maximum recording time is predetermined by the camera memory, and as images are recorded at a rate of 250 fps, the maximum recording time relies on the

resolution of the frame set to establish the length of the recording. The total time for each test in this investigation was set to the maximum available, 60s, and so a total of 15 000 photographic images were recorded using the Photron FASTCAM Viewer software package version 2.1.1.6. Each image was saved individually and labelled as a number sequenced jpeg file. The high speed camera was required to record images concurrently with the voltage readings from the transducer, so that images and pressure readings were comparable. This function was enabled by the use of an analogue trigger.

Two Interfit Stellar tungsten 750 luminaires each positioned on a tripod stand, and housing 3 halogen lamps, provided the appropriate lux levels for the optical lens of the high speed camera to receive and focus the light from the test apparatus, before reaching the sensor and becoming a greyscale image. A high level of lighting was required on the lip of the waterless trap seal in order to provide a sufficient level of contrast between the colour of the trap seal and the colour of the pipe opening. By the theory of depth in photographic studies, it was aimed that within each frame, objects found close in distance to the camera would appear in as light a colour as possible and images further away, appear dark. Quite advantageous to this aim was the fact that darkness existed regardless due to complete closure of the pipe nay the opening of the waterless trap seal.

#### *4.6.2.5 Air pressure measurements*

Air pressure measurements were yielded using transducers which emit a voltage signal alternating in parallel with changes in air pressure. A transducer was connected to the pitot-stat tube near the end of the pipe to measure airflow. The +/- 500 mm wg voltage transducers used during this investigation to determine the static pressure along the pipe, requires a DC supply of 12 volts and so the Thandar ts3022s (a rectifier) was used. The transducer is connected to a hole at the top of the pipe wall and measures the static pressure level $P_{stat}$ by converting the reading in time to a voltage (between 1 to 6 volts). This voltage reading is then fed to the laboratory computer in the form of a digital signal using the 16 bit A/D converter card, and converted to a mm wg measurement.

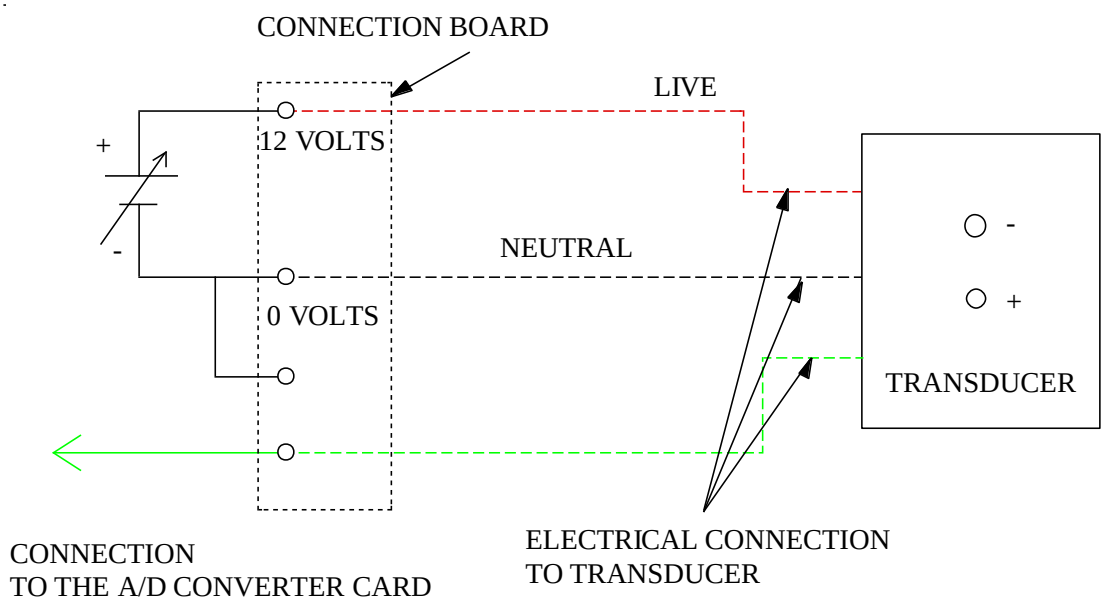


**Figure 4. 21, Schematic of a typical transducer and A/D converter card electrical connection**

The transducer described above is not available as standard and was obtained from the manufacturer as specially made devices.

### *4.6.3 Laboratory setup*

Experiments were carried out on a test rig installed within the services laboratory at Heriot-Watt University. The rig consisted of one Polypipe horizontal Acrylonitrile Butadiene Styrene (ABS) pipe of 1.33 metres length with an internal diameter of 51.79mm and an external diameter of 55.8mm and thickness of 2.39mm, conforming to BS5255. Hereinafter, the pipe shall be referred to as 50mm Ø.

The high speed camera was used to clearly see how the flexible sheath reacted to the propagation of transients. The camera, a Fastcam PC1 R2, allowed accurate visual readings and enhanced resolution of the waters response in greyscale still shots.

The transducers required a D.C. supply so a Tharder ts3022s was used for the conversion of A.C. electrical power. The transducers used were connected to the function generator then to the data acquisition card within the Pc. The voltage output

from both transducers were logged by a Viglen workstation computer through the on board analogue to digital conversion port. This port was capable of monitoring 32 separate channels, which was in excess of what was required but would in no way cause any complications to the actual results.

The laboratory setup and methodology for testing of the commercial waterless trap seal is given below. This setup was used to evaluate the pressure control capabilities of the waterless trap.

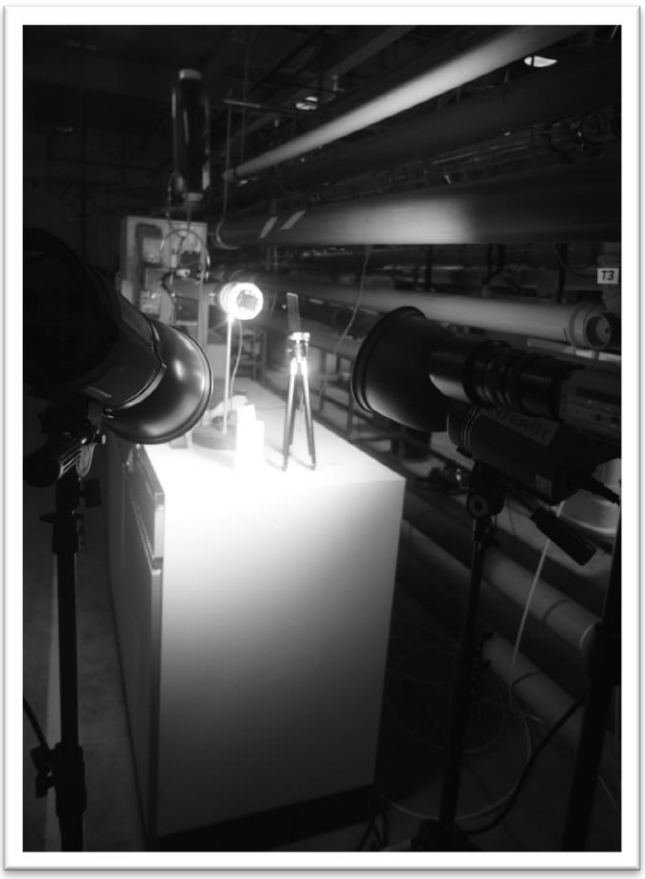

**Figure 4. 22, The setup of the laboratory equipment. Halogen lamps are positioned to illuminate the lips of the waterless trap**

#### *4.6.3.1 Transducer setup*

The transducer operates by linking a known pressure to a voltage reading, therefore the range of expected pressures experienced within the system must lie within the transducers range to afford accurately in the measured data. The accuracy in this measured data is also closely linked to the differential between the transducer output and the actual value. Linearity is the closeness of a calibration curve or output of a transducer to a straight line.

Calibration of the transducer provided a linear relationship between the output voltage and pressure for the $\pm 500\ mm\ wg$ transducer. This relationship is described below.

$$\boldsymbol{V} = 0.01P + 3.393 \qquad \textbf{Eq. 4. 12}$$

Where $P$, pressure, is measured in mm wg.

### *4.6.4 Accuracy of results*

#### *4.6.4.1 Camera*

For the most part, the setup of the camera in relation to the position of the waterless trap seal and by extension the pipe is along its centreline, some distance away. Movement along the $90^0$ plane to this line is noted in the images for Sample 1. The centreline of the devices however where positioned to ensure the centrelines though not always aligned were at least close to parallel.

The calibration of image data, described in Chapter 6 makes note of the scale of the images being equal.

#### *4.6.4.2 Data recording rate*

By calculation of the camera frame rate, the highest expected frequency of the sinusoidal wave is 125Hz assuming half the time step equates to the rise time of the wave. This frequency presents as a possible limitation to the accuracy of the readings as

possible motion could have been missed by the camera. When testing a new product difficulty is faced in ensuring that the equipment chosen is always the best fit for the purpose. In the case of a high speed camera, it is not always possible to fully anticipate the range of motion of an object.

#### *4.6.4.3 Data acquisition*

The data acquisition system is capable of two types of error: system and human error. Accuracy is reduced when mistakes are made during calibration and software setup or via a fault in the hardware or software.

#### *4.6.4.4 Alignment of valve*

Care was taken to ensure that the length of lip of the waterless trap seal was positioned horizontally though movement during operation was observed. Inaccuracy in the height and width measurements is likely as the force applied to the waterless trap seal tends to cause slight rotation about the orifice connection the seal to the pipe. As the orientation cannot be determined via the images, the angle of movement in relation to the pipe pressure cannot be determined. As the degree of rotation is not known, the assumption (in Chapter 6) is that no rotation of significance occurred.

## 4.7 Conclusion

The methodology for laboratory and computational experimentation is presented in this chapter. The chapter begins by providing the details of the software, hardware, numerical models and laboratory set up are given. Data acquisition, from laboratory and CFD systems, is a challenge in the context of the reference products being discussed in this thesis. Significant difficulties surrounding read/write times on the CFD calculations are particularly problematic and were found to be more significant than number of processor cores on a desktop PC. It should be noted again that the use of

commercial CFD software has never been used for boundary condition development before and so, this study possesses a unique view of the pros and cons of the technique. The limitations found are also discussed.

# Chapter 5

## Numerical Analysis of Multiphase flows in Appliance Traps

### 5.1. Introduction

This chapter presents the results of the numerical analysis of low pressure transient propagation in water trap seals. The methodology outlined in Section 4.2, introduced the examination of the flow regime and unsteady friction analysis through the use of CFD. The methodology employs an applied air pressure transient of single frequency which allows the water trap response to be evaluated. The detail provided by computational methods far overreaches that possible in laboratory investigations, leading to potentially more realistic boundary equations. An obvious difficulty however exists in validating this data as in many cases it is not possible to be collected economically through available laboratory methods. Where possible comparison is made to previous research, providing discussions of data validity.

At the centre of the difficulties surrounding the development of boundary equations from laboratory investigation is the complex distribution of frictional forces within a water trap. These frictional forces are unsteady and are not equally distributed throughout the flow area. Unsteady frictional representations for multi-phase water and air mixtures in curved conduit U-bend water traps are not well understood. The friction factor in a closed conduit is determined using the Colebrook-white relationship; however, the body of research leading the development of the Colebrook-white relationship is based on steady, fully developed flow conditions, making its use in transient modelling problematic.

This chapter aims to address Objectives 1, and 2 of this research project; Using CFD as a tool to determine the unsteady flow characteristics of the water trap seal, and develop the analysis method (of the full methodology commenced in Chapter 4) for deriving a deterministic frequency dependent boundary equation suitable for the MoC model.

Section 5.3, highlights the body of data extracted from CFD, while Section 5.4, presents development of a new frequency friction factor for transient flow in appliance water trap seals. Section 5.5 concludes this chapter.

## 5.2. Computational mesh resolution

This section provides the results of the effects of mesh resolution on the computational study of the water movement within the appliance trap seal. In the previous chapter, (Section 4.4.2) it was detailed that two mesh sizes were investigated for the commercial trap seal. This was done in an effort to select a mesh close in resolution to the laboratory trap seal mesh. However, due to time constraints the coarser mesh was selected to perform the main data collection. A comparison of the disparity or similarity between the results is presented below.

The quality of the mesh specified by the user plays a major role in the accuracy of the results as previously noted. It is widely accepted that all simulations are erroneous, but they can however depict realistic flow conditions within reasonable physical variable estimates.

The coarser the mesh the more errors which are introduced into the field of results, but reversely, the more intricate the calculation mesh specified is, the greater the time required to complete the simulation. User discretion is therefore required here in analysing the cost- worth benefit of increased calculation time for a certain percentage increase in model accuracy.

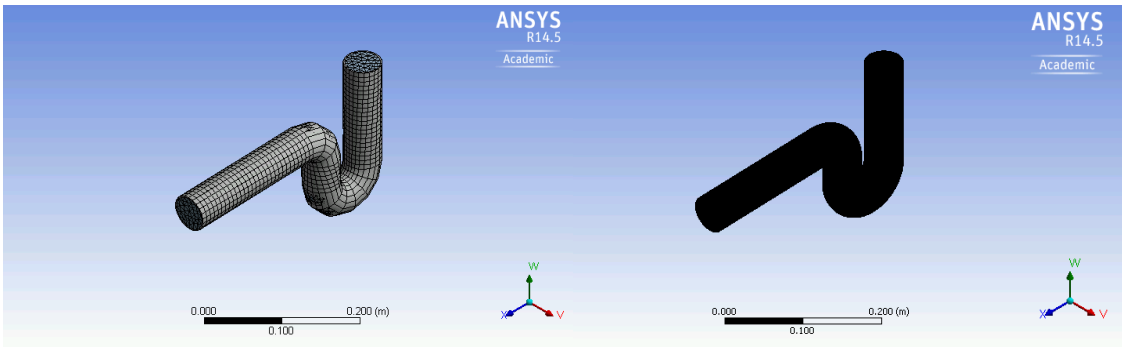


**Figure 5. 1, Screenshots of the commercial appliance water trap with a coarse computational mesh (left) and the commercial appliance water trap with a fine computational mesh (right)**

In this application, the aim of the model is to determine the fluid mechanics in a water trap seal, thus providing designers and researchers with a greater understanding of the conditions likely to compromise the seal between the indoor environment and sewer network. Under research conditions of greater funding and longer time frames, accuracy could be sought to ensure that the flow condition under which depletion of the seal can be satisfactorily predicted. The use of the coarser mesh in this application will however, provide reasonable insight into what would otherwise be shown in greater detail while enabling Objective 2 (the development of new methodology) to be achieved.

### *5.2.1. Accuracy of computational results*

In an effort to express the degree of disparity between the coarse and fine mesh used for the commercial water trap seal assessment, the average and maximum fluid velocity readings within the trap, the average velocity along the seal bend and the disparity in mesh resolution are presented.

The number of elements generated in the coarse mesh and fine mesh is 4541 and 4424807 respectively. The results of the mesh comparison simulations provide that the average velocity in the commercial trap with a coarse mesh is 0.0165m/s and 0.0131m/s in the fine mesh with a max velocity of 0.166 m/s and 0.145 m/s respectively at 0.025s

(when a 10Hz transient air pressure is applied). These results show that there is a difference of 0.0034m/s in average velocity results for a 973 412% increase in the refinement of the mesh. Note from Figures 5.2 and 5.3, the velocity profiles along the bend are alike but differ most significantly at the fluid/fluid interface and inlet. The differential between average velocities in the two simulations along the curve of the trap is 0.00196 m/s.

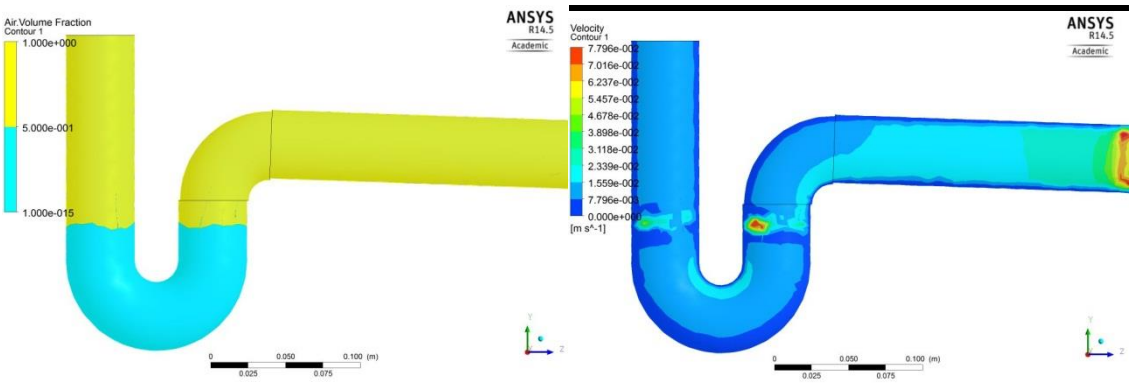


**Figure 5. 2, Screenshots of the commercial appliance water trap (left) volume fraction of air in the coarse mesh simulation (right) fluid velocity in the coarse mesh simulation – 10Hz at 0.025s**

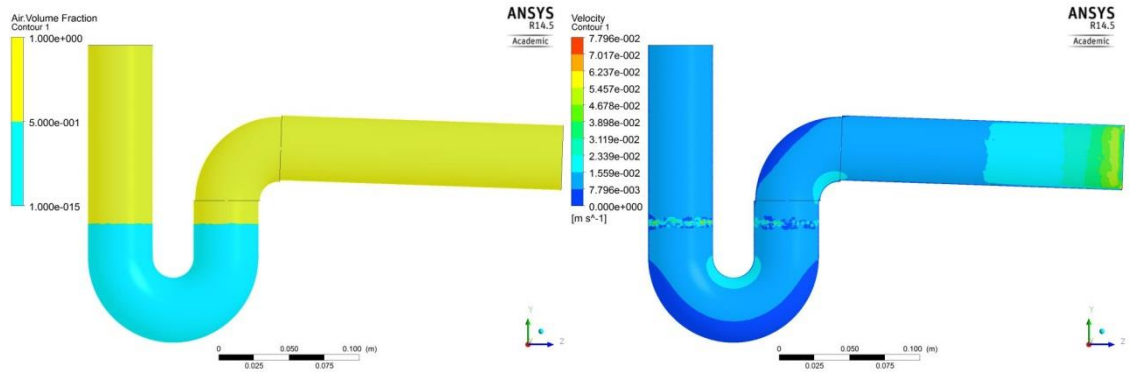


**Figure 5. 3, Screenshots of the (left) volume fraction of air in the fine mesh simulation, (right) fluid velocity in the fine mesh simulation - 10hz at 0.025s**

The quality of the mesh generated for the simulation is significant to the results, as can be seen from the variances in flow regime outside the trap seal. However, a $\pm 2\%$ variance in average readings is sufficiently small to suggest satisfactory accuracy in the coarse mesh data. The interesting point here is that, though a small discrepancy exists in the velocity profile and water volume fraction within the commercial trap seal, across the two simulations of the commercial trap seal, Figures 5.2 and 5.3, show that the velocities along seal bend are consistent.

A judgment on the accuracy of the results based on laboratory comparative data is unobtainable due to the nature of the experiment. Velocities along the bend of the trap seal have never been obtained due to the challenges associated with recording accurate data without influencing and obstructing the fluid flow. The following sections therefore present the data analysis leading towards a new boundary condition methodology using the results of the coarse mesh data.

## 5.3. Fluid flow in the appliance water trap seal

When an air pressure wave comes in contact with water in a trap a shockwave is produced which inevitably changes the flow regime in the trap. This flow regime in a BDS is one whose nature may comprise the characteristics to allow free movement of omnipresent air, and with it, potentially harmful microbiological matter across the trap seal bend, causing cross contamination. Influences such as, the trap design (ratio of inner and outer appliance bend length), inner pipe surface characteristics, the amplitude of the applied pressure, and the duration of the applied pressure transient, all account for the magnitude of the water seal's displacement.

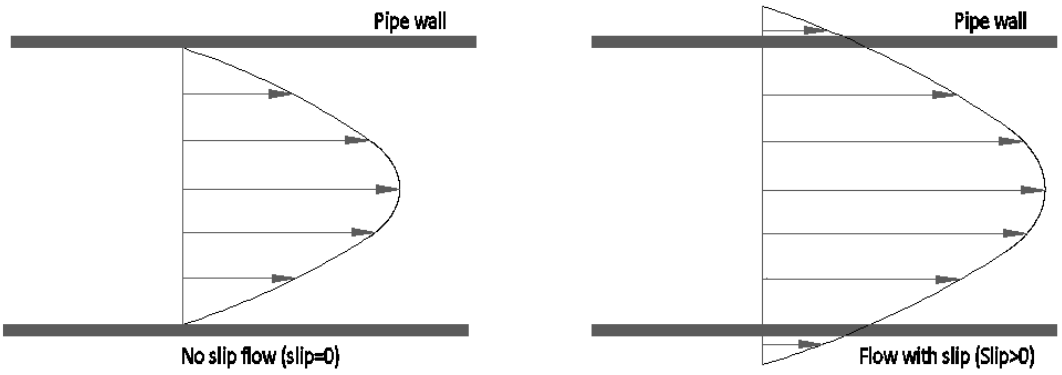


**Figure 5. 4, Air propagation through pipe (a) with no slip condition, (b) with slip**

Consider a no-slip condition in a straight pipe of a finite length. Parallel to the pipe walls the water column is divided into a series of rows which run the entire length of the column. Pressure applied uniformly at the cross sectional entry is expected for the most part, to displace all rows in equal proportion. Relate this scenario to a curved conduit, and uniform displacement becomes unlikely due to the disparity between the lengths. The shortest column will move the greatest distance as (all elements being equal) it presents the least resistance to movement. Under steady state conditions, this row in greatest motion will continue to increase in velocity as more eddies build behind the deformed water column. Newton's second law of motion provides that

$$F = MA \qquad \textbf{Eq. 5. 1}$$

Therefore the smaller the mass of the object (in this instance, water) to be moved the greater the acceleration for an equal force. Friction can be thus said to be a construct of the length of the water column and as the rate of change of the flow conditions is inherently linked to the rate of change of the driving functions, the friction. Generally frictional effects act to damp the pressure fluctuations following pressure transient propagation (Douglas *et al*, 1995).

### *5.3.1. Selection of reference point*

Swaffield, (2010) states that generally, the rise time of appliance discharge is seldom less than 2 or 3 seconds. Therefore the resultant transients are generally slow moving, meaning that the time taken to reach the peak amplitude is lengthy in comparison to the time of a pipe period. For instance, the pipe period in a 20 storey building with a stack height of 60m is 0.3s (Swaffield, 2010). So in the time is takes a wave to reach its maximum within the system, numerous reflections will occur thus increasing the amplitude of, and speed of the applied wave. In order to analyse the effect of the applied pressure transient without alteration due to reflections, a reference point for data comparison should be considerate of the pipe period.

This reference time would enable the collection of results devoid of any reflections. However, in such an instance the amplitude of the applied pressure would vary and so any conclusions would be based on the applied pressure and not the frequency. The first peak data was selected and used as a reference point as it gives the required rise time for a given frequency. After the first peak time a modulation occurs in all simulations which make it difficult to ascertain the effects of the given frequency on the seal. A secondary option which would satisfy this problem is to consider a constant pressure amplitude which occurs in all frequencies before the first reflection is anticipated. Comparisons are therefore made between 0 and 0.25s to avoid the effect of reflections and allow consistent comparison of data at the first positive peak.

Below, images of the effect of the applied pressure wave are presented for all tested frequencies in both laboratory and commercial appliance trap seal. The first time (a) presents the position of water and air in the water trap by making reference to the volume fraction of air, (b) and (c) present the velocities of both fluids in relation to the maximum flow velocity (0.25 m/s) in all simulations.

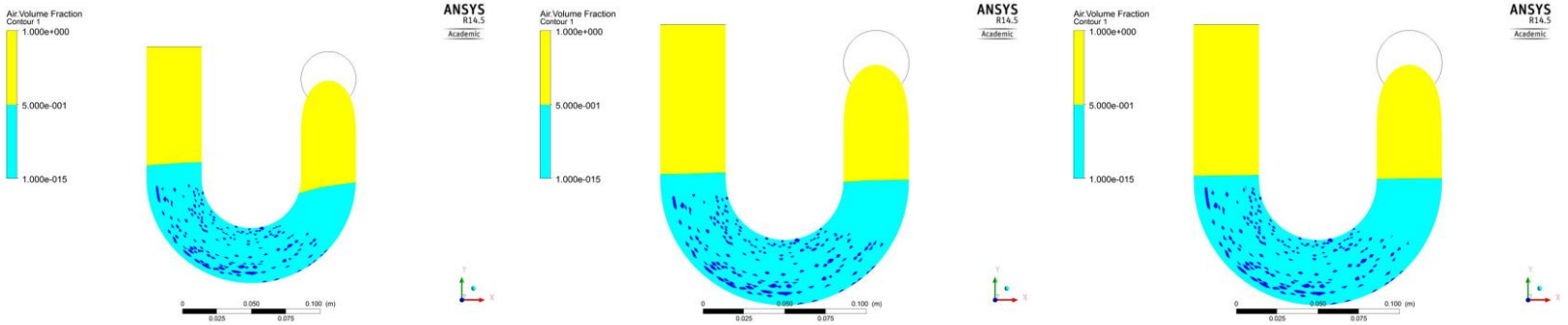


1 Hz (a) 2 Hz (a) 3 Hz (a)

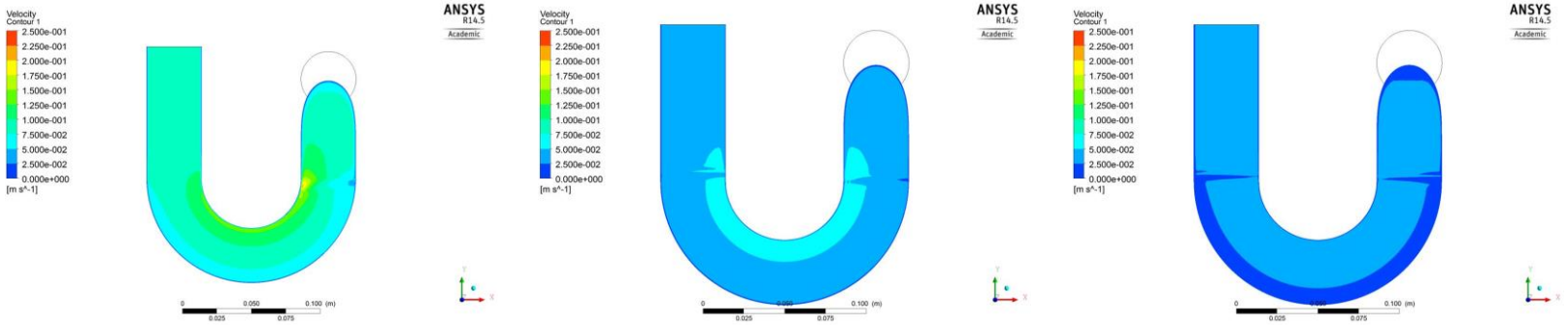


1 Hz (b) 2 Hz (b) 3 Hz (b)

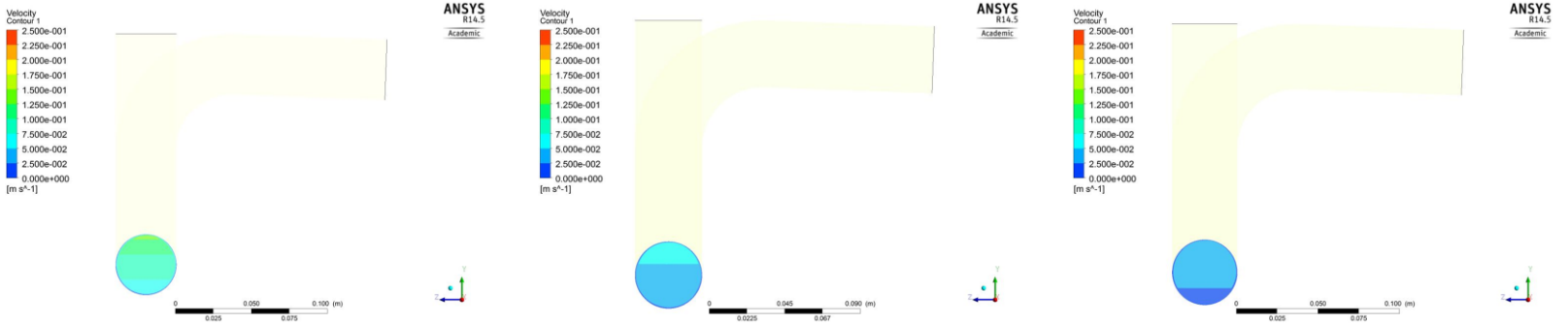


1 Hz (c) 2 Hz (c) 3 Hz (c)

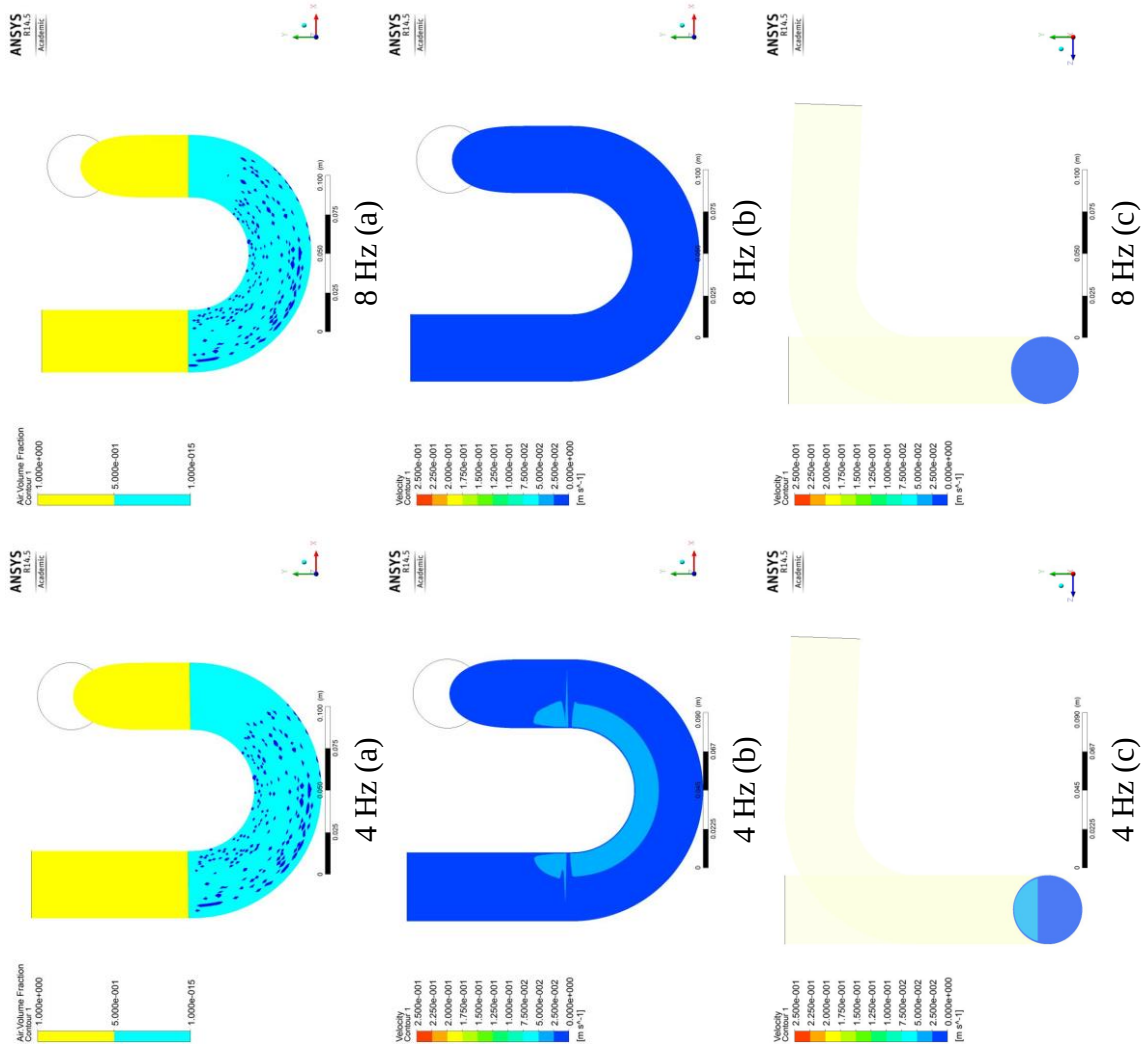


**Figure 5. 5, Screenshots of the: (a) VF of air in the laboratory trap, $Z = 0$ plane (b) fluid velocity, $Z = 0$ (c) fluid velocity, $X = 0$ at 1, 2, 3, 4 & 8 Hz**

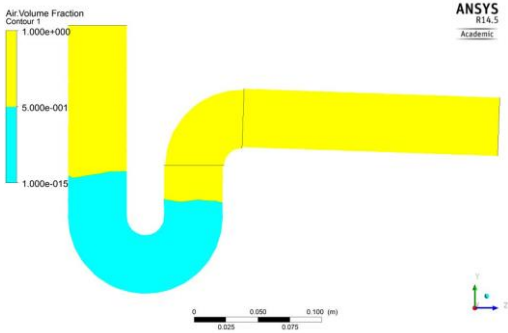


1 Hz (a)

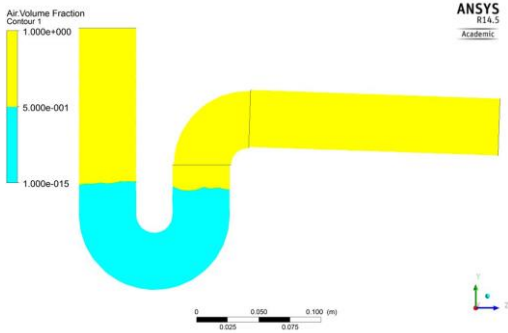


2 Hz (a)

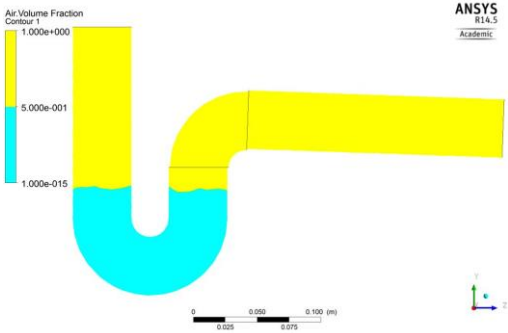


3 Hz (a)

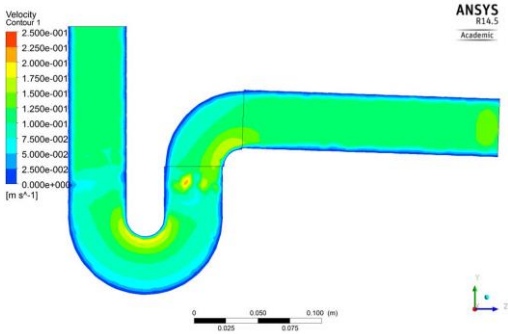


1 Hz (b)

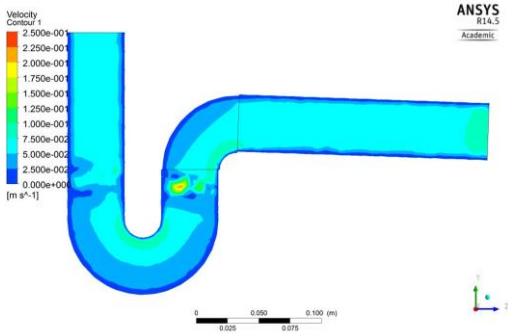


2 Hz (b)

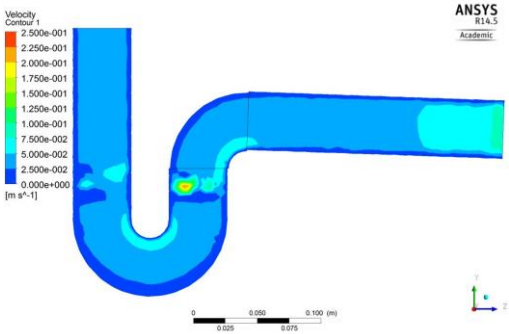


3 Hz (b)

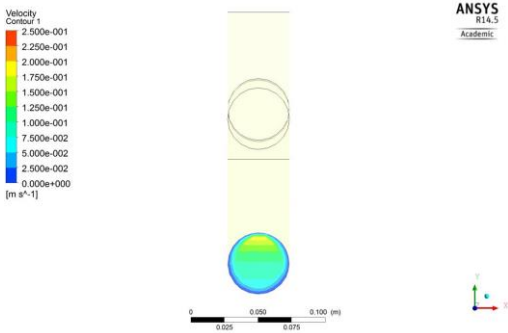


1 Hz (c)

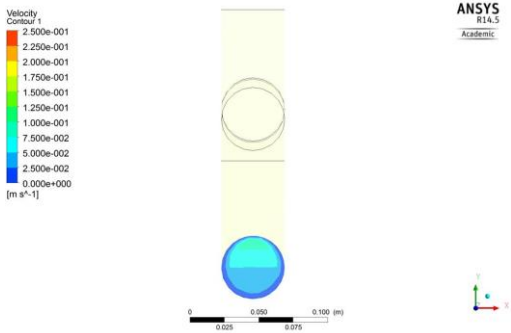


2 Hz (c)

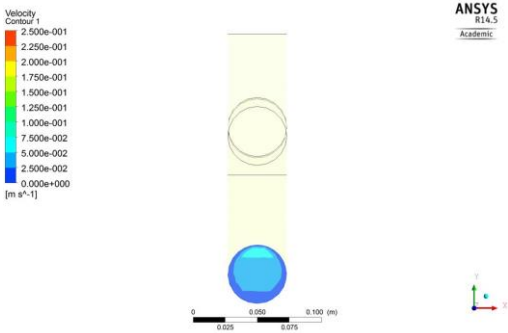


3 Hz (c)

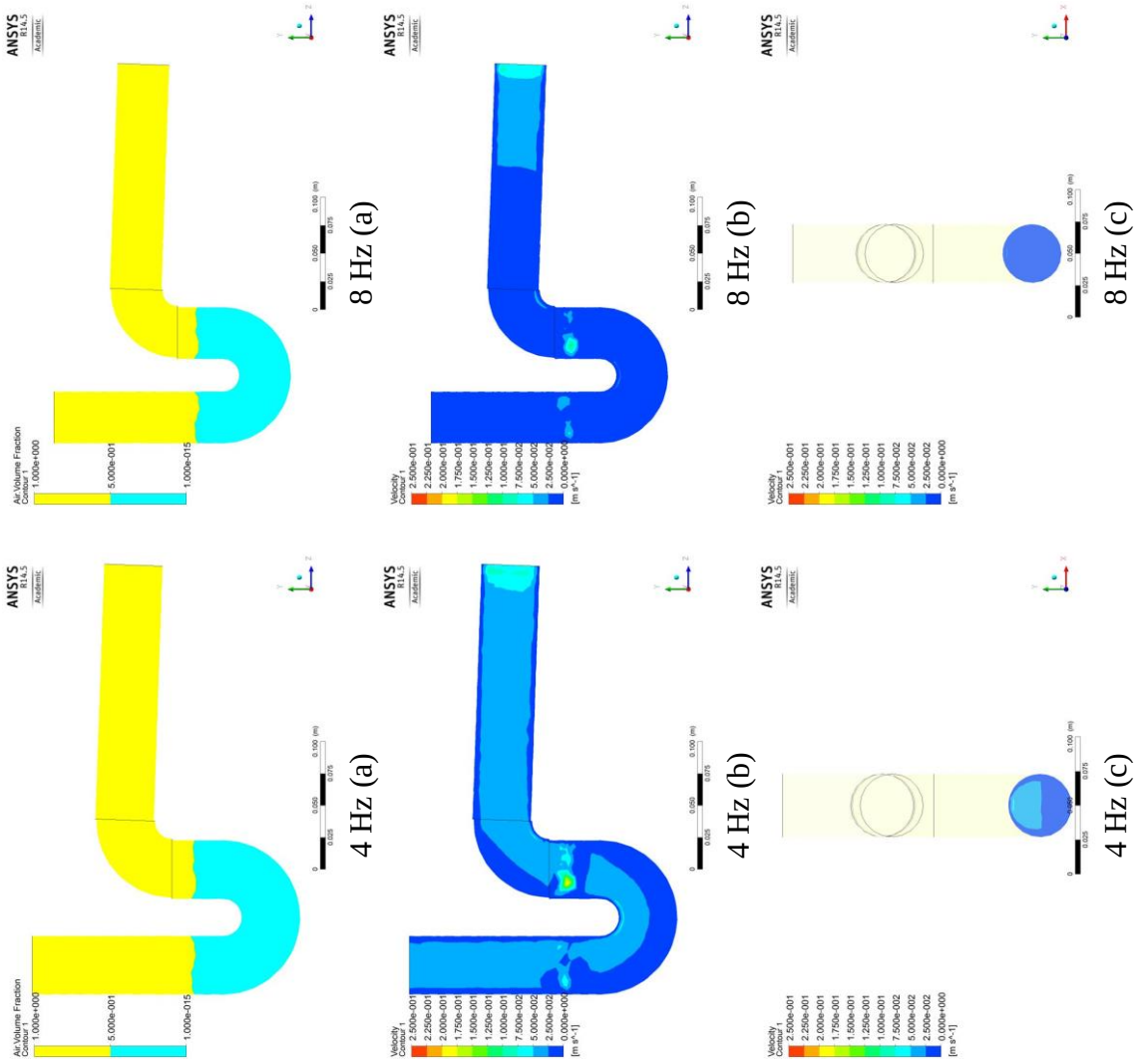


**Figure 5. 6, Screenshots of the: (a) VF of air in the commercial trap, $Z = 0$ plane (b) fluid velocity, $Z = 0$ (c) fluid velocity, $X = 0$ at 1, 2, 3, 4 & 8 Hz**

Figures 5.5 and 5.6 show that the determined relationship between the outer and inner surfaces holds true to Newton's second law of motion, but also that the higher the frequency the lower the average water velocity along the curved conduit. The high velocities at low frequencies are a result of slower rise times which accounts for absorption of energy by the water column. The lower the water velocity and also the lower the inequality between the outer and inner bend length, the less movement observed at the water level.

An interesting point here is also that the test data shows a gradient from high to low related to the inner and outer surface. Velocities along the inner bend of the trap seal are consistently higher along this inner bend than along the outer bend of the trap. Furthermore, the smaller the internal radius of the bend, the greater the velocity noted. Therefore, an advantage of a trap similar to the commercial trap seal is in its ability under negative pressure, to more rapidly, allow air into the branch safe guarding the liquid required for the seal. By this theory, the bottle trap capitalises on this advantage by its bend (of pipe wall thickness).

### *5.3.2. Angled data planes analysis method*

In order to determine another relationship between the water column movement along the bend in the general direction of flow and velocity (not simply along the parallel rows) exists, a simpler method of analysing the probable rate of change is to assess the flow along a range of slice planes. Seven planes were selected at 30º increments from the centre of the bend, and named starting from the right: 0 º, 30 º, 60 º, 90 º, 120 º, 150 º and 180º.

All data in this section is collected at the first positive peak along the sinusoidal cycle to enable comparison based on equivalent applied pressure amplitude (force). A program written in R (by Dr Doug Pender) and modified for this application was used. By first determining the coordinate positions of all relevant points on the slice planes, the code was written to identify the required data which corresponds to the coordinate.

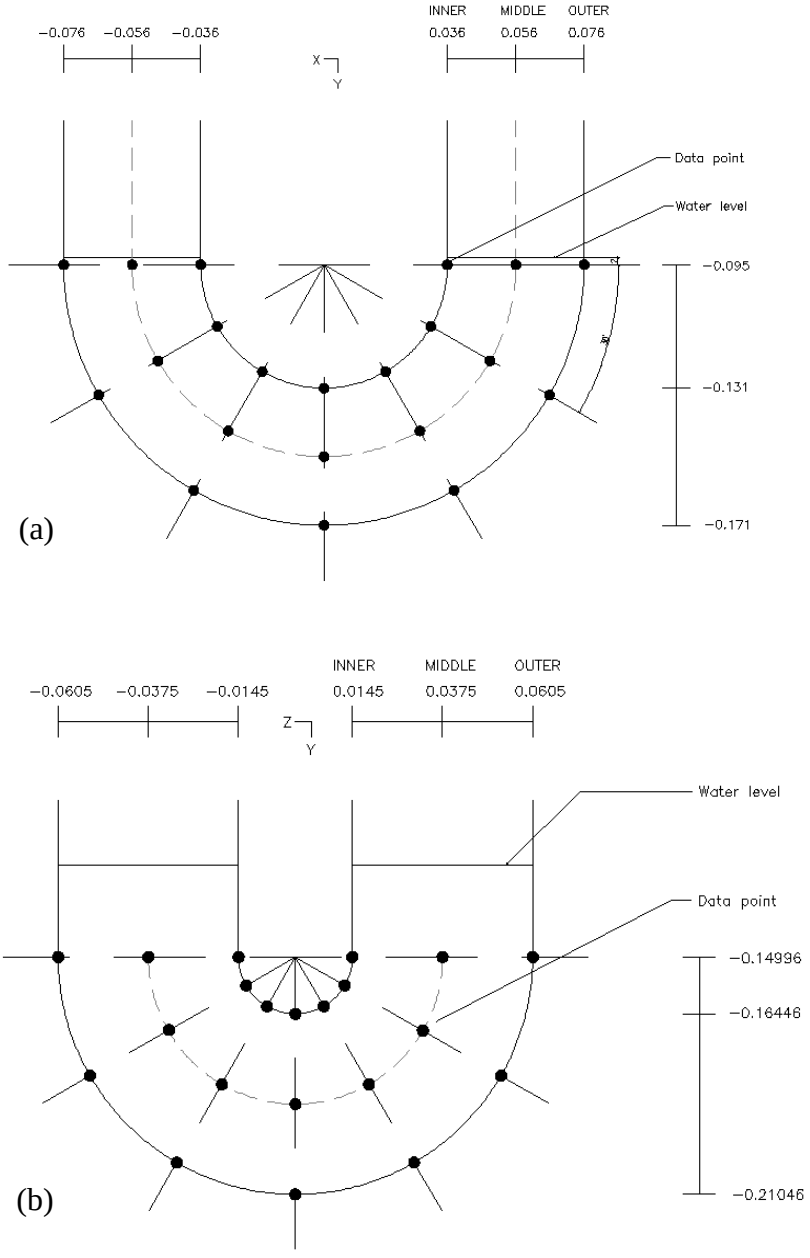


**Figure 5. 7, Geometric representation of the appliance trap seals (a) laboratory trap, (b) Commercial trap seal - 30º increment monitor planes and selected data points (inner, middle & outer points)**

Figure 5.7 presents the position of the data points along the slice planes in the commercial and laboratory appliance water traps, the XY and ZY coordinates for the laboratory and commercial traps respectively, along with the position of the water line at time equals zero is shown.

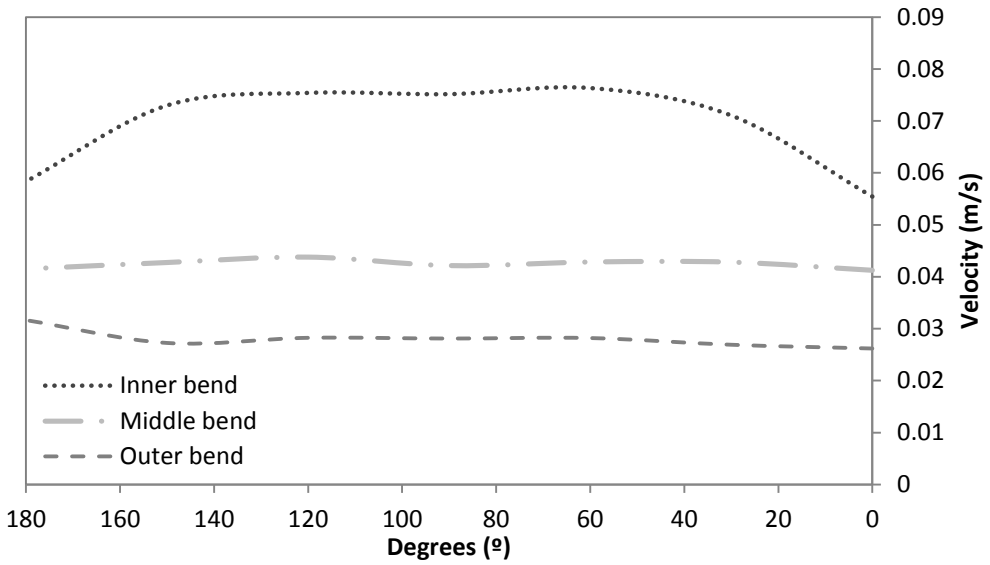


**Figure 5. 8, The average velocity along the inner, middle and outer bend of both appliance trap seals at various angles (clockwise) from the centre of the pipe bend along all frequencies.**

Figure 5.8 shows the general form of fluid flow across all frequencies and traps tested at varying angled planes across the water trap seal; observing flow only along the inner, middle and outer sections on the planes. The flow regime between the velocity along the inner surface, the plane centre and the outer surface of the curved conduit can be seen in Figure 5.8. Little variation to the flow is noted along the centre of the flow and along the outer surface of the trap. The exception to this trend is noticed between 150 º to 180 º where both the velocity along the inner bend (deceleration) and outer (acceleration) surface tends towards the mean. The velocity of water movement is greatest along the inner surface, where a sharp increase is noted between 0 º and 30 º then as mentioned a decrease in velocity between 150 º to 180 º. This pattern can be found repeated in Figures 5.10.

A constant velocity along the middle of points, and the outer surface with the exception between. Along the inner surface of the conduit, the velocity is regarded to increase between 0 º and 30 º, become constant until the 150 º point, and then decreases significantly. These interactions demarcate zones of movement within a trap seal.

These movement zones are:

| | | |
|---|---|---|
| **Zone 1** | 0º to 30º | acceleration in the velocity profile (damping zone) |
| **Zone 2** | 30 º to 150º | largest velocity gradient but velocity across planes remain constant |
| **Zone 3** | 150º to 180º | deceleration in the velocity profile (damping zone) |

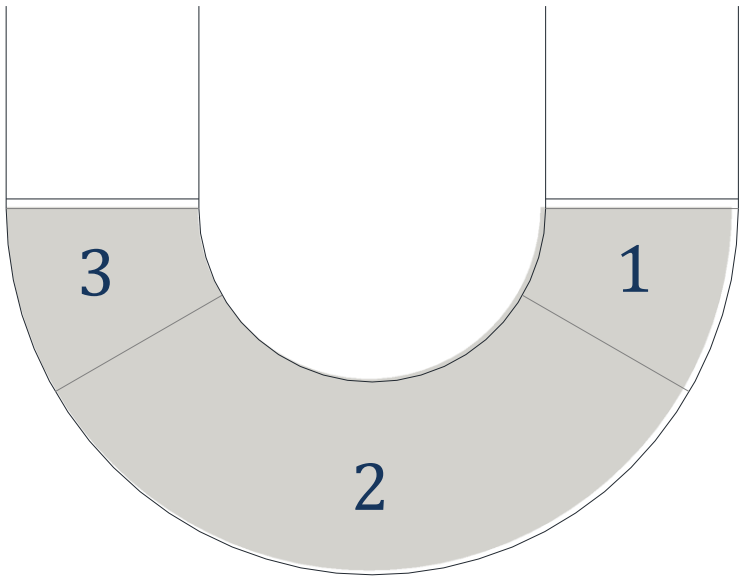


**Figure 5. 9, Representation of the zones of movement in the appliance trap seal**

Section 5.3.2 has identified using Figure 5.8 and Figure 5.9, three zones of differential movement within the appliance trap seals. These zones named zone 1, zone 2 and zone 3. Zone 1 and 3 positioned along the entrance and exit of the seal bend are considered damping zones as they display the greatest resistance to movement. Zone 2 exists along the middle region of the seal. Here, water is found to propagate at a fairly constant rate.

### *5.3.3. Frequency analysis*

The zones of movement identified within the traps in Section 5.3.1 will be explored further in this subsection by regarding the discrepancies and correlations between the flow movement in relation to the applied frequency. Figure 5.10 (a) the laboratory trap seal and (b) the commercial trap seal, show the calculated velocity across the inner, middle and outer bend of the laboratory trap when the input pressure frequency is 1Hz and 8 Hz.

In the laboratory trap seal bend – at low frequencies the acceleration of the flow regime occurs in the first segment (0-30 degrees) along both the inner and the outer surfaces and the sixth segment (150 – 180 degrees) along the outer surface, while the velocity of the flow in the middle of the conduit it found to be greater than that at the inner bend (see Figure 5.10 1Hz (a)). The greatest displacement of the water is found at 1Hz, a finding supported by Beattie (2010) and Swaffield (2010).

Within this case however, as can be seen in Figure 5.10 1Hz (a), in Zone 1 and 3, (at the water surfaces) the water velocity is greatest along the middle bend. This is an anomaly as in all other data collected where the pressure transient frequency is above 1 Hz the inner surface velocity remains greater than anywhere else along the trap.

The greater the frequency of the applied pressure the more common the pattern of fluid flow shown in Figure 5.8 (above) becomes. The zones of movement identified in Figure 5.9 remain applicable in Figure 5.10 (a) 1Hz, 3Hz and 8 HZ of the laboratory appliance trap seal. Here, in the first segment of observed movement, acceleration is recorded at all monitored points with the greatest increase noted along the inner surface of the bend. As in Figure 5.10 1Hz (a) the movement along the $2^{nd}$, $3^{rd}$, $4^{th}$, and $5^{th}$ segments of the curved conduit remain steady along the inner, middle and outer data points.

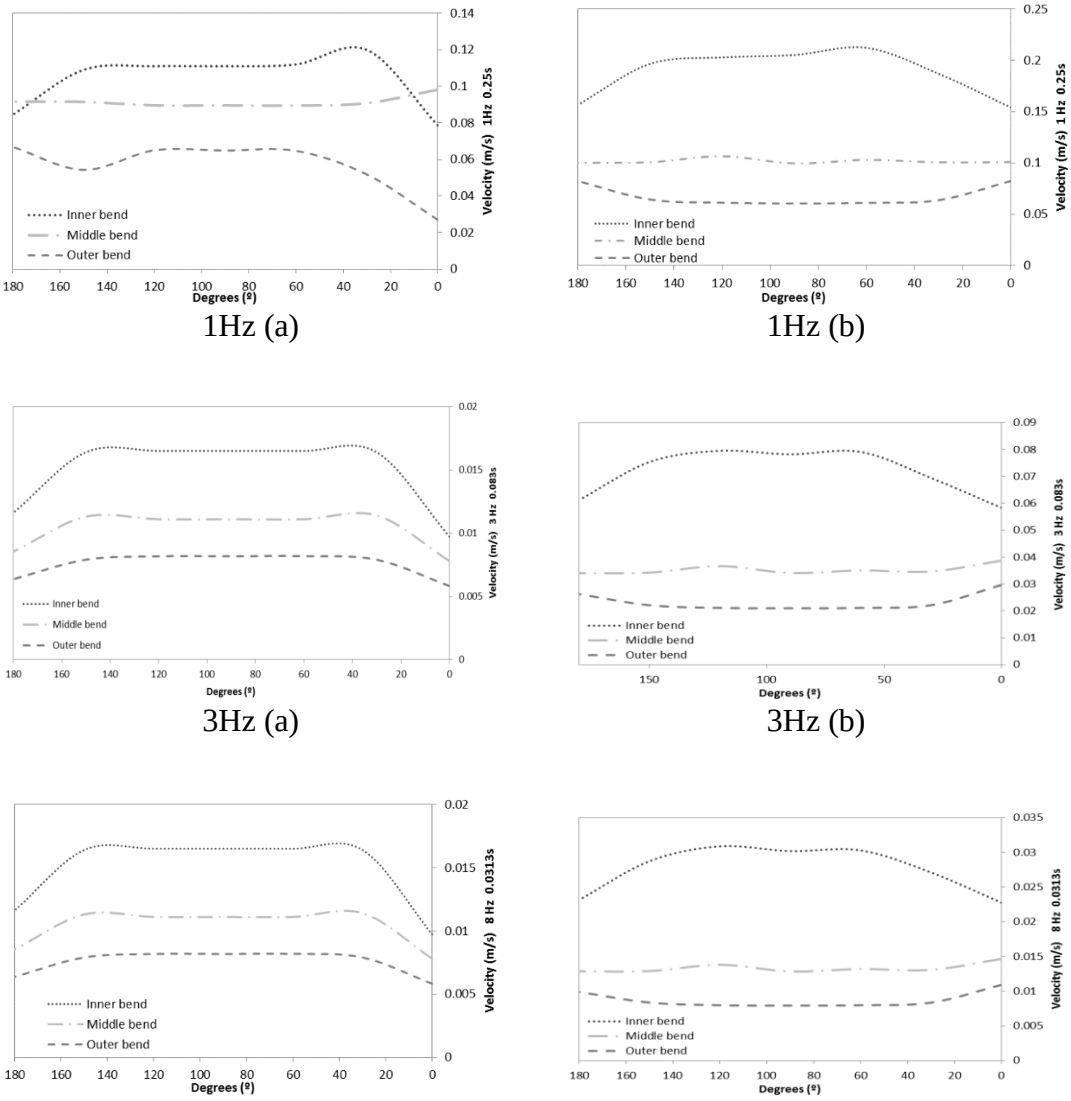


**Figure 5. 10, The velocity along the inner, middle and outer bend of (a) Laboratory trap seal, and (b) Commercial trap seal at various angles (clockwise) from the centre of the pipe bend when input pressure is 1, 3 & 8 Hz**

Figure 5.10 (b) presents the likely flow pattern along the curve of the water seal for frequencies 1Hz, 3Hz and 8Hz in the commercial trap. This flow regime provides an exception to the general zones of movement identified in Figure 5.8, as here, the acceleration along the inner bend is not stopped at 30º, but rather at 60 º. This exception does not hold for the middle and outer bend velocities as they remain as earlier predicted; transitioning at 30º. Figure 5.11 presents a revised pictorial representation of the zonal regions within the commercial appliance water trap.

With this amendment, the inner lengths of zone 1 become 15.3mm and 18.8mm, differing from the original estimation of 7.6mm and 18.8mm for the commercial and laboratory trap seals respectively. This is significant as it leads to a connection between the force (100pa) applied onto the water column and the damping region within this column being a construct of length and not so much the position along the curve. See Figure 5.11 below, and note the difference in the inner lengths of zone 1 and zone 3.

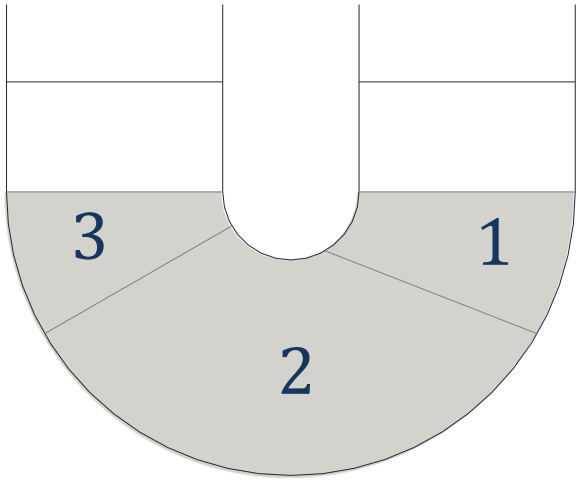


**Figure 5. 11, Representation of the zones of movement in the commercial appliance trap seal**

An additional shared feature between the flow patterns along the two traps is that at 180º (the end of zone 3) all trends tend towards each other. This increased proximity of

velocity ranges is a significant observation as it suggests reduced movement of the water.

Zone 1

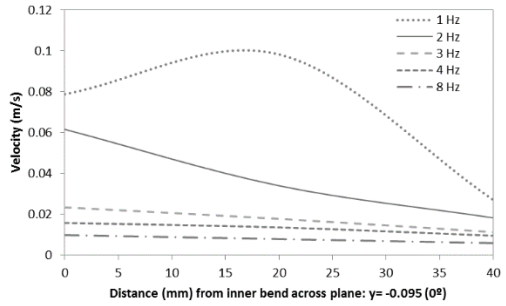


(a)

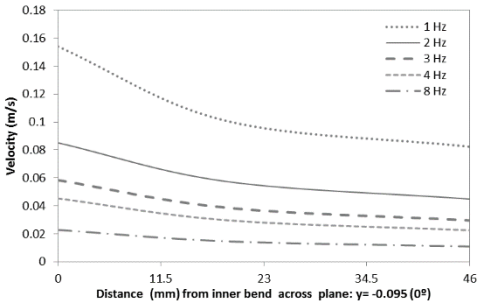


(b)

Zone 2

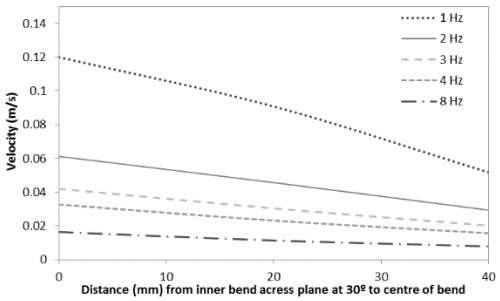


(a)

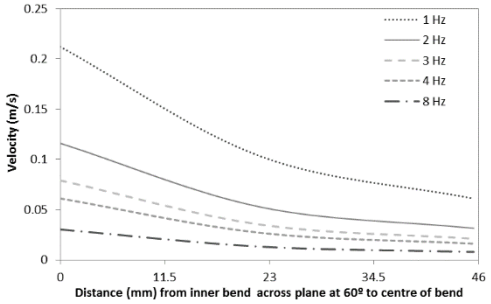


(b)

Zone 3

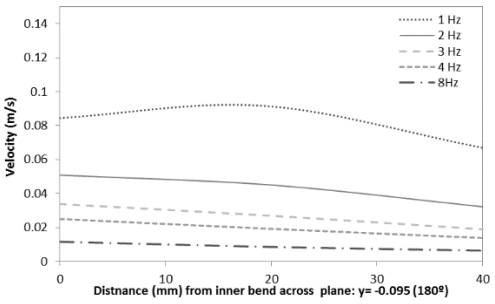


(a)

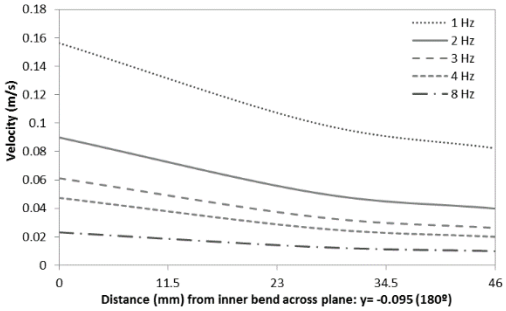


(b)

**Figure 5. 12, Velocity along Zone 1, 2 and 3 for all applied pressure frequencies in the laboratory appliance trap (a) and the commercial appliance trap (b). Distance along the x plane is a measure from the intersection of plane with the inner bend.**

Figure 5.12 presents the velocity along the slice planes at 0º (Zone 1), the beginning of Zone 2 and the end of Zone 3 in the laboratory trap seal (a) and the commercial trap seal (b) for all frequencies. The data presents information which can be found pictorially in a more ambiguous nature in Figure 5.5 and 5.6. It can be concluded that for the same applied pressure the rise time is critical to the speed at which the water column is moved in response. The data for the two traps presented show conclusively, that the greater the applied frequency of the generated transient, the slower the recorded water velocities, and the disparity between the velocity across the planes is greatest at the low frequencies. Note also that, in the laboratory trap seal with a 1Hz transient input flow, buckling is seen along the middle of the bend for 0º, 30º and 180º, a factor not mimicked in the commercial trap, thus leading to an assumption that this laminar like movement is a consequence of the trap's geometric design.

This flow regime noticed in the laboratory trap water column provides evidence that as the incoming flow is laminar, the larger the inner bend, the more likely the flow is to remain uniform. Frictional effects along the wall of the pipe lead to greater velocities along the middle line, depicting very clearly under a larger time frame and response to a higher pressure input, that laminar frictional representation is likely. This however, occurs only in one instance of the simulations conducted, leading to the general conclusion that in all other instances specifically in the commercial trap seal, laminar frictional representation is highly unlikely.

### *5.3.4. Comparison of the two traps*

Comparisons between the behaviour of the water column in the two modelled appliance water traps have been made in the previous section. It has been shown that:

1. The water velocity along the trap with the smaller inner length is consistently greater than that in the trap with the larger inner circumference regardless of the applied frequency.

2. That rise time (and therefore wave frequency) of the low amplitude pressure transient plays a critical role in the recorded water velocity
3. The inner length of Zone 1 is the only length comparable between two differing U-bend trap seals.
4. The greater the applied frequency of the generated transient, the lower the disparity between the velocity across the planes
5. At low frequencies the flow in the Laboratory trap becomes increasingly unsteady whereas in the Commercial trap the general flow trends remain consistent.

A difficulty of multiphase flow simulation is the identification of the position of water or air along the mesh. Noting not just what the fluid velocity is, but the water velocity and the air velocity, and thus understanding the reason for changes in flow behaviour and establishing a valid comparison between the tests.

Figure 5.13 (a) and (b) presents the velocity gradients of the flow along the slice planes at the various applied frequencies. These graphs show the anomaly that is the flow behaviour along the 0º plane of the laboratory trap. An explanation for this behaviour is found in that the water level is 2mm above this plane at time equal to zero. At 0.25s in the 1Hz simulation the water level is below this original point. The recorded water volume fractions along this plane are: 0.00000185 (inner), 0.0000031 (middle) and 0.00218(outer). At low frequencies there is greater movement of water and this 0 º plane or rather this seemingly free surface plane, would be the first to approach a water volume fraction less than 1. The greater the frequency of the applied low pressure transient the less movement detected, and so the recorded water volume fractions along the 0º plane is 0.631 (inner), 0.872 (middle), 0.973 (outer) and 0.953 (inner), 0.998 (middle), 0.999 (outer) for 3 Hz and 4 Hz respectively. The commercial trap on the other hand has a 24mm head of water above the 0º plane at time equal to zero. The recorded water volume fractions across this plane are: 0.9945 (inner), 0.9821(middle) and 0.9968 (outer). Therefore, the irregularity shown for the 0º plane can be attributed to the velocity of air along the plane and not water. Across all planes and within both appliance traps regardless of the fluid present two regions are clearly presented. The

flow when the low amplitude pressure transient is less than 3 or 4Hz and the flow when the low amplitude pressure transient is greater than 4Hz.

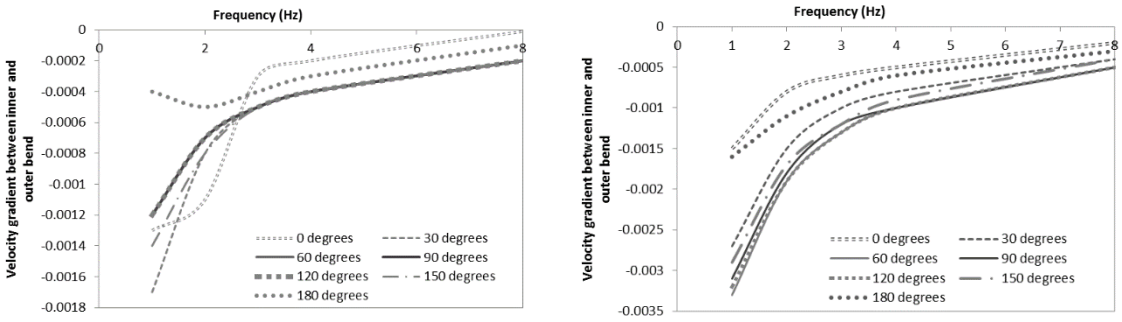


(a) (b)

**Figure 5. 13, Velocity gradient across the planes set at 30º increments according to frequency in the laboratory appliance trap (a) and the commercial appliance trap (b)**

As the diameters of the traps differ by 6mm, the following equation was employed to present a platform for comparison at various points along the planes.

$$i = \frac{d}{D} \qquad \textbf{Eq. 5. 2}$$

Where, $d$ is the distance from the inner surface, and $D$ is the internal diameter of the trap.

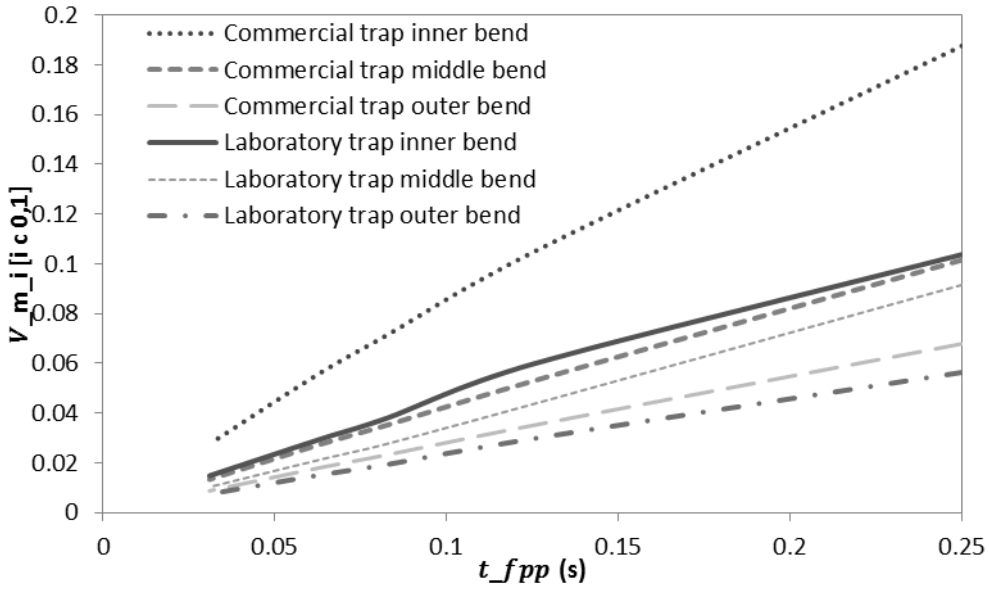


**Figure 5. 14, The average velocities along the inner, middle and outer surface of the commercial and laboratory trap against the applied pressure frequency**

Figure 5.14 shows that with the same applied pressure in the two water trap seals, the commercial trap records a vast increase in the velocities along the inner bend of the trap and at the lower frequencies. The velocities along the outer bend of the traps however, are more akin.

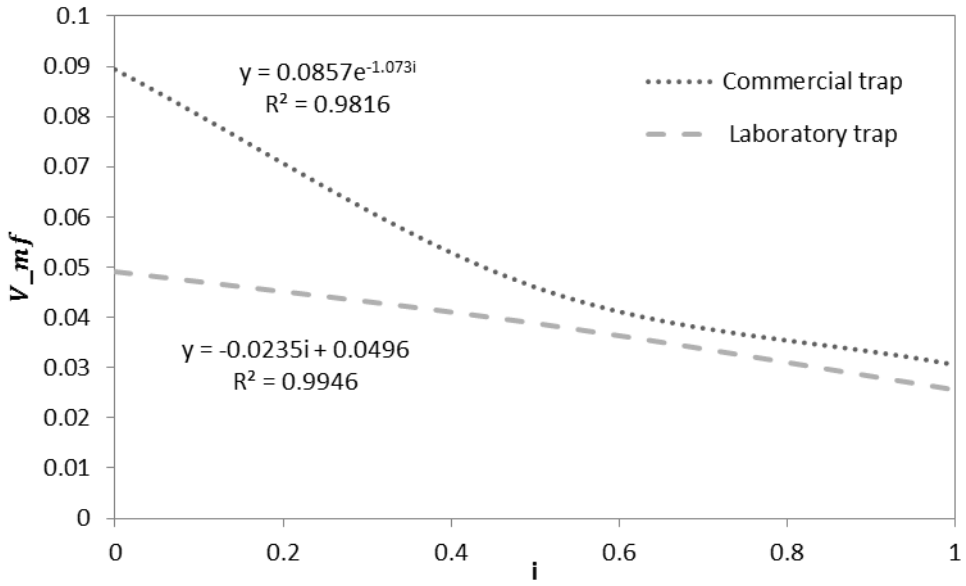


**Figure 5. 15, The average velocity across the two traps measuring from the inner $(\boldsymbol{i = 0})$ to the outer edge $(\boldsymbol{i = 1})$**

Figure 5.15 presents the relationship between the average velocities across the traps. In the commercial trap seal the relationship is described as follows,

$$\frac{\sum_{i=0}^{n} V_{mf}}{n} = \frac{\sum_{i=0}^{n} 0.0857e^{-1.234i}}{n}, \qquad i \in [0,1] \qquad \textbf{Eq. 5. 3}$$

In the laboratory trap seal equation the mean velocity is

$$\frac{\sum_{i=0}^{n} V_{mf}}{n} = \frac{\sum_{i=0}^{n} 0.0235i + 0.0496}{n}, \qquad i \in [0,1] \qquad \textbf{Eq. 5. 4}$$

Where, $n$ is the number of points along the plane selected.

Using an averages relationship shown in Eq 5.3 and 5.4, as the basis for a water trap boundary condition negates the possibility of the critical influence that frequency has on the depletion of the trap. Figure 5.14, shows that there is a distinct increase in the velocity of the water movement in the commercial trap (,the trap with the shorter inner

bend length). The commercial trap however, has the larger width of the two traps (extending by 6mm) which would be expected to slow the movement along the pipe, however in this scenario all values along the inner, middle and outer bend are higher than corresponding points in the laboratory trap. It is suggested then, that the factors of greatest consequence to the velocity of the water under an applied pressure (overlooking the influence of pressure) are the frequency and the length of the trap bend when small discrepancies in diameter exist.

| Appliance traps | t_fpp / i | 0.25s | 0.125s | 0.083s | 0.0625s | 0.0313s | Average |
|---|---|---|---|---|---|---|---|
| Commercial trap | 0 | 0.187614 | 0.104554 | 0.071603 | 0.055549 | 0.02759 | 0.089382 |
| | 0.5 | 0.101531 | 0.052826 | 0.035327 | 0.027117 | 0.013329 | 0.046026 |
| | 1 | 0.067873 | 0.035027 | 0.023316 | 0.017857 | 0.008764 | 0.030567 |
| Laboratory trap | 0 | 0.103729 | 0.059657 | 0.038171 | 0.0292 | 0.014804 | 0.049112 |
| | 0.5 | 0.091543 | 0.043543 | 0.027786 | 0.021071 | 0.010333 | 0.038855 |
| | 1 | 0.056371 | 0.029686 | 0.019429 | 0.014963 | 0.0075 | 0.02559 |

**Table 5. 1, The average velocity (m/s) in the commercial trap seal and laboratory trap seal along i=0, 0.5, and 1.**

Tables 5.1, examines more closely the relationships between the two traps. A coefficient is used to describe the

$$\frac{V_{\mathbf{T1}}}{V_{\mathbf{T2}}} \qquad \textbf{Eq. 5. 5}$$

Where, $V_{\mathbf{T1}}$ denotes the average velocity along a bend or plane in trap 1(the laboratory trap),and $V_{\mathbf{T2}}$ is the average velocity along bend in Trap 2 (the commercial trap).

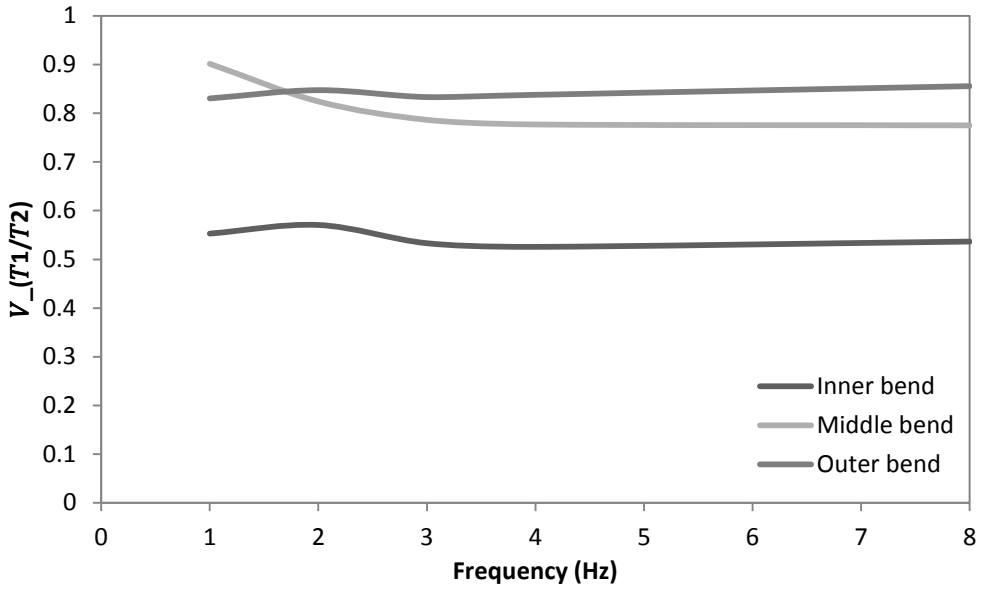


**Figure 5. 16, Relationship between the average velocities along the inner, middle and outer surface of the commercial and laboratory trap against the applied pressure frequency**

Figure 5.16, examines the proportional relationship between the velocities along the inner, middle and outer bend of the two traps, and reiterates that not only does the movement of water become consistent at velocities greater than 3Hz, but suggests the relationship between this movement in traps of differing geometric characteristics is constant between 3Hz and 8Hz. As stated previously, two distinct regions exist: below and above 3Hz. Henceforth, due to Figures 5.13 and 5.16, the transitional region will be considered to occur between 3 and 4 Hz.

The relationship between the velocities in the two traps introduces a new concept to the analysis of the water trap seal. This is as, if a linear relationship exists, then the velocity of water movement could be reduced to a function of the geometry of the trap and the applied pressure transient.

This circumference of the inner bend was calculated to be:

- 45.6 mm in the commercial trap
- 113.1 mm in the laboratory trap

The ratio of the inner bend length ($L_I$) and the outer bend length ($L_O$) in the commercial trap and laboratory trap is 0.242 and 0.473 respectively.

It has already been established the importance of frequency to the rate of movement in the trap and the two regions which exist in applied frequencies.

The use of a coefficient to define the relationship between velocity and a length function < 1 would be useful to the prediction of flow according to the dimensions of the inner and outer bend length if pressure and frequency are known.

Let

$$v_L = v * \frac{L_I}{L_O} \qquad \textbf{Eq. 5. 6}$$

Where, $v$ is the velocity at the data point, and $\frac{L_I}{L_O}$ is the ratio between the inner and outer bend circumference.

and

$$V_L = \frac{\sum_{i=0}^{n}(v * \frac{L_I}{L_O})}{n} \qquad \textbf{Eq. 5. 7}$$

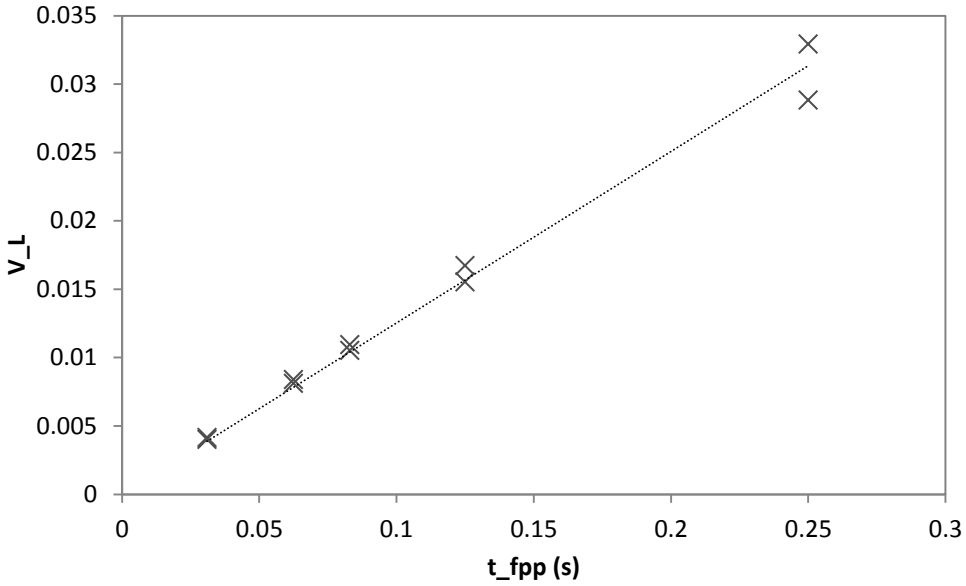


**Figure 5. 17, The average velocity coefficient ($V_L$) across both traps against the rise time of the first applied pressure wave in both traps. $R^2$ = 0.9877**

This data was determined by taking the average velocity across all data points for each frequency then multiplying it by the $L_I/L_O$ ratio. The following relationships were found:

$$V_L = 0.1253 t_{fpp} \qquad \textbf{Eq. 5. 8}$$

Where, $V_L$is the mean velocity as a function of the bend length ratio, and $t_{fpp}$ is time at first positive peak. It follows that:

$$t_{fpp} = \frac{1}{4f} \qquad \textbf{Eq. 5. 9}$$

Figure 5.14 showed the average velocity along the inner, middle and outer curve of the conduits. Figure 5.17 re-evaluates the relationship between the traps by making the values a product of the $L_I/L_O$ ratio then calculating for each frequency.

If the rows of movement (analogue) is to be considered vital to the displacement of the water column, simply taking the average velocity of flow in the trap cannot be deemed a suitable method for modelling the trap seal behaviour, and so the following relationships were discovered:

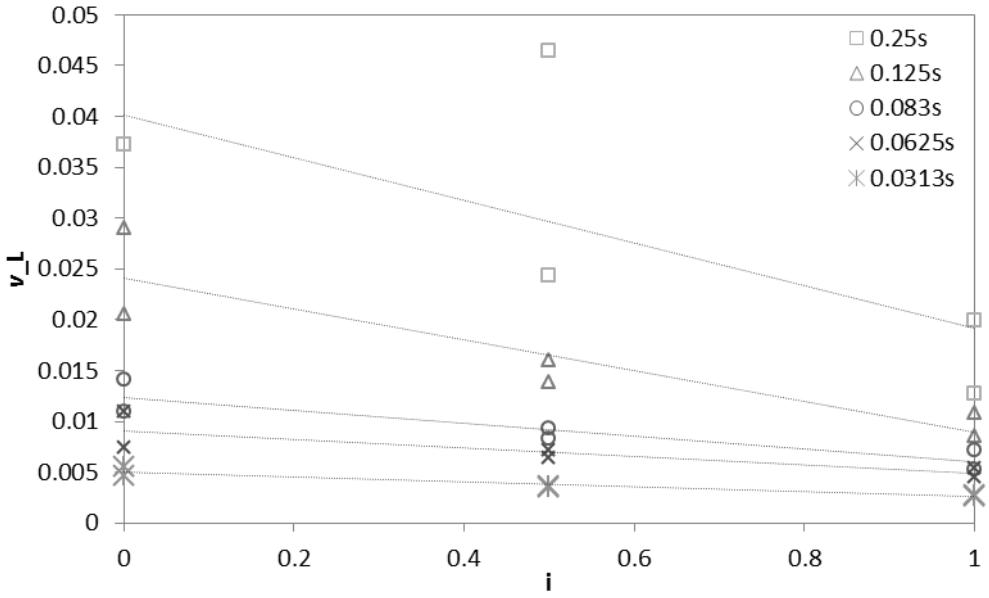


**Figure 5. 18, Velocity as a product of the pipe ratio against the distance along the pipe from the inner curve at the various first positive pressure peaks**

Using the general form $y = mx + c$, the following relationship was developed. In the form,

$$v_L = S_v i + c_L \qquad \textbf{Eq. 5. 10}$$

The differential between the two trend lines in the Figure 5.20 is the representation of frequency dependant friction in the appliance trap seal. If friction is the resistance to motion then the relationship presented in Figure 5.20 graphically presented the differential between flow rates between the outer and inner zones of the trap seal. This information has never before been gained and provides the basis for a new friction factor for whole BDS simulation and specifically the prediction of water flow across the curved conduit.

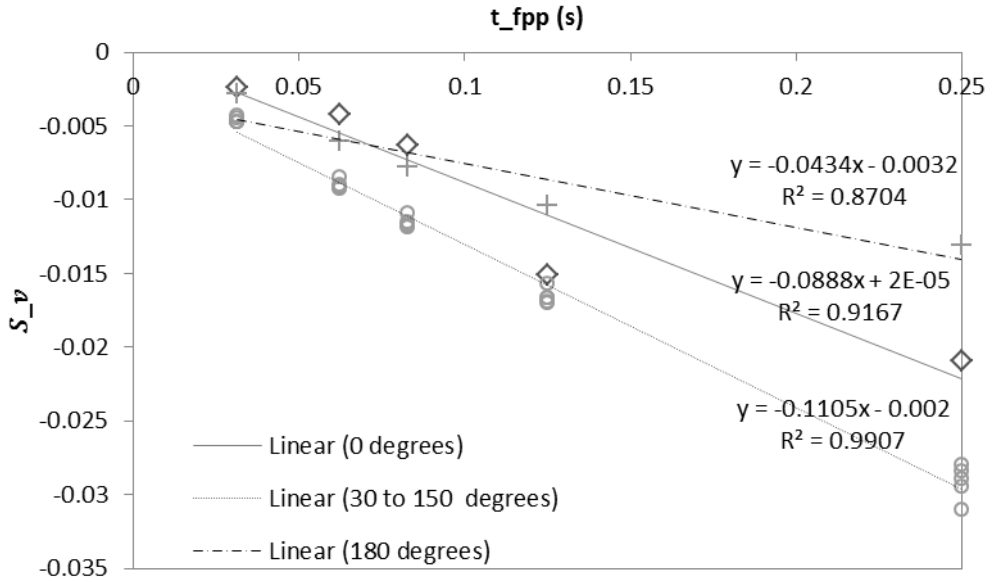


**Figure 5. 19, The gradient of velocity against the rise time of the first pressure peak**

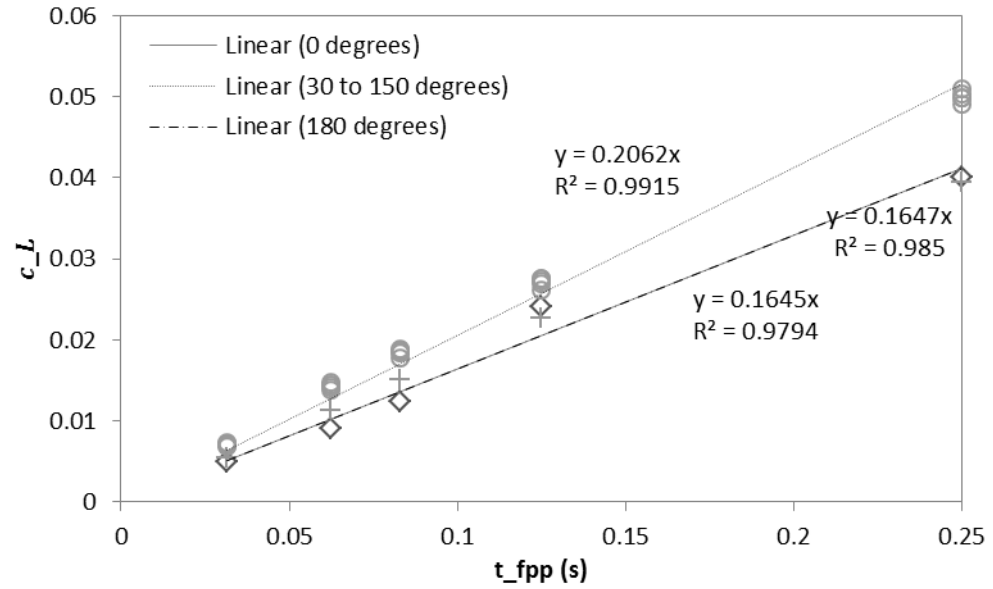


**Figure 5. 20, The intercept or inner curve velocity against the rise time of the wave**

The following equations serve as a general description for velocity in the laboratory or commercial appliance water trap, and enable prediction of water seal flow rate dependent on trap geometry. They are written in the form $(S_v i + \boldsymbol{c}_L)\frac{L_O}{L_I}$.

$$v = \left(\left(-0.0888t_{fpp} + 0.00002\right)i + 0.1645t_{fpp}\right)\frac{L_O}{L_I}, \qquad if\ \theta \in [0º] \qquad \textbf{Eq. 5. 11}$$

$$v = \left(\left(-0.1105t_{fpp} - 0.002\right)i + 0.2062t_{fpp}\right)\frac{L_O}{L_I}\ , if\ \theta \in [30º, 150º] \qquad \textbf{Eq. 5. 12}$$

$$v = \left(\left(-0.0434t_{fpp} - 0.0032\right)i + 0.1647t_{fpp}\right)\frac{L_O}{L_I}\ \ , if\ \theta \in [180º] \qquad \textbf{Eq. 5. 13}$$

Figures 5.21 and 5.22 show the results of the CFD analysis (measured) plotted against the results of Eq 5.11, Eq.5.12 and Eq. 5.13.

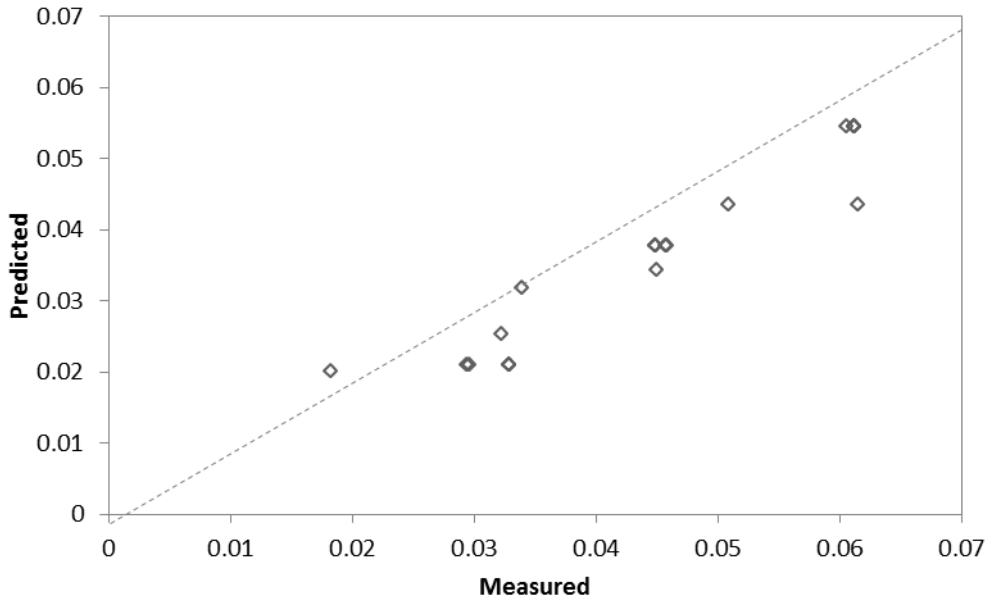


**Figure 5. 21**, **Measured (CFD) vs predicted velocity along the Laboratory trap seal at 2Hz (time: 0.125s) $R^2$ = 0.9163**

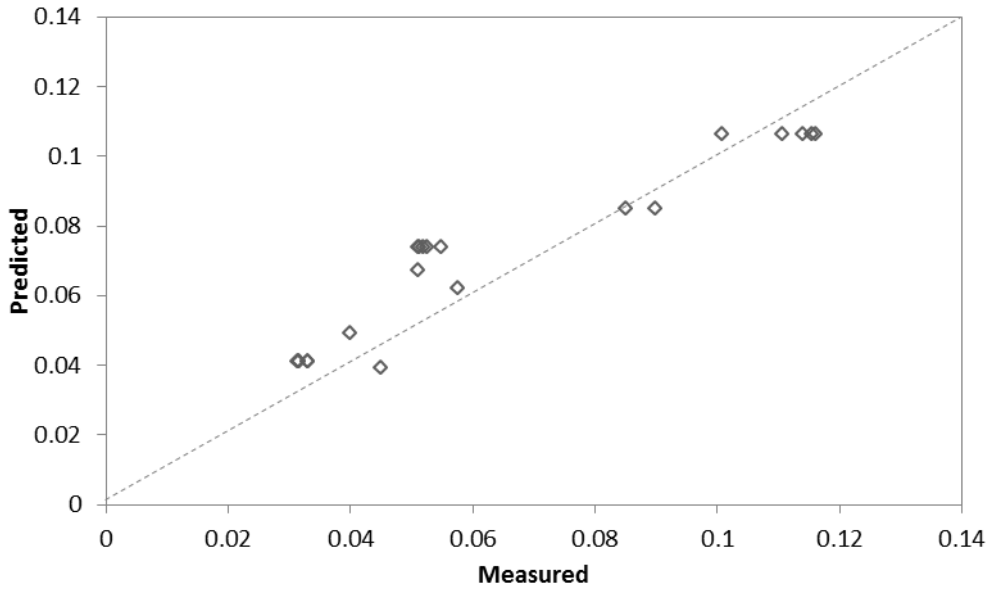


**Figure 5. 22**, **Measured (CFD) vs predicted velocity along the Commercial trap seal at 2Hz (time: 0.125s). $R^2$ = 0.8948**

### *5.3.5. Summary*

Section 5.3 has provided an analysis of the multiphase flow simulation using ANSYS CFX. The data generated was analysed by isolating the variables related to six angled planes of 30 degree increments. These planes highlighted the zones of motion which existed along the bend. These three zones are regarded to exhibit acceleration, constant flow, and deceleration. Zones 1, and 3 where acceleration and deceleration are found respectively, are considered damping zones. It was found through comparison of the laboratory and commercial trap seals, that geometric characteristics of the zones are comparable as they occurred between 15-18mm of the beginning of the bend, then until the 150 degree plane, and from the 150 to 180 degree plane. This segmentation correlates to zones 1, 2 and 3 respectively.

The main finding of subsection 5.3.2 was of a transition between the velocity in the trap if the applied frequency was below 3 or 4 Hz or greater than 3 or 4Hz. The section continues in subsection 5.3.3, where the equations describing the flow across the zones

of movement were developed. This suite of 3 equations is expressed as a function of the inner and outer length of the seal bend.

This section has addressed in full Objective 1 of the research study.

## 5.4. Development of a frequency dependent internal energy factor

The Colebrook white equations describing friction, are based on steady state conditions and therefore do not consider the effect of pressure transients which are common place in a BDS. This section seeks to develop a new factor which considers both friction and separation losses, and is able to accurately predict water column oscillatory behaviour in relation to the characteristics of the applied air pressure transient.

Section 5.3 showed, that zones 1 and 3 constantly exhibit velocity profiles lower than that in zone 2.The internal energy therefore can be said to be a measure of the differential between the zones of movement.

Using the average velocity along the trap or along a plane does not allow for the accurate prediction (within the MoC) of the moment of trap vulnerability and thus cross contamination. The maximum velocity which occurs along the inner curve is of greater importance to the accuracy of the model, though it does pose the risk of overestimating the depletion time. First though, the following data presented, takes into consideration the recorded flow at the data points along the inner bend.

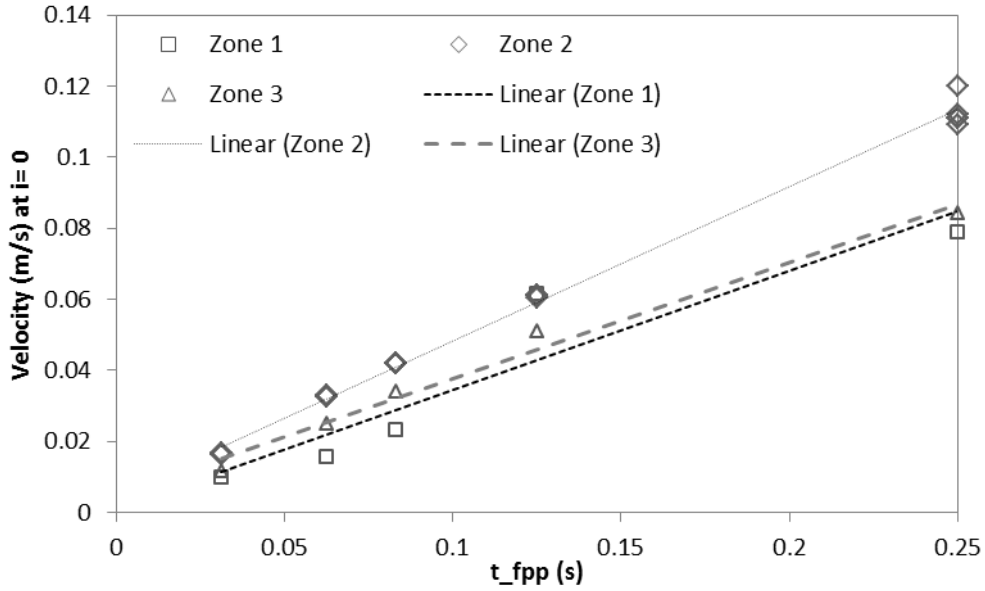


**Figure 5. 23, The velocity at $i = 0$ along the three zones against the rise time of the first applied pressure wave in laboratory trap. $R^2$ = 0.8773, $R^2$ = 0.9956, and $R^2$ = 0.9856 for Zone 1, 2 and 3 respectively.**

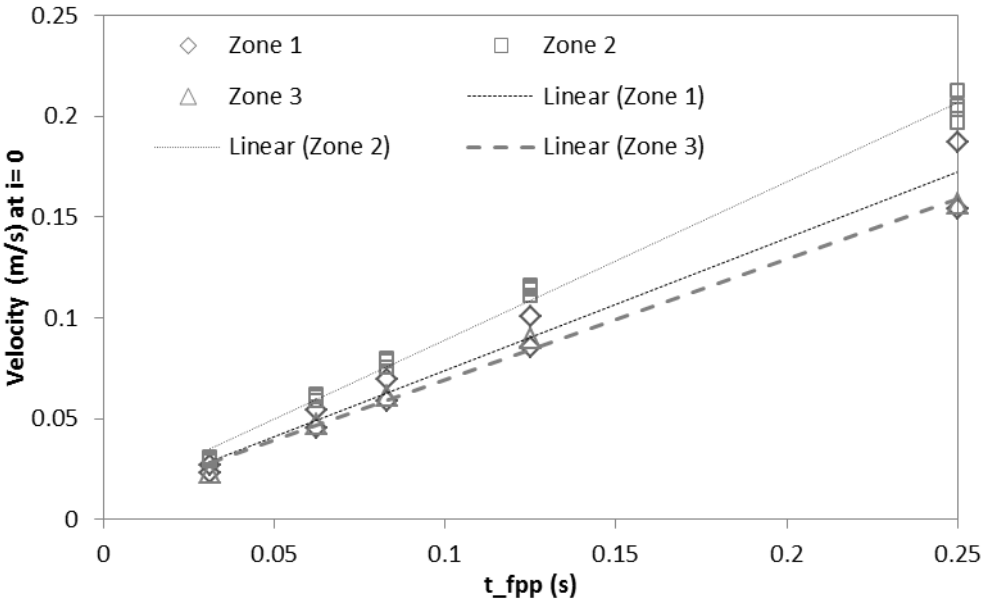


**Figure 5. 24, The velocity at $i = 0$ along the three zones against the rise time of the first applied pressure wave in commercial trap. $R^2$ = 0.9682, $R^2$ = 0.9939 and $R^2$ = 0.9934 for Zone 1, 2 and 3 respectively.**

From Figure 5.25 the (below) relationship for the commercial and laboratory trap is found.

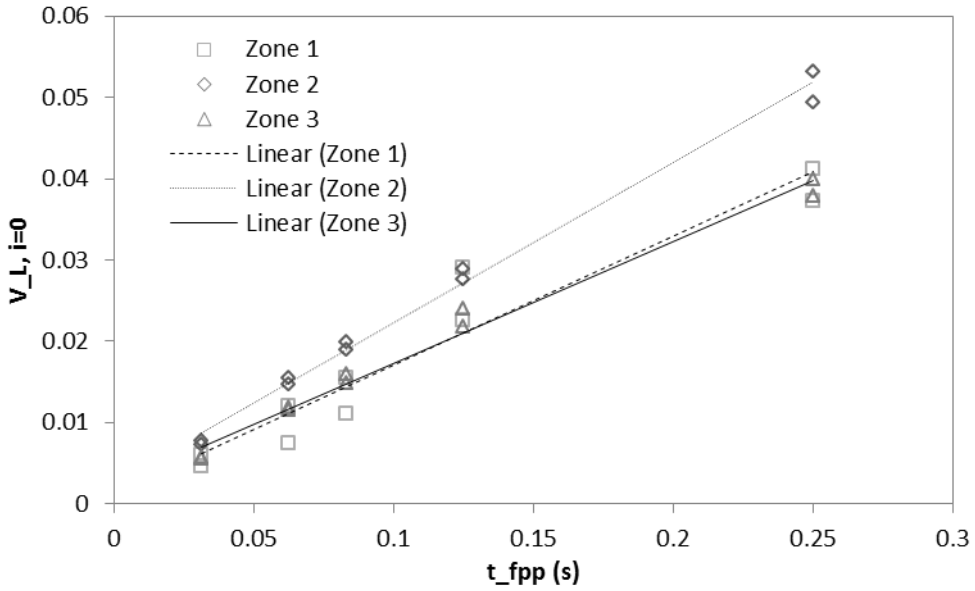


**Figure 5. 25, The velocity ratio at $i = 0$ along the three zones against the rise time of the first applied pressure wave in both traps. $R^2 = 0.9301$, $R^2 = 0.9934$ and $R^2 = 0.9858$ for Zone 1, 2 and 3 respectively.**

The following data determines the relationships between the maximum recorded velocity along the inner bend (which occurs within zone 2) and the velocities in zone 1 and 3.

| | t_fpp (s) | Zone 1 (0) | Zone 2 (Max) | Zone 3 (180) | Av Z1:Z3 |
|---|---|---|---|---|---|
| Laboratory trap | 0.25 | 0.0787 | 0.12 | 0.0844 | 0.08155 |
| | 0.125 | 0.0615 | 0.0615 | 0.0508 | 0.05615 |
| | 0.083 | 0.0233 | 0.0421 | 0.0338 | 0.02855 |
| | 0.0625 | 0.0157 | 0.0328 | 0.025 | 0.02035 |
| | 0.0313 | 0.00973 | 0.0165 | 0.0116 | 0.010665 |
| Commercial trap | 0.25 | 0.1447 | 0.2121 | 0.1528 | 0.14875 |
| | 0.125 | 0.0807 | 0.1161 | 0.0873 | 0.084 |
| | 0.083 | 0.0553 | 0.07912 | 0.0594 | 0.05735 |
| | 0.0625 | 0.0429 | 0.06113 | 0.046 | 0.04445 |
| | 0.0313 | 0.0215 | 0.0303 | 0.0225 | 0.022 |

**Table 5. 2, The velocity (m/s) in all zones and the average velocity in zone 1 and zone 3 at $i = 0$ at corresponding first positive peak time**

| | t_fpp (s) | Zone 1 | Zone 2 (Av) | Zone 3 | $v_{max}* L$ | Z2-Z3 |
|---|---|---|---|---|---|---|
| Laboratory trap | 0.25 | 0.03721 | 0.053238 | 0.039905 | 0.056736 | 0.013333 |
| | 0.125 | 0.029077 | 0.028869 | 0.024018 | 0.029077 | 0.004851 |
| | 0.083 | 0.011016 | 0.019867 | 0.015981 | 0.019905 | 0.003886 |
| | 0.0625 | 0.007423 | 0.01548 | 0.01182 | 0.015508 | 0.003659 |
| | 0.0313 | 0.0046 | 0.007782 | 0.005485 | 0.007801 | 0.002298 |
| Commercial trap | 0.25 | 0.041255 | 0.049402 | 0.037841 | 0.051351 | 0.011561 |
| | 0.125 | 0.022504 | 0.027606 | 0.02176 | 0.028108 | 0.005846 |
| | 0.083 | 0.015471 | 0.018898 | 0.014817 | 0.019155 | 0.004081 |
| | 0.0625 | 0.012024 | 0.014653 | 0.011478 | 0.0148 | 0.003175 |
| | 0.0313 | 0.006039 | 0.007269 | 0.005602 | 0.007336 | 0.001667 |

**Table 5. 3, The velocity coefficient ( $V_L$or $v_L$) in all zones and the variance between zone 2 and zone 3 at $i = 0$ at corresponding first positive peak time**

The damping effect of the zone 1 and 3 is considered to be the difference between the velocity between zone 1 and 2, and, zone 3 and 2. This damping effect or measure of friction is investigated below.

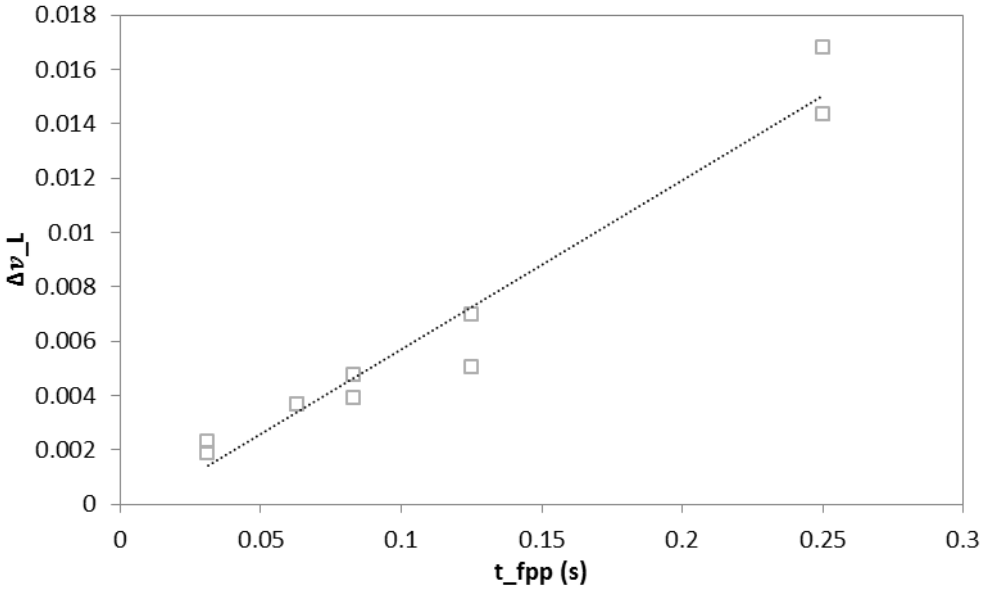


**Figure 5. 26, The differential velocity at $i = 0$ along the three zones against the rise time of the first applied pressure wave in both reference traps**

The relationship between the maximum pressure (found along the 60º plane) in zone 2, and either: the velocity in zone 1, velocity in zone 3 or the average velocity of zones 1 and 3; $R^2 = 0.6954$, $R^2 = 0.9562$, and $R^2 = 0.8514$ respectively. Best correlation in data variance across the frequencies is shown in Figure 5.26 and found using Eq.5.14 and 5.15 (below).

$$(v_{max} - v_{z3}) * \frac{L_I}{L_O} \qquad \textbf{Eq. 5. 14}$$

Here,

$$\Delta v_L = 0.0623 t_{fpp} - 0.0005 \qquad \textbf{Eq. 5. 15}$$

Using the average velocity across zone 2 as it covers a wider area of movement than zones 1 and 3, Figure 5.27 presents the friction factor as a function of L for the two appliance trap seals.

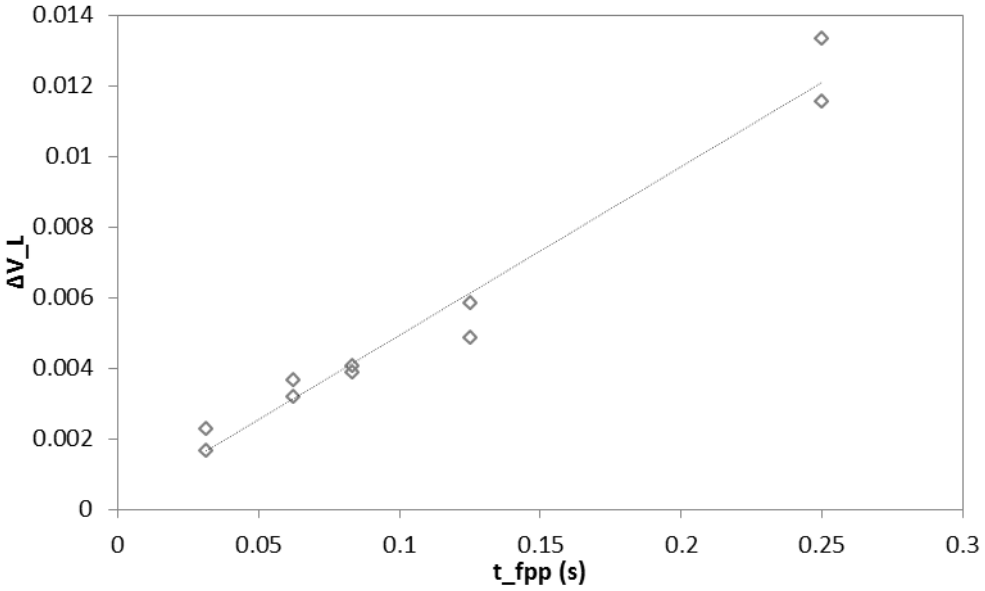


**Figure 5. 27, The variance in velocity between zone 2 and zone 3 using V_L at $i = 0$ against the rise time of the first applied pressure wave in both reference traps. $R^2$ = 0.9688**

$$\Delta v_L = 0.0478 t_{fpp} + 0.0002 \qquad \textbf{Eq. 5. 16}$$

As data for both traps present water at plane 180, the data on this plane is used as the base to measure the resistance of motion of water nearest the free surface of the water column. From Figure 5.27 the relationship presented in Eq 5.16 is gained. This finding addresses Objective 2 of this study, along with the findings noted at the beginning of Section 5.3.3. The unsteady frequency dependant frictional relationship is established along with a methodology basis for the development of Eq 5.16. These findings will be reiterated in Section 5.5.

## 5.5. Conclusion

This chapter has investigated the unsteady flow characteristics of the water trap seal due to the nature of the applied pressure transient frequency, satisfying objective 1, and

presenting the analysis method for developing the deterministic frequency dependent friction factor required to address Objective 2.

Velocities within the water trap below 3 Hz and above 4Hz were found to differ significantly, confirming an earlier finding by Gormley and Beattie (2010) that a transitional zone between 3 and 4Hz exists. The research has also found that three zones of movements exist in both trap seals, and a likely link between the inner length of Zone 1 (irrespective of geometry) is suggested. This notion of velocity as a paradigm irrespective of geometry was entertained further, forming a base line from which velocity is a construct of the inner and outer bend length was developed. Subsection 5.3.3, provides a suite of 3 equations in this form which express velocity along the trap seal bend.

It is also noted in this chapter that the appliance trap seal with the shorter inner bend is more vulnerable to induced siphonage due to the higher recorded velocities. This insight into the velocity profile, zones of movement within the seal, and the notion of velocity as a function of geometry between all water trap seals (u-bends), has never before been gained and offers researchers in this field an interesting platform for further research.

An assessment of the zones of movement led the rationale for the difference between the damping zone (zones 1 and 3) and the region of constant movement as a friction representative. A new frequency friction factor expresses this relationship, highlighting the effects of frequency of applied air pressure wave on water velocity in the trap.

# Chapter 6

## Fluid Structure Interaction – Laboratory and Numerical Investigations

### 6.1. Introduction

Airflows in Building Drainage Systems are inherently transient, presenting both computational and experimental challenges. The effect of these transient air flows on the characteristic movement of non-rigid self-sealing valves - waterless traps, has been investigated through laboratory and computational methods to satisfy Objective 3 of this research. The employed methods allow analysis of shapes and patterns, and enumerate the flow changes by observing closely the opening and closing movement. These laboratory and computational techniques, though not previously used in this application provide a qualitative and quantitative representation of the deformable valve's oscillatory movement.

In this chapter the term sheath refers to the simplification of the shape of the waterless trap seal to a cylindrical tube of uniform cross sectional area, while, the term valve is used to express a device or system through which fluid flows and in turn self-oscillates over a range of frequencies. The chapter provides a description of the waterless trap seal and draws on the work of others for an initial classification of a fundamental mathematical model for the device. Research from areas as diverse as; the definition of

human lip movement for embouchure analysis in musical physics, to, vocal cord visualisation studies in the field of medicine, were consulted and have played a role in helping to define the complex mechanical motion associated with waterless trap opening and closing.

The term photogrammetric is used to define a novel analytical technique coupling photographic image data with system pressure data. The photographic imagery is transformed into a 2 dimensional grid matrix defining each pixel in a binary fashion and linked to system pressure in preparation for further investigation by Fourier analysis to relate the opening and closing of the valve to applied transient air pressures. This coding of images and pressure data has proved to be a powerful tool with which to define complex moving parts and the methodologic procedures, together with the derived frequency dependent boundary equations for the reference product waterless traps are described in full in this chapter.

## 6.2. Mechanical properties of the valve

In general terms, an oscillation describes the repetitive forward and backward movement of an object. This phenomenon occurs commonly when an object is struck for example, a church bell, a swing, or a pendulum. The likelihood of flow induced oscillation depends largely on the design, the material composition of the product, and the applied force (direct, reflected or attenuated). In the case of the waterless trap seal, the periodic force of airflow on a valve is expected to disturb the position of rest, and result in the valve's lips producing differing size deformations, therefore relating not just material composition, but the importance of the airflow characteristics to the valve's motion or the valve's motion on pipe reflections.

A useful starting point for the analysis of the waterless trap seal is to identify the similarities of this device with that of research in different fields of science. If we consider the waterless trap seal to be a valve like any other which allows the propagation of a liquid or gas through it, this valve can be likened to biological

elements, such as vocal cords and lips reeds; both of which act as air suppression and control devices.

Research of vocal cord movement (the coupling of both mechanical and medical science), is a fairly recent development with early research being by Flanagan and Landgraf (1968), and Ishizaka and Flanagan (1972). These researchers investigated the vocal cord vibration as a result of an applied airflow and developed a simplified model of self-sustained oscillations. These models are the one mass model by Flanagan and Landgraf (1968), and the two mass model by Ishizaka and Flanagan (1972). These common descriptions of the vocal folds use a "source filter" theory, where the valve is depicted to operate in complete independence of its surrounding elements and their associated acoustic field (Newton, 2009).

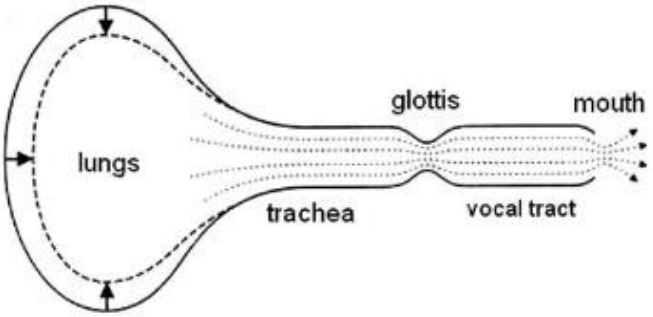


**Figure 6. 1, Representation of the voice production system. Source: originally adapted from Titze,(1994) cited in Cataldo *et al* (2006)**

The complicated geometry of the vocal cord valve is generally condensed down into a small number of discrete masses using the 'lumped element' method (Newton, 2009). This method used by Flanagan and Landgraf (1968) and Ishizaka and Flanagan (1972), is found in numerous lip reed and vocal cord studies and describes the mechanical response of the reactive valve (see Newton, (2009); Bromage, (2007); Stevenson, (2009); Story and Titze, (1995).

The lumped element model or lumped parameter model is based on the analogue of an electrical circuit where the lumped elements of a circuit: the resistance, capacitance and inductor are equalled to the force, the mass and the acceleration terms in a mechanical system.

$$\boldsymbol{V} = L\frac{\partial I}{\partial t}\ \ equals, F = \ m\frac{\partial v}{\partial t} \qquad \textbf{Eq. 6. 1}$$

The relationship between frequency of the applied force and the amplitude of an opening can be formed using this simplification of movement. The disadvantage to using this modelling approach however is in the level to detail lost. The fewer the elements existing in the system, the less likely it is that the system behaviour is realistically captured. Figure 6.2 and 6.3 show pictorially the depiction of the oscillatory motion in relationship to a springs, viscous damper and mass system. Here, by Hooke's law $F = Kd$ is considered.

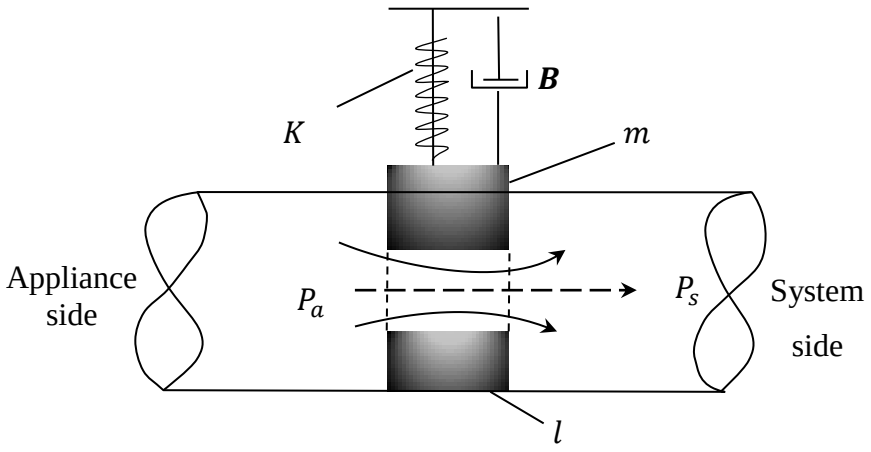


**Figure 6. 2, The simple one mass model of the valve (laid horizontally), where the lips are assumed to behave like masses on springs. A constant pressure $p_a$ is applied pressure on the appliance side of the pipe and the pressure exiting the valve channel is $p_s$.**

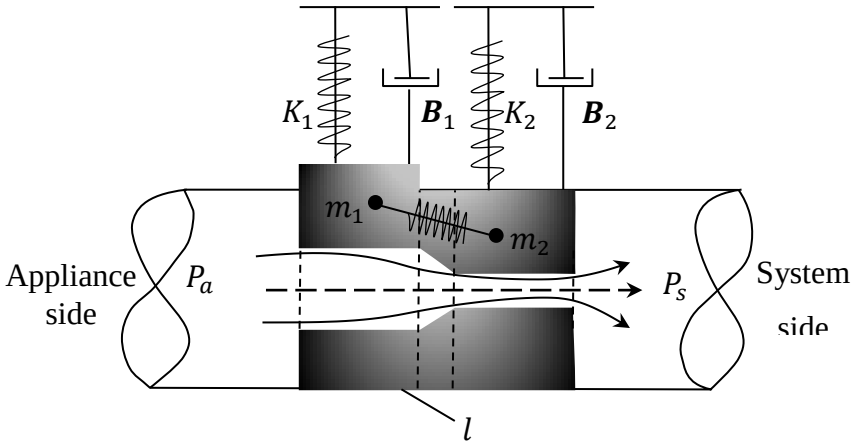


**Figure 6. 3, The two mass model of the valve (laid horizontally), where the lips are assumed to behave like masses on springs. A constant pressure $\boldsymbol{p_a}$ is applied in the pipe and a volume flow $\boldsymbol{v}$ enters the lip channel, whose height is denoted by h. the pressure exiting the valve channel is $\boldsymbol{p}$. (adapted from Ishizaka and Flanagan (1972))**

For the one mass model, the following applies,

$$M\ddot{x} + \boldsymbol{B}\dot{x} + Kx = F(t) \qquad \textbf{Eq. 6. 2}$$

Where $x(t)$ is the displacement of mass $M$, $\boldsymbol{B}$ is the viscous damper, $K$ is the spring stiffness, and F is the force.

## 6.3. Image analysis procedure

The methods employed throughout this chapter seek to enable a simpler representation of pipe opening to be developed, using photogrammetric data. Previous research for instance Kuo *et al*, (2013), used images captured from an endoscopy video and transformed them into binary format. Here the size of the opening was determined and a process developed for the selection of the largest and smallest opening area images.

In order to determine the mechanical response of the valve, high speed digital frames were recorded using the Photron Fastcam PCI Monochrome 500. This device records images in greyscale, (see Figure 6.5) at a rate of 250 frames per second. A total of 15000 images were gathered for each test run; spanning the stepped incremental increases in pressure applied to the trap. This data will be analysed in great detail in the subsequent sections and subsections within this chapter.

A custom program was written for the analysis of the greyscale photographic data. This code written in $C^{++}$ language converts the image into a series of corresponding black or white pixels relating to the original image.

The binary image code comprises of five main elements:

- An executable program (*.exe)
- A text input file detailing the threshold parameter and instructions for conversion of images (*.txt)
- Photograph input folder storing all original images to be converted to black and white images. (in jpeg format)
- Photograph output folder – gathering all converted black and white images (in jpeg format)
- The results (percentage, height and width) from each image in the output folder recorded in sequential order in comma separated valves format (*.csv)

### *6.3.1. Binary image processing*

The binary image system processes the information in a greyscale image via the recognition of an object apart from the background from all corresponding grey values. The system translates the greyscale images to monochromatic images with a single bit; 0 or 1. The cell/pixel colour recognition software compiled in Microsoft visual studio and written in $C^{++}$ language, was developed by the Heriot Watt Drainage group and customised for this application, created the binary image system for this project. This tool for data analysis was used previously by Filsell (2006) in the studies of water

curtain, rolling waves, and annular flows in vertical stack drainage, and was found to be of great use in flow analysis. This early edition of the software was re-written for the requirements of this project. The enhancements include the measurements of height and width and the colour of the target object. As shown in Figure 6.4, the dark regions are coloured white and the light regions are coloured dark. This logic was reversed here, so that the opening area of the pipe which is noted as dark in colour due to no lighting within the pipe, remained as is, and all other external features in the laboratory setup were converted to white.

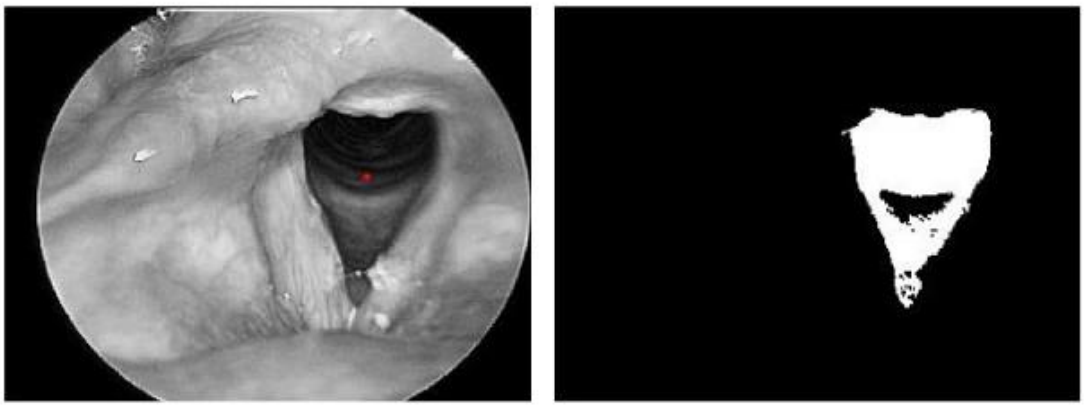

**Figure 6. 4, Image of vocal folds (left) and corresponding binary image of opening area (right) Source: Kuo, C. *et al*, 2013**

By ignoring the variations to movement along the length of the value and isolating a single opening area, this tool was able to record the valve's mechanical/ structural response to the pressure transients. Figure 6.5, shows an image for each reference waterless trap seal during testing. The $C^{++}$ code converts the images to binary format and a count of the image dimensions is made. The program uses the Portable Binary Map (PBM) file format and displays images using the binary logic.

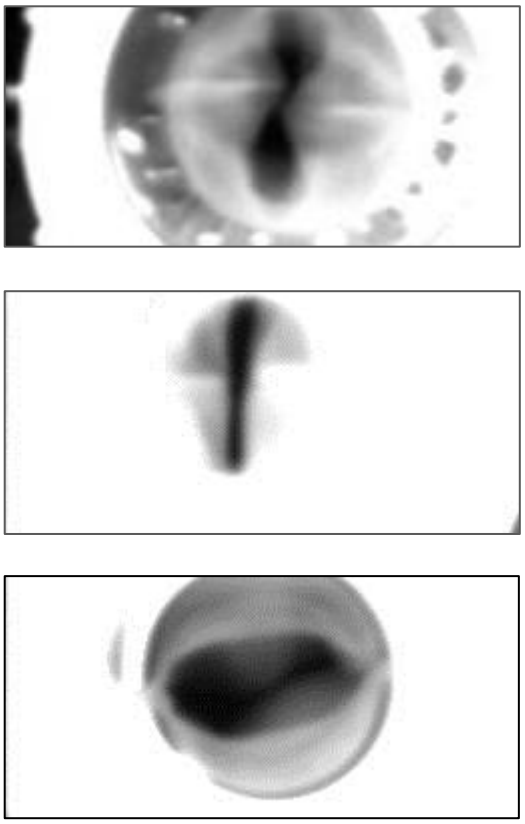

(a)

(b)

(c)

**Figure 6. 5, Greyscale recorded images of Sample 1 (a), Sample 2 (b), and Sample 3 (c)**

#### *6.3.1.1* ***Segmentation***

All pixels in an image hold an intensity value; a simple commonality. The process of segmentation through thresholding, allows the separating of light and dark regions in a frame by the masking of an object is a binary picture. Once the image has been separated into two regions, the background and object, its topological and geometric properties useful to image analysis are attained.

This research project required the separation of the trap opening (object) and the valve, pipe, orifice, and setup apparatus (collectively grouped as the background). The $C^{++}$

code first checks if the PBM files are valid, then scans each pixel within the photograph and separates pixels relating to the trap opening from the pixel relating to the rest of the elements in the frame. The logic configured here is: the opening of the water less trap seal is logic 0, while all other external elements are logic 1. The process of pixel threshold selection is vital to the accuracy of the geometric results

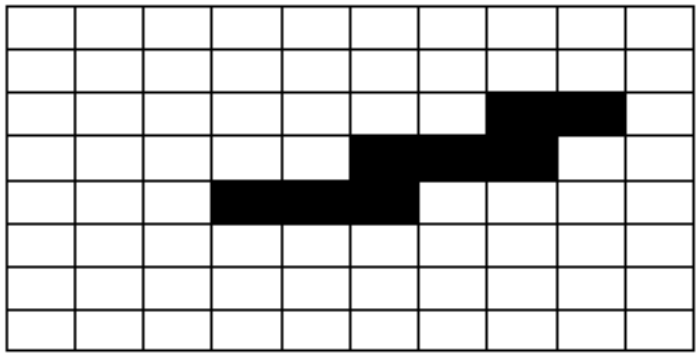

| | | | | | | | | | |
|---|---|---|---|---|---|---|---|---|---|
| 1 | 1 | 1 | 1 | 1 | 1 | 1 | 1 | 1 | 1 |
| 1 | 1 | 1 | 1 | 1 | 1 | 1 | 1 | 1 | 1 |
| 1 | 1 | 1 | 1 | 1 | 1 | 1 | 0 | 0 | 1 |
| 1 | 1 | 1 | 1 | 1 | 0 | 0 | 0 | 1 | 1 |
| 1 | 1 | 1 | 0 | 0 | 0 | 1 | 1 | 1 | 1 |
| 1 | 1 | 1 | 1 | 1 | 1 | 1 | 1 | 1 | 1 |
| 1 | 1 | 1 | 1 | 1 | 1 | 1 | 1 | 1 | 1 |
| 1 | 1 | 1 | 1 | 1 | 1 | 1 | 1 | 1 | 1 |

**Figure 6. 6, Pixelated image and corresponding image in binary format**

#### *6.3.1.2 **Threshold and averaging***

Variations in daylighting, reflections due to the colour and material of the trap along with the oscillatory frequency (aternating with pressure) lead to changes in illumination across the waterless trap seal throughout the test period. Local thresholding is advantageous as global thresholding does not compensated for changes in illumination within a single image, and thus changes in the greysscale opening area pixel colour. Global thresholding runs the risk of introducing extraneous pixels data into the binary image. Due to the size of the image the effect of lighting in a single frame is believed to secondary to the effect of variations over time. Therefore, the photographic data was subdivided into regions based on the pressure profile and a global thresholding scheme adopted.

$$f_t(x,y) = \begin{cases} b_1 & if\ f(x,y) > T \\ b_0 & if\ f(x,y) \leq T \end{cases} \qquad \textbf{Eq. 6. 3}$$

Where: T is the threshold, $f_t$ is the binary image function, $f$ pixel intensity, $b_1$ binary locic 1, $b_0$ binary logic 0, and $(x,y)$ is the spatial cordinate. The gray level 0 is the darkest and the gray level 1 is the lightest.

```
Averaging          // Comparison method - set to Averaging or Polling
5                  // Surround in pixels when calculating brightness
51                 // Cut-off value for black / white (0-255)
```

**Figure 6. 7, Screenshot of requirements of the text file**

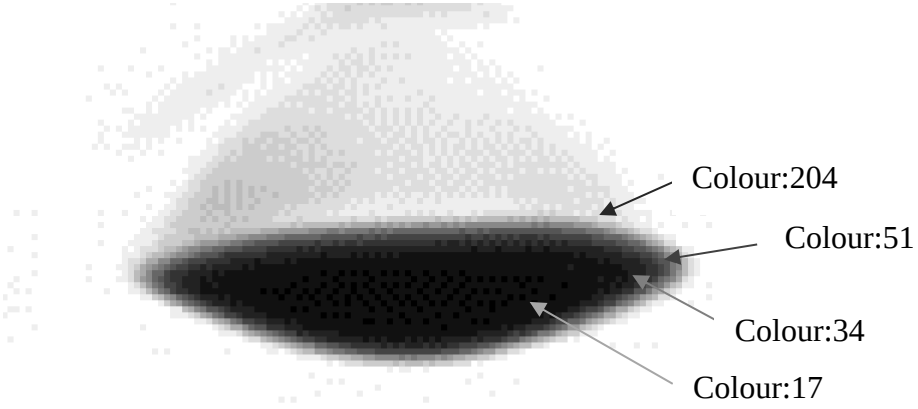


**Figure 6. 8, Screenshot of pixel colour variation for a Sample 2 image**

Local thresholding enables the identification of the intensity of the opening area within each subdivided region. It was found possible for image intensity within the samples from a single test to vary according to the quality of lighting levels. Using a loop system, the executable file was run to determine if the isolated threshold colour (referred to as cut-off value in Figure 6.7) provided results which were alike to the raw data. If unsatisfactory the colour intensity is reinvestigated until results gained for each data set are true to the unaltered images. The second variable – averaging, is altered upon the requirements of each data set accorrding to the concentration of the threshold colour outide the target object.

Averaging acts as a size filter, filtering any noise out of the binary image. An average value of 1 regards only the pixel data for the pixel under regard. An average of large value (>1, say 5), regards the intensity of surrounding pixels choosing its identity based on the identity of surround pixels. Figure 6.9 and Figure 6.10 display the influence of threshold selection and averaging on the resulting binary image of Figure 6.5c.

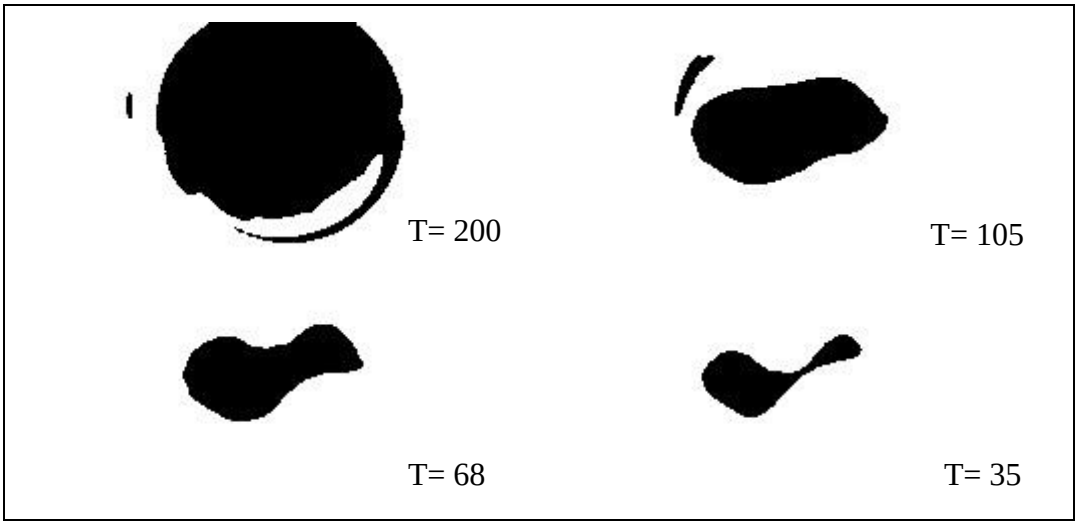


**Figure 6. 9, Conversion of Figure 6.5c (Sample 3 image) into a binary image using different threshold but a constant averaging of 1. Where T is the threshold**

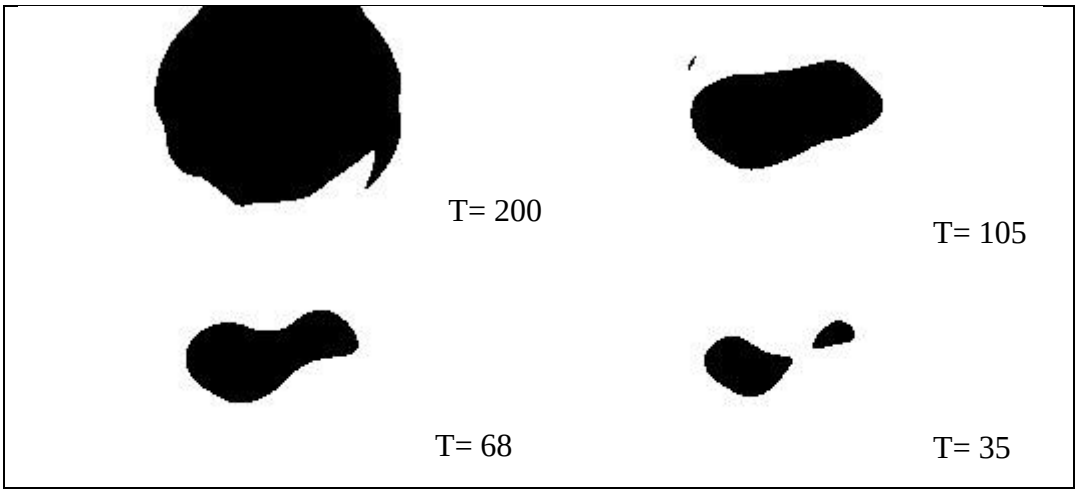


**Figure 6. 10, Conversion of Figure 6.5c (Sample 3 image) into a binary image using different threshold but a constant averaging of 5. Where T is the threshold**

It should be noted that Figure 6.5a is processed into a binary image with averaging value of 5 to ensure that the dark region to the left of the photograph is not shown in the

binary image. This dark region is not found in Samples 2 and 3, and so, an averaging value of 1 is commonly adopted. The commonly noted thresholds for the three samples is $T = 51$ for Sample 1, $T = 34$ for Sample 2 and $T = 68$ for Sample 3.

### 6.4. Calibration of Pixels to metric measurements

This section introduces the method of converting the data which is gathered by the cell/pixel recognition software to a metric scale of distance. This information about the opening of the orifice in relation to the connected pipe is important, as it provides a sense of scale to the measured readings. Up till now, all readings are referenced to the size of the image frame.

The recordings by the program of the binary image geometric characteristics are of the: height, width, and percentage logic 0 to logic 1 in the frame. The height is determined by a count along each column for the max number of logic 0 and the process is repeated along each row for the max number of logic 0 to determine width.

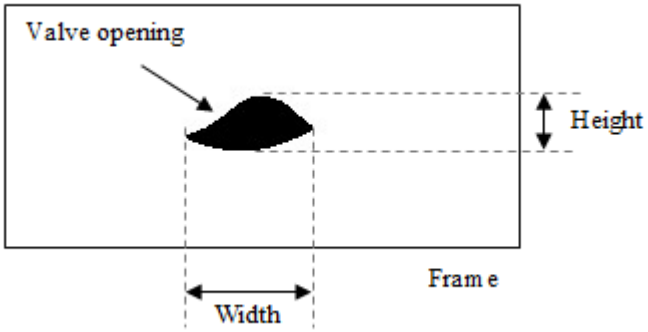


**Figure 6. 11, Schematic showing the valve wall boundary and the definition of area, height and width of the opening.**

All data thus far has been enumerated in pixels and with reference to the image resolution. In order to develop boundary conditions the data regardless of the unit of measure is required to be comparable to the pipe dimensions. Therefore, a relationship

must be developed to relate this data to actual physical units of measure. The data was calibrated by first establishing a commonality between all readings. The orifice (the end of the pipe fitting) which enables connection between the waterless trap seal and the 50mm pipe is used as the constant between the trap seals, as due to overexposure, the connection between the fitting and the waterless trap seal is only clearly displayed in the Sample 3 test images (see Figure 6.5). This constant however is valid (regardless of the slight variations in dimension) as, in the event a reference trap seals is blown out of its original position upon prodding, the orifice would remain and be considered the maximum opening to the pipe.

The area of a binary image is given by:

$$A = \sum_{i=1}^{n} \sum_{j=1}^{m} B|i,j| \qquad \textbf{Eq. 6. 4}$$

Where, $B|i,j|$ is the binary region

In order to determine the relationship between the pixel data and the real measurements of the trap seal and thus determine and analyse the openings of the trap seal, the binary images were used to first determine the width and height of the waterless trap seal. The converted image in this step is shown in Figure 6.5(b). Once this geometric data was known, the photograph is manipulated by converting the entire waterless trap to a colour 0 region. This new edited binary photograph is then processed by the software in much the same way it would a colour photograph, and the height, width and percentage area of the orifice to the frame (120 x 256 pixels) is calculated. This data is validated by comparison with the recordings from the first processed image (Figure 6.5(b)). This method of calibrating photographs was also followed for samples 1,and 2, but difficulty was encountered in producing images for samples 1 and 2 similar to Fig 6.12c (where all elements outside the pipe orifice are produced as colour 1). As the pipe orifice is constant for all tests the calibration results for sample 3 are used. This process is presented in greater detail in Figure 6.12

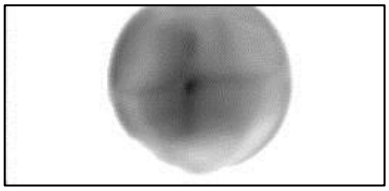

(a)

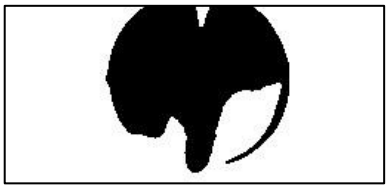

(b)

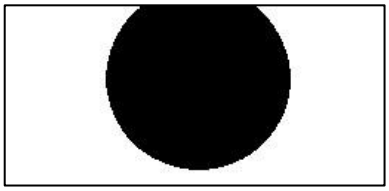

(c)

**Figure 6. 12, From the Sample 3 data set: reference image (a), corresponding binary image (b), edited binary image (c)**

To ensure accuracy in the measurement of the orifice area in pixels, multiple images were processed until certainty in the results was reached. From the measured diameter of 31.89mm the following relationship were determined.

$$1\,mm = 3.455 pixel \qquad \textbf{Eq. 6. 5}$$

$$A = 25.736 a_f \qquad \textbf{Eq. 6. 6}$$

Where, $A$ is the opening area, and $a_f$ is the % opening of the frame

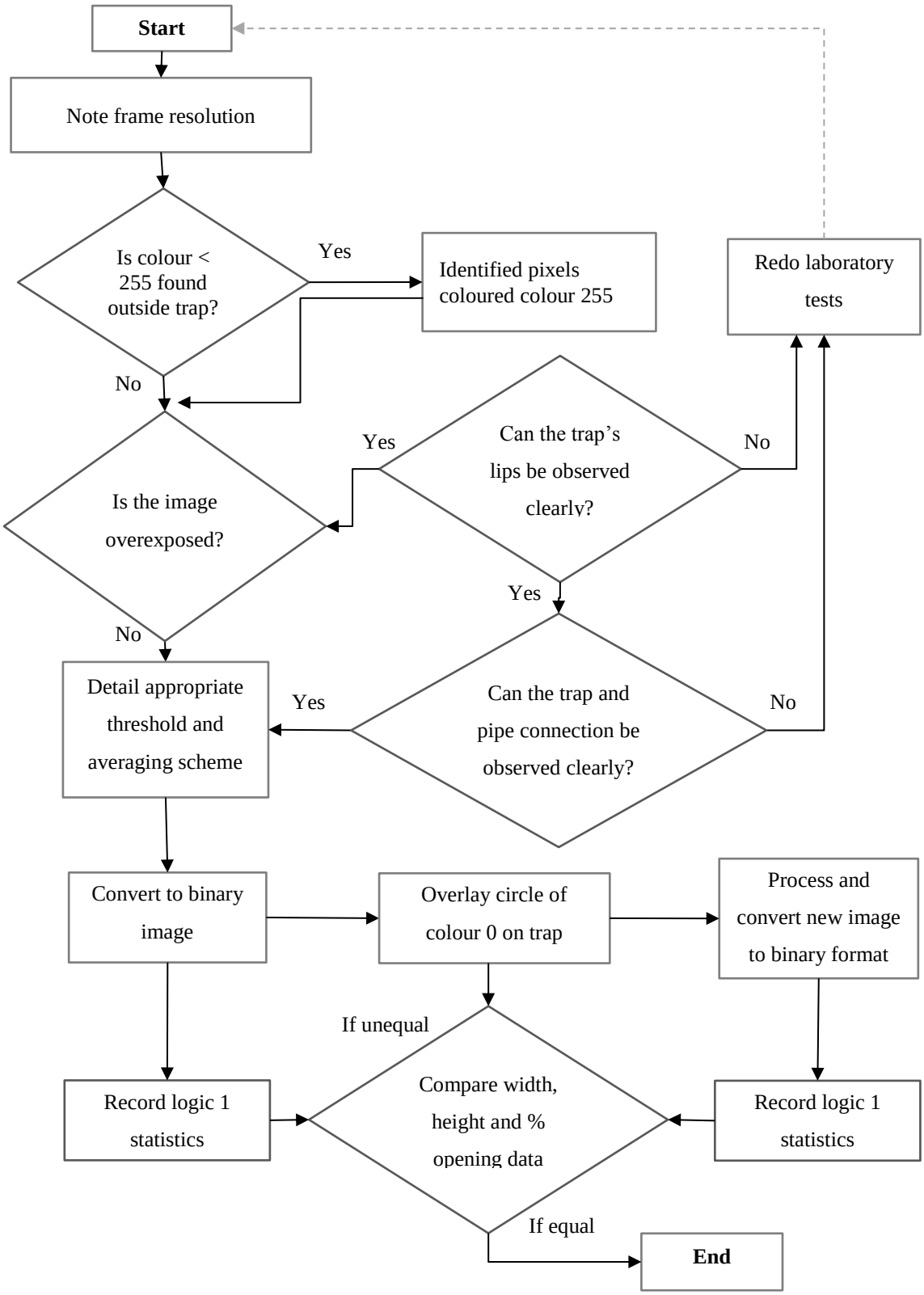


**Figure 6. 13, Method to establish the size of the waterless trap seal orifice in pixels**

| | | |
|---|---|---|
| Radius | 62.5 pixels | 31.89 mm |
| Max opening area of orifice (pixel²) | 12271.85 | 1028.1 mm² |
| Frame resolution | 30720 pixels² (256 x 120 pixels) | 2565.6 mm² (73.98 x 34.68 mm) |

**Table 6. 1, Relevant measurements in pixels and the corresponding metric measurements**

## 6.5. Accuracy

### *6.5.1. The effect of the reference products*

Using the reference image shown in Figure 6.12, the calibration of pixels to millimetres was obtained. An error is likely when using the calibrated measurements from Sample 3 as the conversion measure for Sample 1 and Sample 2 image readings. Though it is not suspected that an error should be noted as this data was taken in the same experimental session slight inline movements to the camera and lighting were made when needed during the experimental process. Additionally, as different reference products present differently in the images and provide less clarity than shown in Figure 6.12a it is not possible to calculate the degree of accuracy in the readings.

### *6.5.2. Thresholding*

Each sample data set is not only reliant on the conversion measure to millimetres, but also on the selection of threshold colour to the accuracy of the measured data. For Sample 2 it was determined that if the threshold colour was selected to be $T = 160$, then the resulting opening area would be 82.1 mm², or for $T = 34$ for the same image, the resulting opening area 35.52 mm². A 131.1% differential is found between the

calculations, showing the importance of the threshold estimation which at T=160 could regard the valve as being open when the opposite is true.

## 6.6. Laboratory results

This section presents the only laboratory component of this research. As described in Chapter 5, three waterless trap seals were investigated. Section 6.5 explained the photogrammetric methods used to analyse the large data set to provide quantitative data from photographic data which presents mainly as qualitative data.

The transient variation in the pressure reading within the pipe correspond to the mechanical motion of the waterless trap seal; noted by the opening size – opening percentage (to frame size), height, and width. This data was determined through the process described in Section 6.3. The following subsections detail the analysis of the pressure readings, the opening shape and the opening size in time.

Pressure traces relating the oscillatory movement of the waterless trap seal were increased in increments spanning a total time of 60 seconds. Within this time 16, 16, and 11 pressure increments were noted for Sample 1, 2 and 3 tests respectively. The four highlighted data sets in Figures 6.14, 6.15 and 6.16 represent comparable regions of steady pressure for opening threshold, low, medium and high pressure. These ranges are selected to present a platform for comparison of movement as either pressure or opening area during the range can be likened.

It is important to make note that the division of the data sets were determined first, and then within these incremental sets, observations of movement were noted. The threshold range may not always be absolute as first opening may in actuality occur between the considered sets. Models developed in Section 6.7 however, will aim to mimic the opening area shown in the data set, and so to in the previous data set where the trap should remain closed in relation to the corresponding pressure trace. Therefore, the

predicted threshold should occur as measured between the data sets, through accuracy in the timing is not expected.

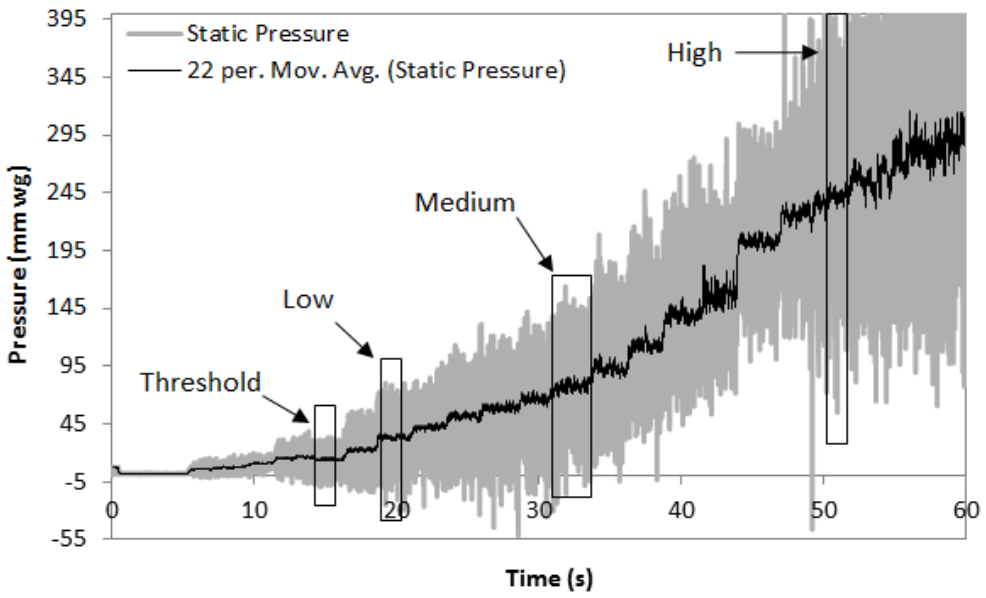


**Figure 6. 14, Pipe pressure readings during the testing of sample 1. Regions: threshold, low, medium, and high.**

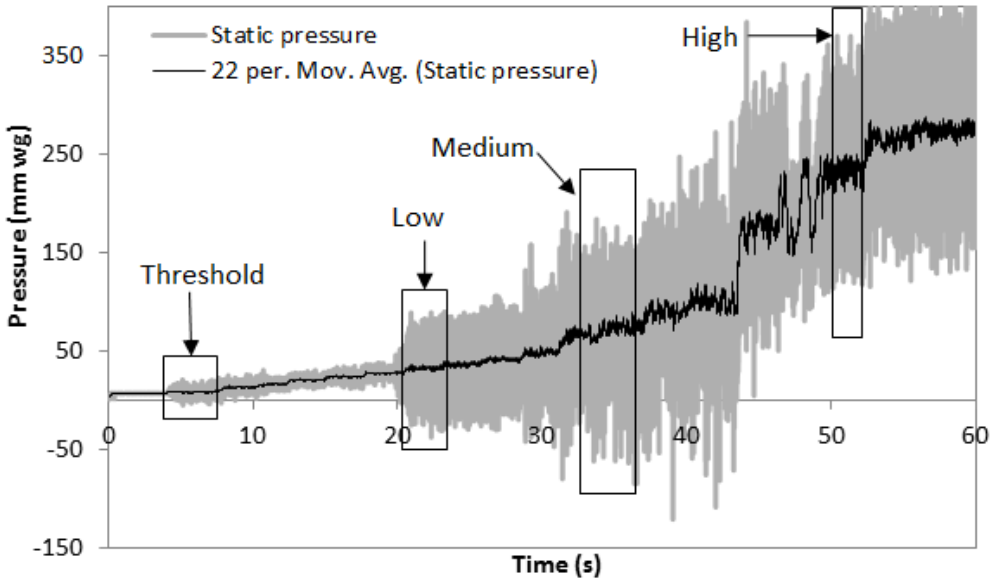


**Figure 6. 15, Pipe pressure readings during the testing of Sample 2. Regions: threshold, low, medium, and high.**

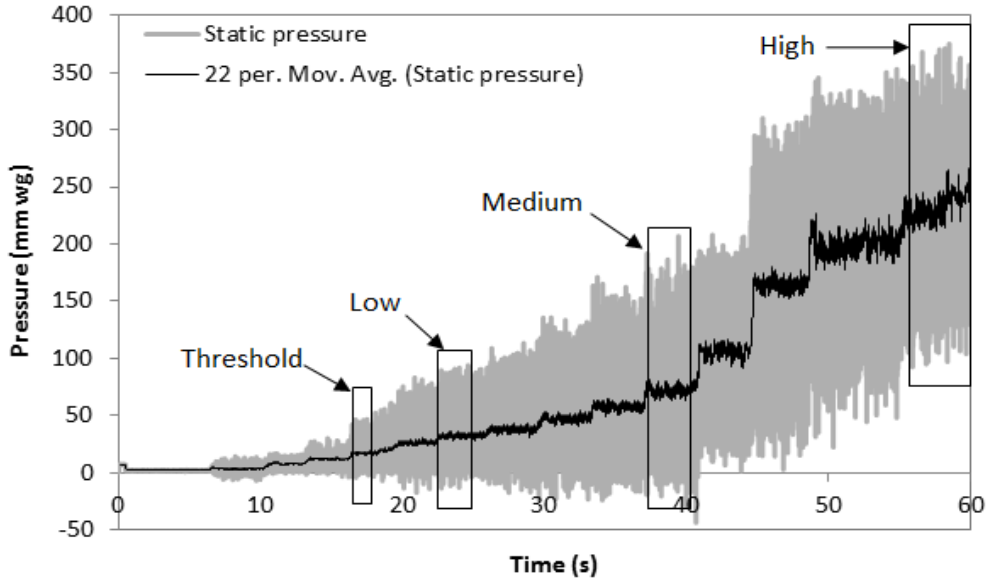


**Figure 6. 16, Pipe pressure readings during the testing of Sample 3. Regions: threshold, low, medium, and high.**

The regions of valve opening threshold, along with low, medium and high pressure regions are presented in Table 6.2.

| Range | Sample 1 | | Sample 2 | | Sample 3 | |
|---|---|---|---|---|---|---|
| | Time (s) | Pressure (mm wg) | Time (s) | Pressure (mm wg) | Time (s) | Pressure (mm wg) |
| **Threshold** | 14 to 15s | 14.598 | 4 to 8s | 8.484 | 17 to 17.3s | 16.675 |
| **Low** | 19 to 20s | 33.049 | 21 to 23s | 32.464 | 23 to 25s | 31.973 |
| **Med** | 31 to 33s | 76.994 | 33 to 36s | 70.919 | 37 to 40s | 71.446 |
| **High** | 50 to 51s | 239.255 | 50 to 52s | 232.374 | 56 to 60s | 233.818 |

**Table 6. 2, Comparable average pressure readings for data between the opening threshold, low, medium and high pressure regions.**

As shown in Table 6.2, this section has identified 4 comparable ranges which will be used throughout this chapter to present analysis of the results of the laboratory study.

### *6.6.1. Measurements of repeatable patterns*

Movement patterns were distinguished by the shape of the pipe opening, common opening size, and the consistent repetition of those sizes and opening shapes. In the instance where Sample 1 is installed, the number of images per cycles decreases steadily with an increase in pressure. Between the mean pressures of 17.18 mm wg and 39.5 mm wg a 5 image cycle is noted, 46.29mm wg and 73.26 mm wg a 4 image cycle, 82.8 mm wg and 113.19 mm wg a 3 image cycle and so on (See Figure 6.18).

Anomalies within identified opening cycles are sometimes found. The data for the threshold opening of Sample 1 shows a 6 shape opening cycle however 5 images instead of six may present in 1 of the 4 cycles. In general, the opening area to the pipe increases between the low to medium range but reduces in the high range. Another anomaly is found in the motions of Sample 3. Unlike Sample 1 and 2, Sample 3 presents a pattern of two valve open images per cycle between 16.7mm wg and 46.9 mm wg. At these pressures, the other waterless trap seals remain constantly open and no cyclical pattern is recorded.

Discerning a pattern in this Sample 1 data range proved difficult as the images at first assessment were regarded to be random; with no consistent pattern. The 4 cycles shown in Figure 6.17 were however noted to exist among a significant amount of random motion.

Similarities were not just noticed in the shape displayed by the waterless trap but also by the size of the opening. Figures 6.17 to 6.19, show that the opening size of the trap seal can be predicted as the shape (approximately equal in size) repeats every cycle.

| Cycle | Image 1 | Image 2 | Image 3 |
|---|---|---|---|
| 1 |  | | |
| 2 |  |  | |
| 3 |  | | |
| 4 |  | | |

**Figure 6. 17, The repeated oscillatory pattern over 12 images (over 4 image cycles) of Sample 1 (Med) openings between 31s - 33s of the test. Images 7916 to 7927 of 15001 processed to display only colours 0 and 255. Threshold colour for opening is 51 with averaging 5.**

| Cycle | Image 1 | Image 2 | Image 3 | Image 4 | Image 5 | Image 6 |
|---|---|---|---|---|---|---|
| 1 |  |  |  |  |  | n/a |
| 2 |  |  |  |  | |  |
| 3 |  |  |  |  |  | n/a |
| 4 |  |  |  |  | | n/a |

**Figure 6. 18, The repeated oscillatory pattern over 21 images (over 4 image cycles) of Sample 2 (Low) openings between 21s - 23s of test. Images 5282 to 5302 of 150010 processed to display only colours 0 and 255. Threshold colour for opening is 34 with averaging 1.**

| Cycle | Image 1 | Image 2 | Image 3 | Image 4 |
|---|---|---|---|---|
| 1 |  |  |  |  |
| 2 |  |  |  |  |
| 3 |  |  |  |  |
| 4 |  | |  |  |

**Figure 6. 19, The repeated oscillatory pattern over 16 images (over 4 image cycles) of Sample 3 (Med) openings between 37s – 40s of the test. Images 9385 to 9400 of 15001 processed to display only colours 0 and 255. Threshold colour for opening is 51 with averaging 1.**

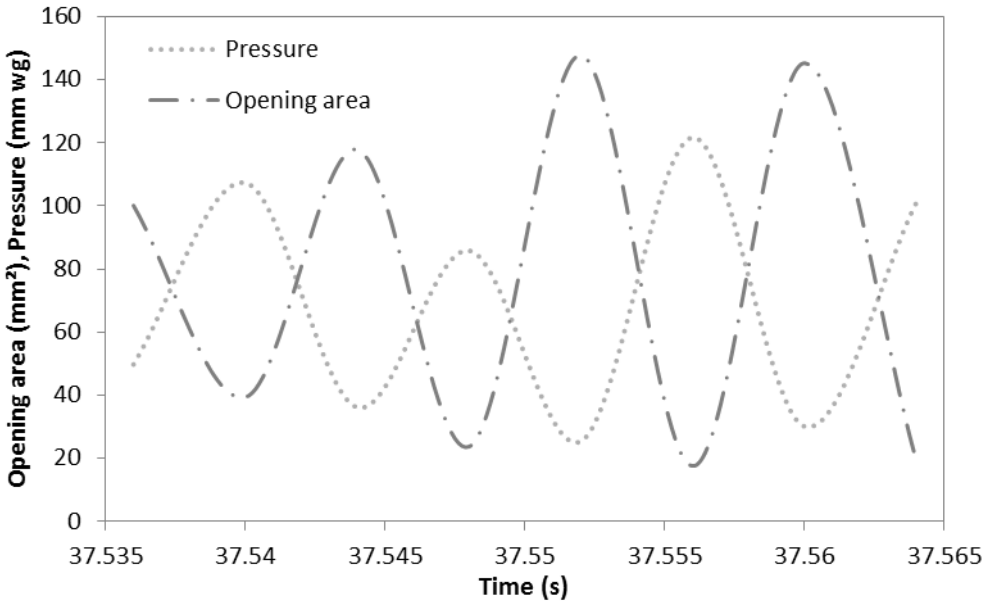


**Figure 6. 20, Opening area for images 9385 to 9400 and the corresponding pressure readings plotted against time. This plot relates to the cycle images shown in Figure 6.17**

Figure 6.20 shows the plot of the opening area and pressure for the cyclical images for Sample 3 in the medium range. The plot expresses the relationship between the build-up of pressure in the pipe during closure and the instantaneous reduction in pressure upon the opening of the valve. This relationship between pressure and opening area is expected to yield comparable frequency readings as the oscillatory motion and pressure gradient operate in unison. Of significance here, is the opposing phase of the opening and closing of the trap, and the pressure amplitude within the trap.

Frequency of movement can also be regarded from the number of images per cycle. Figure 6.21 excludes the data sets where no image data is recorded, but shows that Sample 1 reduces most steadily in the length of a cycle as the pressure is increased on the valve. Sample 2 remains constantly open at low pressures but quickly mimics the pattern found in Sample 1 at high pressure ranges (greater than 140 mm). While Sample 9 it was found to provide no consistent pattern. Once above the RMS pressure value of 45.23mm wg the cycle length becomes more difficult to predict. However above 100 mm wg the cycle length constantly increases.

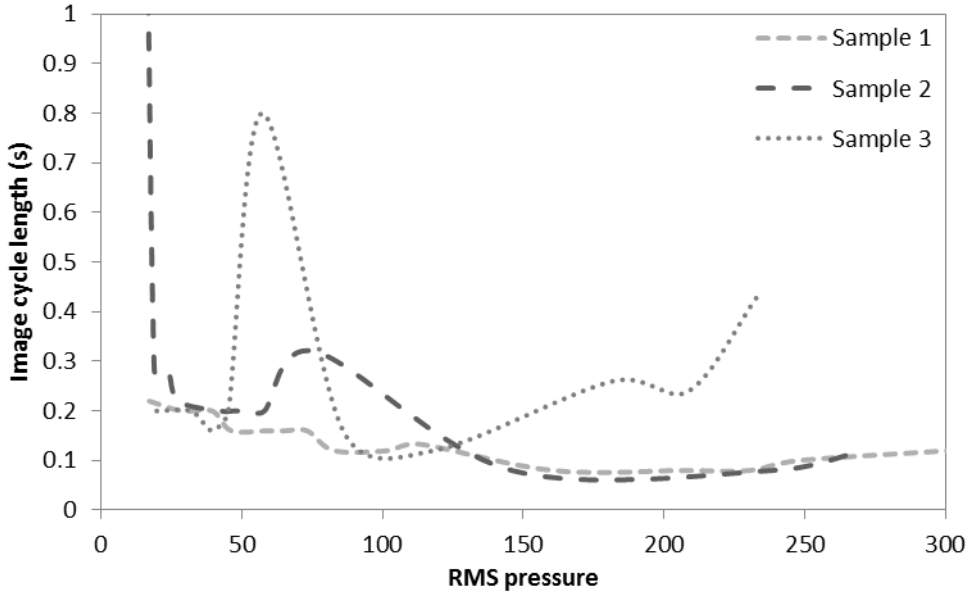


**Figure 6. 21, Duration of each cycle of a repeated oscillatory pattern across the range of applied pressures for the installed reference products**

The consistencies of found cyclical images throughout the data ranges in all tested prototypes suggests that the oscillatory motion of the waterless trap seal can be predicted. All further analysis is aimed at mathematically reproducing the motion observed and shown in this section.

### *6.6.2. Determining the opening area by the linear measurements*

This section examines the relationships which exist between the opening area of the waterless trap seal and the maximum height and maximum width of the opening as the opening shapes displayed in Section 6.6.1 showed the commonly formed arbitrary geometries.

Similar studies in other scientific fields such as acoustic modelling, aim to develop an artificial system which links pressure and opening size, to the pitch or note of a played instrument. The intended outcome of this examination is to determine the mathematical relationship between the opening area of the valve and the linear measurements, additionally, determine whether through this numerical approximation the valve opening is a function of its elasticity.

Figure 6.22 and Figure 6.23 show the plot of the opening area of Samples 1, 2 and 3 in the medium pressure range against the width, and the opening area against the height respectively. From all pressure range plots of this data, it is noted that in general Sample 2 records the largest opening area, largest height and largest width. The largest area is noted in the medium range, and is seconded by Sample 2 opening in the low range. The largest height is recorded in Sample 2 high range and the largest width is in Sample 2 medium range. The largest width is seconded by Sample 3 high range data. Though these correlations are significant to understanding the differences in the trap behaviour, when presented in this form the correlation between width and height of the trap to the opening area seem arbitrary.

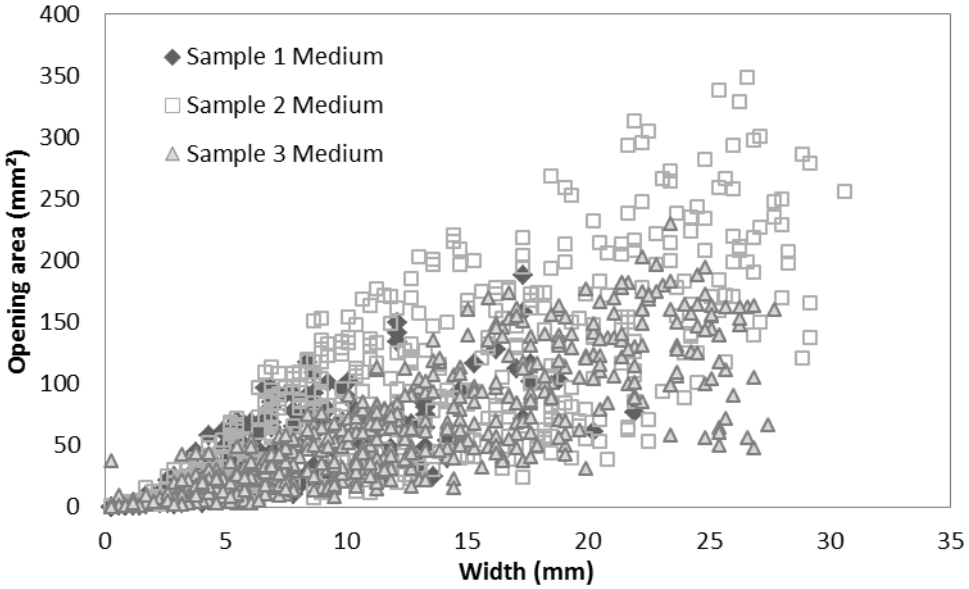


**Figure 6. 22, Opening area of the pipe against the opening width for sample 1, 2 and 3 when a medium-range static pressure is recorded in the pipe**

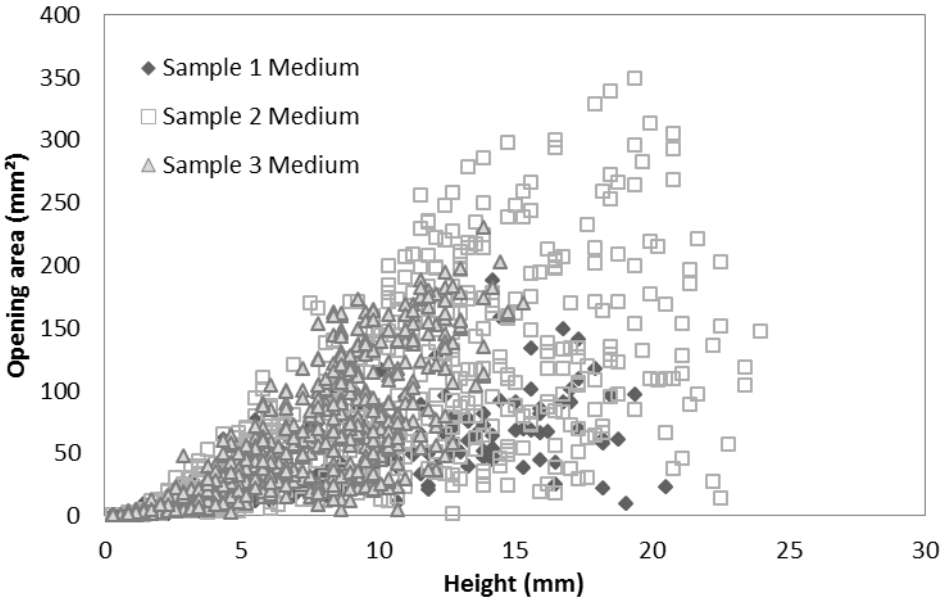


**Figure 6. 23, Opening area of the pipe against the opening height for sample 1, 2 and 3 when a medium-range static pressure is recorded in the pipe**

The max height and max width of the opening was not found to adequately describe the characteristics of the opening shape and so using principles from electrical engineering, the following relationship is yielded.

$$A_{av} = \frac{1}{T}\int_0^T A\, dt \qquad \textbf{Eq. 6. 7}$$

Here, the average opening area $A_{av}$ replaces the term $P$ (average power), and $A$ replaces $p$, the power in time.

Integrating over $2\pi$ rather than T, we obtain:

$$A = \frac{1}{2\pi}\int_0^{2\pi} \hat{w}\hat{h}\,[\sin(\omega\, t\, \emptyset)\, sin\, \omega\, t]d\omega t \qquad \textbf{Eq. 6. 8}$$

Which becomes,

$$A = \frac{1}{2\pi}\int_0^{2\pi} \hat{w}\hat{h}\,[\sin 2\omega\, t\, cos\emptyset \quad + sin\emptyset sin\, \omega\, t\, cos\omega\, t]d\omega t \qquad \textbf{Eq. 6. 9}$$

From the $\cos(a + b) = \cos a \cos b - \sin a \sin b$ relationship, the equation can be rewritten as

$$A = \frac{wh}{2} \pm cos\emptyset + \frac{wh}{2} cos\emptyset \cos 2\omega\, t - \frac{wh}{2} \sin 2\omega\, t\, sin\emptyset \qquad \textbf{Eq. 6. 10}$$

Then since over one time period,

$$\frac{wh}{2} cos\emptyset \cos 2\omega\, t - \frac{wh}{2} \sin 2\omega\, t\, sin\emptyset = 0 \qquad \textbf{Eq. 6. 11}$$

The approximation of the opening area is given by

$$A = \frac{\hat{h}}{\sqrt{2}} \frac{\hat{w}}{\sqrt{2}} cos\emptyset \qquad \textbf{Eq. 6. 12}$$

$\frac{\hat{h}}{\sqrt{2}}$ and $\frac{\hat{w}}{\sqrt{2}}$ are the RMS values of the height and width, and so $A$ in Eq 6.13 can be simplified further if $cos\emptyset$ (which represents the phase shift between the movement of the height and the movement of the width of the valve) equals 1 when the elasticity of the valve is inconsequential, and $\emptyset$ is equal to 0. In effect the representation of the relationship between area, width and height of opening is analogous to the Ohm's law relationship between Power, Voltage and Current in an electrical circuit so that;

$$A = h_{rms} * w_{rms} \qquad \textbf{Eq. 6. 13}$$

Note however that $\emptyset$ is likely to increase as elastic deformation of the waterless trap seal occurs. This deformation causes the membrane to stretch under the applied force making the movement of height and width arbitrary on occasion.

This relationship is likened to Eq.6.14, used for the approximation of opening area in simplified models of lip motion where the lip aperture is regarded as rectangular (see Bromage , 2007).

$$A = W(t) * H(t) \qquad \textbf{Eq. 6. 14}$$

Where, $H$ is the mean height, and $W$ is the constant width written as, $S(t) * h(t)$.

Stevenson (2009) explains that when Eq 6.14 is used in the lip motion analysis, the model assumes that the width remains constant throughout the playing of a brass instrument, but the height of the players' lips vary. The study measured the mean height and with this variable approximated the opening area of the lip. Early work by Saneyoshi *et al* (1987) is among the first to makes use of this linear relationship between the breadth and height of an opening.

A more recent physical model (Msallam *et al*, 1997) has instead of the linear equation, used a quadratic relationship to describe the lip motion of a bass player. In a want for an improvement on linear relationship, Eq.6.15 was assumed.

$$A = w(t) * h(t)^q \qquad \textbf{Eq. 6. 15}$$

Predictions using Eq. 6.16 were found to be more realistic in lip motion analysis than the earlier linear relationship

$$\boldsymbol{A = S(t) * h(t)^2} \qquad \textbf{Eq. 6. 16}$$

The prediction of the waterless trap seal movement differs from the lip motion analysis as the width of the opening is not constant. Both the height and width of the trap seal vary with time and applied pressure. The RMS value of the maximum height and maximum width provide a mean linear measure of the opening. This measure when used in Eq. 6.13 however provides realistic predictions of the waterless trap seal opening area. Figure 6.24 provides a plot of the measured against the predicted opening area of Sample 2 in the medium pressure range data. Results from all other samples and ranges are presented in Table 6.3. These all show very good correlations.

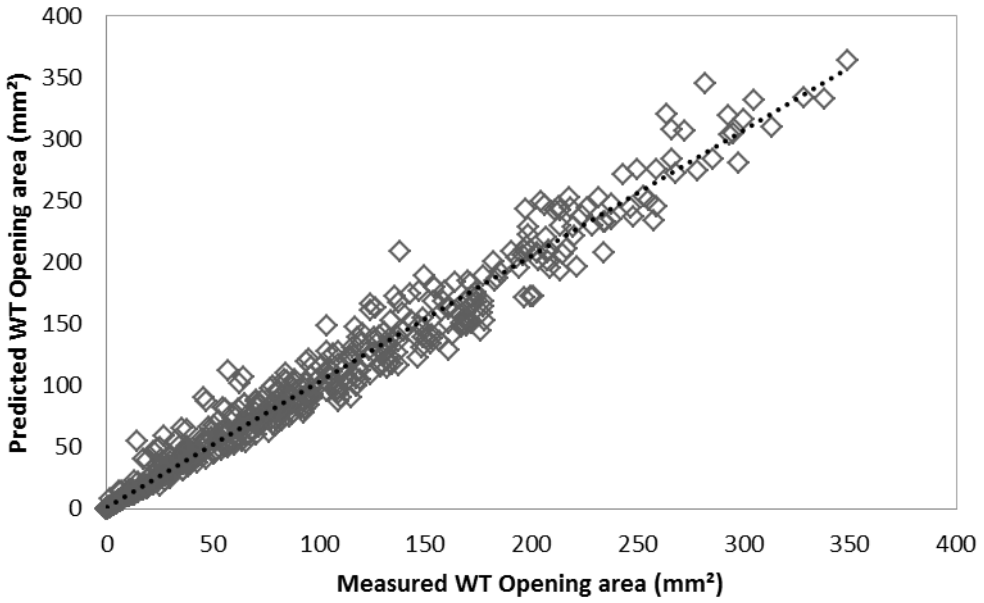


**Figure 6. 24, Measured against predicted opening area plotted for the medium-range pressure data in Sample 2 tests. $R^2$=0.978**

| | Sample 1 $R^2$ | Sample 2 $R^2$ | Sample 3 $R^2$ |
|---|---|---|---|
| Threshold | 0.9971 | 0.9859 | 0.9972 |
| Low | 0.9829 | 0.9468 | 0.9871 |
| Med | 0.9728 | 0.978 | 0.9643 |
| High | 0.938 | 0.8878 | 0.8946 |

**Table 6. 3, The correlation coefficient $R^2$ of the measured against predicted opening area plots for Samples 1, 2, and 3 using RMS values of the height and width of the valve opening**

#### *6.6.2.1 **Summary***

It has been shown in this subsection that the geometry of the opening can be predicted with the knowledge of two variables, be it width and height, opening and height or opening and width, though the lumped element model approach. This data however does not aid in the real time prediction of waterless trap seal movement in relation to the flow conditions within a BDS. The equations of motion for the lumped element system are required to be coupled to the aerodynamic driving forces; where the pressure exerted within inner pipe, produces oscillations to the valve. In return, this pressure in the pipe will depend on the open area.

For this purpose the link between pressure and the opening movement is required. The following subsections within Section 6.6 investigates existing relationships using Fourier analysis of the complex multi parameter datasets

### *6.6.3. Fourier spectral processing*

The length of the cycle images provides frequency information of the valve movement. While this information is detailed it presents particular analytical challenges due to the vast complex datasets involved. Spectral analysis offers an opportunity to establish fundamental relationships from which boundary equations can be developed.

Spectral analysis was conducted using Fast Fourier Transform (FFT) which is a signal processing algorithm. This algorithm was used to determine the dominant frequencies (of opening and closing fluctuations) within time domain waveforms. These waveforms describe the transient pipe pressure and valve opening.

Discrete Fourier Transform (DFT) is a broader transform from which the FFT algorithm is derived. The difference between the calculation methods is that, the DFT is an order $n^2$ procedure and the FFT is an $n * log_2(n)$ operation, and so the difference in

processing time is dramatic with large data sets. The FFT is therefore a faster calculation method for producing the discrete Fourier transform (DFT).

FFT transform enables a wave (a function of time, or space) to be broken up into the sum of their contributing exponentials (sines and/ or cosines). So for instance as Filsell (2006) describes, a sample wave of 1KHz may contain two dominant frequencies of 4 and 16 Hz. The resultant or original wave is the summation of these contributing sinusoids. This relationship is expressed in Eq. 6.18.

$$x(t) = Asin(8\pi t) + Bsin(32\pi t) \qquad \textbf{Eq. 6. 17}$$

The FFT transform however, does not provide details of the time within a wave when this frequency occurs, Probability of the wave frequency is the only measure gained and is suggested by the acoustic strength of the noted frequency. Autosignal, the software package used for this application regards the Fourier basis functions as phase bearing sinusoids and so the complete signal is a mere summation (Nspex) of the constituent frequencies. Therefore it is possible to reconstruct the signal for any time period. This feature will be discussed later in this chapter.

$$y(t) = \sum_{k=1}^{Nspec} A_k \sin(2\pi v_k t + \theta_k) \qquad \textbf{Eq. 6. 18}$$

Here, A is the amplitude, $v$ is the frequency, and $\theta$ is the phase.

### *6.6.4. Fourier frequency spectrum - Pressure*

The resultant frequency of the air pressure transient measured in the pipe is a reaction to the frequency of the applied wave originating from the pressure transient generator and the reflections induced by the closures to the waterless trap seal within an oscillatory

cycle. This oscillatory motion does not occur at all frequencies however. Dependent on the trap characteristics and an applied low amplitude pressure transient, the waterless trap seal is likely to remain in an open position for the entirety of the wave. The spectral analysis data derived from FFT transformation for the amplitude of the pressure wave in time is provided in the left hand column of Figure 6.25. The graph shows the FFT output (in the right hand column) for the pressure amplitude data in the Threshold, Low, Med, and High pressure regions.

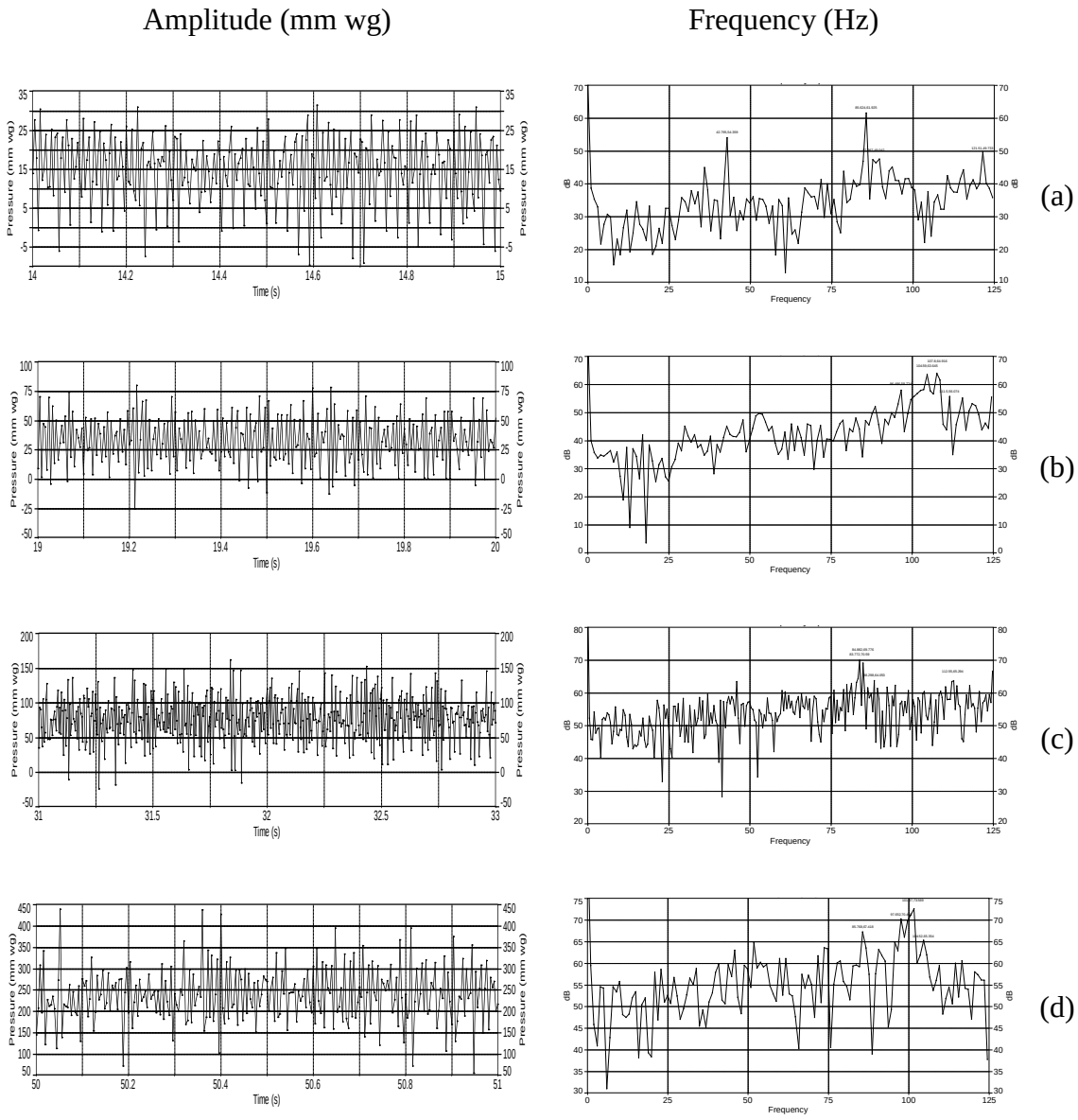


**Figure 6. 25, Pipe pressure reading (left) presented alongside Fourier pressure frequency analysis (right) Sample 1. Demarked regions: (a) threshold, (b) low, (c) medium, and (d) high pressure**

In Figure 6.25, and in all except the threshold data, the dominant and secondary frequencies all range between 80-110 Hz with minimum amplitude of 60dB. The dominant pressure frequency across all data sets within the Sample 1 test, range between 83 Hz and 124Hz.

A commonality was discovered between the threshold, low and medium regions in Samples 2 and 3, as the dominant frequencies lie between 48.99 -125Hz and more specifically in Sample 2 between 80 and 125Hz. In the high pressure range, the prominent frequencies lie in two regions, 0 -25Hz and 100- 125Hz for Sample 1 and between 0 and 25Hz in Sample 3. Additionally, when Sample 3 is used, the dominant pressure frequencies for threshold, low and medium lie in two regions, at approximately 50Hz and approximately 100 Hz.

### *6.6.5. Valve opening frequency spectrum*

Section 6.6.1 discussed the outcomes of the measure of repeatable image cycle data and the lengths recorded for these cycles. A more comprehensive method of gathering this information is to determine the frequency of motion by using the AutoSignal software to determine the Fourier spectrum of the photogrammetric data determined through calculations in Section 6.3 and 6.4.

The data gathered here however, using the high speed camera is deemed valid as the frequency readings do not rise above 123Hz. On the other hand, readings of 100Hz are common in both the pressure and opening data readings and therefore could be a result of missed data between the requisite image capture time period. This information can only be confirmed by the use of a high speed camera with a larger image capture frame rate.

Sample 3 shows a more distributed range of frequencies than found in the static pressure traces shown in Sample 1. However, the dominant opening frequency ranges between 83 Hz and 124Hz and so can be likened to the pressure frequency in all ranges except the threshold range in the Sample 1 test.

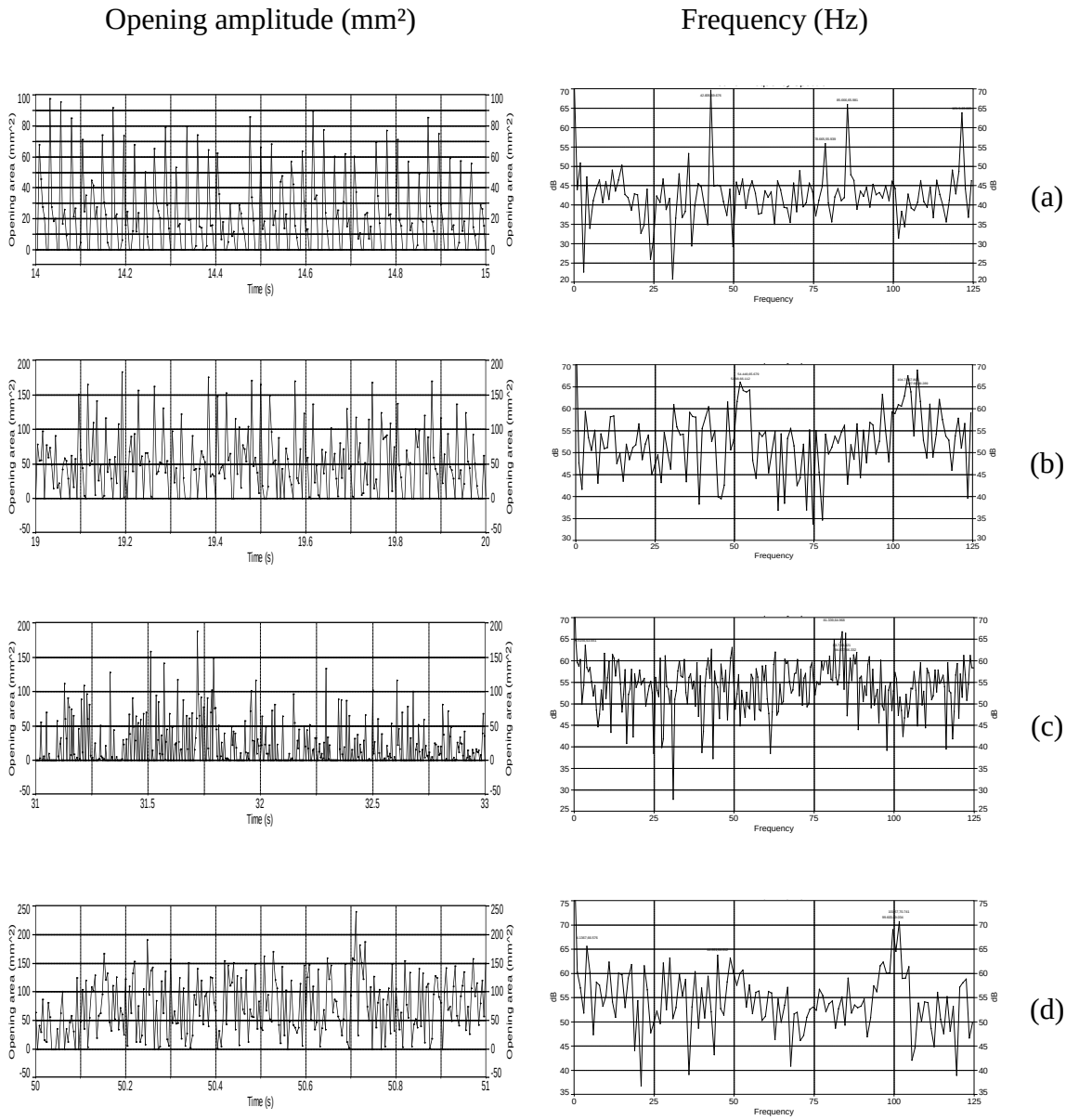


**Figure 6. 26, The opening area of the pipe in time (left) presented alongside Fourier opening frequency analysis (right) Sample 1. Demarked regions: (a) threshold, (b) low, (c) medium, and (d) high**

A commonality between the dominant pressure frequency is only seen in the low and high pressure amplitude ranges between 80 -100Hz and <25Hz.

Threshold and low frequency are similar to the pressure frequency (approximately 50 Hz and approximately 100Hz)

High range Fourier analysis presents no significantly dominant frequency and no correlation to the earlier presented pressure frequency at this range when Sample 3 is installed.

| Pressure range | Data set analysis | Sample 1 (Hz) | Sample 2 (Hz) | Sample 3 (Hz) |
|---|---|---|---|---|
| Threshold | Opening frequency | 42.84 | 0.98 | 51.55 |
| | Pressure frequency | 85.62 | 78.83 (94.371) | 102.07 (51.97) |
| Low | Opening frequency | 107.66 | 97.16 | 49.06 |
| | Pressure frequency | 107.8 | 93.65 | 48.99 |
| Medium | Opening frequency | 83.70 | 3.74 | 58.6 |
| | Pressure frequency | 83.77 | 115.66 (102.16) | 58.6 (59.6) |
| High | Opening frequency | 101.57 | 35.69 | 119.24 |
| | Pressure frequency | 101.37 | 19.42 | 11.3 (20.54) |

**Table 6. 4, Dominant results of Fourier spectrum image cycle analysis and Fourier spectrum of corresponding pressure data for data sets.**

Using the same method of frequency analysis applied to the data sets above, the frequency of the trap opening and pressure data for each repeatable 4 image cycles noted was determined and listed in in Table 6.5. This data shows similar results to the opening and pressure frequencies noted for Sample 1 (threshold, low, and medium range), Sample 2 (low range), and Sample 3 (low range).

No data is available for the Sample 1 and Sample 2 at high range as the images per cycle are too low in number to provide sufficient data for analysis.

| Pressure range | Image cycle analysis | Sample 1 (Hz) | Sample 2 (Hz) | Sample 3 (Hz) |
|---|---|---|---|---|
| Threshold | Opening frequency | 43.48 (86.51) | 25.21 (74.90) | 52.078 (104.86) |
| | Pressure frequency | 87.93 (42.76) | 74.63 (101.37) | 52.53 (106.18) |
| Low | Opening frequency | 100.23 (50.30) | 96.41 (47.76) | 54.43 (106.38) |
| | Pressure frequency | 111.62 (50.50) | 96.52 (30.62) | 106.66 (52.00) |
| Medium | Opening frequency | 83.89 (39.79) | 30.54 (62.94) | 86.48 |
| | Pressure frequency | 83.96 (45.37) | 99.66 (69.47) | 42.069 |
| High | Opening frequency | n/a | n/a | 34.90 (105.03) |
| | Pressure frequency | n/a | n/a | 22.46 (40.87) |

**Table 6. 5, Results of Fourier spectrum image cycle analysis and Fourier spectrum of corresponding pressure data**

The data in brackets in Tables 6.4 and 6.5 are the secondary dominant opening and the corresponding pressure frequencies obtained from the FFT analysis of the opening and pressure data. It should be noted that a relationship exists here which was not found in the whole data set analysis. For instance, in sample 1 threshold data, it is the secondary frequency which can be likened to the dominant pressure frequency and vice versa. This relationship is not noted in the Fourier spectrum of the entire data set. This relationship is seen again in Sample 3 (low).

### *6.6.6. Summary*

This section of Chapter 6 has confirmed (shape and opening pattern analysis, along with analysis of the pressure data) that there is a correlation between the opening area and the applied pressure. The reference waterless trap seals (Sample 1, 2 and 3) all oscillate predominantly in reoccurring pattern when a fairly steady transient flow is exists within the pipe. Interestingly, in Samples 1 and 2 the length of the image cycle reduces with an increase in pressure. This data is shown in Fig 6.21.

Sections 6.6.3 and 6.6.4 noted that pressure frequency in many cases proving that the oscillations change the flow regime of the applied pressure due to constant reflections these reflections occur at the same frequency of the closing. The correlation between the pressure frequency and the opening frequency is noted in some results but not across the board. The following section will evaluate the advantage to using a single dominant frequency value or considering more fully four main pressure and opening frequencies recorded.

## 6.7. Evaluating the relationships between dominant pressure frequency, dominant opening frequency, opening measurements and pressure

It has thus far been determined that a pattern exists within the majority of the accessed data set images. The total number of data sets is: 16 for the Sample 1 test, 16 in the Sample 2 test, and 11 in the Sample 3 test.

This section details the relationships which exist between the pressure frequency readings, opening area frequency readings and the opening area. In order to develop a model for the prediction of waterless trap seal movement the opening conditions must be determined first. Figure 6.27 shows the extent of the data obtained and gives a measure of the challenges faced in producing meaningful generalisations and equations from the raw unprocessed data.

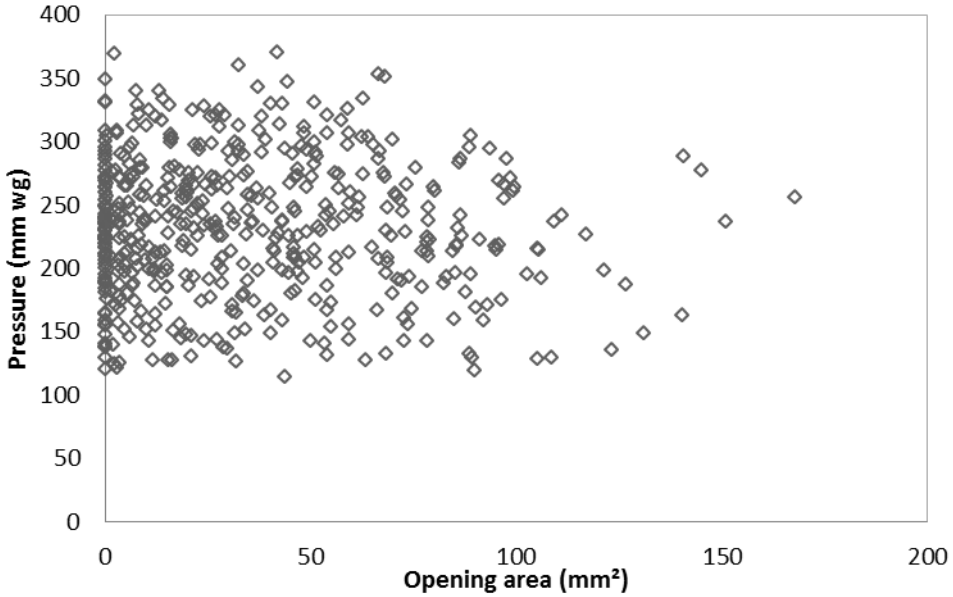


**Figure 6. 27, Plotted pressure readings (at high range) against the waterless trap seal (Sample 2) opening area**

### *6.7.1. Opening area as a function of transient static pressure*

This subsection of Section 6.7 seeks to develop relationships for pressure wave amplitude through the use of a single value per variable per data set. The method chosen to assess the pressure and opening area relationship, recorded a single value for pressure within each data set and likewise for the opening area. These values are the averages, the mean of the variable over the data set (RMS) and the maximum variable value over the data set.

The RMS value or the quadratic mean has been used in approximation of the mean opening height in Section 6.6.2. The RMS of a data set provides the most probable pressure or opening area within the transient conditions of the set. This mean is calculated by taking the square root of the sum of the variables

$$P_{rms} = \sqrt{\frac{\sum_1^n P}{n}} \qquad \textbf{Eq. 6. 19}$$

Probability of open area at given pressure

$$a_{rms} = \sqrt{\frac{\sum_1^n a}{n}} \qquad \textbf{Eq. 6. 20}$$

$a$ is the measured opening area, RMS opening area plotted against the corresponding RMS Pressure for the Samples 1, 2 and 3 to a 5$^{th}$ order polynomial

The developed relationship equations take the general form

$$P\varepsilon_{xi} = aP_{xi}^{x+n} \ \ldots + bP_{xi}^{x+2} \ + cP_{xi}^{x+1} \ + dP_{xi}^{x} \ + C \qquad \textbf{Eq. 6. 21}$$

Where, $P\varepsilon$ is the predicted variable, $P$ is the pipe pressure and the subscript $_{xi}$ denotes the method employed.

The first assumption of $P\varepsilon_{xi}$ is $A_{rms}$ which as noted in the subscript, uses the RMS of the opening area.

$$A_{rms} = aP_{rms}^{x+n} \ \ldots + bP_{rms}^{x+2} \ + cP_{rms}^{x+1} \ + dP_{rms}^{x} + C \qquad \textbf{Eq. 6. 22}$$

Where, $A_{rms}$ is the quadratic mean of the opening area, and $P_{rms}$ is the quadratic mean of the pressure

This general relationship however, was determined to be inappropriate as by considering the probable opening area at a probable pressure within wide ranging and seemingly random data sets, overestimation of the opening area becomes likely. To

counteract this issue, the maximum area associated with a given pressure was determined to be better suited to this application. If the max pressure and maximum opening area relationship is used, the prediction within that data set will not exceed the measured maximum and therefore acts as a limit for the prediction.

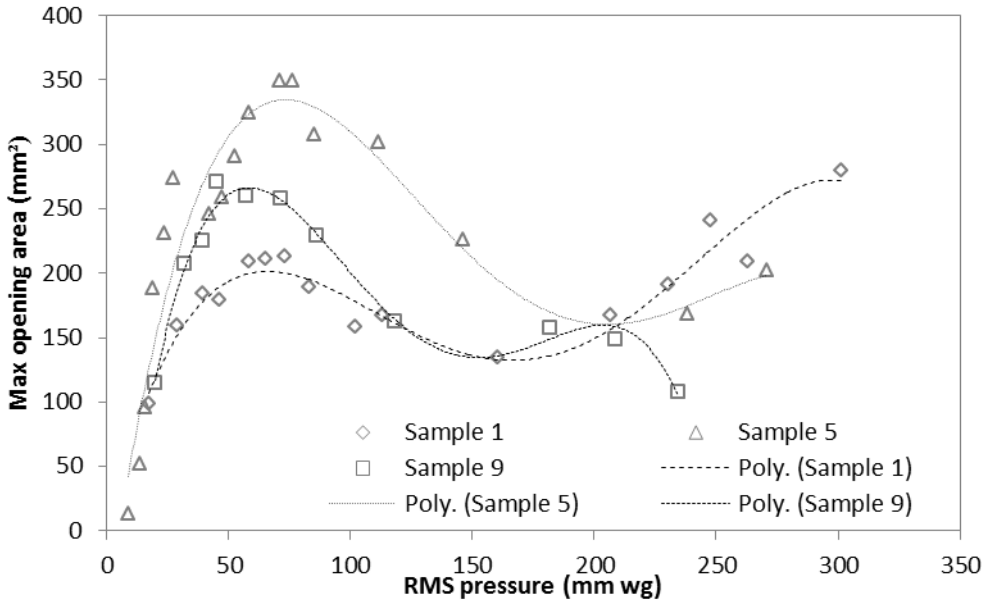


**Figure 6. 28, Maximum opening area against the corresponding RMS pressure for Samples 1, 2 and 3 to a 4th order polynomial presented correlations of $R^2$ = 0.8247, $R^2$ = 0.9074, and $R^2$ = 0.9783 respectively.**

Figure 6.28, $P\varepsilon$ shows that the predicted variable in Eq.6.21 becomes $A$, which denotes the opening area (in mm²), P is the pipe pressure and the subscript $xi$ becomes MR, denoting the relationship: Maximum opening area ($A_{max}$) against RMS Pressure ($P_{rms}$) .

$$P\varepsilon_x = A_{MR^x} \qquad \textbf{Eq. 6. 23}$$

The equations describing this relationship for the three samples are:

$$A_{MR^4} = -8 * 10^{-7}P^4 + 0.0005P^3 - 0.1067P^2 + 8.0075P - 3.0856$$

Sample 1 **Eq. 6. 24**

$$A_{MR^4} = -2 * 10^{-7}P^4 + 0.0003P^3 - 0.1061P^2 + 11.639P - 73.822$$

Sample 2 **Eq. 6. 25**

$$A_{MR^4} = -2 * 10^{-6}P^4 + 0.0012P^3 - 0.227P^2 + 15.683P - 111.24$$

Sample 3 **Eq. 6. 26**

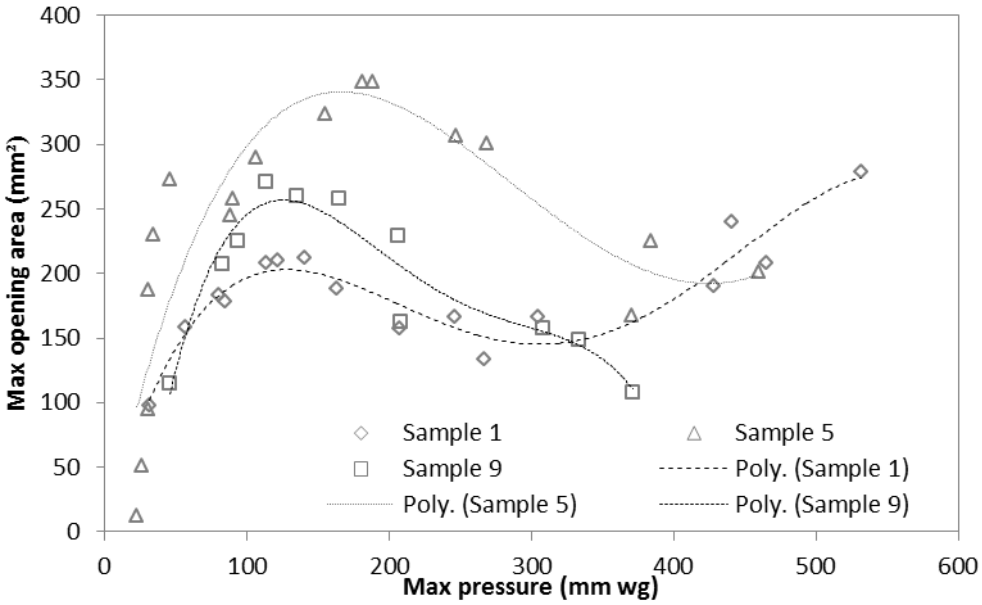


**Figure 6. 29, Max opening area against the corresponding maximum pressure for Samples 1,2 and 3 to a 4th order polynomial presented correlations of $R^2 = 0.7765$, $R^2 = 0.7751$, and $R^2 = 0.9737$ respectively.**

Here in Figure 6.29, $P\varepsilon$ the predicted variable in Eq.6.21 becomes $A$, which denotes the opening area (in mm²), P is the pipe pressure and the subscript $xi$ becomes max, denoting the relationship: Maximum opening area ($A_{max}$) against Maximum Pressure ($P_{max}$ ).

$$P\varepsilon_x = A_{Max^x} \qquad \textbf{Eq. 6. 27}$$

The equations describing this relationship for the three samples are:

Sample 1, $$A_{Max^4} = -5 * 10^{-8}P^4 + 6 * 10^{-5}P^3 - 0.0256P^2 + 3.9654P + 0.5787 \qquad \textbf{Eq. 6. 28}$$

Sample 2, $$A_{Max^4} = -2 * 10^{-8}P^4 + 4 * 10^{-5}P^3 - 0.0235\,P^2 + 5.0434\,P - 5.6976 \qquad \textbf{Eq. 6. 29}$$

Sample 3, $$A_{Max^4} = -2 * 10^{-7}P^4 + 0.0002P^3 - 0.072P^2 + 9.9944\,P - 218.59 \qquad \textbf{Eq. 6. 30}$$

This Section has looked closely at the link between opening area amplitude at a given applied pressure. Equations 6.24 and 6.28 provide methods of predicting the opening area of Sample 1, Equations 6.25 and 6.29 for Sample 2, and Equations 6.26 and 6.30 for Sample 3. The method best suited to predict the opening area of the traps is discussed later in Section 6.8.

### *6.7.2. Opening frequency as a function of transient static pressure*

This section aims to continue that done in Section 6.7.1 by developing equations which may be suitable for the prediction of the waterless trap seal opening frequency. The option of modelling the opening area of the pipe using the dominant frequency in a sinusoidal wave was found to be challenging. This being as, for each data set numerous frequencies are found in the wave spectrum. Neglecting those frequencies in the spectrum close in amplitude to the dominant frequency can result in a significant misrepresentation of the trap seal's response to varying pressure wave. Therefore a maximum of 4 dominant frequencies were recorded using the FFT algorithm for each data set By using the data set frequency readings as an alternative to the cycle image data and time frequency readings, it could be ensured that no unobserved patterns are disregarded.

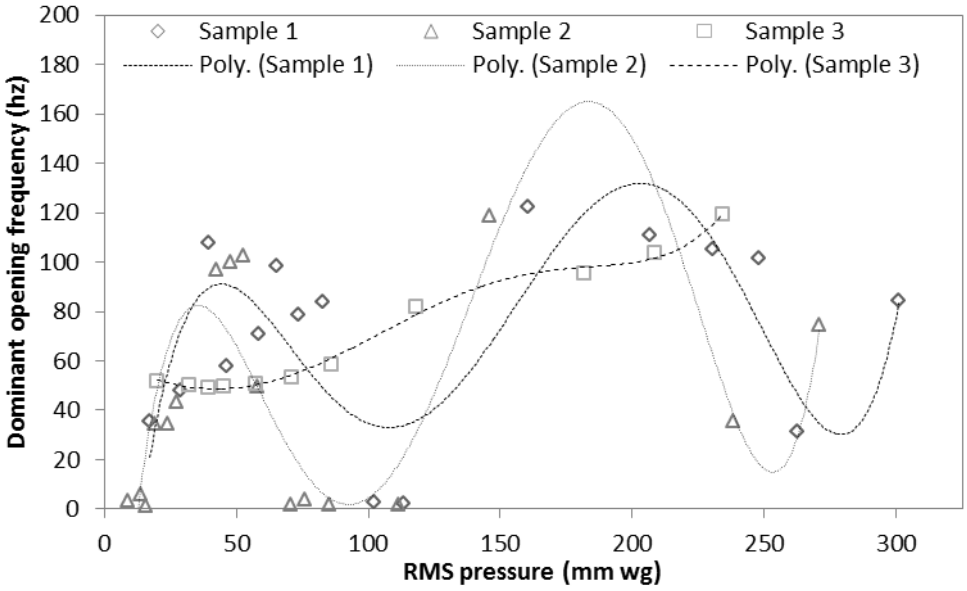


**Figure 6. 30, Dominant opening frequency plotted against the RMS pressure for Sample 1, 2,and 3 to the 5th or 6th order polynomial, presented correlations of $R^2$ =0.603,$R^2$= 0.7114, and $R^2$=0.9955 respectively.**

From Figure 6.30, $P\varepsilon$ the predicted variable becomes $f_D'$ which denotes the opening frequency (a function of the dominant measured opening frequencies), $P$ is the pipe

pressure and the subscript $xi$ which denotes the method employed is replaced by $rms^5$ or $rms^6$. The predictive equation becomes,

$$P\varepsilon_x = f'_{D_{rms^x}} \qquad \textbf{Eq. 6. 31}$$

The equations describing this relationship for the three samples are:

Sample 1, $$f'_{D_{rms^6}} = 2 * 10^{-11}P^6 - 8 * 10^{-9}P^5 - 2 * 10^{-6}P^4 + 0.0012P^3 - 0.1941P^2 + 10.82P + 109.9 \qquad \textbf{Eq. 6. 32}$$

Sample 2, $$f'_{D_{rms^5}} = 2 * 10^{-8}P^5 + 2 * 10^{-5}P^4 + 0.004P^3 - 0.4222P^2 + 17.456P - 161.13 \qquad \textbf{Eq. 6. 33}$$

Sample 3, $$f'_{D_{rms^5}} = 2 * 10^{-9}P^5 - 9 * 10^{-7}P^4 + 0.0001P^3 - 0.0001P^2 - 0.4199P + 59.729 \qquad \textbf{Eq. 6. 34}$$

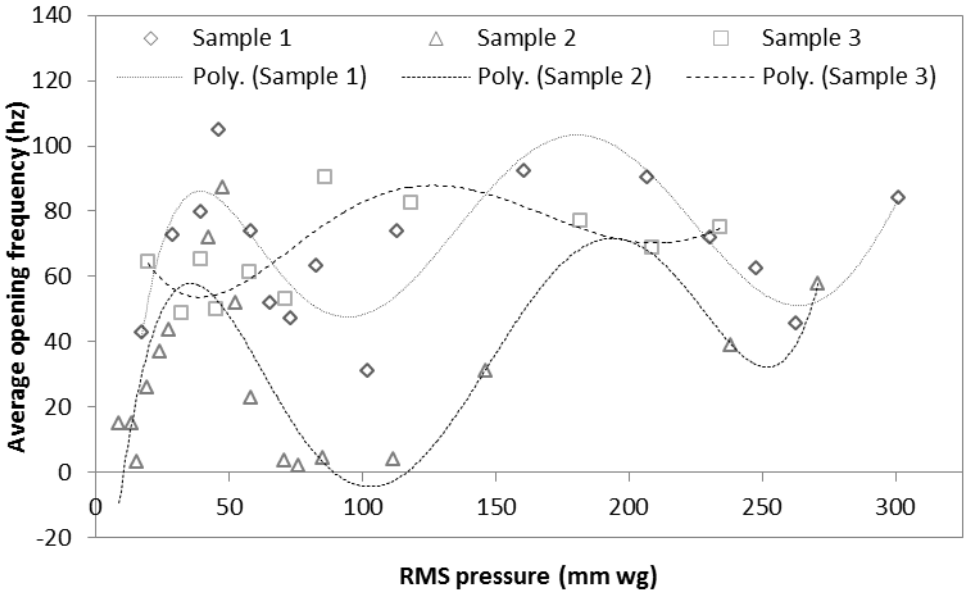


**Figure 6. 31, Average opening frequency plotted against the RMS pressure for Sample 1, 2 and 3 with trend lines to the 5th and 6th polynomial present correlations of $R^2$=0.7177, $R^2$=0.6666, $R^2$= 0.651 respectively.**

Here, $P\varepsilon$ the predicted variable becomes, $f'_{av}$ which denotes the opening frequency (a function of the average measured opening frequencies), P is the pipe pressure and the subscript $_{xi}$ denotes the method employed $rms^5$ or $rms^6$.

$$P\varepsilon_x = f'_{av_{rms^{x+n}}} \qquad \textbf{Eq. 6. 35}$$

The equations describing this relationship for the three samples are:

$$\text{Sample 1,} \quad f'_{av_{rms^6}} = -4 * 10^{-11} P_{rms}^6 + 4 * 10^{-8} P_{rms}^5 - 2 * 10^{-5} P_{rms}^4 + 0.0034 P_{rms}^3 - 0.3218 P_{rms}^2 + 13.266 P_{rms} \qquad \textbf{Eq. 6. 36}$$

Sample 2, $$f'_{av_{rms^5}} = 1 * 10^{-8}P_{rms}^5 - 8 * 10^{-6}P_{rms}^4 + 0.002P_{rms}^3 - 0.2238P_{rms}^2 + 9.5177P_{rms} - 77.063$$ **Eq. 6. 37**

Sample 3, $$f'_{av_{rms^5}} = -2 * 10^{-9}P_{rms}^5 + 2 * 10^{-6}P_{rms}^4 - 0.0006P_{rms}^3 + 0.0714P_{rms}^2 - 3.4374P_{rms} + 108.25$$ **Eq. 6. 38**

Best fit polynomials are used to provide an accurate description of the relationship between RMS pressure and opening average or dominant frequency. An interesting finding here is that between 75-100mm wg a change in frequency, is always noted, however, more so in samples 1 and 2.

Equations 6.32 and 6.36 provide equations predicting the opening frequency of Sample 1, Equations 6.33 and 6.37 for Sample 2, and Equations 6.34 and 6.38 for Sample 3. The method best suited to predict the opening frequency of the traps is discussed later in Section 6.8.

### *6.7.3. Reproducibility of movements*

In order to replicate the movement of the waterless trap seal in a computational model such as AIRNET, the altering opening area with time is required. Simply, the trap opening can be likened to an orifice at the end of a pipe whose size changes in time.

The model developed in this section is required to meet two standards:

- It must mimic reasonably the total time the trap is open- opening area over time
- It must satisfactorily mimic the oscillation frequency for a given applied (varying) pressure.

This fluctuating relationship can be likened to a sinsusoidal function where multiple frequences account for the wave pattern:

$$A(\sin\alpha \pm \sin\beta) = A\left(2\sin\frac{1}{2}(\alpha \pm \beta)\cos\frac{1}{2}(\alpha \mp \beta)\right) \quad \textbf{Eq. 6. 39}$$

Where, α and $\beta$ are the two most dominant frequencies.

Another approach which would use a single frequency at a single time uses the general form of the equation

$$A(\sin\omega) \quad \textbf{Eq. 6. 40}$$

Here, the angular frequency is expressed as a polynomial dependent on the immediate pressure at

$$\omega = 2\pi(\ ap^3 + bp^2 + cp \quad + c) \quad \textbf{Eq. 6. 41}$$

Of the 20 predictive methods that were used, 7 best fit methods were further analysed by determining the frequency spectrum of the predicted data. The results found that no single method is capable of predicting the response adequately over all pressures.

Therefore, $A_\alpha$ is the predicted area and a sequenced integer associated with each prediction method to denote the method of calculation. These predictors are detailed below.

$$A_{\alpha 1} = A_{MR} * \sin(2\pi\, f'_{D_{rms}}) \quad \textbf{Eq. 6. 42}$$

$$A_{\alpha 2} = A_{MR} * \sin(2\pi f'_{av_{rms}}) \quad \textbf{Eq. 6. 43}$$

$$A_{\alpha 3} = A_{Max} * \sin(2\pi f'_{D_{rms}}) \quad \textbf{Eq. 6. 44}$$

$$A_{\alpha 4} = A_{max} * \sin(2\pi f'_{av_{rms}}) \quad \textbf{Eq. 6. 45}$$

$$A_{\alpha 5} = A_{Max} * \cos(2\pi f'_{D_{rms}}) \quad \textbf{Eq. 6. 46}$$

$$A_{\alpha 6} = A_{max} * \cos(2\pi f'_{av_{rms}}) \quad \textbf{Eq. 6. 47}$$

## 6.8. Waterless trap seal opening predictions

### *6.8.1. Waterless trap seal opening amplitude Predictions*

This subsection presents a series of plots of the measured valve opening (left) alongside a corresponding prediction (right), for a synchronised pressure transient within the comparable ranges identified in Section 6.6. Sample 1 plots are presented in Figure 6.32, and Sample 3 in Figure 6.33.

Measured Predicted

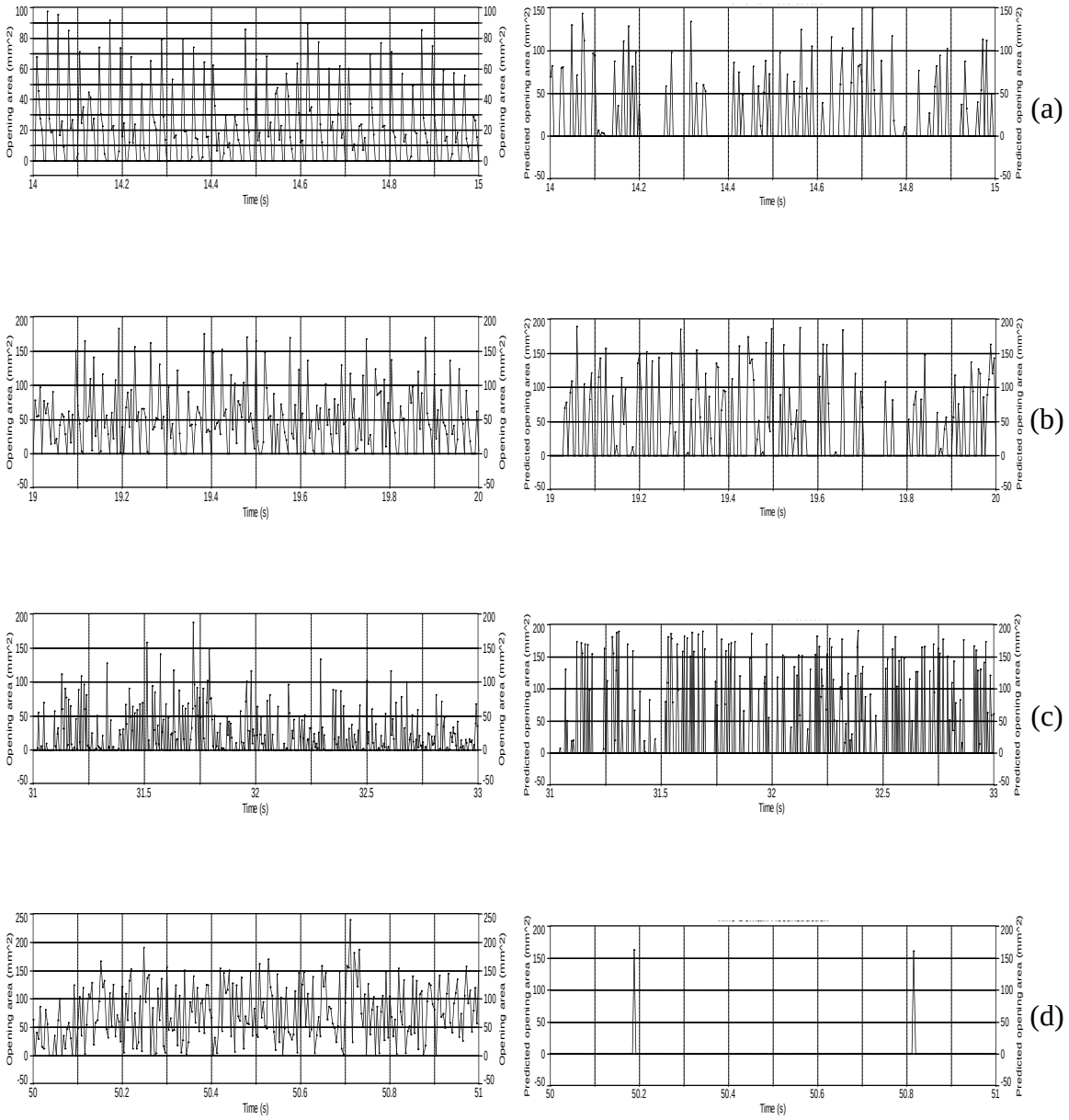


**Figure 6. 32, The measured opening area of the pipe in time (left) presented alongside the predicted opening area ($A_{\alpha 1^4}$) of the pipe in time (right) for Sample 1. Demarked regions: (a) threshold, (b) low, (c) medium, and (d) high**

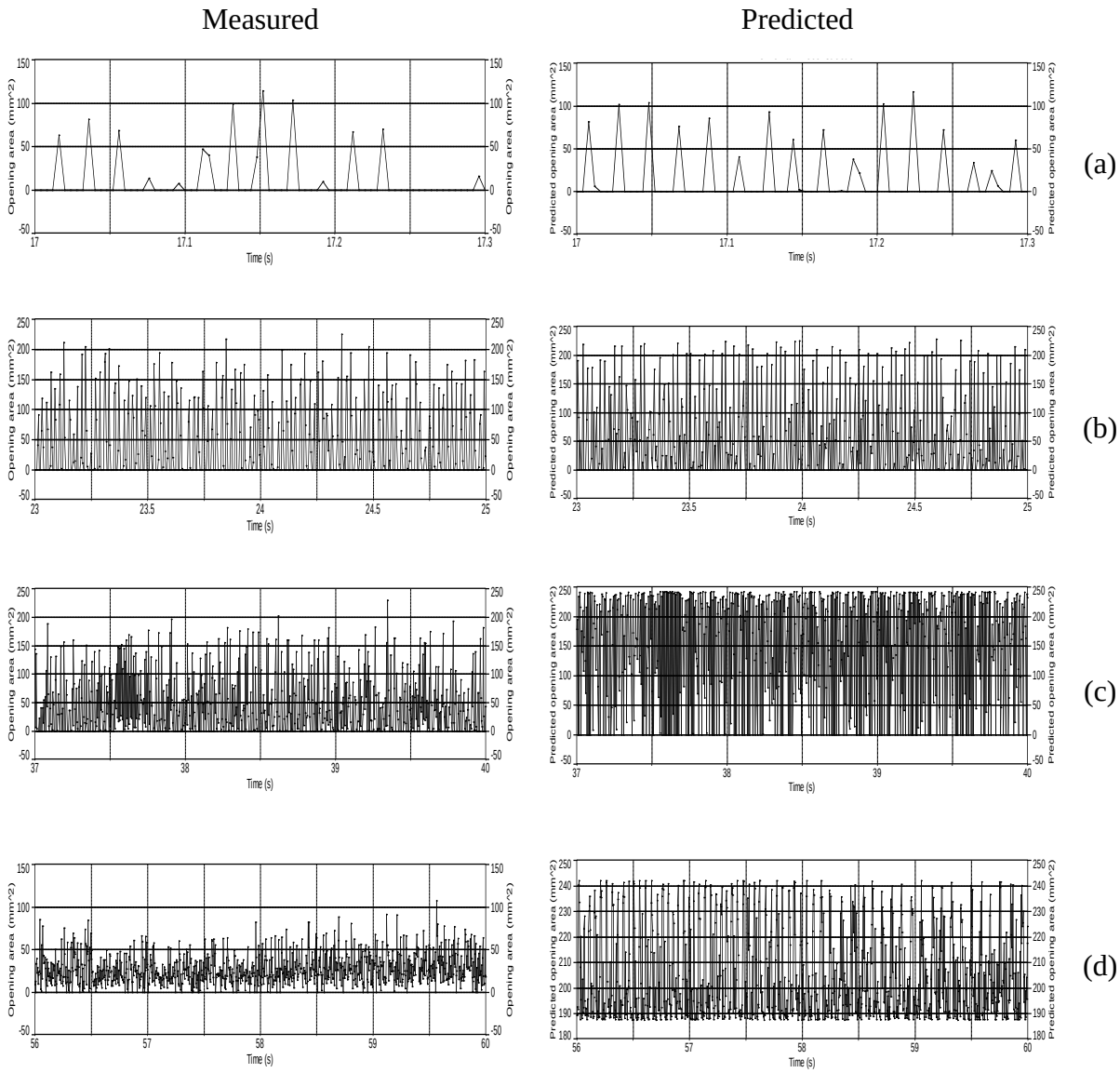


**Figure 6. 33, The measured opening area of the pipe in time (left) presented alongside the predicted opening area ($A_{Max^4}$) of the pipe in time (right) for Sample 3. Demarked regions: (a) threshold, (b) low, (c) medium, and (d) high**

Neglecting the results of the three data points highlighted in colour red in Figure 6.38 by considering them to be anomalies, the relationship presented in Figure 6.39 is found.

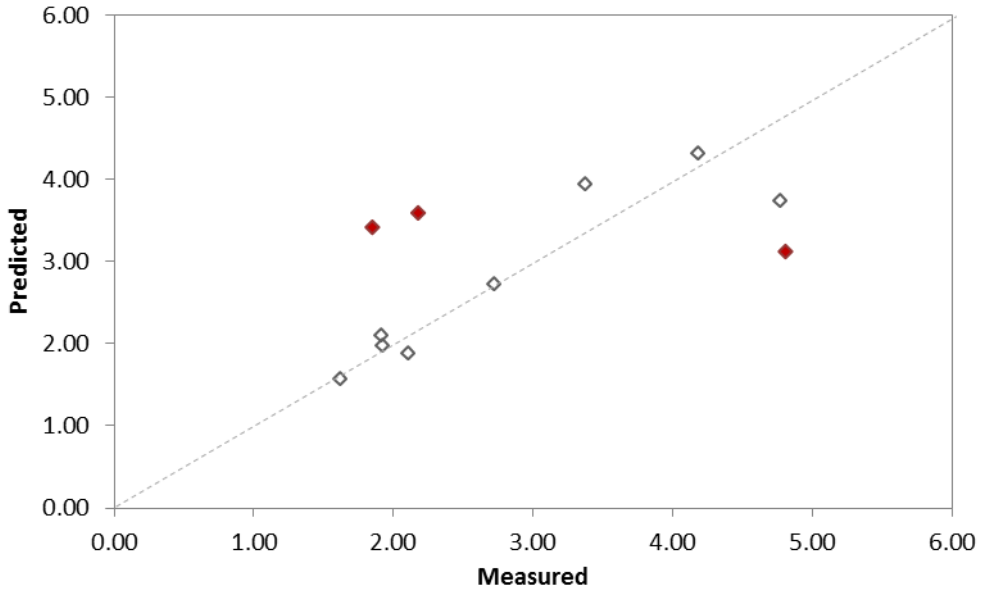


**Figure 6. 34, Plot of Sample 1 measured against predicted % opening of the pipe over 1 second across all data sets. $A_{\alpha 1}$**

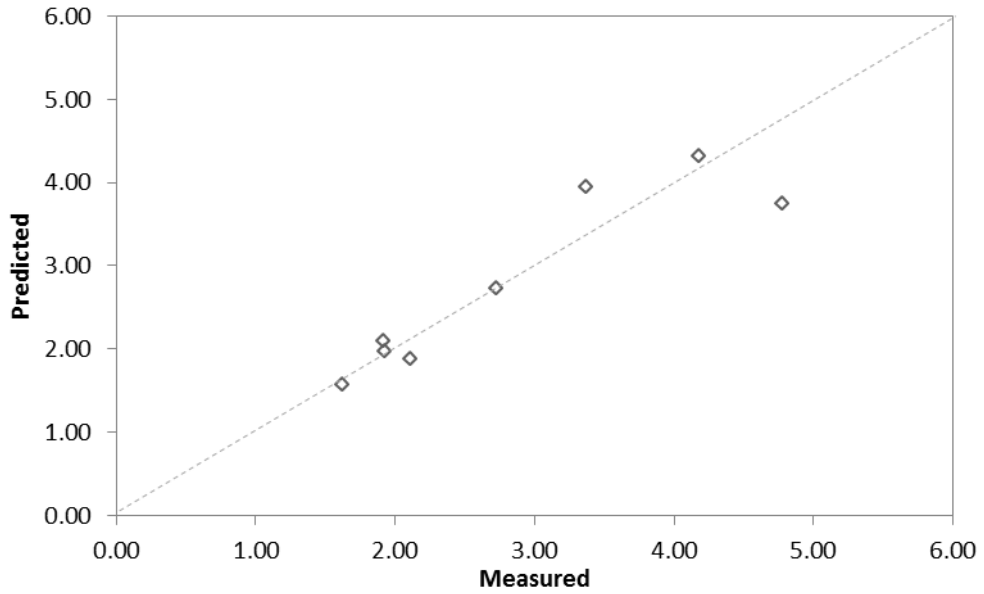


**Figure 6. 35, Plot of Sample 1 measured against predicted % opening of the pipe over 1 second in instances where the RMS pressure value is equal to or below 160.49 mm wg. $A_{\alpha 1}$ provides $R^2 = 0.8432$**

It was found that a more accurate prediction is made using the $A_{\alpha 1}$ equation over the $A_{\alpha 2}$equation where the average frequency is used. Though this however is shown to be true, $A_{\alpha 2}$ equations were found to produce satisfactory accuracy in the amplitude and frequency spectrum of the models.

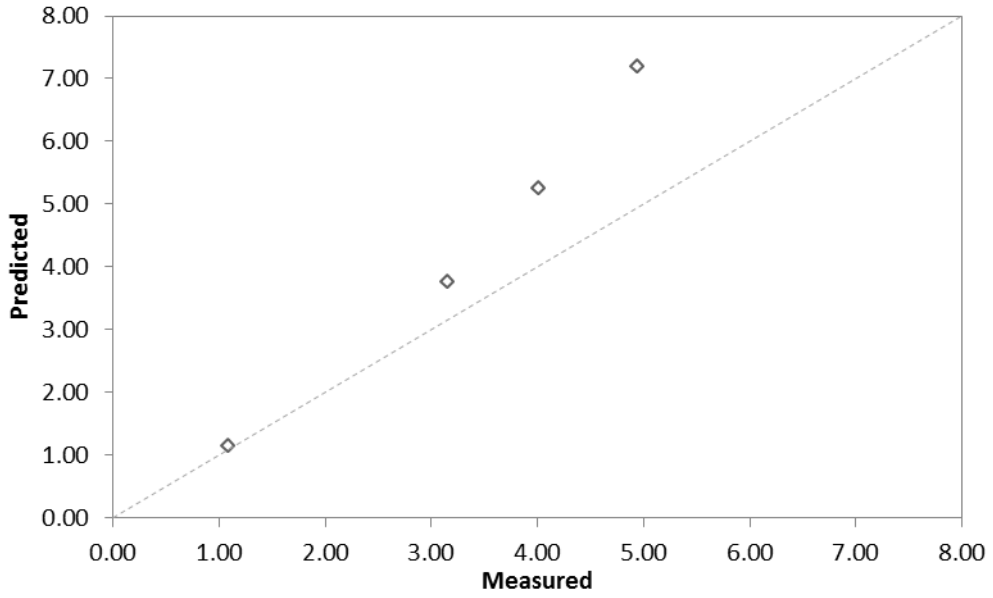


**Figure 6. 36, Measured against predicted % opening of the pipe over 1 second Sample 3 in instances where the RMS valve is equal to or below 45.23. $A_{Max^4}$ provides $R^2 = 0.9838$**

The best fit predictor of the oscillatory movement of Sample 3 was found to be the $A_{Max^4}$ equation. This equation is a satisfactory predictor of pressure transient response up to the RMS pressure value of below 45.23 mm wg or a maximum pressure of 113 mm wg.

As the criteria for a successful model required that the frequency and amplitude mimic the measured data, the following sections assess the Fourier spectrum of the predicted data, and provide comparison with the measured frequency for four pressure ranges.

### *6.8.2. Waterless trap seal opening frequency predictions*

This subsection presents a comparison of the measured opening frequency against the predicted opening area frequency across the data in the threshold, low, medium and high data sets.

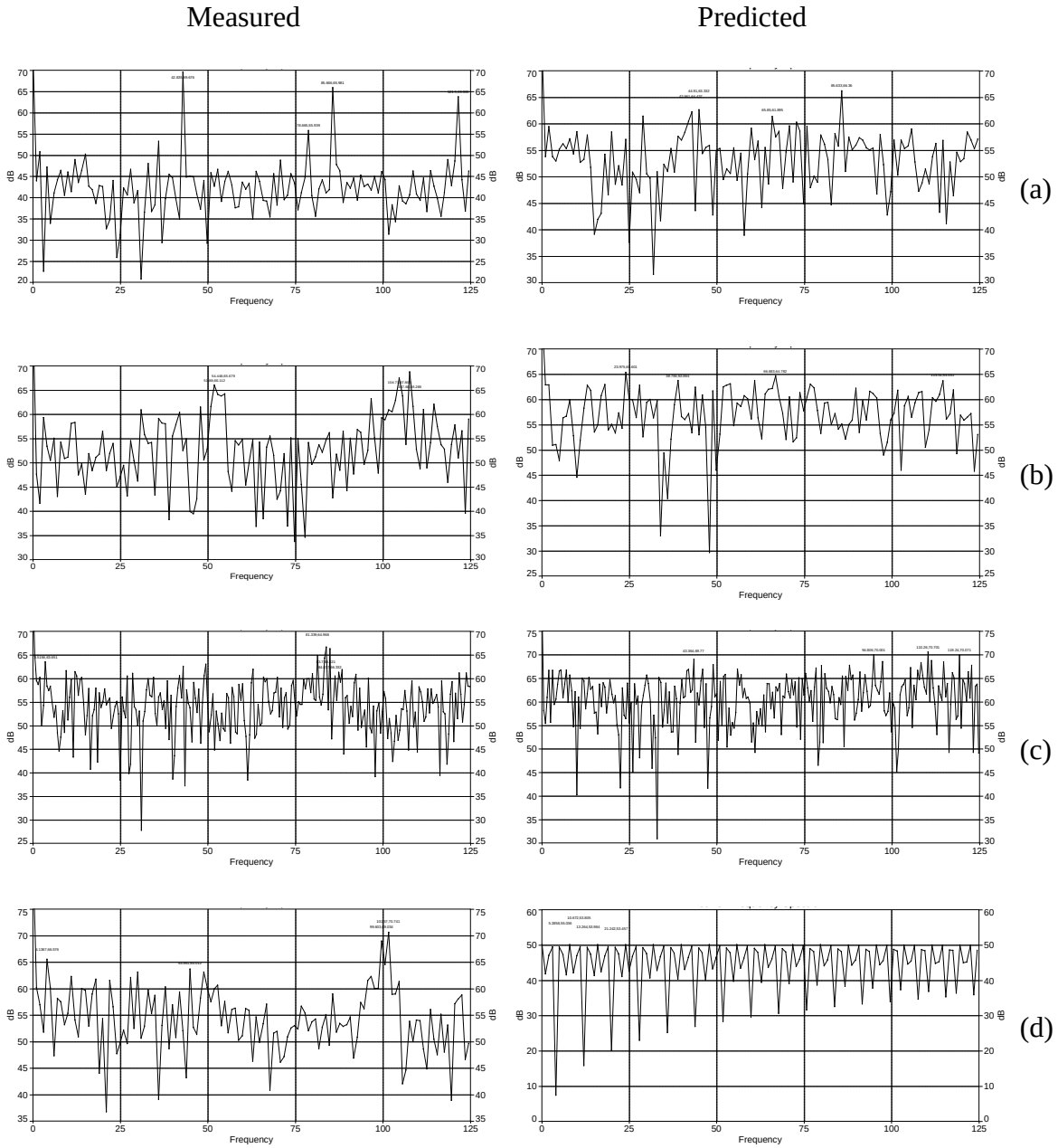


**Figure 6. 37, The measured Fourier opening frequency analysis (left) presented alongside predicted Fourier opening frequency analysis (for $A_{\alpha 1^4}$ data) (right) Sample 1. Demarked regions: (a) threshold, (b) low, (c) medium, and (d) high**

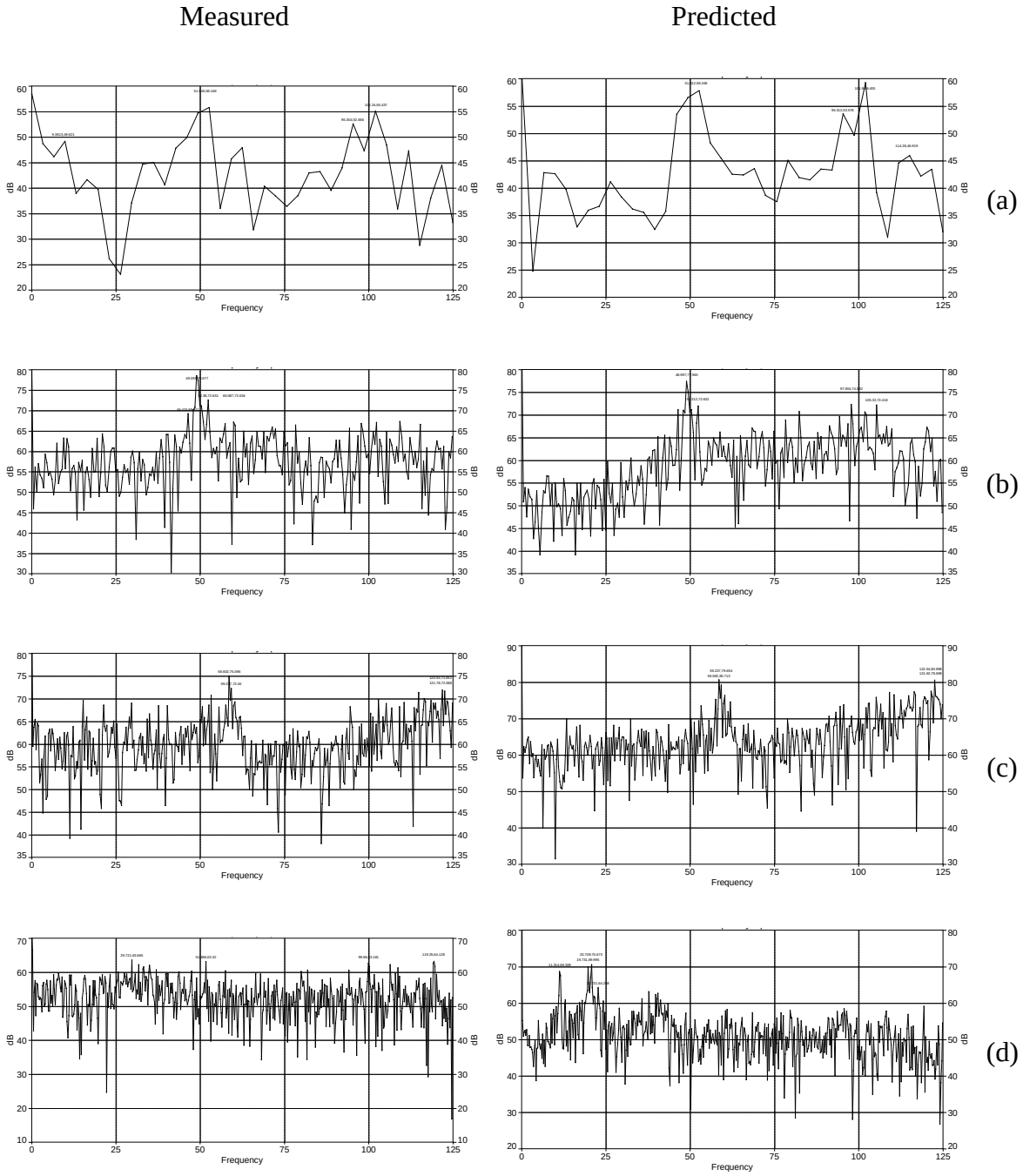


**Figure 6. 38, The measured Fourier opening frequency analysis (left) presented alongside predicted Fourier opening frequency analysis (for $A_{Max^4}$ data) (right) Sample 3. Demarked regions: (a) threshold, (b) low, (c) medium, and (d) high**

### *6.8.3. Summary*

This section of Chapter 6 has established a predictive method for the oscillatory motion of Samples 1 and 3. The model for predicting sample 2 was deemed unsuitable for predicting opening area and frequency across a wide range of pressures. The best results however, were obtained from the simple relationship $A_{Max^6}$ .

Using a sinusoidal relationship requiring both an amplitude and frequency, The prediction method for Sample 1 utilised the amplitude relationship from Eq. 6.24 and dominant frequency relationship from Eq. 6.32, the resulting equation is shown below.

$$A = (-8 * 10^{-7}P^4 + 0.0005P^3 - 0.1067P^2 + 8.0075P - 3.0856)Sin\left(2\pi\left(\frac{2 * 10^{-11}P^6 - 8 * 10^{-9}P^5 - 2 * 10^{-6}}{P^4 + 0.0012P^3 - 0.1941P^2 + 10.82P + 109.9}\right)\right) \quad \textbf{Eq. 6. 48}$$

The prediction method for Sample 3 differs as the amplitude relationship was found to b the only requirement for this trap seal. The amplitude relationship restated here is found from Eq 6.30.

$$A = -2 * 10^{-7}P^4 + 0.0002P^3 - 0.072P^2 + 9.9944\,P - 218.59 \quad \textbf{Eq. 6. 49}$$

It has been shown in Section 6.8 that the movement of the waterless trap seal can be predicted through the novel use of photogrammetric methods. This approach has never before been used to develop boundary conditions and has been found to provide equations which satisfactorily predict the opening area of the pipe with an installed waterless trap seal. A limitation however, of this method is in the qualitative analysis of the mechanical response of the valve. Photogrammetric methods using a single high speed camera provided only a 2 dimension perspective of the trap operation.

## 6.9. Co-simulation FSI results

Fluid structure interaction (FSI) was conducted through the coupling of two ANSYS solvers; a fluid (ANSYS CFX) and a solid (ANSYS Mechanical) solver. These results show the movement of a non-rigid tube modelled to a generalised likeness of a waterless trap seal. This section aims to provide an insight into boundary condition development using this technique.

The otherwise flat when stationary lip of the waterless trap seal (of width 35.1mm) was modelled as a uniformly circular tube with an equivalent diameter of 22.34mm. A simulation of this nature is typically lengthy due to the read/write requirements across the two solvers

The calculated displacement of the non-rigid sheath under a constant pressure of 1500pa (150mm wg) after 0.0082s is presented in Figure 6.39. Figure 6.40 presents pictorially the calculated displacement of the sheath of equal dimensions at 0.005s, 0.01s and 0.0128s of the simulation with a stepped up constant pressure of 1000Pa is presented.

It should be noted that pressure henceforth is calculated in Pascals and not mm wg.

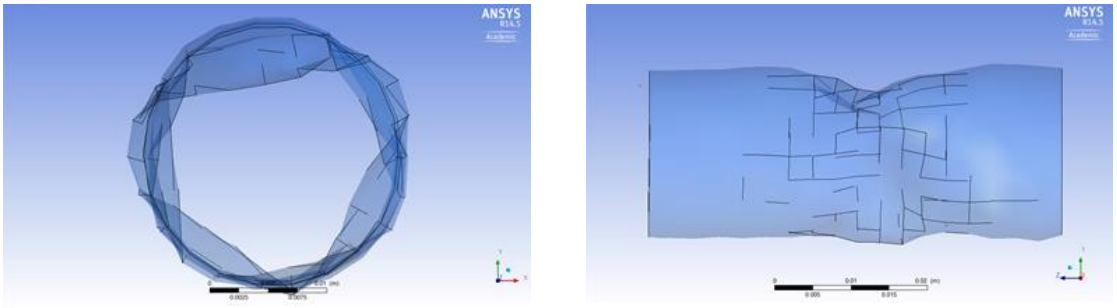


**Figure 6. 39**, The deformation along the sheath with the coarse structural mesh undulating in accordance with the applied pressure.

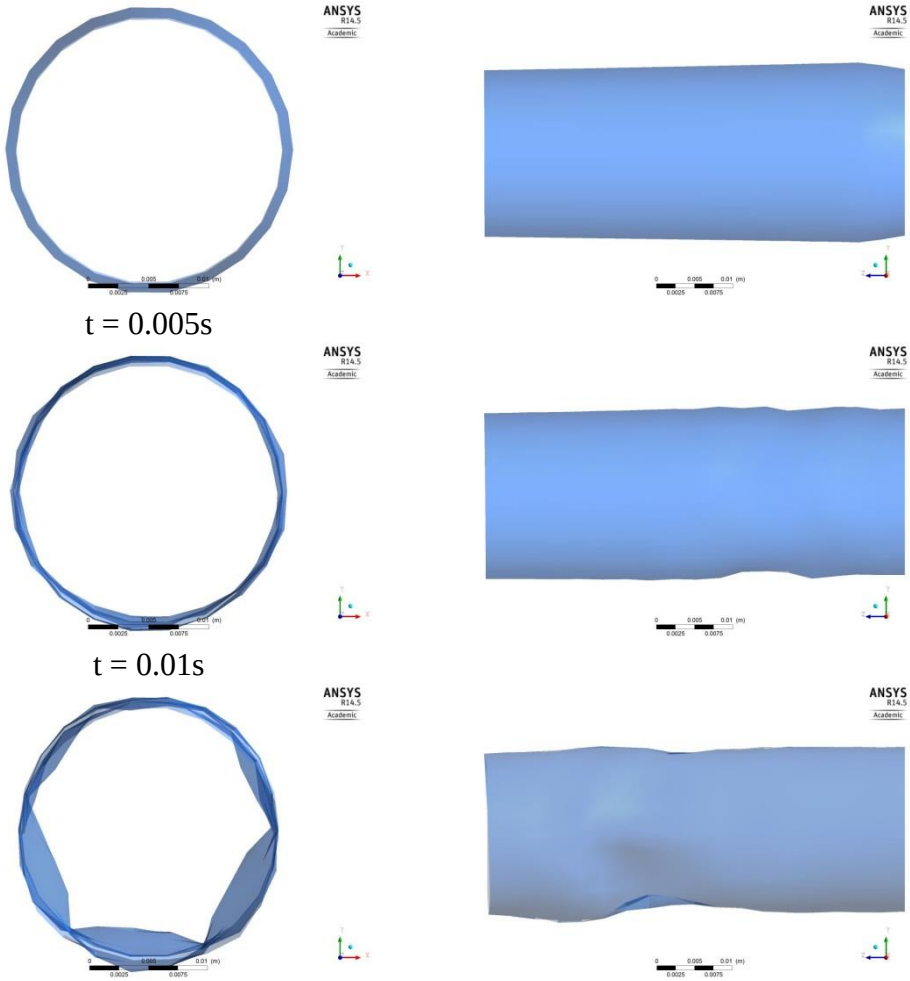


**Figure 6. 40, The deformation of the flexible sheath. (a) the front view of the deformation in time, (b) the side view of the deformation in time. The inlet is position to the far right of the image.**

Considering the points along the centre line of the sheath, the following data relating the opening area, velocity and the pressure is noted.

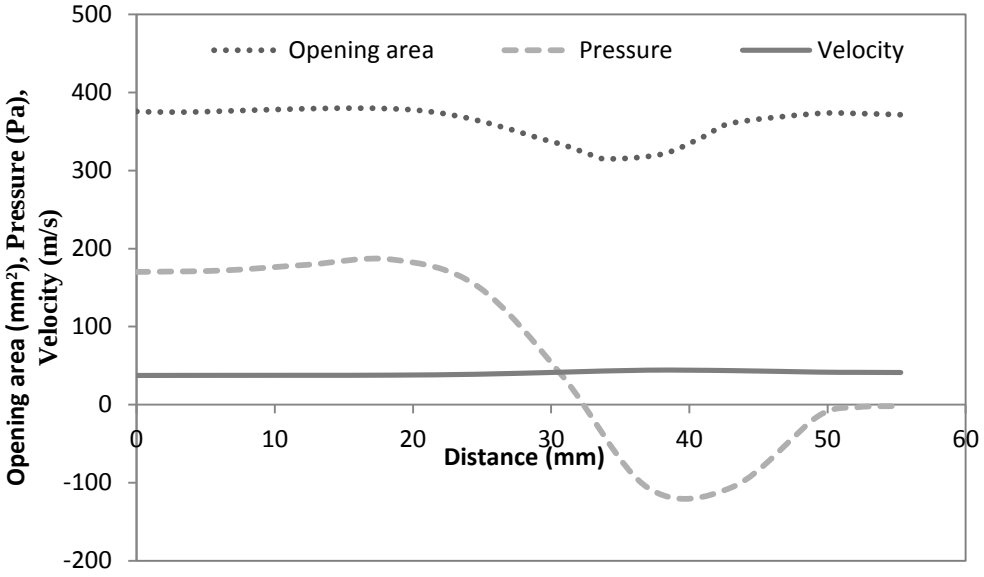


**Figure 6. 41, Comparison of the Opening area, Pressure, and Velocity at 0.128s along the centre line of the sheath**

Figure 6.41 shows the expected correlation between opening area, pressure and velocity. As the sheath narrows in cross sectional area along the middle of its length, an increase in pressure is noted downstream and a drastic decrease in pressure as air flow nears atmospheric conditions. Directly proportional to the mesh displacement is the velocity which increases with a decrease in cross sectional area.

The Figures 6.42 and 6.43 provide the pressure and velocity regimes along 5 slice planes along the length of the sheath.

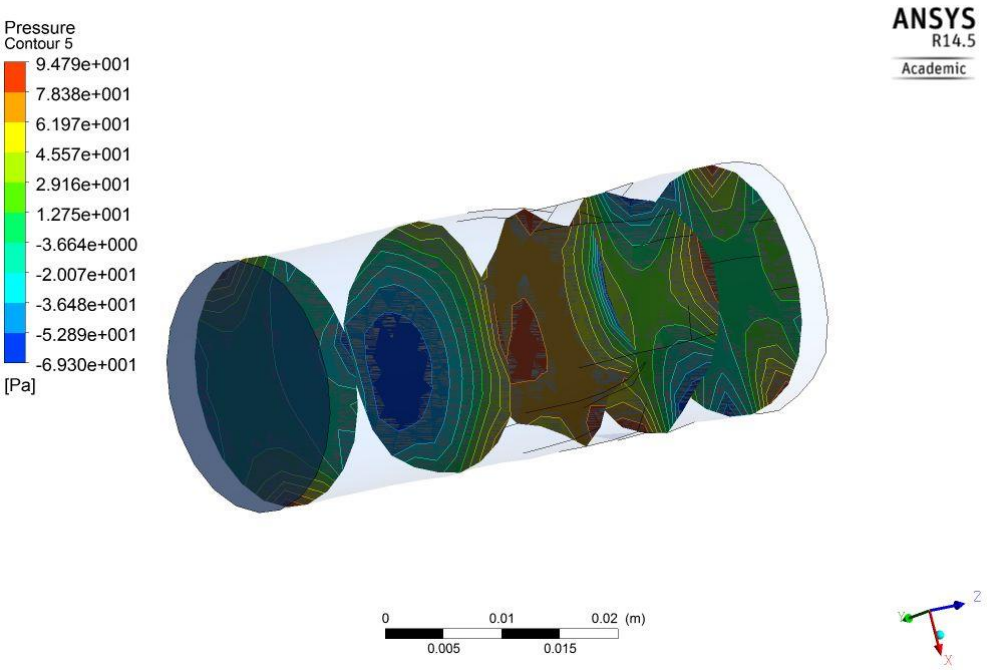


**Figure 6. 42, Pressure displayed on slice planes along the length of the sheath at 0.128s. The inlet of the sheath is placed to the left of the image.**

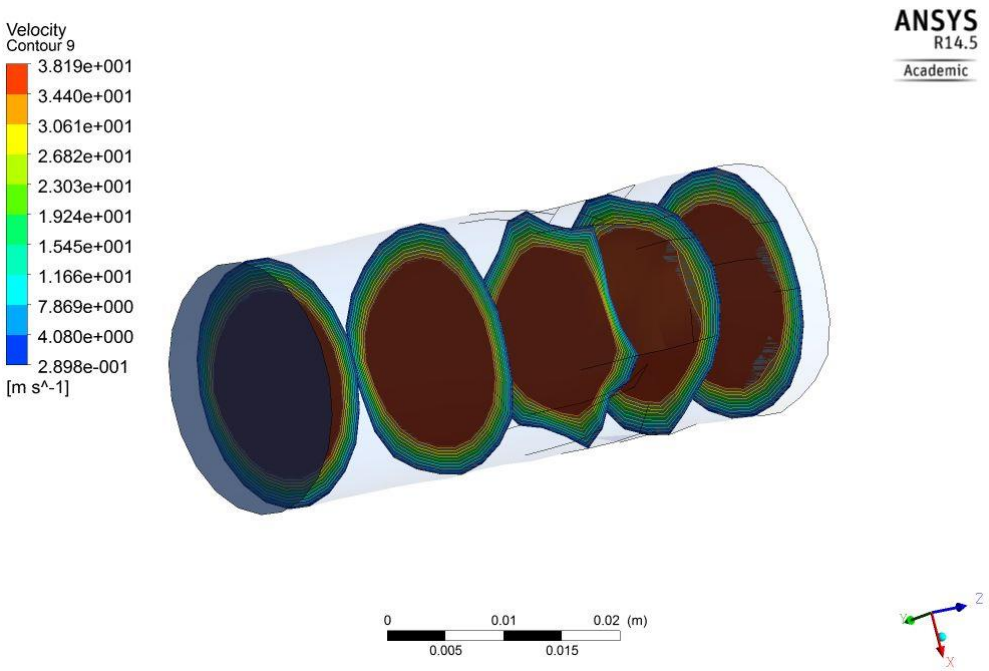


**Figure 6. 43, Fluid velocity displayed on slice planes along the length of the sheath at 0.128s. The inlet of the sheath is placed to the left of the image.**

Newton, (2009) states that the process of separating a flow phenomenon into for instance its mechanical and fluid properties is a classic example of the scientific principle whereby a system is greatly simplified before being described by the smallest possible set of equations. This simplification of the complete Navier Stokes equations allows models to depict more easily the reality of a particular problem. Such simplification is mentioned for instance in Chapter 3 with the conversion of the Navier Stokes equations to the Euler equations by not considering viscosity, or the Navier Stokes equations to the St. Venant equations, by solely considering the flow problem laterally. The lateral consideration of flow dynamics between two points, when applied to the Euler equation gives the Bernoulli equation (below).

$$\frac{p_1}{\rho} + \frac{v_1^2}{2} + gz_1 = \frac{p_2}{\rho} + \frac{v_2^2}{2} + gz_2 = constant \qquad \text{Eq. 6. 50}$$

This knowledge along with the relationship provided by Eq. 6.13 provides that a one mass model is suitable for the approximation of the waterless trap seal. Meaning that, from Figure 6.43 is can be seen that a single dominant area of displacement exists along the length of the sheath. This displacement laterally points to a one mass model. The equation developed in Section 6.6.2 using the lumped element approach provides that a linear relationship exists between the opening area, the height and the width.

Pressure upstream of the valve presented in Story and Titze (1995) under the conditions that the cord length and thickness are ignored, and area is considered, yields the relationship expressed below.

$$P(a) = P_i - \frac{1}{2}\rho v^2 \left(\frac{1}{{a_m}^2} - \frac{1}{a_i^2}\right) \qquad \textbf{Eq. 6. 51}$$

This two mass glottal model when adapted to the theory of the waterless trap seal, $P_i$ denotes the valve pressure, $a_m$ is the minimum cross sectional area of the valve, and $a_i$ is the corresponding pipe area.

This simplified version of the Bernoulli equation Ishizaka and Matsudaira (1972) follows,

$$P_m = P_i - \frac{1}{2}\rho k_e v^2 \left(\frac{1}{{a_m}^2}\right) \qquad \textbf{Eq. 6. 52}$$

$P_i$ is the input pressure, $P_m$ is the pressure at the minimum cross sectional area of the valve, $k_e$ is the exit pressure coefficient.

The loss coefficient is not a new concept to the field of BDS modelling. In actuality all boundary conditions to date in the AIRNET model require this definition. However, though FSI has provided a more in-depth understanding of the flow regime within the sheath, it can also be used to develop more traditional relationships.

These results and relationships confirm that the modelling technique is a valid method for evaluating flexible products. Future work in this area should seek to fully validate the findings against laboratory data.

## 6.10. Conclusion

Chapter 6 has presented the results of the digital and laboratory experiments along with the details of the photogrammetric analysis methods developed, and the Fourier analysis methods employed. These methods of analysis, allowed the assessment and derivation of significant information. Photogrammetric analysis proved very useful in analysing shape and patterns, and providing geometric data from which correlations and boundary conditions can be derived.

This research has found that waterless trap seals generate reflected air pressure transients which are opening frequency dependent, and can compromise water seals in other parts of the system. It was also found that not all waterless trap seals can be modelled accurately, and not to all pressure ranges, due to the randomness of the oscillatory motion across the range of pressure even though image cycles proved the trap's opening patter could be repeated, this was not found to be consistently so.

The use of a lumped element model enabled the defining of the relationship between the opening area and the length and height of the trap seal opening. The RMS value was also found critical to the approximation of the waterless trap seal opening area using known variables – length and width.

This appliance seal, unlike the water trap seal, is a non-rigid structure and so the numerical study of fluid flow behaviour of such a material is a more complex and time consuming process. The use of FSI proved advantageous to gaining an in-depth assessment of the flow conditions within the finite nodes of the model. This method enables the development of boundary conditions using traditional methods of determining the loss coefficient, or by assessing the smallest opening area of the sheath in time.

These methods are all new techniques to the Building Drainage and Plumbing field, and are suitable for boundary condition derivation and thus incorporation in a holistic boundary condition methodology.

# Chapter 7

## Discussion and Validation of Boundary Condition Development Techniques

### 7.1 Introduction

The flow characteristics of the waterless and the water trap seal were determined through laboratory and computational experimental methods and were presented in the preceding Chapters 5 and 6. The research findings satisfactorily lead to the development of boundary conditions -providing oscillatory orifice area approximations of the waterless trap seal in response to system pressures, and a new frequency dependant representation of velocity change in the water trap seal. These developments led to novel boundary condition methodologies enabling the development of suitable boundary conditions for inclusion in the MoC based model, AIRNET. These methodologies are presented in detail in this chapter and effectively satisfy Objectives 2 and 3 of this research project.

Validation of the new boundary conditions is problematic since whole system response under normal operating conditions would not yield useful data due to the random nature of system pressures which would make it impossible to disaggregate the influence of the water traps or waterless traps from other randomly operating devices. There is however a real need to validate the boundary conditions against known predictable baselines to increase confidence that whole system responses accurately reflect reality.

Two main principles gained from the analysis were used to validate the equations. Firstly, for a water trap it is known that as the frequency of an applied pressure wave increases, the expected water level movement in the trap will decrease; such that there should be little discernible movement at frequencies above 8 Hz, this principle is well understood, and easily observable. Secondly, for a waterless trap as pipe termination, the mean static pressure in the pipe is proportional to the effective opening area of the waterless trap as it fluctuates between open and closed under a constant applied pressure. This principle is difficult to understand, however if extreme conditions are considered then it may be easier to visualise – that is, if the pipe is completely open then no pressurisation will occur since there is no boundary, conversely, if the pipe is terminated in a dead end then the pipe will continue to pressurise. The level of opening of the waterless trap allows some pressurisation, and that level is also, by logic, related to the opening area. By using these principles in the validation process it is possible to test the accuracy of the boundary equations derived by the methods discussed in chapters 5 and 6.

## 7.2 Development of a Water trap seal boundary conditions

For traditional water trap seal modelling, equations are used to describe the forces acting within a system which cause the displacement of water. One such equation within AIRNET presents the frictional resistance in an oscillating trap seal.

$$A\big(p(j,N(j)+1)-p(ref)\big)+\rho_w(H_S-H_A)-\ \tau_0 L_w P=\frac{\rho_L L_I A dV_L}{\Delta t} \qquad \textbf{Eq. 7. 1}$$

Where, $\big(p(j,N(j)+1)\big)$ represents the air pressure on the system side of the trap, $(p(ref))$ is the air pressure on the appliance side of the trap, P is the wetted perimeter, $p$ is pressure, $\rho$ is density of the liquid, $H_S$ is the water height from free surface on the system side to the base of the trap, $H_A$ is the water height from free surface on the

appliance side to the base of the trap, A is the cross sectional area of the trap, $V_w$ is the liquid column velocity.

The new boundary condition which considers the effect of a frequency dependant friction factor is,

$$A\big(p(j,N(j)+1)-p(ref)\big)+\rho_w(H_S-H_A)-\ \tau_0 L_w P = \frac{\rho_L L_I A d V_L}{\Delta t}-\Delta v \qquad \textbf{Eq. 7. 2}$$

The new expression Eq 7.2 holds true to the original theory of the boundary condition requiring a relationship between the flow depth at both the trap inlet and trap outlet to the flow rate, but allowing the model to predict the variance in flow movement according to changes in transient conditions.

The method of developing this frequency dependent friction factor required the digital reproduction of the appliance water trap, the computational setup involving the VOF method which established the regions of water and air, and calculates the movement of the phase according to the fraction of the fluid element in each control volume. Upon the specification of all physical criteria, and the solution and convergence controls, the solution commences. Once complete, the results are viewed and extracted from the post processor and the process of data analysis begins. Figure 7.1 highlights the process.

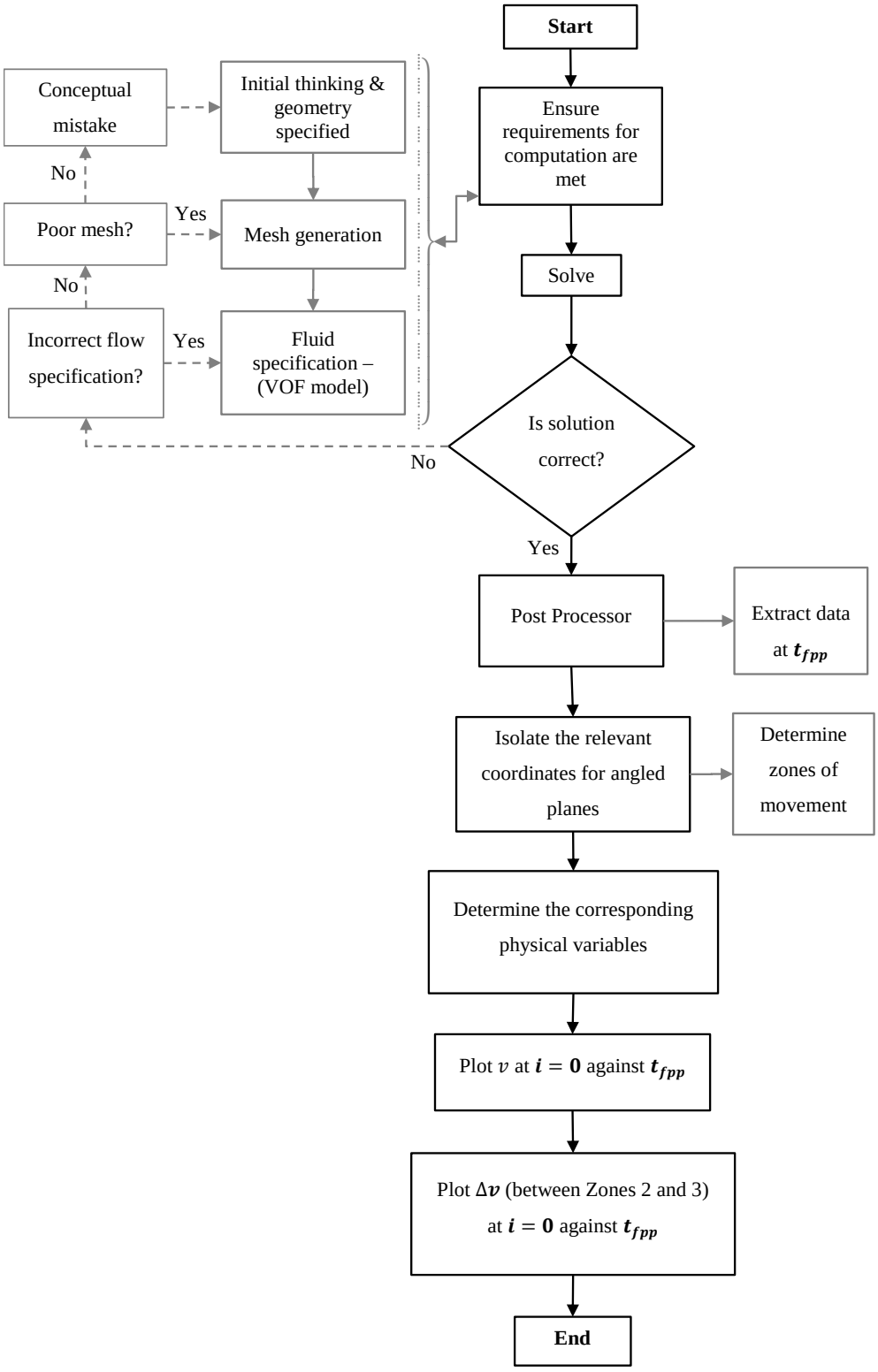


**Figure 7. 1, Methodology flowchart for boundary condition development of the water trap seal.**

The analysis process requires first determination of the number of equally spaced reference planes, then the isolation of the relevant coordinates and corresponding data. With this data, zones according to relative movement are determined, and friction and separation losses can be calculated. Calculated along water planes is recommended and so data should be cross reference to the volume fraction is advised.

### *7.2.1 Validation of multiphase simulation results*

This section seeks to establish a strong correlation between the results of the CFD model and the previous research of the water trap seal performance. Though it is not always possible to validate a CFD simulation as similar measurements may not be feasible in a laboratory setting, in this instance research by Gormley and Beattie (2010) and Beattie (2007) offers the visual observations of the frequency response of the trap seal movement along with findings from the pressure response.

#### *7.2.1.1 Frequency response*

Gormley and Beattie (2010) identified the transitional zone of movement through laboratory investigation of the response of water trap seal to a number of pressure frequencies. This zone is confirmed by the CFD simulations of the laboratory of like geometric proportions in Section 5.3.2. Here the analysis of the results found that a transitional zone of significant altering of trap velocity is between 3 and 4 Hz. The results continued by showing this region of velocity change in the commercial trap seal data proving that this zone is not only a consequence of trap design by purely the response to frequency. This change in velocity however was linked in the rate of rise to the first positive peak of the applied wave.

#### *7.2.1.2 Mesh quality*

Validation was also initiated in Chapter 5, by considering the effect of mesh resolution. Figure 5.2 was used to validate the data in the coarse mesh presented in Figure 5.3. It is well noted, that the higher the mesh resolution, the greater the degree of accuracy afforded. A factor which could diminish confidence in the coarse mesh results, however, as time presented a significant restriction on the resolution of simulation, validation of the suitability of a coarse mesh was deemed useful. The results of this comparison found that a $\pm 2\%$ disparity exists. This small disparity is found to be insignificant for the purpose of methodology development.

#### *7.2.1.3 Visual observation*

Due to the nature of CFD and the depth and breadth of information gained in many instances comparison of flow field data is not always possible. Visual observation is found to be an accepted method of validation. In this instance, analysis of photographic data provided by Beattie (2007) is used to verify the accuracy of water column displacement in accordance to the applied low amplitude pressure wave frequency.

**Figure 7. 2, Observation of the displacement of water in the appliance trap in the Heriot watt University drainage laboratory.**

Figures 7.2 and 7.3, show the disproportional displacement of water along the bend as air displaces the water. This is a result of a positive pressure transient in the laboratory and CFD investigation when an air pressure of significant amplitude and/or frequency is applied. Notice from the images that the air column along the inner bend approaches the vertical section of the pipe while the water column along the outer surface of the bend remains closer in proximity to its original position. It is important to note that under normal operation after this occurrence where air propagates across the seal via bubbles or free surface flow, upon flow stoppage the water will return to rest and reseal the appliance trap if sufficient fluid remains.

This pattern of movement in the laboratory trap validates the flow regime in the CFD model. However when the photographs are overlaid a discrepancy is noted to the right of the outer bend. This area in highlighted in Figure 7.4.

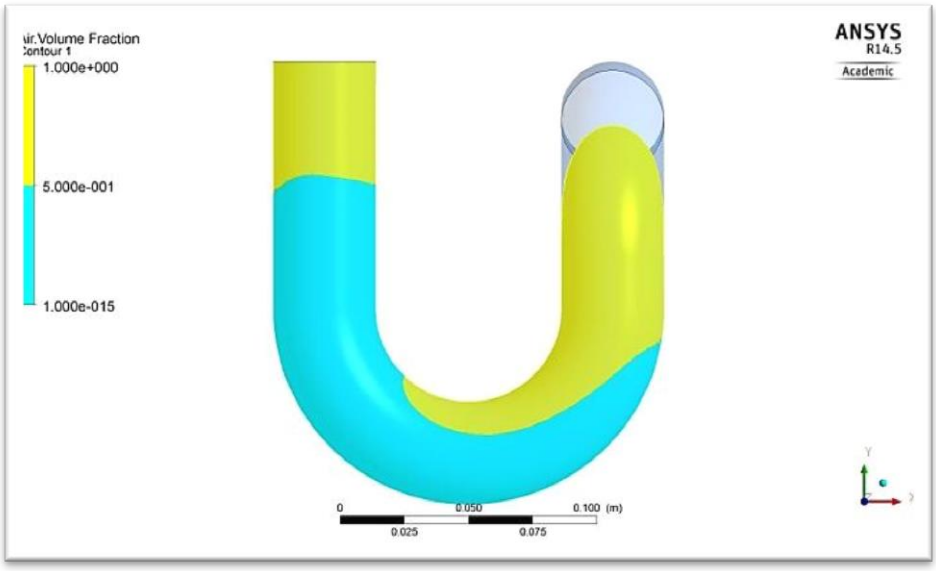


**Figure 7. 3, Air volume fraction across the XY plane (Z=0) in the laboratory appliance water trap at 0.5s when an applied 1Hz pressure transient.**

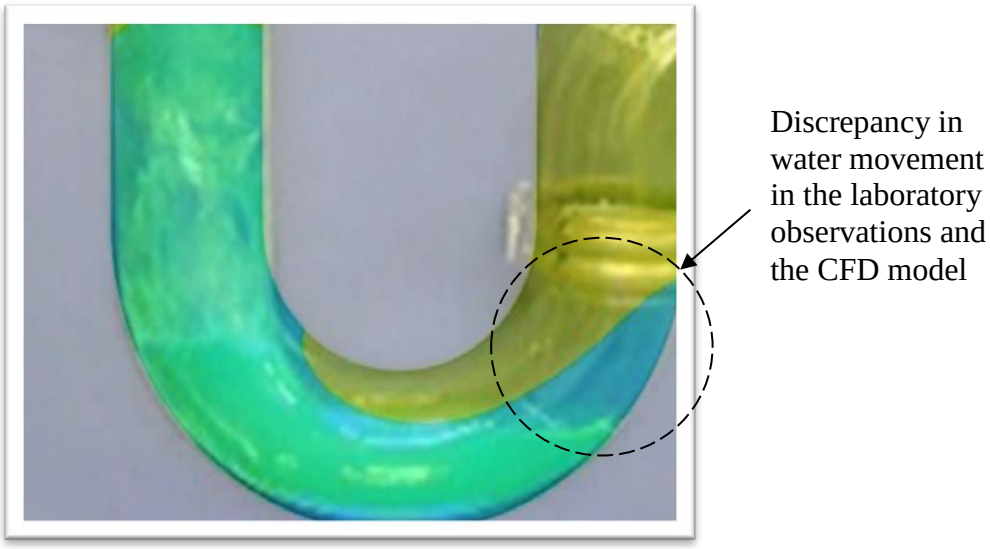


**Figure 7. 4, The overlay of the laboratory observation image and the VF results of the appliance trap seal from ANSYS CFX**

It should be noted that the experiments were not conducted under consistent applied pressures or time frames, however it is expected that the movement of water should be

relatively alike. Figure 7.4 shows that CFD is able to fairly accurately predict the movement of the water along the inner bend of the trap seal, but that possible errors are likely in the region highlighted. This may be due to an underestimation of the velocity of water movement along the outer bend of the trap seal. Confirmation of this discrepancy and further details of the degree of accuracy requires further laboratory research of a like to like situation which outreaches the scope of this study.

Beattie (2007), using a high speed camera, to capture the trap seal movement along the appliance side of the trap. His research offers a larger time scale of assessment than allowed for in this project. Figure 7.5 presents the comparable images above the base line height and for frequencies, 1,2,3,4 and 8 for the 38mm trap seal test.

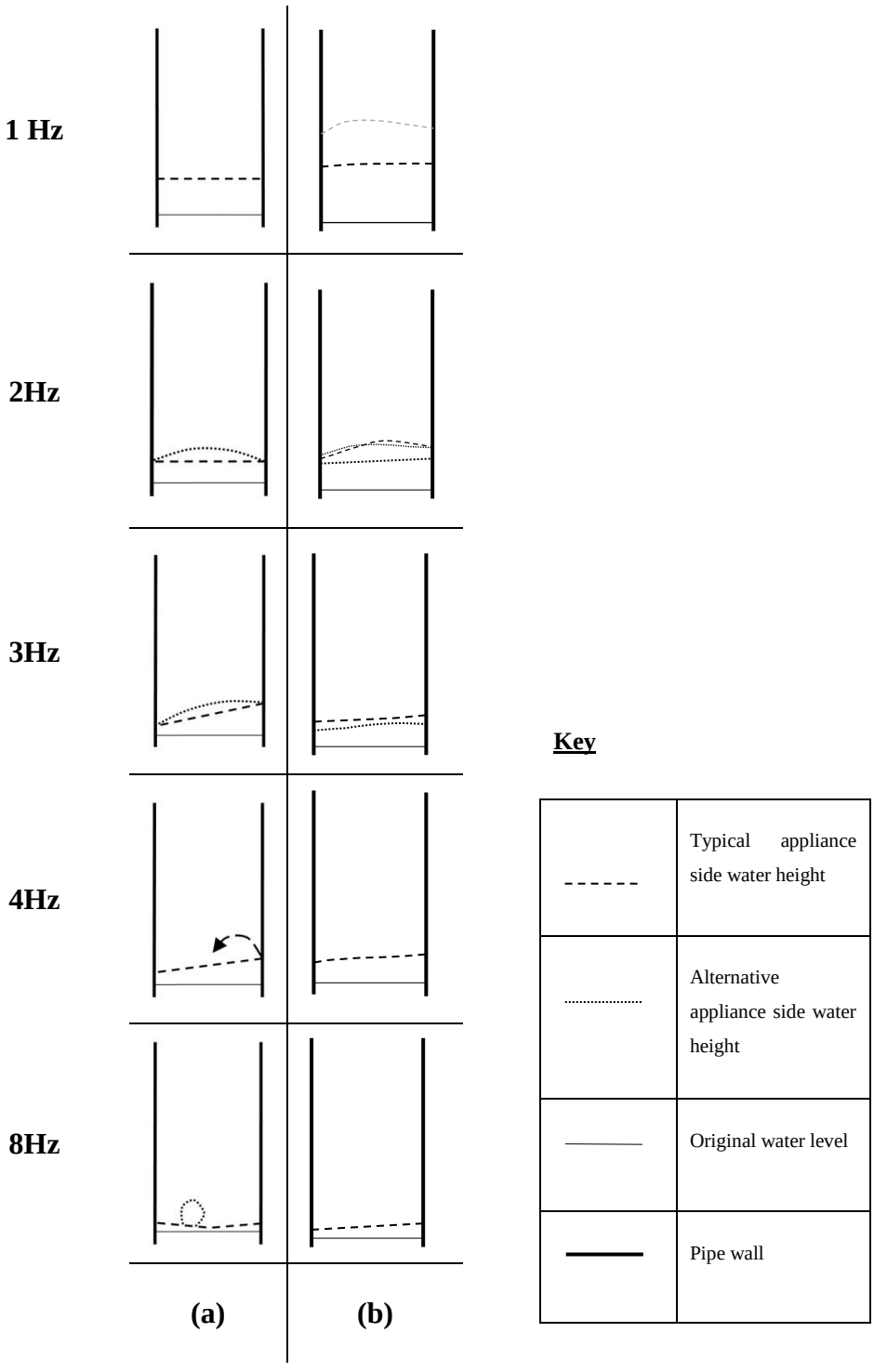


**Figure 7. 5, Representative sketches of the water oscillations for each tested frequency (a) Measured at 38mm water trap depth, Beattie (2007), (b) Predicted using ANSYS CFX at 38mm water trap depth**

These water profile images are compared to the corresponding image from ANSYS CFX. Scaled and pencilled image are presented below.

The pattern of water movement along the appliance side of the water trap seal is found to be similar to that calculated by ANSYS CFX. This data through visual assessment can there be said to be valid.

### *7.2.2 Validation of Frequency dependant representation of velocity change*

The following presents the AIRNET water trap response predictions for a pressure input to the branch of 1 metre length connected to the likened virtual model of the laboratory trap. A single peak pressure is applied to the virtual water trap seal at frequencies 1, 3, 5, 8, and 10. Figures 7.6 to 7.9 show the results of when the existing boundary condition shown in Eq 7.1 is used over a 3s period.

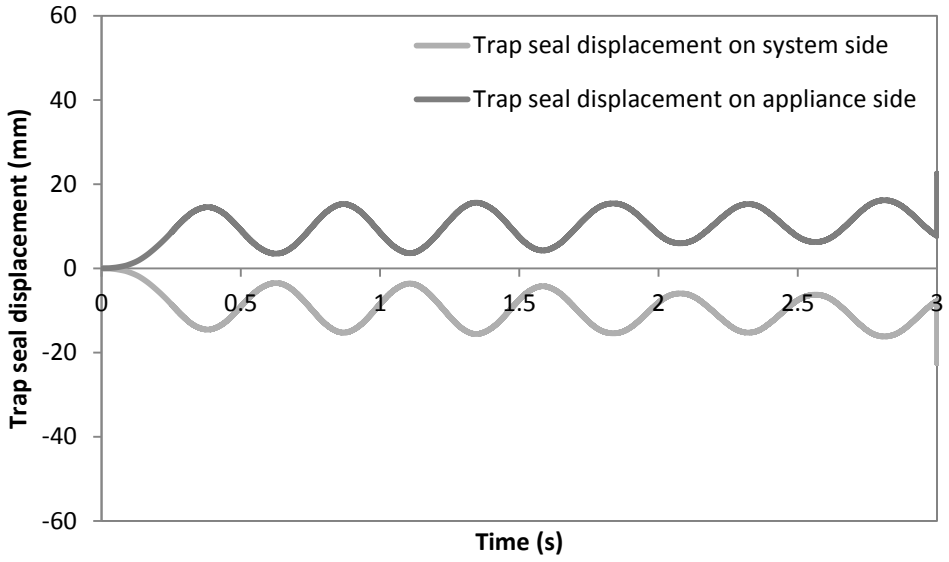


**Figure 7. 6, Results of the AIRNET simulation when the applied airpressure wave equals 1Hz**

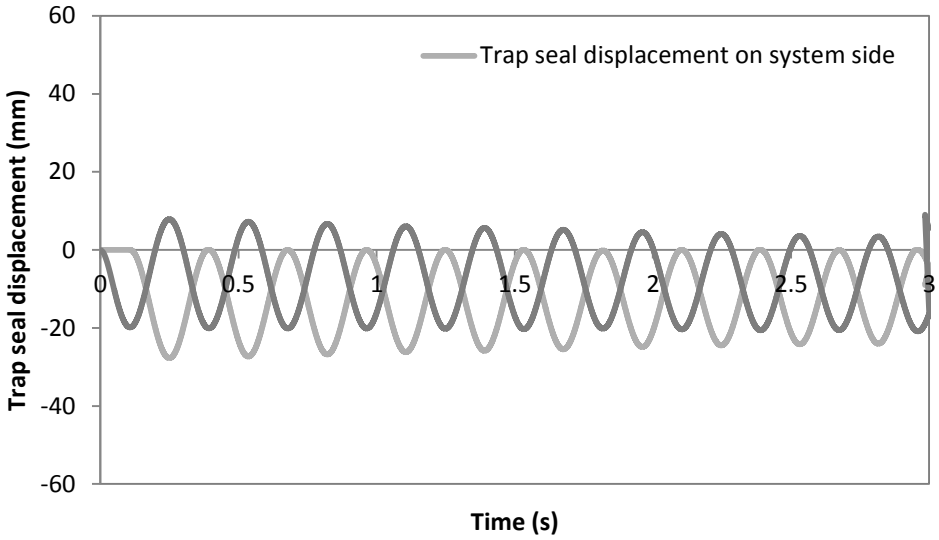


**Figure 7. 7, Results of the AIRNET simulation when the applied airpressure wave equals 5Hz**

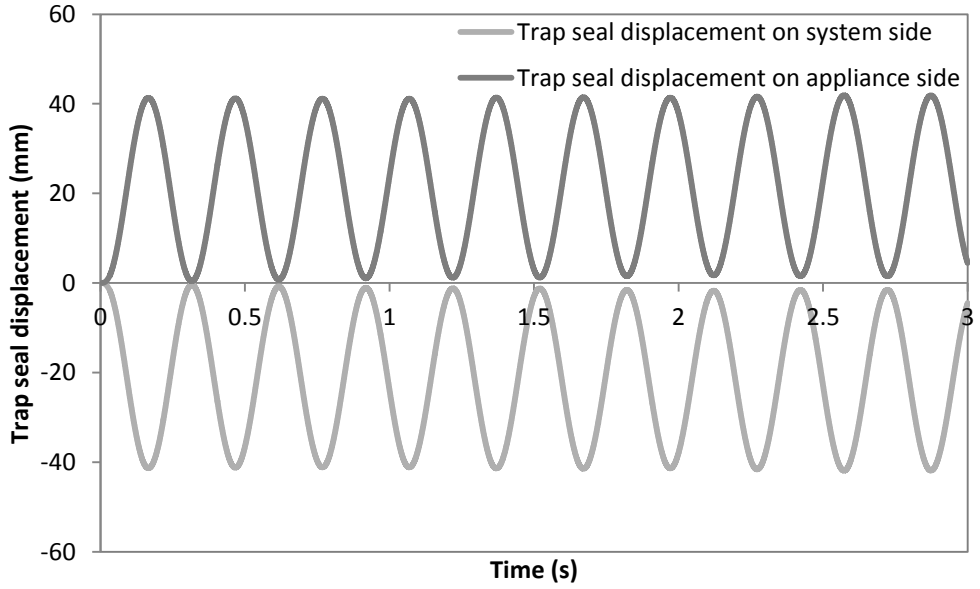


**Figure 7. 8, Results of the AIRNET simulation when the applied airpressure wave equals 8Hz**

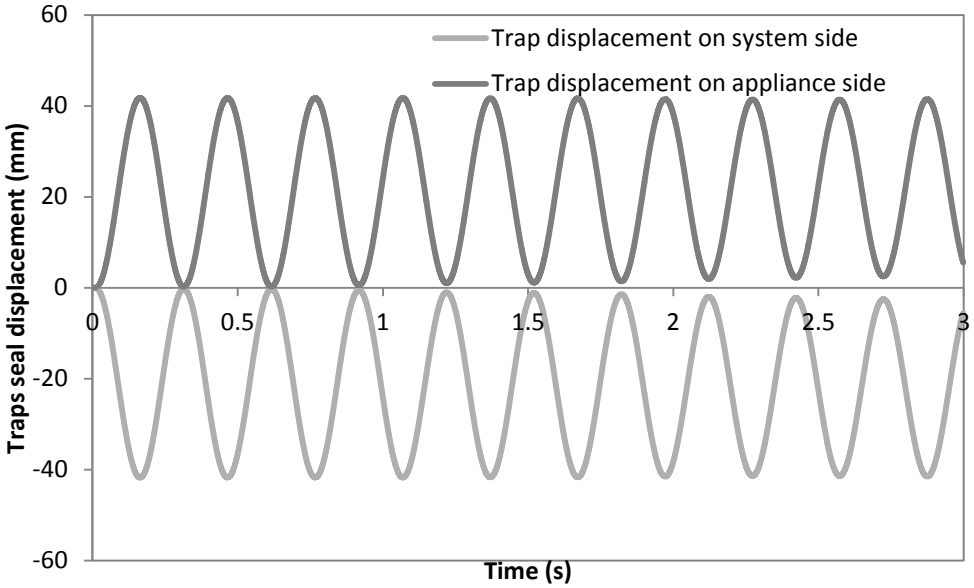


**Figure 7. 9, Results of the AIRNET simulation when the applied airpressure wave equals 10 Hz**

These figures show that the existing boundary condition, trap seal displacement is considered greater with every increase in the applied frequency. This numerical assessment of the trap seal displacement is contrary to that found by Beattie (2007) and Gormley and Beattie (2010).

The following presents the results of the water seal movement in the virtually tested appliance trap seal using the detla *v*. note that the following Figures 7.10 – 7.13 all hold a max value in the y axis of 20mm trap seal displacement over the 60mm in Figures 7.6 – 7.9.

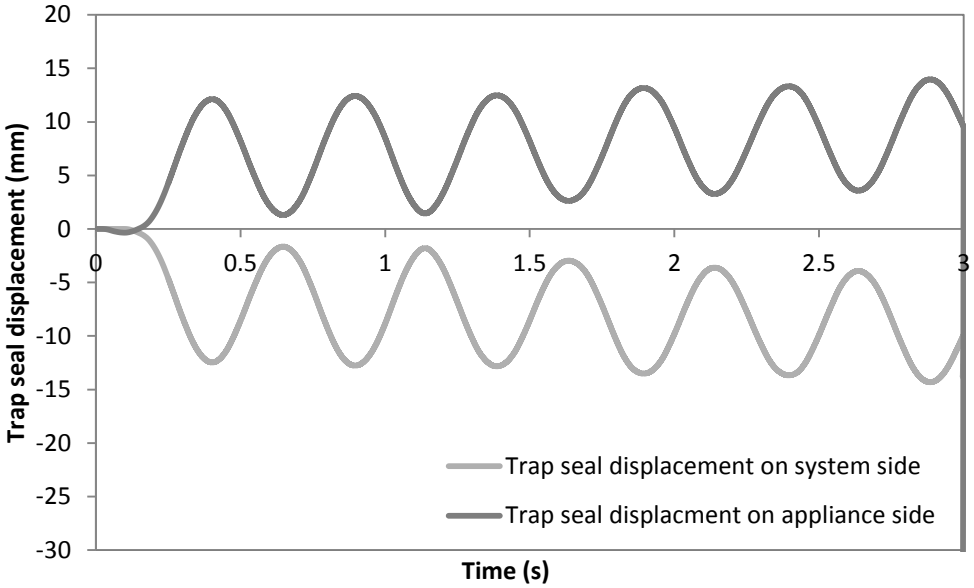


**Figure 7. 10, Results of the AIRNET simulation using detla *v* when the applied airpressure wave equals 1Hz**

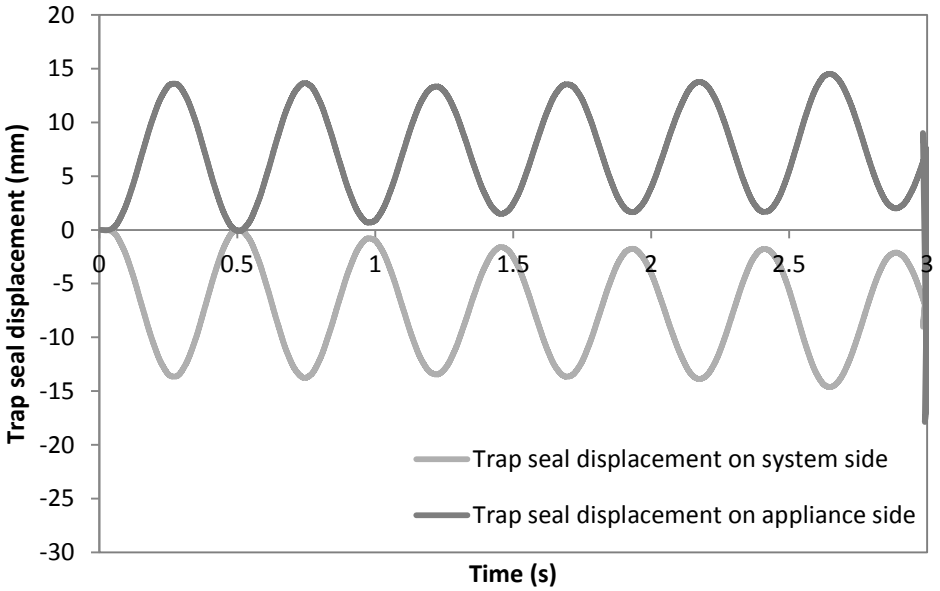


**Figure 7. 11, Results of the AIRNET simulation using detla *v* when the applied airpressure wave equals 3Hz**

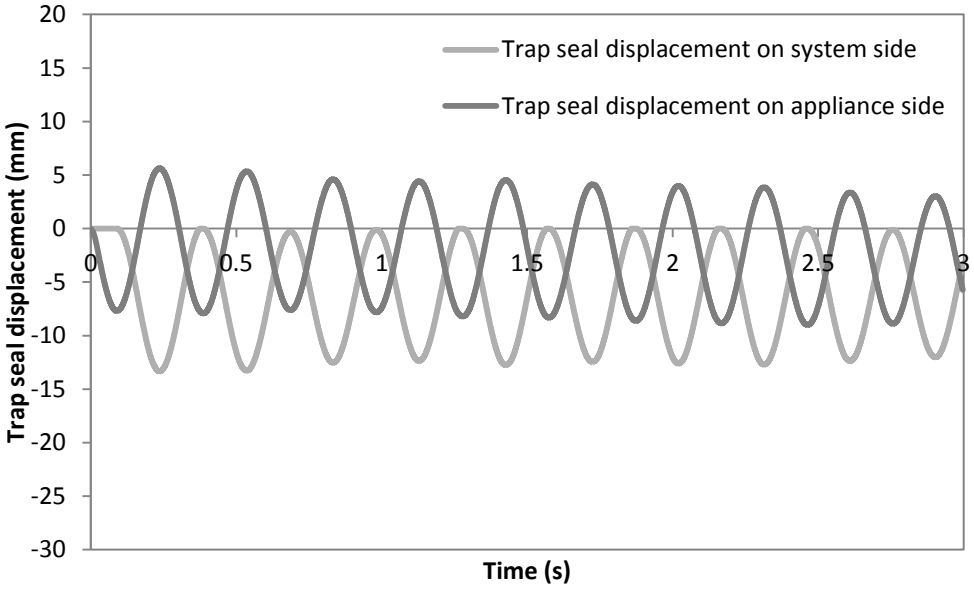


**Figure 7. 12, Results of the AIRNET simulation using detla *v* when the applied airpressure wave equals 8Hz**

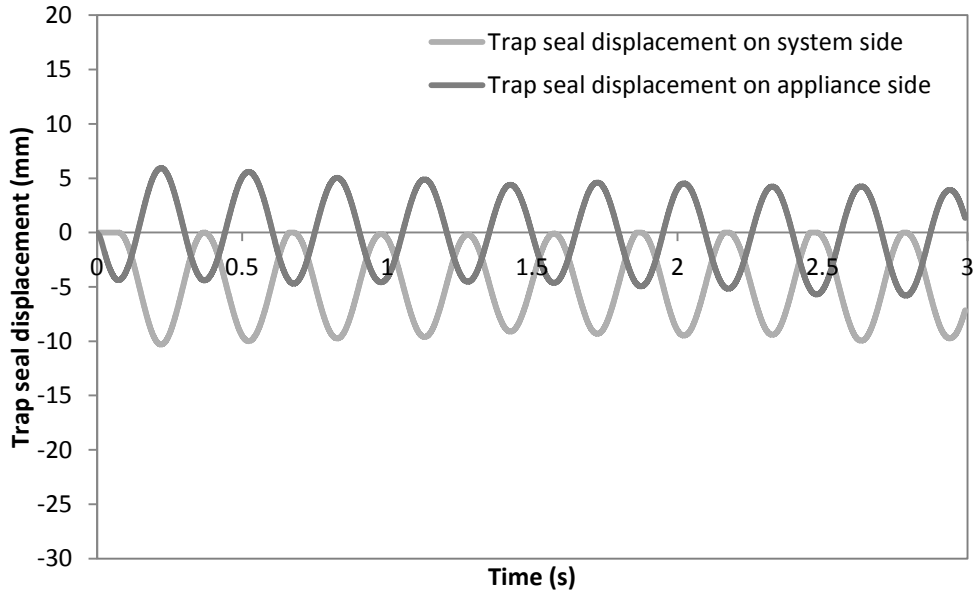


**Figure 7. 13, Results of the AIRNET simulation using detla *v* when the applied airpressure wave equals 10Hz**

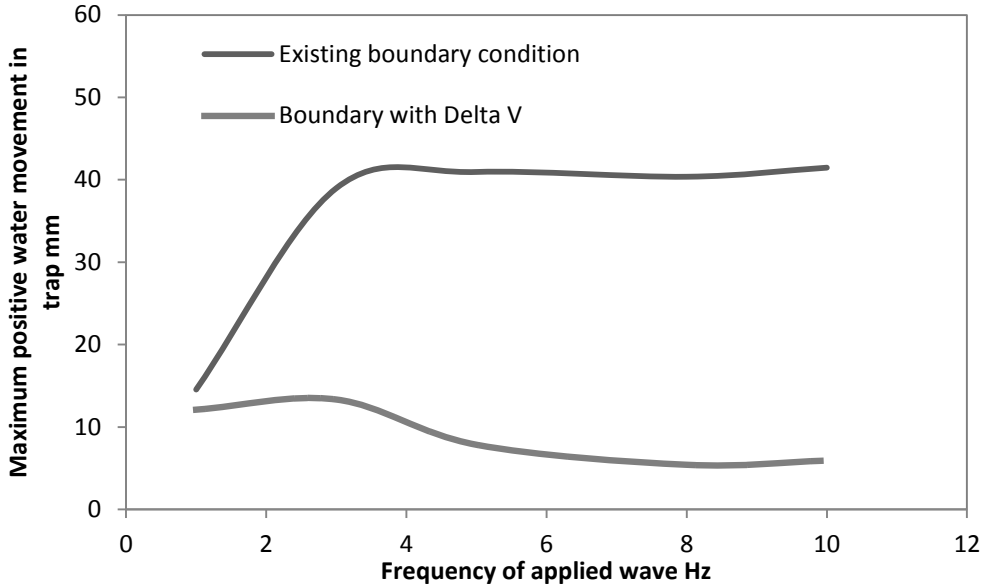


**Figure 7. 14, Comparison of the trap seal displacement results modelling system operation with the existing and new detla *v* boundary conditions.**

Here, the AIRNET prediction with the existing boundary condition, do not reflect the reality of trap seal movement. It is known that trap seal displacement increases with a decreasing frequency which is presented in the comparison data – the prediction with $\Delta v$.

Generally the existing boundary condition overestimates the trap movement. This leads to an overestimation of seal loss. This overestimation therefore leads to inaccurate whole system assessment of the system's operational characteristics. The new boundary condition is frequency dependent, providing more realistic estimation of effects of air pressure transient propagation, trap water movement and therefore trap seal loss.

It is also an improvement on the Zilke equations in that there is no 'setting time' i.e. the first peak will still be as large with Zilke - it will then attenuate Figure 7.14 presents graphically the disparity between the two methods of predicting seal movement and the vast level of estimation shown also in Figures 7.6 – 7.9.

### *7.2.3 Summary*

The validation of the computational data through comparison with existing data and through comparison with the results of the AIRNET model, have provided sufficient data to render the use of the tool a satisfactory alternative to traditional laboratory testing. This finding addresses Objective 4 of this research.

Where possible, data from previous research, from the laboratory investigations, CFD and FSI analysis is used to increase confidence levels in the validity of the equations. Previous attempts to introduce an unsteady friction component into the water trap seal boundary condition have been far from perfect. The most deterministic of these methods was due to Zilke (Swaffield 2010) as discussed in Chapter 2. The application of Zilke in this context is computationally challenging for a 1-D model and significantly increases calculation time. The method is also time dependent – where accuracy developed over time, thus rendering initial calculations inaccurate with ongoing consequences for whole system modelling. Gormley and Beattie's (2010) β co-efficient was easier to implement, however it was restricted to the single water trap analysed, and so was not considered robust enough for whole system modelling.

## 7.3 Development for waterless trap seals Boundary conditions

The traditional method employed for any previous developed boundary conditions for AIRNET, required the determination of the loss coefficient factor $K$ using the equation below. The velocity and pressure readings required to transpose and solve for $K$, were determined through laboratory investigation. Chapter 6 has presented the use of FSI data to provide that which could alternatively be found through laboratory testing and determine to a larger degree the range of movement which exists within the product and what condition induce constant, minute and extreme reactions in movement. 2D analysis across the length of the sheath leads to the development of a multiple mass lumped element model through which flow characteristics can be simplified without ignoring substantial characteristics.

In its operation the waterless trap behaves much like the air admittance valve which was first developed in 1980 in Scandinavia. Invented as a surge protector for the retention of trap seal, the major concern of this new device was its ability to adequately seal under positive pressure conditions and prevent the occurrence of cross contamination. The boundary condition which describes this opening and closing phenomenon presently in AIRNET is

$$\Delta p = 0.5\rho K_t V|V| \qquad \textbf{Eq. 7. 3}$$

Though the AAV can be likened to a waterless trap seal, this simplified approach to its movement, over estimates the amount of time the pipe is fully open and any influence transients may have on the responsive behaviour of the trap opening or closing.

Chapter 6 of this thesis provided the equations below, where the orifice area equals,

$$A = (-8 * 10^{-7}P^4 + 0.0005P^3 - 0.1067P^2 + 8.0075P - 3.0856)$$
$$Sin\left(2\pi\left(\begin{matrix}2 * 10^{-11}P^6 - 8\,\alpha 10^{-9}P^5 - 2\,\alpha 10^{-6} \\ P^4 + 0.0012P^3 - 0.1941P^2 + 10.82P + 109.9\end{matrix}\right)\right) \qquad \textbf{Eq. 7. 4}$$

or

$$A = -2 * 10^{-7}P^4 + 0.0002P^3 - 0.072P^2 + 9.9944\,P - 218.59 \qquad \textbf{Eq. 7. 5}$$

Development of the waterless trap seal boundary condition or any similar BDS appliance made up primarily of a flexible of moving membrane, can be investigated and characterised by the method employed in this study. The process involved the selection of the product, which can then be analysed via one of two methods depending on the available resources – laboratory or computational methods.

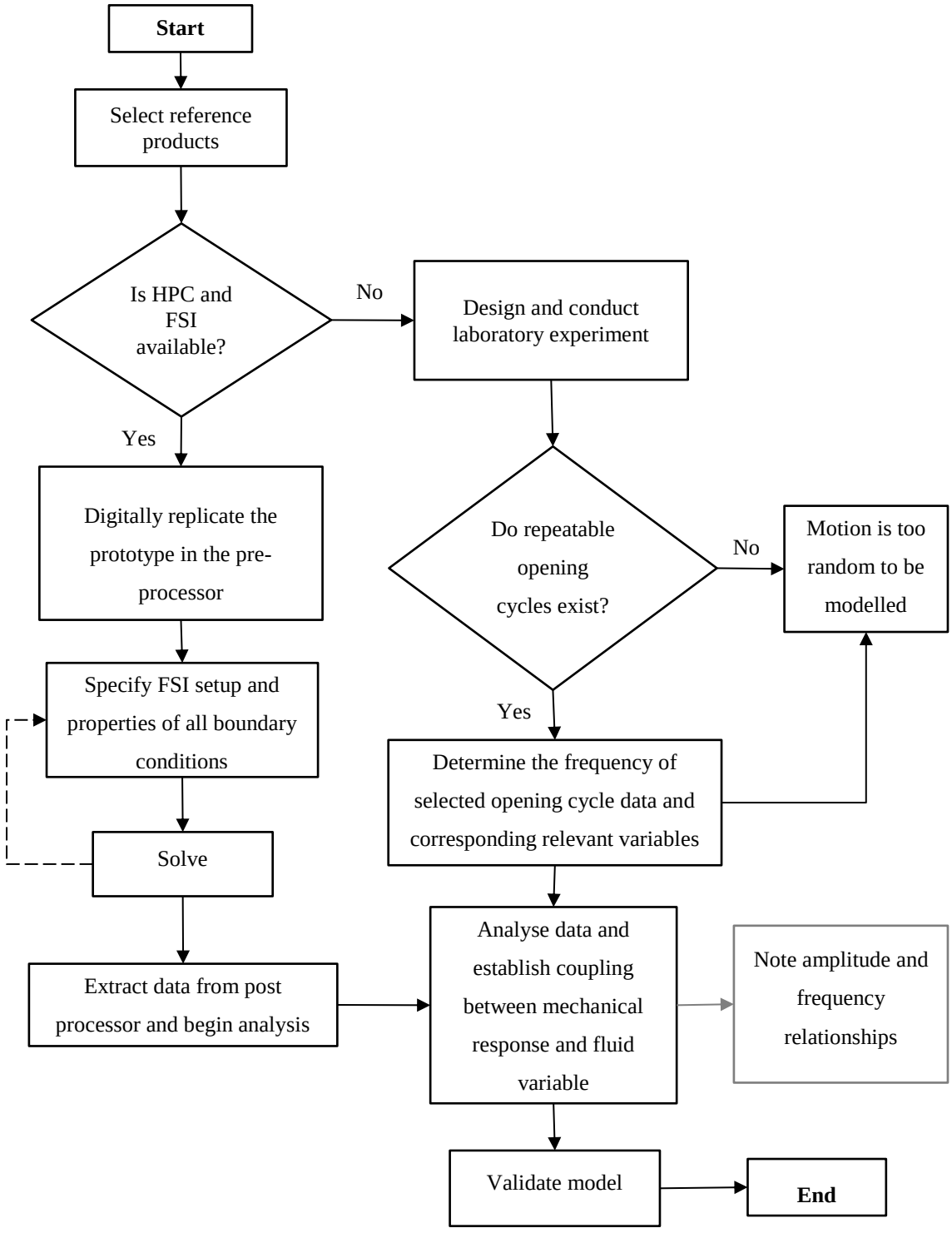


**Figure 7. 15, Methodology flow chart for Waterless trap seal boundary condition development**

This novel method of boundary condition development is presented in a flowchart in Figure 7.15.

This section seeks to provide a more realistic model of the aerodynamic behaviour of an elastic membrane (non-rigid valve) as pressure and frequency vary in a BDS. The validity of previous models to the true behaviour of the waterless trap seal has been expressed. Newly developed methods and boundary conditions will be validated in Section 7.3.1

### *7.3.1 Validation of waterless trap seal model*

Validation of the boundary condition technique is conducted through the use of the already validated AIRNET model. The equation describing Sample 3 was selected as it provides greater simplicity for programming than that for Sample 1.

Under normal conditions the AIRNET model calculates the opening area of the pipe based on the pressure profile within the branch connecting the trap. This opening will present a reflection (downstream) into the branch from which a new pipe opening area will be approximated. This relationship describes the intended fluid structure interaction calculation of the waterless trap seal in AIRNET. The ability of the model to accurately perform this process will enable AIRNET to become a single solution FSI method without requiring the solution of governing mechanical principles.

The assessment was conducted through a series of steady state calculations. The system model was designed in AIRNET builder and comprised of a 50mm vertical pipe with pressure input at the base and a dead end at the other. A 50mm branch connected to this main stack, and presented at the end an orifice of maximum diameter of 31.89mm. A constant air pressure was input to the system and the results are recorded below. It is approximated that the applied pressure to the pipe is twice the amplitude of the static pressure at approximately 0.5m from the end of the pipe.

Assuming, from laboratory observation

$$p_a \cong 2p_s \qquad \textbf{Eq. 7. 6}$$

The opening area was determined for a required pipe static pressure, and the opening assumed to be circular in shape using the calculated equivalent diameter. This shape is known however, to be contradictory to reality, as irregular and non-symmetrical movements are expected by the waterless trap seal opening.

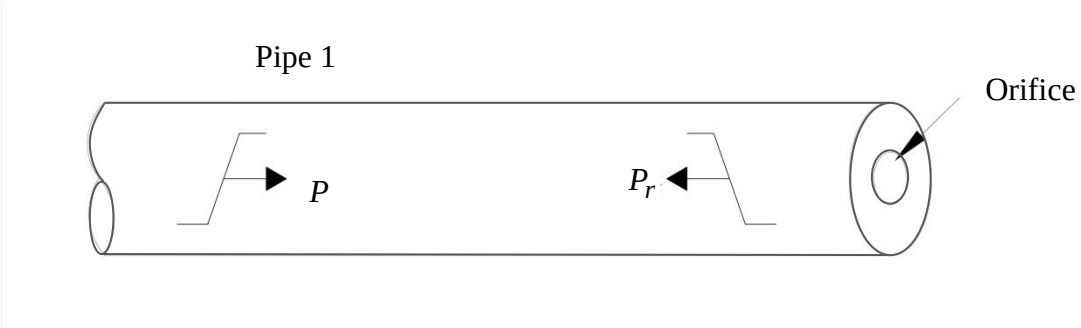


**Figure 7. 16, AIRNET model setup**

The waterless trap seal was simplified to an orifice of constant size. A recording of the changing opening area was not possible but changing pressure was.

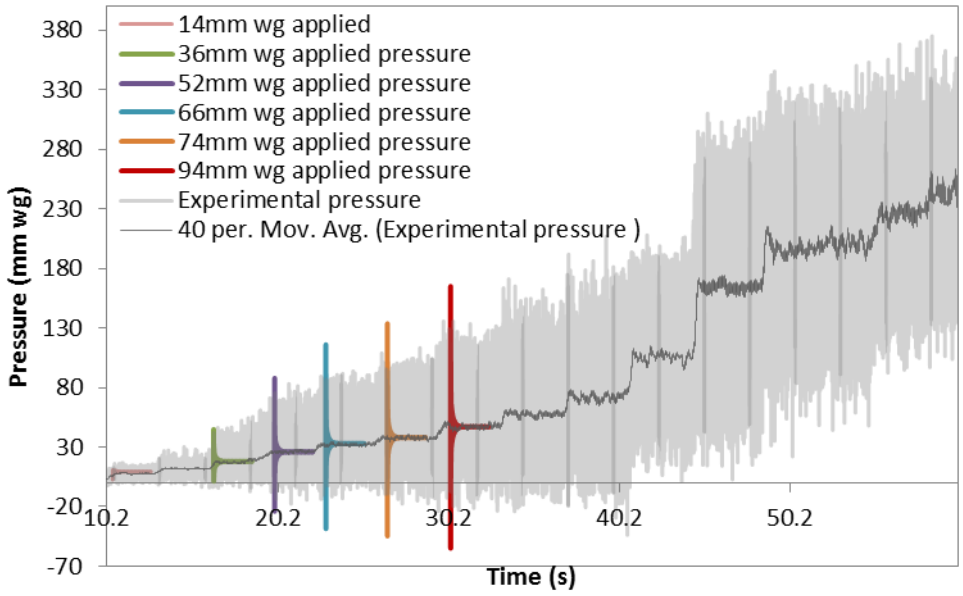


**Figure 7. 17, Predicted data overlaid onto Sample 3 pressure amplitude results**

Figure 7.17, shows that the greater the pressure the greater the over estimation. Regardless of this fact, Figure 7.17 shows clearly that the recorded predicted static pressure for the measured opening area corresponds satisfactorily within the correct data set the average pressure of the measured data correlates to the static pressure after 0.5s of constant unaltered pressure.

Figure 7.18 shows that after a 0.324s of the run, the pressure is observed to reach a fairly steady state of gently undulating form about the moving average of the measured data

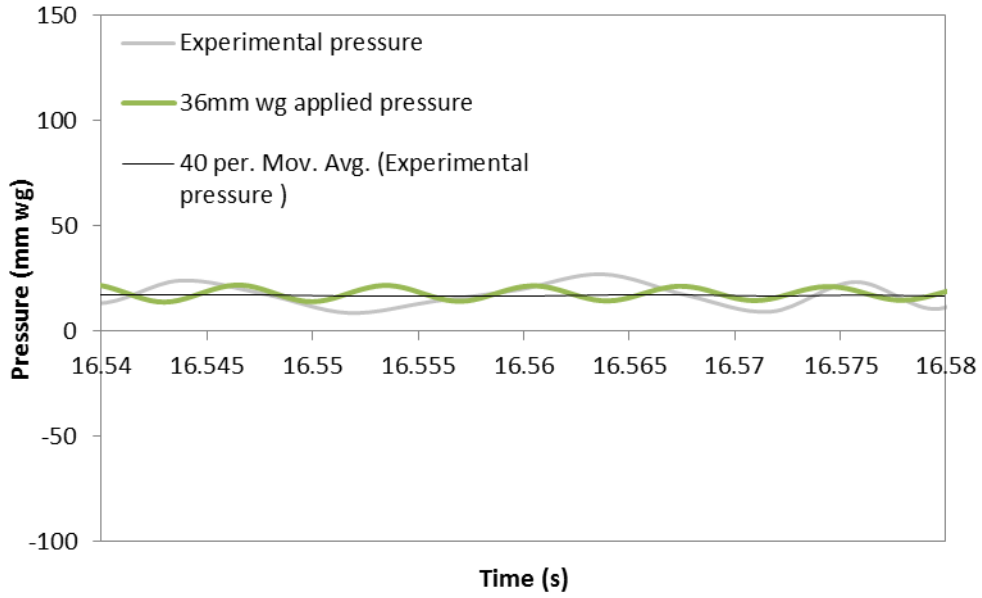


**Figure 7. 18, between 16.54s and 16.58s**

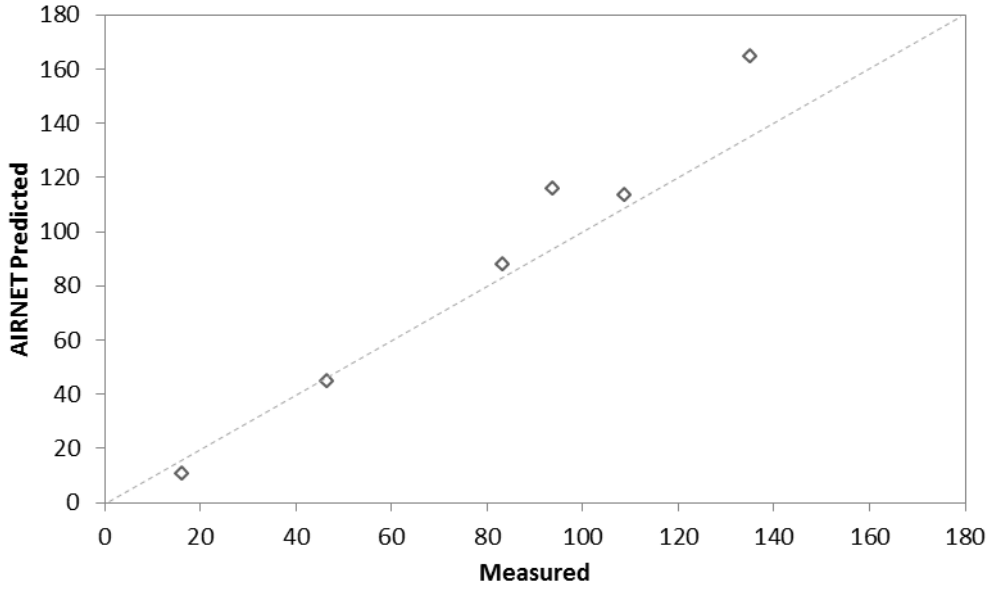


**Figure 7. 19, Measured maximum pressure against AIRNET predicted maximum pressure of selected data sets. $R^2 = 0.9799$**

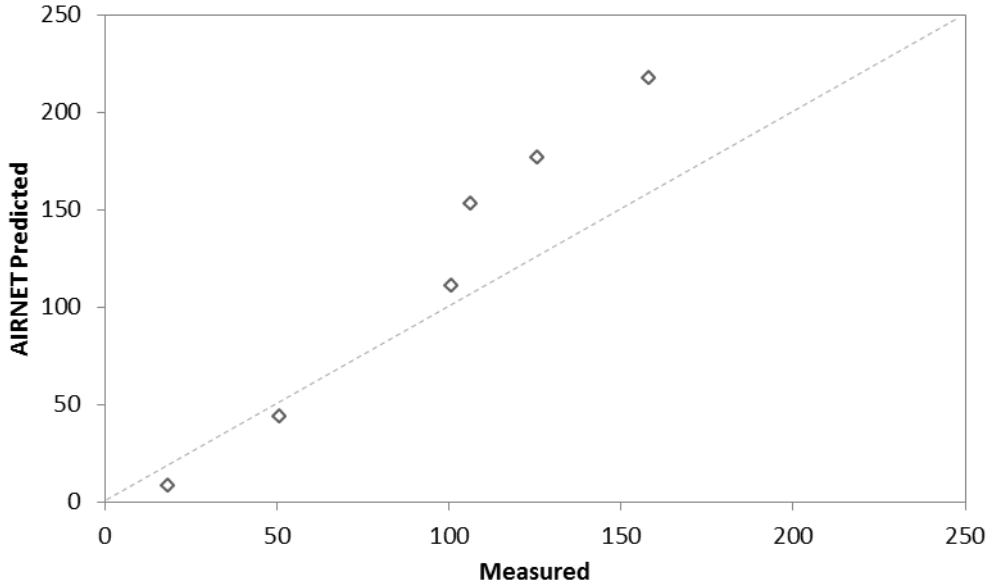


**Figure 7. 20, Measured pressure range against predicted pressure range of selected data sets $R^2 = 0.9766$**

This data provides validation to the method of predicting pressure response to changes in waterless trap seal opening size. Sections 7.2.2 and 7.3.1 accomplish Objective 5 of this research.

The validity of CFD and FSI as a comparable method to traditional laboratory evaluation was presented. It is suggested that given adequate computational hardware for the tasks required, CFD and FSI would prove to be less time consuming than traditional methods, enabling quicker analysis of the effect of minute changes of physical properties. All this, while providing greater information than possible in the laboratory. The disadvantage of computational methods however, lies as previously stated in preceding chapters, in the ability to validate that experimental data. Sections 7.2.2 and 7.3.1 prove that validation however is a realistic possibility through non-conventional methods.

## 7.4 Conclusions

This chapter has presented novel methodologies for the development of boundary conditions. The methods employed to successfully validate the equations were in themselves novel, given the difficulty in disaggregating the influence of trap seal response from other reflective boundaries in a large system. The governing principles of reducing water trap movement with increasing frequency and system pressurisation due to waterless trap mean opening area were found to successfully describe the device operation in a way that could be validated.

Test simulation runs incorporating the $\Delta v$ co-efficient in AIRNET clearly demonstrated that water trap response was frequency dependent, with little movement at higher frequencies. Similarly, AIRNET predicted a pressurisation of a virtual test pipe when the new boundary equation for the waterless trap was included.

Overall, the use of CFD to analyse the hitherto ill-defined internal flows in a water trap has proved invaluable in generating a more robust and accurate boundary condition for inclusion in AIRNET. The use of photogrammetric analysis in conjunction with more traditional frequency related analytical tools such as Fourier analysis has led to the development of boundary equations which fully describe the complex fluid to structure interactions associated with flexible sheath waterless traps in building drainage systems.

The benefits of these new boundary conditions are clear. More accurate water trap response means that more effective protection systems can be tailored to real system responses to the inevitable air pressure transients experienced in building drainage systems.

# Chapter 8

## Conclusions and Recommendations for Future Study

### 8.1 Conclusions

The inclusion of a barrier between the Building Drainage System (BDS) and the habitable space is arguably the single most significant development in Public Health Engineering in modern history. The inclusion of the appliance trap seal actively isolates people inside the building from disease in the plumbing and sewerage system

The airflows in BDSs are characterised by their humidity and temperature, and can contain toxic sewer gases and harmful pathogens, notwithstanding the nuisance of malodour, which in the 19$^{th}$ century was considered synonymous with disease. The main defence against this ingress is the 'trap seal' which comes in two forms; the 'water trap seal' and the 'waterless trap seal'. Whilst these devices form effective barriers in the main, they are vulnerable to transient air pressure fluctuations in the system which can lead to protection systems being compromised. Greater understanding of the operational characteristics of both these device types is essential for better protection strategies.

The sole purpose of the BDS is to safely and rapidly remove physiological waste from habitable spaces - preventing the spread of disease and infection through host contact with fluids and solid waste which housed these microorganisms. The SARS epidemic at the Amoy Gardens (in Hong Kong) in 2003, provided testament to the theory, that

disease transmission could occur through the BDS, and so, continued emphasis has been placed by researchers and Public Health Engineers on meeting the system criteria and preventing instances of cross contamination.

Numerical modelling of the whole building drainage network enables rapid assessment of the suitability of a BDS design to meet the system criteria. AIRNET provides a powerful tool for the analysis of BDS performance, but first, requires appropriate equations in order to continue calculations at system boundaries. This method of assessment currently uses a laboratory only approach to allow a single loss co-efficient to be developed for a device, regardless of physical properties. These boundary conditions are inherently static and do not account for moving, flexible structures.

This research has produced new methodologies to evaluate performance and generate dynamic boundary conditions suitable for inclusion in the existing 1-D MoC based model, AIRNET, which solves for pressure and velocity via the St. Venant equations of continuity and momentum in a finite difference scheme.

The overarching aim of this project was to provide greater insight into how BDS protection devices function and determine under what conditions fundamental vulnerabilities existed. Alongside this, there is a need for new methods of boundary condition development; methods which provided the MoC technique and the user with greater detail of system operation were than found through traditional methods, therefore enabling greater accuracy to whole system modelling. As with all models, AIRNET has limitations and is constantly under improvement. One particular limitation from observation is that the model overestimates water level fluctuations, particularly at higher frequencies. The output from this research has gone a long way to redressing this inconsistency.

To achieve this aim, laboratory and computational testing was conducted on 3 waterless trap seals, a typical PVC water trap and the laboratory glass water trap. Computational Fluid Dynamics (CFD) offers opportunities for analysis of systems on a minute scale, however, it is very costly and time-consuming. Research using this method found that

the protection afforded by trap seals of all types is dependent on the frequency of the applied pressure wave as on the amplitude of force applied. The frequency response of the commercial water trap modelled in CFD suggests that the smaller inner bend length leads the trap seal to be more vulnerable to induced siphonage (due to the high flow rate response), than the laboratory trap seal under the same conditions. It was found that three zones of movement existed within the bend of the seal and that a relationship existed between the inner bend length of zone 1. Velocity was also found to become a construct of the inner and outer bend length from which the velocities along the bend could be calculated. Objective 1 was met by the analysis of this flow regime within the appliance trap seals

The use of CFD offered the potential for design optimisation, together with insight into the complex processes involved in trap seal operation, however data analysis proved very challenging. The large quantity of data generated and ability to assess fluid dynamics properties at any point in the geometry proved very challenging, particularly since there had been no previous work carried out in this area. The definition of zones of movement within a standard U-bend formed the basis for analysis leading to the development of a dynamic velocity decrement model encapsulating unsteady friction and separation losses linked to device geometry for the first time. These findings led to the identification of a frequency dependent internal energy factor $\Delta v$ suitable for predicting the effect of frequency of an air pressure transient, on trap seal displacement. This finding satisfied Objective 2 of the research project, and is validated using AIRNET to satisfy Objective 5.

Through the laboratory assessment of the fluid structural interaction of the waterless trap seal, it was found that, reflections as a result of the repeated closing of the waterless trap seal, if generated at a sufficiently low frequency (particularly <4Hz), low amplitude air pressure transients could under certain conditions compromise the integrity of other water trap seals in the system. This movement of air, typically unsteady in nature, is a direct result of the patterns of usage and discharge profiles of sanitary appliances in the building and now the reflection of a waterless trap seal. These appliances generate time

dependent flows and thus subject the system to a range of both negative and positive air pressures. Modern building drainage installations are complex systems involving many different technologies which must react to one another as no division within the pipe network exists. It is no longer possible to solely describe the nature of systems component interactions through a single loss coefficient, particularly given the dynamic frequency dependency of the system, without the use of sophisticated methods such as those described in this thesis. CFD and FSI are shown to offer opportunities for analysis of systems on a minute scale, however substantial economic resources are required.

The analysis of the waterless trap seal through laboratory and computational FSI techniques, also led to the development of a boundary condition methodology which integrates the two techniques. The use of a novel technique, integrating digitized photographic data and system pressure data transformed via a new method known as photogrammetric analysis, offers the potential for future similar work on flexible structures and has proved to be immensely powerful in this research. The boundary conditions for Samples 1 and 3, developed by these techniques, describe the oscillatory motion of the devices for pressures typical to the BDS. The RMS value calculation and lumped model assessment was found to be particularly useful in providing the tools to establish new relationships between the opening area, opening height and width, and later opening area and pressure. These relationships allow AIRNET to become a single solution method for the approximation of the water less trap seal fluid structural interaction problems.

Within Chapters 5 and 6, validation (addressing Objective 4) is also conducted through a series of comparisons with laboratory and CFD data. Identification of the transitional frequency region comparable to the Gormley and Beattie (2010) findings along with the visual observations of the pattern of flow movement are considered to render this technique a suitable alternative to laboratory testing.

Chapters 4 to Chapter 6, present the step by step methodology for the development of the boundary condition for the water trap seal and the waterless trap seal. The methodology is presented in its entirety in Chapter 7. Here, the presentation is found to

satisfy Objectives 2 and 3. It should be noted that two of the three tested trap seals could be modelled fairly accurately over a range of pressures. The numerical expression developed to describe the behaviour of Sample 2 across the range of induced pressures was found to be inconsistent and so no single relationship was found suitable. This however, is likely to be due to the use of compromised data but unfortunately time limitations prevented the assertion of this assumption.

In closing, the MoC numerical model (AIRNET) enables the quick and accurate analysis of the real systems. Ongoing development is vital, as only with accurate boundary conditions can the model realistically predict the conditions under which, the BDS is compromised, and for what length of time. The first technique developed a novel boundary condition methodology combining photographic imagery, pressure data, photogrammetric and Fourier analysis techniques to produce a mathematical representation of the dynamic opening and closing of a waterless trap under transient pressures. This dynamic fluid structure interaction was also carried out through the coupling of ANSYS Mechanical and ANSYS CFX, however computing power limitations precluded full replication of the laboratory experiments. The second technique developed focussed on the dynamic response of a water trap seal. Current boundary conditions use a steady state representation of friction and ignore U-bend separation losses. Analysis via ANSYS allowed a frequency dependent dynamic representation of velocity change in the water trap seal to be developed, incorporating representations of unsteady friction and separation losses to be included for the first time.

## 8.2 Recommendations for future study

Following the findings of this investigation of the performance of appliance trap seals in BDS, the areas that require further work have been identified.

(i). In this study, a relatively uniform mesh was generated for the analysis of the water trap seal, however recent CFD research suggests the advantage of

inflation layers to the accuracy of generated data. Further investigation of the zones of movement within the water trap seal using a fine mesh with inflation layers is suggested as an enhancement to the methodology and derived boundary conditions.

(ii). This research has taken into account the effect of a single applied low amplitude pressure and focussed on the effects the frequency, discounting the transient pressure on the water trap seal in two appliance traps. Further research is needed to expand the model and assess the suitability of the developed frequency dependent friction factor to the approximation of various applied low amplitude pressures within the same basin of applied frequencies. Additionally, as the Frequency Factor is developed for the 38mm water trap seal it is critical to assess its suitability to the prediction of water trap seals more likely to be found in the system (50mm and 75mm seals),

(iii). The findings of Chapter 6 and 7, suggest an opportunity for the expansion of the analysis of the waterless trap seal under unsteady and steady conditions through FSI for a more lengthened time frame. This research has shown that the relationship between pressure and the solid structure, in other non-rigid conduits, can be applied to the sheath and that digital experimentation can provide the necessary data to determine the separation loss of the fitting. Like with the water trap seal, computational experimentation holds the ability to assess the unsteady nature of waterless trap seals in far greater detail than attained in the laboratory, enabling novel boundary condition methods outside those developed in this thesis to be discovered.

# References


Abbott, M. (1979). *Computational hydraulics*. London: Pitman Pub.

Abbott, M. and Basco, D. (1989). *Computational fluid dynamics*. Harlow, Essex, England: Longman Scientific & Technical.

Amsallem D, Farhat C and Lieu T (2007) Aeroelastic analysis of F-16 and F-18/A configurations using adapted CFD-based reduced-order models *48th AIAA/ASME/ASCE/AHS/ASC Structures, Structural Dynamics, and Materials Conference*, vol. AIAA 2007-2364, pp. 1– 20, Honolulu, Hawaii.

Andersson, B. (2012). *Computational fluid dynamics for engineers*. Cambridge: Cambridge University Press.

Angelakis, A. and Rose, J. (2014). *Evolution of sanitation and wastewater technologies through the centuries*. London: IWA Publishing.

ANSYS (2012). ANSYS CFX Rel 12.0 Documentation. PA, US: ANSYS Incorporated.

Antaki, G. (2003). *Piping and pipeline engineering*. New York: Marcel Dekker.

Argyris, J. (1955). Energy Theorems and Structural Analysis. *Aircraft Engineering and Aerospace Technology*, 27(3), pp.80-94.

Augier, N. (2001). Case Study: Globalisation; Location; Everywhere; Together, in Sickness and in Health. *The NY Times Magazine*. [online] Available at:

http://www.nytimes.com/2001/05/06/magazine/1-case-study-globalization-location-everywhere-together-sickness-health.html [Accessed 9 Apr. 2015].

Bazilevs, Y., Calo, V., Zhang, Y. and Hughes, T. (2006). Isogeometric Fluid–structure Interaction Analysis with Applications to Arterial Blood Flow. *Computational Mechanics*, 38(4-5), pp.310-322.

Beattie, R. (2007). *Derivation of an empirical frequency dependent friction factor for transient analysis of water trap seals in building drainage systems*. MSc thesis, Heriot Watt University, Edinburgh.

Beattie, R. (2013). *The effect of weather and climate change on siphonic rainwater drainage system operation*. PhD thesis, Heriot Watt University, Edinburgh.

Bennett, J. and Brachman, P. (1998). *Hospital infections*. Philadelphia: Lippincott-Raven.

Bessems, D., Rutten, M. and Van De Vosse, F. (2007). A wave propagation model of blood flow in large vessels using an approximate velocity profile function. *Journal of Fluid Mechanics*, 580, p.145.

*Bhagavad-gita*

Billington, N. and Roberts, B. (1982). *Building services engineering*. Oxford: Pergamon Press.

Boldy, A. (1976). Waterhammer analysis in hydroelectric pumped storage installation. In: *Proc. 2nd Int. Pressure Surge Conference, BHRA.*

Booth, G.R. (1853). *The London sewerage question: Some serious observations and suggestions upon the defective plan of sewerage proposed by the Metropolitan Board of Works, Together with a method for remedying the evil*. London.

Boseley, S. (2007). Sanitation rated the greatest medical advance in 150 years. *The Guardian*. [online] Available at:

http://www.theguardian.com/society/2007/jan/19/health.medicineandhealth3 [Accessed 6 Jun. 2015].

Braess, D. and Schumaker, L. (2002). *Finite elements*. Cambridge [u.a.]: Cambridge Univ. Press.

Bromage, S. (2007). *Visualisation of the Lip Motion of Brass Instrument Players, and Investigations of an Artificial Mouth as a Tool for Comparative studies of Instruments*. PhD thesis. Edinburgh University.

BS EN274-2 : 2002 *Waste fittings for sanitary appliances — Part 2: Test methods,* , British Standards Institute, London

BS EN 12056:2000 *Gravity Drainage Systems inside buildings Part 2: Sanitary Pipework, layout and calculation*s, British Standards Institute, London

Campbell, D. (1992). *Mathematical Modelling of Air Pressure Transients in Building Drainage and Vent Systems*. PhD thesis collection. Heriot Watt University.

Carr, R. (2001). Excreta-related infections and the role of sanitation in the control of transmission. In: WHO, ed., *Water quality - Guidelines, Standards and Health: Assessment of risk and risk management for water-related infectious disease*, 1st ed. [online] London: IWA Publishing. Available at: http://www.who.int/water_sanitation_health/dwq/iwachap5.pdf [Accessed 29 Feb. 2015].

Carstens, M. and Roller, J. (1959). Boundary-shear stress in unsteady turbulent pipe flow. *Journal of the Hydraulic Division, ASCE,* 65(HY2), pp.67-81.

Cataldo, E., Leta, F., Lucero, J. and Nicolato, L. (2006). Synthesis of voiced sounds using low-dimensional models of the vocal cords and time-varying subglottal pressure. *Mechanics Research Communications,* 33(2), pp.250-260.

Centre for Disease Control and Prevention Newsroom, (2013). *Measles Still Threatens Health Security | Press Release | CDC Online Newsroom | CDC*. [online] Cdc.gov. Available at: http://www.cdc.gov/media/releases/2013/p1205-meales-threat.html [Accessed 19 Mar. 2015].

Centre for Disease Control and Prevention, (2014). *CDC Global Health - Global Health Security - Why It Matters*. [online] Cdc.gov. Available at: http://www.cdc.gov/globalhealth/security/why.htm [Accessed 19 Mar. 2015].

Chadderton, D. (2004). *Building services engineering*. London: Spon Press.

Chadwick, E. (1842). *Report on the sanitary conditions of the labouring population of Great Britain*. London: Printed by W. Clowes and Sons for H.M. Stationery Off.

Chan, W. (2006). *Simulation of Arterial Stenosis Incorporating Fluid Structural Interaction and Non-Newtonian Blood Flow*. Mphil Thesis collection. RMIT University, Australia.

Cheng, H. (2003). *Proposed Guidelines of using CFD and the validity of the CFD models in the numerical simulations of wind environments around buildings*. PhD thesis collection. Heriot Watt University.

Chung, T. (2010). *Computational fluid dynamics*. Cambridge: Cambridge University Press.

Connolly, M. and Heymann, D. (2002). Deadly comrades: war and infectious diseases. *The Lancet*, 360, pp.s23-s24.

Courant, R. and Friedrichs, K. (1948). *Supersonic flow and shock waves*. New York: Interscience Publishers.

Courant, R., Friedrichs, K. and Lewy, H. (1928). ber die partiellen Differenzengleichungen der mathematischen Physik. *Math. Ann.*, 100(1), pp.32-74.

Degroote, J. (2010). *Development of Algorithms for the paritioned simulation of strongly coupled Fluid -Structure Ineraction problems*. PhD Thesis. Gent University, Belgium.

Degroote, J., Haelterman, R., Annerel, S., Bruggeman, P. and Vierendeels, J. (2010). Performance of partitioned procedures in fluid–structure interaction. *Computers & Structures*, 88(7-8), pp.446-457.

Douglas, J., Gasiorek, J. and Swaffield, J. (1995). Fluid mechanics. Harlow, Essex, England: Longman Scientific & Technical.

Douglas, J., Gasiorek, J., Swaffield, J. and Jack L. (2011). *Fluid mechanics*. Harlow, Essex, England: Longman Scientific & Technical.

Dumont, K., Vierendeels, J., Segers, P., Van Nooten, G. and Verdonck, P. (2005). Predicting ATS open pivot (TM) heart valve performance with computational fluid dynamics. *Journal of Heart Valve Disease*, 14(3), pp.393-399.

Eesa, M. (2009). *CFD studies of complex flows in pipes*. PhD Thesis. Univesity of Birmingham, U.K.

Environment Agency, and Natural Resources Wales, (2013). *Water stress areas - final classification*. [online] Available at: https://www.gov.uk/government/uploads/system/uploads/attachment_data/file/244333/water-stressed-classification-2013.pdf [Accessed 20 Feb. 2015].

Evangelisti, G. (1969). Waterhammer Analysis by the Method of Characteristics. *L'Energia Elettrica*, XLVI, Milano.

Eymard, R., Hilhorst, D. and Vohralík, M. (2006). A combined finite volume–nonconforming/mixed-hybrid finite element scheme for degenerate parabolic problems. *Numer. Math.*, 105(1), pp.73-131.

Farhat, C., van der Zee, K. and Geuzaine, P. (2006). Provably second-order time-accurate loosely-coupled solution algorithms for transient nonlinear computational aeroelasticity. *Computer Methods in Applied Mechanics and Engineering*, 195(17-18), pp.1973-2001.

Ferziger, J. and Perić, M. (2002). *Computational methods for fluid dynamics*. Berlin: Springer.

Fewtrell, L. and Bartram, J. (2001). *Water quality*. London: IWA Pub.

Fidler, D. (1996). Globalization, International Law, and Emerging Infectious Diseases. *Emerg. Infect. Dis.*, 2(2), pp.77-84.

Flanagan, J. and Landgraf, L. (1968). Self-oscillating source for vocal-tract synthesizers. *IEEE Transactions on Audio and Electroacoustics*, 16(1), pp.57-64.

Fletcher, C. (1997). *Computational techniques for fluid dynamics*. Berlin: Springer.

Fox, J. (1968). *The use of the digital computer in the solution of water-hammer problems. ICE Proceedings*, 39(1), pp.127-131.

Fox, J. (1989). *Transient flow in pipes, open channels, and sewers*. Chichester [England]: Ellis Horwood.

Frontinus, S. and [trans. Charles Bennett], (1961). Stratagems and the Aqueducts of Rome. *Cambridge: Harvard University Press*, p.p.357-.

Giannopapa, C. (2004). *Fluid structure interaction in flexible vessels*. PhD Thesis. King's College London (University of London).

Godunov, S. (1959). Finite difference method for numerical computation of discontinuous solutions of the equations of fluid dynamics. *Mat. Sb*, 47, pp.271-306.

Goldin, I. (2014). Ebola outbreak is latest example of globalization's risks. *PBS Newshour*. [online] Available at: http://www.pbs.org/newshour/making-sense/ebola-outbreak-latest-example-globalizations-risks/ [Accessed 21 Feb. 2015].

Gormley, M. (2002). *Development of a positive air pressure attenuatorfor use in Building Drainage Systems*. Mphil. Thesis, Heriot Watt University.

Gormley. M. (2011) 'Assessment of the impact of low flush volume WCs on building drainage system operation' Scottish Government Report

Gormley, M. and Beattie, R. (2010). Derivation of an empirical frequency-dependent friction factor for transient response analysis of water trap seals in building drainage systems. Building Services Engineering Research and Technology, 31(3), pp.221-236.

Gormley, M. and Kelly D. A., (2011) 'Pathogen Loading and Environmental Conditions Found in Hospital Building Drainage System Wastewater and Airflows.' CIB W62 International Symposium, Portugal.

Gormley, M., Swaffield, J., Sleigh, P. and Noakes, C. (2011). An assessment of, and response to, potential cross-contamination routes due to defective appliance water trap seals in building drainage systems. *Building Services Engineering Research and Technology*, 33(2), pp.203-222.

Gray C.A.M, (1953). Analysis of the dissipation of energy in waterhammer. *Proc. ASCE*, Vol 119, Paper 274, pp 1176-1194.

Griebel, M., Dornseifer, T. and Neunhoeffer, T. (1997). *Numerical simulation in fluid dynamics*. Philadelphia, Pa.: Society for Industrial and Applied Mathematics (SIAM, 3600 Market Street, Floor 6, Philadelphia, PA 19104).

Harington, J. (1596). *A new discourse of a stale subject, called The metamorphosis of Aiax*. [London]: Printed by J. Windet.

Hathway, E., Noakes, C., Sleigh, P. and Fletcher, L. (2011). CFD simulation of airborne pathogen transport due to human activities. *Building and Environment*, 46(12), pp.2500-2511.

Hirt, C., Amsden, A. and Cook, J. (1974). An Abitrary Lagrangian-Eulerian computing method for all flow speeds. *Journal of Computational Physics*, 14(3), pp.227-253.

Hrennikoff, A. P., 1941. Solution of problems in elasticity by the framework method. Transactions of the American Society of Mechanical Engineers. Journal of applied mechanics, vol. 8, pp. A169 – A175

Hughes, T. and Lubliner, J. (1973). On the one-dimensional theory of blood flow in the larger vessels. *Mathematical Biosciences*, 18(1-2), pp.161-170.

Hunter, R. (1924). *Minimum requirements for plumbing*. US Department of Commerce, Plumbing Code Report.

Hunter, R. (1940). *Methods of estimating loads on plumbing systems*. Washington DC: BMS 65 and BMS 79, National Bureau of Standards.

IPCC, (2007). *Chapter 3: Freshwater Resources and their Management*. IPCC 4th Assessment Report, Climate Change. IPCC.

IPCC, (2014). *Mitigation of Climate Change*. IPCC 5th Assessment Report, Climate Change. IPCC: Cambridge University Press, USA.

Ishizaka, K. and Flanagan, J. (1972). Synthesis of Voiced Sounds From a Two-Mass Model of the Vocal Cords. *Bell System Technical Journal*, 51(6), pp.1233-1268.

Ishizaka, K. and Matsudaira, M. (1972). *Fluid mechanical considerations of vocal cord vibration*. Santa Barbara, CA: SCRL Monograph 8, Speech Communication Research Laboratory.

Izhar, A., Qureshi, A. and Khushnood, S. (2013). Simulation of Fluid Structure Interaction of Heat Exchanger Tube Using ANSYS CFX. *Life Science Journal*, [online]

10(2), pp.2317-2328. Available at: http://www.lifesciencesite.com/lsj/life1002/324_19108life1002_2317_2328.pdf [Accessed 16 Mar. 2014].

Jack, L. (1997). *An investigation of the air pressure regime within building drainage vent systems*, PhD Thesis, Heriot Watt University.

Jack, L. (2000). Developments in the definition of fluid traction forces within building drainage vent systems. *Building Services Engineering Research and Technology*, 21(4), pp.266-273.

Joukowsky, N. (1900). Uber den hydraulisher Stoss in WasserlietungsrohenMemoirs de l'Academie Imperiale des Sciences de St Petersburg. *translated by Miss O Simin, Proceedings: American Water Works Associations*, 24(1904), pp.p. 341-424.

Kelly, D.A (2009). Controlling the risk of cross-contamination from the building drainage system using the reflected wave technique to identify depleted water trap seals'. Heriot Watt University theses collection. Edinburgh, U.K.

Kenover, J. (2009). *Mohenjo-daro the Ancient Indus Valley City in Photographs*. [online] Mohenjodaro.net. Available at: http://www.mohenjodaro.net [Accessed 26 Feb. 2015].

Knobler, S., Mahmoud, A. and Lemon, S. (2006). *The impact of globalization on infectious disease emergence and control*. Washington, DC: National Academies Press.

Knossos, Crete. (n.d.). [image] Available at: http://mythagora.com/photo/gallery17/intro17.html [Accessed 26 Feb. 2015].

Kumar, V., Abbas, A., Fausto, N. and Mitchell, R. (2007). *Robbins basic pathology*. 8th ed. Philadelphia, PA: Saunders.

Kuntz, M. and Menter F.R., (2004). Simulation of fluid-structure interactions in aeronautical applications. European Congress on Computational Methods in Applied Sciences and Engineering (ECCOMAS)

Kuo, C., Chu, Y., Wang, P., Lai, C., Chu, W., Leu, Y. and Wang, H. (2013). Using image processing technology and mathematical algorithm in the automatic selection of vocal cord opening and closing images from the larynx endoscopy video. *Computer Methods and Programs in Biomedicine*, 112(3), pp.455-465.

Lamb, H., (1898). On the velocity of in a tube, as affected by the elasticity of the walls, *Memoirs and proceedings of the Manchester Literary and Philosophical Society*, Manchester U.K.,.42(9), pp1-16.

Lamoen, J., (1947). *Le coup de belier d'Allievi, compte tenu des pertes de charge continues*. Bull. Centre de Etudes, de Recherches et d'Essais Scientifiques des Constructions du Gerrie Civil et Hydraulique Fluviale, Tome II, Doseor, Liege.

Lawrence, K. (2007). *Ansys tutorial*. [Mission, KS]: SDC Publications.

Lawrence, K. (2007). *ANSYS Workbench Tutorial*. [Mission, Kansas]: Schroff Development Corp.

Lax, P. (1954). Weak solutions of nonlinear hyperbolic equations and their numerical computation. *Communications on Pure and Applied Mathematics*, 7(1), pp.159-193.

Lax, P. and Wendroff, B. (1960). Systems of conservation laws. *Communications on Pure and Applied Mathematics*, 13(2), pp.217-237.

Lee, K. W. and Xu, X. Y. Modelling of flow and wall behaviour in a mildly stenosed tube. *Medical Engineering & Physics*, 24: 575-586, 2002

Lieu, T. and Lesoinne, M. (2004). Parameter adaptation of reduced order models for three-dimensional flutter analysis. *AIAA Paper*, pp.2004-0888.

Lillywhite, M.S.T and Wise, A.F.E. (1969) Towards a general method for the design of drainage systems in large buildings, Journal IPHE, Vol 68, No4.

Lin, T.C and Morgan, G. W. (1956a). Wave propagation through fluid contained in a cylindrical elastic shell. *Journal of Applied Mechanics*, 23, pp.255-261.

Lin, T.C and Morgan, G. W. (1956b). Wave Propagation through Fluid Contained in a Cylindrical, Elastic Shell. *J. Acoust. Soc. Am.*, 28(6), pp.1165-1176.

Lister, M.,(1960). Numerical simulation of hyperbolic partial differential equations by the Method of Characteristics, in Ralston and Wilf (eds) *Mathematical Methods for Digital Computers*, John Wiley, New York, pp. 165-179.

Logan, D. (2010). *A first course in the finite element method*. 4th ed. Pacific Grove, CA: Brooks/Cole.

MacCormack, R. (1969). The Effect of Viscosity in Hypervelocity Impact Cratering. *AIAA Paper*, pp.66-354.

MacCormack, R. (1971). Numerical solution of the interaction of a shock wave with laminar boundary layer. In: *Proceedings of 2nd International Conference on Numerical Methods in Fluid Dynamics*.

Massau,J. (1900). Memoirs sur l'integration graphique des equations aux derives partialles, Ann Ass. Ingrs. Sortis des Ecols Speciales de Grand, 23, 95-214. Translated as Unsteady flow, H.J. Putman, Rocky Mountain Hydraulic Lab, Colorado, 1948.

McDougall J.A. (1995) 'Mathematical modelling of solid transport in defective building drainage systems'. PhD thesis, Heriot Watt University, Edinburgh.

McHenry, D. (1943). A lattice analogy for the solution of plane stress problems. *Jour. ICE*. 21, pp.59-82.

Menter, F. (2009). Review of the shear-stress transport turbulence model experience from an industrial perspective. *International Journal of Computational Fluid Dynamics*, 23(4), pp.305-316.

Monge, G.(1789) Mémoire sur quelques phénomènes de la vision. *Annales de chimie et de physique* 3 (1789):147.

Murzionak, A. (2013). *Rocket Based Combined Cycle Exchange Inlet Performance Estimation at Supersonic Speeds*. MSc Thesis. Carleton University, Ontario, Canada.

Nelson, K. and Williams, C. (2007). *Infectious disease epidemiology*. Sudbury, Mass.: Jones and Bartlett Publishers.

Newton, M. (2009). *Experiemental Mechanical and Fluid Mechanical Investigation of the Brass Instrument Lip-reed and Human Vocal Folds*. PhD Thesis. Edinburgh University.

Nicholls-Lee, R.F. (2011*). Adaptive composite blades for horizontal axis tidal turbines*. PhD Thesis, University of Southampton.

Niyogi, P. (2006). *Introduction to computational fluid dynamics*. New Delhi: Dorling Kindersley.

Oden, J. (1973). Some results of finite element applications in finite elasticity. *Computers & Structures*, 3(1), pp.175-194.

Paidoussis, M. (2003). *Slender structures and axial flow*. London: Elsevier Academic Press.

Païdoussis, M. and Denise, J. (1972). Flutter of thin cylindrical shells conveying fluid. *Journal of Sound and Vibration*, 20(1), pp.9-26. Parliamentary papers (1846) Pg 12 (40)

Parmley, R. (2001). *Hydraulics field manual*. 2nd ed. New York: McGraw-Hill.

Peiro J.,and Sherwin,S. (2005). 'Handbook of Materials Modelling. Volume I: Methods and Models,C 8.2.'Netherlands [online] Available from: *www2.imperial.ac.uk/ssherw/spectralhp/papers/HandBook.pdf* [Assessed *21/08/2011]*

Pericevic, I. and Moatamedi, M. (2007). Application of the penalty coupling method for the analysis of blood vessels. *Revue européenne de mécanique numérique*, 16(3-4), pp.537-548.

Perktold, K. and Rappitsch, G. (1995). Computer simulation of local blood flow and vessel mechanics in a compliant carotid artery bifurcation model. *Journal of Biomechanics*, 28(7), pp.845-856.

Peskin CS. (1972). *Flow patterns around heart valves: a digital computer method for solving the equations of motion.* PhD thesis. Phys- iol., Albert Einstein Coll. Med., Univ. Mi- crofilms. 378:72–30

Reuderink, P., Hoogstraten, H., Sipkema, P., Hillen, B. and Westerhof, N. (1989). Linear and nonlinear one-dimensional models of pulse wave transmission at high Womersley numbers. *Journal of Biomechanics*, 22(8-9), pp.819-827.

Richardson, L. (1910). On the Approximate Arithmetical Solution by Finite Differences of Physical Problems Involving Differential Equations, with an Application to the Stresses in a Masonry Dam. *Proceedings of the Royal Society A: Mathematical, Physical and Engineering Sciences*, 83(563), pp.335-336.

Sahoo, P., Soltani, S. and Wong, A. (1988). A survey of thresholding techniques. *Computer Vision, Graphics, and Image Processing*, 41(2), pp.233-260.

Saneyoshi, J., Teramura, H. and Yoshikawa, S. (1987). Woodwind and brasswind instruments. *Acustica*, 62, pp.194-210.

Shaw, C. (1992). *Using computational fluid dynamics*. New York: Prentice Hall.

Skalak, R. (1956). An extension of the theory of waterhammer. Transactions of the ASME, 78, pp.105-116

SKK (HK), (2015). [image] Available at: http://www.skkhk.com.hk/UserFiles/Image/Job_reference/0089.jpg [Accessed 5 Feb. 2015].

Stevenson, S. (2009). *Experimental Investigation of Lip Motion in Brass Instrument Playing*. PhD thesis. Edinburgh University.

Story, B. and Titze, I. (1995). Voice simulation with a body-cover model of the vocal folds. *J. Acoust. Soc. Am.*, 97(2), pp.1249-1260.

Streeter, V., (1969). Waterhammer Analysis, *Jour.. Hyd Div ASCE*, 88(HY3), 79-113.

Streeter, V. and Lai, C. (1962). Waterhammer analysis with fluid friction. *Jour. Hyd. Div ASCE*, 128, paper No. 3502 Part 1, pp.1491-1552.

Stubley G. D., (2008) '*Computational Fluid Dynamics for Fluids Engineering Design – ANSYS CFX STUDENT USER MANUALVersion11'*. University of Waterloo, Canada.

Swaffield, J. (2006). Sealed building drainage and vent systems—an application of active air pressure transient control and suppression. *Building and Environment*, 41(10), pp.1435-1446.

Swaffield, J., (2007). *Influence of unsteady friction on trap seal depletion*, CIBW62 Water Supply and Drainage Conference, Brno, September 19-21.

Swaffield, J. (2010). *Transient airflow in building drainage systems*. Abingdon, Oxon: Spon Press.

Swaffield, J. and Boldy, A. (1993). *Pressure surge in pipe and duct systems*. Aldershot, Hants, England: Ashgate Pub.

Swaffield, J. and Campbell, D. (1992a). Air pressure transient propagation in building drainage vent systems, an application of unsteady flow analysis. *Building and Environment*, 27(3), pp.357-365.

Swaffield, J. and Campbell, D. (1992b). Numerical modelling of air pressure transient propagation in building drainage systems, including the influence of mechanical boundary conditions. *Building and Environment*, 27(4), pp.455-467.

Swaffield, J. and Campbell, D. (1995). The simulation of air pressure propagation in building drainage and vent systems. *Building and Environment*, 30(1), pp.115-127.

Swaffield, J. and Galowin, L. (1992). *The engineered design of building drainage systems*. Aldershot, Hants, England: Ashgate.

Swaffield, J., Campbell, D. and Gormley, M. (2005). Pressure transient control: Part II—simulation and design of a positive surge protection device for building drainage networks. *Building Services Engineering Research and Technology*, 26(3), pp.195-212.

Swaffield, J., Jack, L. and Campbell, D. (2004). Control and suppression of air pressure transients in building drainage and vent systems. *Building and Environment*, 39(7), pp.783-794.

Swaffield, J., Jack, L. and Campbell, D. (2004). Control and suppression of air pressure transients in building drainage and vent systems. *Building and Environment*, 39(7), pp.783-794.

Swaffield, J., Gormley, M., Wright, G., McDougall, I. (2015.). *Transient free surface flows in building drainage systems*. Taylor & Francis, U.K.

Tenth Annual Report of the Registrar-General, (1847), pp.xvii.

*The Bible.* Christian Community Bible, Catholic Pastoral Edition.

The Independent, (2015). *Mediterranean migrant crisis 2015*. [image] Available at: http://www.independent.co.uk/incoming/article10302153.ece/alternates/w620/migrants-AFP.jpg [Accessed 6 Jun. 2015].

Transport for London, (2015). *Rolling stock - Transport for London*. [online] Tfl.gov.uk. Available at: https://www.tfl.gov.uk/corporate/about-tfl/what-we-do/london-underground/rolling-stock [Accessed 6 Jun. 2015].

Tu, J., Yeoh, G. and Liu, C. (2008). *Computational fluid dynamics*. Amsterdam: Butterworth-Heinemann.

Turner, M., Clough, R., Martin, H. and Topp, L. (1956). Stiffness and Deflection Analysis of Complex Structures. *Journal of the Aeronautical Sciences (Institute of the Aeronautical Sciences)*, 23(9), pp.805-823.

United Nations, (2015). *United Nations Millennium Development Goals*. [online] Available at: http://www.un.org/millenniumgoals/endopendefecation.shtml [Accessed 6 Jun. 2015].

Versteeg, H. and Malalasekera, W. (1995). *An introduction to computational fluid dynamics*. Harlow, England: Pearson Education Ltd.

Wilcox, D. (1993). *Turbulence modeling for CFD*. La Cãnada, CA: DCW Industries, Inc.

Winslow, C. (1920). The conveyance of bacteria by sewer air. *Journal of the American Medical Association*, LIII(18), pp.1490.

Wise, A.F.E (1957). *Drainage pipework in dwellings*. London: HMSO.

Wise, A.F.E and Croft, J. (1954). Investigation of single stack drainage for multi-storey flats. *Journal of Royal Sanitary Institute,* Vol 74, No 9, pp797-826.

Witzig, K. (1914).Uber erzwungene wellenbegungen zaher, inkopressible flussigkeit-edn in elastischen rohren.PhD theses, University of Bern

Womersley, J. (1957). Oscillatory Flow in Arteries: the Constrained Elastic Tube as a Model of Arterial Flow and Pulse Transmission. *Physics in Medicine and Biology*, 2(2), pp.178-187.

World Health Organisation, (2003). *Final Report: Amoy Gardens*. WHO Environmental Investigation. WHO.

World Health Organisation, (2005). *Using climate to predict infectious disease epidemics*. [online] Geneva: World Health Organisation. Available at: http://www.who.int/globalchange/publications/infectdiseases.pdf [Accessed 19 Feb. 2015].

World Health Organisation, (2009). *WHO | Cholera in Zimbabwe - update 4*. [online] Who.int. Available at: http://www.who.int/csr/don/2009_06_09/en/ [Accessed 5 Mar. 2015].

World Health Organisation, (2015). *Ebola data and statistics*. [online] Apps.who.int. Available at: http://apps.who.int/gho/data/node.ebola-sitrep.ebola-summary?lang=en [Accessed 23 Feb. 2015].

Wright G.B. (1997). *Mathematical modelling of sub-surface building drainage networks and their associated mechanical vent systems,* PhD Thesis, Heriot Watt University.

Wylie, E. and Streeter, V. (1978). *Fluid transients*. New York: McGraw-Hill International Book Co.

Young, T. (1808). Hydraulic investigations, subservient to an intended Croonian lecture on motion of the blood. *Philosophical Transactions of the Royal Society (London*), 98, pp.164-186.

Zienkiewicz, O. and Cheung, Y (1964) The Finite Element Method for Analysis of Elastic Isotropic and Orthotropic slabs, *ICE Proceedings*, 28(4), pp471-488.

Zilke W. (1968). Frequency dependant friction in transient pipe flow, *Journal of Basic Engineering*. Trans. ASME, Vol 90, No. 1, pp.109-115.

**Abbreviations**

| | |
|---|---|
| ASME | American Society of Mechanical Engineers |
| CIBW62 | International Council for Research and Innovation in Building and Construction Working Commission W62 'Water Supply and Drainage for Buildings' |
| ICE | Institute of Civil Engineering |
| IPHE | Institute of Public Health Engineering |
| WHO | World Health Organisation |